Preparation of Brand New Ligand Architectures Incorporating N-Heterocyclic Carbene Complexes with Carboranyl Substituents: Coordination Chemistry, Catalytic Evaluation and Anticancer Properties

Jordan Holmes

Submitted in accordance with the requirements for the degree of

Doctor of Philosophy

The University of Leeds

July 2017

The candidate confirms that the work submitted is his/her own, except where work which has formed part of jointly authored publications has been included. The contribution of the candidate and the other authors to this work has been explicitly indicated below. The candidate confirms that appropriate credit has been given within the thesis where reference has been made to the work of others.

Jointly Authored Publications

Tethered N-heterocyclic carbene–carboranes: unique ligands that exhibit unprecedented and versatile coordination modes at rhodium

Jordan Holmes, Christopher M. Pask, Mark A. Fox and Charlotte E. Willans.

Chem. Commun., 2016, **52**, 6443–6446.

CANDIDATE'S CONTRIBUTION

The work described within this publication is presented in Chapters 2 and 3 of this thesis. The candidate synthesised and characterised all of the compounds reported in the manuscript. The X-ray crystallographic data was all collected by the candidate. The manuscript was prepared by Dr C E. Willans.

Chelating N-heterocyclic carbene–carboranes offer flexible ligand coordination to Ir^{III}, Rh^{III} and Ru^{II}: effect of ligand cyclometallation in catalytic transfer hydrogenation

Jordan Holmes, Christopher M. Pask and Charlotte E. Willans.

Dalt. Trans., 2016, **45**, 15818–15827.

CANDIDATE'S CONTRIBUTION

The work described within this publication is presented in Chapter 5 of this thesis. The candidate synthesised and characterised all of the compounds reported in the manuscript. The X-ray crystallographic data was all collected by the candidate. The manuscript was prepared by Dr C E. Willans.

This thesis is dedicated to my parents.

For their endless love, support and encouragement

Acknowledgements

First of all I would like to thank my supervisor, Dr Charlotte E. Willans, for all her support and guidance over the last few years. Her seemingly limitless patience and understanding have been invaluable to me and are greatly appreciated.

A huge thank you to all the past and current members of the Willans group. Especially to Mike, aka Baby, our shared passion for Arnold Schwarzenegger made the lab a very enjoyable place to work, and I will truly miss shouting each of his 150 best quotes across the lab to each other. Likewise, thanks go to Frances with whom I could share the highs and lows of carborane chemistry with. I would also like to thank Bank who has to be the most stylish chemist, and dresses each day as if it was a Ralph Lauren photo shoot.

I would also like to thank members of the Hardie group who have also made the past few years an enjoyable experience. Especially Jonny who has to be the keenest chemist I have ever met, and Sam for his pessimistic outlook on life.

I also extend my thanks to all members of the Halcrow and McGowan groups, in addition to all technical staff here at Leeds, especially Dr C M. Pask for his help with X-ray crystallography. I would also like to thank Mr S. Atallah who works under the supervision of Prof R. Phillips at The University of Huddersfield for conducting the cell line screening studies.

A special thanks goes to my parents, without your love and support this journey would not be possible, and making you proud of me has pushed me to strive to be the best person I can be.

Finally, I would like to thank my girlfriend Tegan. She is truly one of the most genuine, kind hearted people I have ever met, and I cannot thank her enough for her support over the last two years. Not to mention the countless number of lifts to and from work at ridiculous times of the day!

Scope of Thesis

In this thesis two very different types of ligand classes are brought together, namely N-heterocyclic carbenes (NHCs) and carboranes. Chapter one discusses the fundamental structure and bonding involved in these two types of compound. An account of the synthetic strategies employed in the literature for the synthesis of NHCs and carboranes, and the techniques employed to coordinate these ligands to various metal centres is discussed.

Chapter two discusses the synthetic strategies explored towards a new hybrid ligand scaffold that fuses N-heterocyclic carbenes (NHCs) and *o*-carborane. A focal point of this work was to demonstrate the tailorability of this novel ligand system. A detailed account of the techniques employed for the characterisation of these novel ligands is given.

Chapter three discusses the synthetic challenges associated with deprotonation of the zwitterionic ligand precursors reported in Chapter 2. A deprotonation study revealed that the ligand must possess an ethyl linker or longer between the imidazolium and the carborane for a free carbene to be isolated. Subsequent coordination to various metal centres, including titanium, iron and rhodium, is explored.

The synthesis and full characterisation of Rh^{I}-NHC complexes that exhibit *closo*-carboranyl substituents is described in Chapter four. These complexes display unprecedented chemistry with a rare example of a Rh^{I}-metallacycle coordinating through both the NHC and the carbon vertex of the carborane. The catalytic activity of these complexes was probed in the hydrosilylation of acetophenone.

Chapter five investigates the application of our NHC-carborane ligands to the higher oxidation states of Rh^{III} and Ir^{III} as well as Ru^{II}. We have discovered that the nature of the α-substituent of the NHC, as well as reaction conditions, can determine the vertex at which cyclometallation occurs. A series of Ir^{III} complexes were successfully cyclometallated through the NHC and either a carbon atom or the B3/B6 vertex of the cage. Examination of the Ir complexes in the transfer hydrogenation of acetophenone revealed that cyclometallation through the carborane has a profound effect on the catalytic activity, indicating a bifunctional mechanism and involvement of the carborane moiety.

Chapter six describes the diverse coordination modes of NHC-carborane ligands at Ag^{I}. The steric nature of the ligand precursor plays a crucial role in the overall stability and the type of silver complex formed, with the first structurally elucidated example of Ag^{I} directly bound through the carborane reported. In addition, a series of carboranyl complexes derived from the natural product theobromine were synthesised. The antiproliferative properties of these complexes against the HCT116 (colon) cancer cell line was evaluated.

Table of Contents

List of Figures

List of Schemes

List of Tables

Abbreviations

2c-2e	two centre two electron (bond)
3c-2e	three centre two electron (bond)
Adm	Adamantyl
Å	Angstrom
AE	Antipodal Effect
^{n}Bu	Butyl group (-C_4H_9)
br.	Broad
BE	Butterfly Effect
COD	Cyclooctadiene
COSY	Correlation Spectroscopy
Cp	Cyclopentadienyl (C_5H_5)
Cp*	1,2,3,4,5-Pentamethylcyclopentadiene (C_5Me_5)
d	doublet
DCE	Dichloroethane
DCM	Dichloromethane
DFT	Density Functional Theory
DMSO	Dimethyl sulfoxide
DSD	Diamond-Square-Diamond
δ	chemical shift
e.d	electron density
ee	enantiomeric excess
eq	equivalent
ESI	Electron Spray Ionisation
Et_2O	Diethyl ether
g	grams
HMQC	Heteronuclear Multiple-Quantum Correlation
HRMS	High Resolution Mass Spectrometry
Hz	hertz
J	NMR coupling constant
K	kelvin
m-	*meta*-
LDA	Lithium diisopropylamide
LiHMDS	Lithium bis(trimethylsilyl)amide
M^+	Parent ion
M	Metal

Me	Methyl group (-CH_3)
MeCN	Acetonitrile
Mes	Mesityl group (-C_9H_{11})
MHz	megahertz
mg	milligrams
mol	moles
mmol	millimoles
m	multiplet
m/z	mass to charge ratio
NE	Neighbour Effect
NBS	*N*-bromosuccinimide
NHC	N-heterocyclic carbene
NMR	Nuclear Magnetic Resonance
NOE	Nuclear Overhauser Effect
OLED	Organic Light-Emitting Diode
o-	*ortho-*
p-	*para-*
p-cymene	$CH_3C_6H_4CH(CH_3)_2$
Ph	Phenyl group (-C_6H_5)
ppm	parts per million
q	quartet
RBF	Round-bottomed flask
rt	room temperature
s	singlet
TEA	Triethylamine
TMEDA	N,N',N'-Tetramethylethylenediamine
^{t}Bu	*tert*-Butyl (-C_4H_9)
t	triplet
Δ	splitting distortion
TFR	Triangular Face Rotation
TH	Transfer Hydrogenation
THF	Tetrahydrofuran
Ueq	Thermal parameter
VCD	Vertex-to-centroid distance
xs	excess

Chapter 1

Introduction

In this thesis two very different types of ligand classes are brought together, namely N-heterocyclic carbenes (NHCs) and carboranes. This chapter discusses the fundamental structure and bonding involved in these two types of compound. An account of the synthetic strategies employed in the literature for the synthesis of NHCs and carboranes, and the techniques employed to coordinate these ligands to various metal centres is discussed.

1.1 Structure and bonding of boranes and their derivatives

The behaviour of boron atoms originates from their electron deficiency, *i.e.* from the presence of only three bonding electrons and four available atomic orbitals. As a consequence, in order for boron to satisfy the octet rule it can partake in a combination of 2c2e (two-centre, two-electron) and 3c2e (three-centre, two-electron) electron-pair bonds. This can be observed in the simplest of boron hydrides (B_2H_6) in which four of the valence electrons, two of which are from the boron atoms, are delocalised within two bridging B-H-B units (**Figure 1.1**).[1]

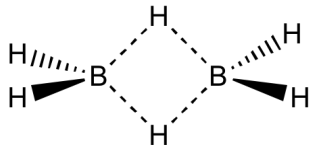

Figure 1.1 Structure of B_2H_6.

The most unique property of boron is its ability to form polyhedral skeletons, comprised of combinations of 2c2e and 3c2e bonds, with the principle building block consisting of triangular boron facets (**1**) (**Figure 1.2**). Every additional boron atom combines with one or more edges forming a new triangular face, and due to the approximate sp^3-hybridisation of each boron, triangles joined at an edge possess an obtuse angle (**2**). Successive addition of boron atoms gives a nest structure (**3**) and ultimately the closed icosahedron (**4**).

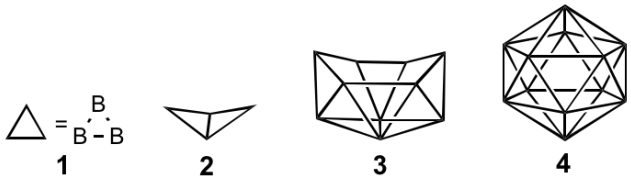

Figure 1.2 Successive building of boranes: the principle building blocking (**1**), obtuse angle formed upon addition of another boron (**2**), nest structure (**3**) and the closed icosahedron (**4**).

A common misconception is that these polyhedral structures are electron deficient, when in truth they have precisely the right number of orbitals and electrons for maximum stability. To illustrate this the different types of localised bonds involved in the molecular structure of *nido*-2,3-$C_2B_4H_8$ is presented **(Figure 1.3)**. The structure possesses a total of ten 2c2e bonds (2 C−H, 2 C−B, 4 B−H, 1 C−C and 1 B−B) and four 3c2e bonds (2 B−H−B and 2 C−B−B), requiring fourteen electron pairs, which are supplied by two carbons, four borons, and eight hydrogens. In addition, each carbon and boron has four neighbouring atoms, requiring four atomic orbitals for binding.

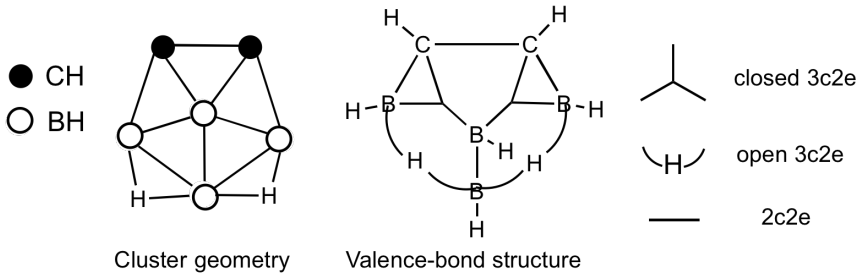

Figure 1.3 Molecular structure of *nido*-2,3-$C_2B_4H_8$ and the different types of localised bonds.[2]

The requirement for a precise number of orbitals and electrons led to Lipscomb and co-workers developing a topological model, which predicted a limited range of possible structures for any given borane, and could even predict those yet to be discovered.[3] The theory worked well for smaller boranes but failed at predicting larger structures. In 1971, Wade's rules were developed for predicting the structure of boranes, which not only worked but can also be easily applied to heteroboranes and other main group cluster compounds.[4] The method simply involves counting the number of skeletal electrons to determine the geometry of the cage. For a detailed account on the main principles behind Wade's rules see Grimes's book "Carboranes (Second edition)".[2]

1.2 Nomenclature

Dicarba-dodecaborane ($C_2B_{10}H_{12}$) possesses three common isomeric forms; 1,2- (*ortho*), 1,7- (*meta*) and 1,12- (*para*), with the numbers describing the positioning of the CH vertices in the cage. The numbering of the cage starts at the top vertex and successive belts are numbered in a clockwise fashion. Heteroatoms are numbered corresponding to their atomic number, with atoms of the highest atomic number usually holding the highest precedence (**Figure 1.4**). In this thesis, *ortho*- *meta*- and *para*- or *o*-, *m*- and *p*- are used interchangeably for brevity. The loss of a BH vertex gives the corresponding *nido*-dicarbaundecaborates, with the numbering of the cage now starting at the opposing vertex to the open face. In this thesis, the numbering system of the cage does not change upon loss of a BH vertex which simplifies matters when discussing the vertices of a cage between an *ortho*-carboranyl compound and its *nido*-derivative (**Figure 1.5**).

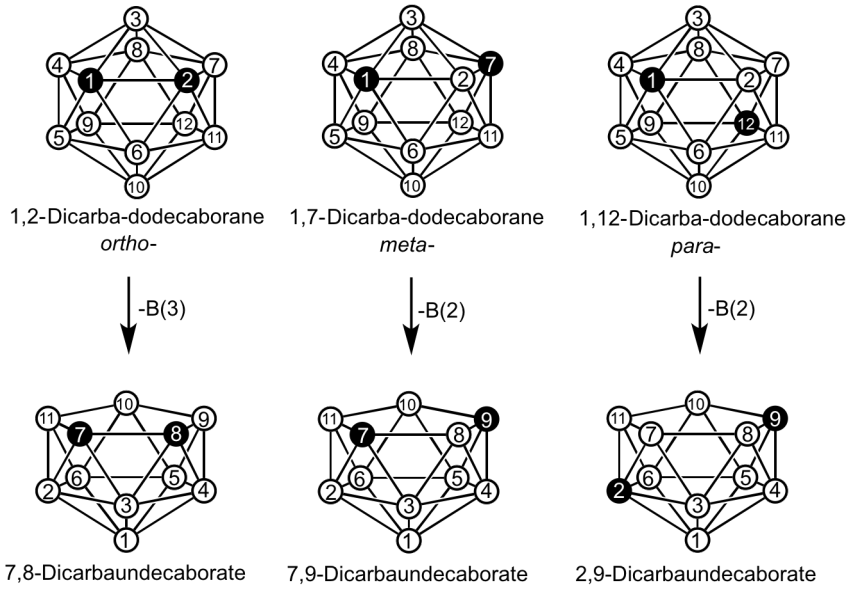

Figure 1.4 Numbering system used in the literature for *ortho*- *meta*- and *para*-carborane and their respective *nido*-species.

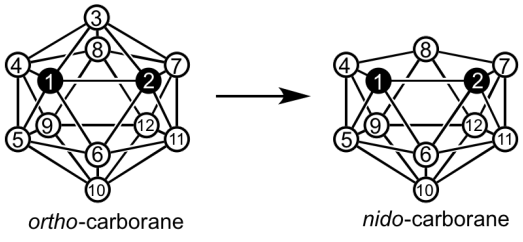

Figure 1.5 The numbering system adopted in this thesis.

1.3 Synthesis of carboranes

1.3.1 Alkyne insertion

The synthesis of *o*-carborane (**3**), involves the insertion of carbon into a polyborane framework, namely decaborane (**1**). Electron donors such as MeCN readily react with **1** to form the considerably more stable Lewis base adduct $B_{10}H_{12}(MeCN)_2$ (**2**).[5] Alkynes are the most commonly employed insertion reagents, and the reaction of **2** with acetylene gives **3** in high yields, with the carbon atoms of acetylene becoming the vicinal carbon atoms in the cage (**Scheme 1.1**).[6] In practice, the Lewis base adducts are usually not isolated, and the reaction can be conducted in a one pot synthesis by treating **1** with an alkyne in the presence of an electron donor. It is noteworthy that acetylene is an extremely flammable gas and requires an elaborate setup to use.[7] *o*-Carborane is therefore usually prepared from 1,2-bis(hydroxymethyl)- or 1,2-bis(acetoxymethyl)-*ortho*-carborane.[8,9]

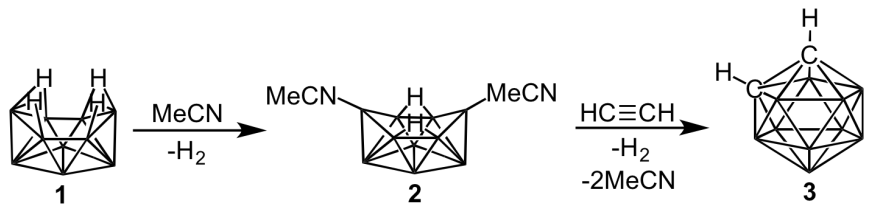

Scheme 1.1 Carborane synthesis *via* alkyne insertion.[4,5]

o-Carborane is the most widely utilised of its 3 isomers, and its derivatives are reported with numbers into the thousands with an extensive compilation gathered in Grimes's book "Carboranes (Second edition)".[2] By simply changing the substituent on the alkyne one has access to a plethora of potential carborane derivatives. However, there is one major drawback to this synthetic method; attaching bulky substituents directly to the alkyne, or use of alkynes which possess high Lewis basicity, leads to unfavourable carborane formation and the products are obtained in very low yields. The mechanism for insertion of the alkyne into the polyborane framework is complex, though the widely accepted mechanism includes two reactive intermediates: 1) the dissociation of a molecule of the electron donor (MeCN) (**4**), which is postulated following kinetic studies,[10,11] and 2) the coordination of the alkyne to **4** (**4.adduct**), where the alkyne first acts as a ligand before carborane formation (**Scheme 1.2**).

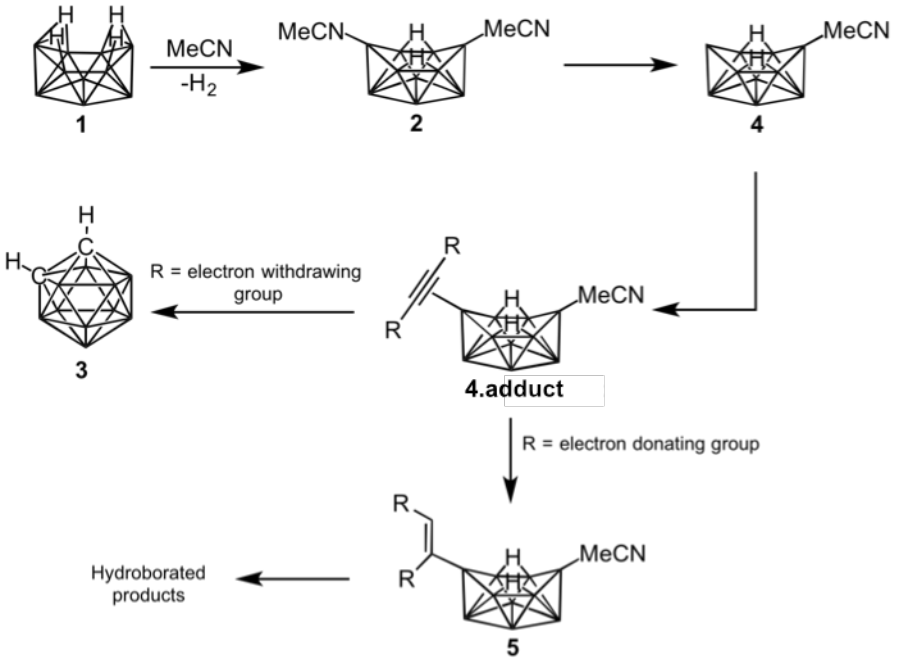

Scheme 1.2 Plausible mechanism for carborane formation *via* alkyne insertion.

This long standing issue of being restricted to alkynes that do not possess high Lewis basicity or bulky substituents directly attached to the vicinal carbons has led a number of researchers looking at why carborane formation is so unfavourable, and to optimise reaction conditions (**Figure 1.6**). The first milestone came through the work of Sneddon and co-workers in 2004, who reported the use of ionic liquids, which not only increased the yield but allowed products from internal alkynes to be isolated, which by conventional methods either fail or give much lower yields.[12] Almost a decade later, Valliant's preliminary work with $AgNO_3$ as a heterogeneous catalyst was able to drastically improve the yields using a range of substituted alkynes with $B_{10}H_{12}(MeCN)_2$.[13] It was proposed that the alkyne coordinates to silver, lowering both its Lewis basicity and the activation energy to formation of the desired product. A year later, Valliant reported the synthesis of a tailored homogenous catalyst allowing some reactions to be carried out at room temperature.[14]

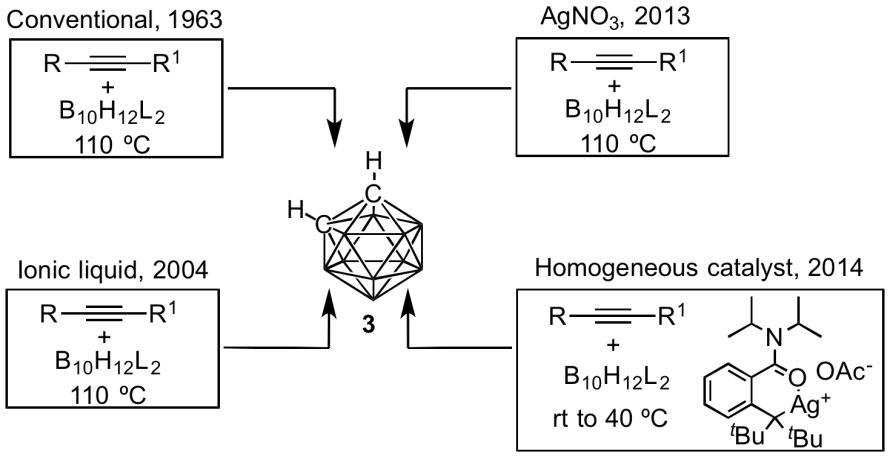

Figure 1.6 Evolution of carborane synthesis *via* the alkyne insertion route.[6,12-14]

1.3.2 Metalation at the C-vertex

An alternative synthetic route to substituted carboranes is to functionalise *o*-carborane directly through deprotonation of the most acidic carboranyl protons with a strong base such as ^{n}BuLi, to give C-lithiated carborane **6** (**Scheme 1.3, A**). It is noteworthy that **6** exists in equilibrium with the parent carborane (**3**) which often leads to a mixture of mono- (**6**) and di-C-substituted (**7**) products. This complication can be averted by either carrying out the lithiation in dimethoxyethane, which affords **6** exclusively, or by blocking the C2- position with a silyl moiety (**8**) that can later be removed to give the desired mono-substituted product (**10**) (**Scheme 1.3, B**). This synthetic method is considered much more versatile in comparison to the alkyne insertion method (see Grimes's book and references therein for a detailed account of the chemical transformations in which lithiated carboranes such as **3**, **7** and **9** have been utilised).[2]

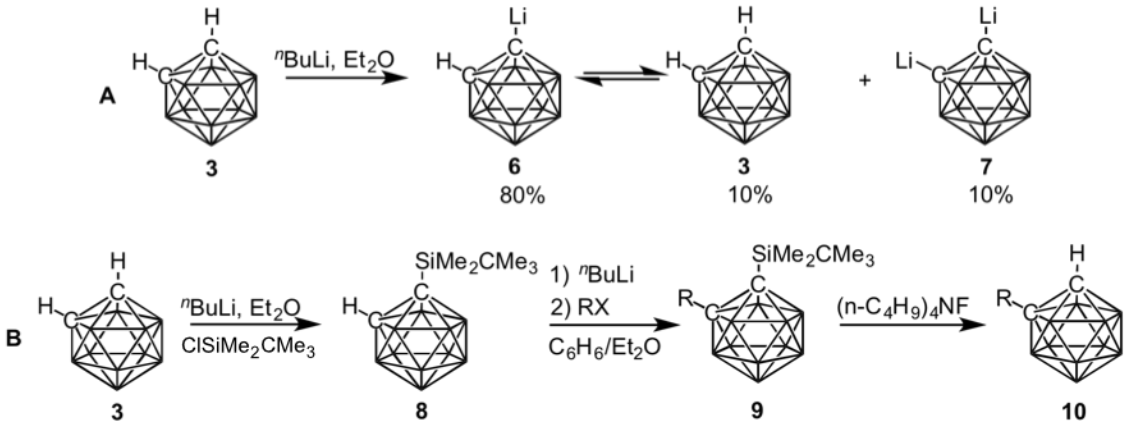

Scheme 1.3 Lithiation reactions with *o*-carborane.[2]

1.4 Metallacarboranes

Metallacarboranes fall into one of two classes, π- or σ-metallacarboranes, with the former describing the bonding of a metal through the open face of the carborane cluster. Conversely, a metal can bind through a linked periphery of the icosahedral cage, through a boron or carbon vertex. This chapter will focus on π-metallacarboranes, with *exo*-metallated derivatives discussed in later chapters.

The field of metallacarborane chemistry was developed on the basis of two key chemical advances. The first was the degradation reaction of *o*-carborane to the dianion $[C_2B_9H_{11}]^{2-}$,[15] and the second was the reaction of this species with $FeCl_2$ to give the first metallacarborane reported by Hawthorne and co-workers in 1965 (**Scheme 1.4**).[16] The open face of the dicarbollide dianion $[C_2B_9H_{11}]^{2-}$ is considered isolobal to that of the cyclopentadienide ion $[C_5H_5]^-$, with an η^5-coordination to the metal centre. The Fe metallacarborane showed improved stability over its Cp analogue achieved through 'peanut-like' bonding, which describes the more effective orbital overlap between the two icosahedral clusters and the metal centre (**Scheme 1.4**). Furthermore, due to the divalent charge of the dicarbollide ligands they are able to stabilise complexes of higher oxidation state with Fe metallacarboranes preferring the Fe^{3+} oxidation state to their Fe^{2+} Cp derivatives.

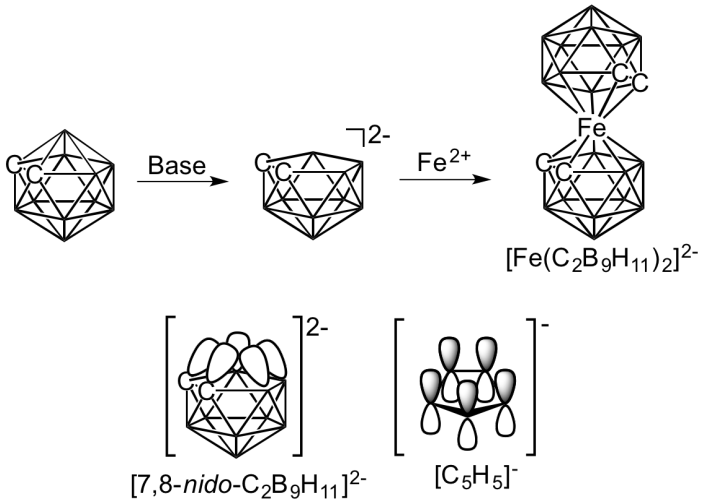

Scheme 1.4 Synthesis of the first metallacarborane and a representation of the orbitals in *nido*-carborane and Cp.[2]

Preparative routes to metallacarboranes are both diverse and plentiful, but the most utilised due to its versatility and accessibility is through 7,8-RR'$C_2B_9H_9^{2-}$, which yields 12-vertex icosahedral *closo*-MC_2B_9 clusters.[2,17–19] **Scheme 1.5** presents some of the synthetic methods employed for the synthesis of these clusters.

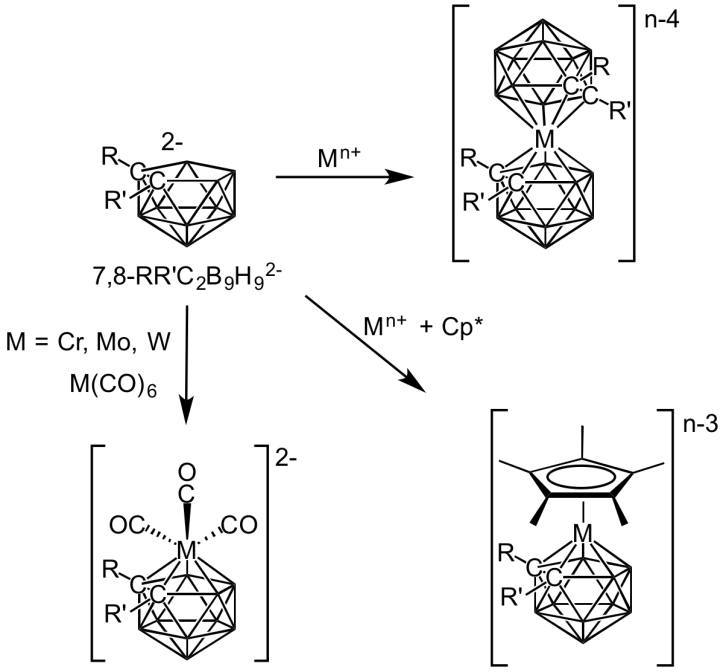

Scheme 1.5 Formation of metallacarboranes *via* insertion of transition metals into $7,8\text{-}RR'C_2B_9H_9^{2-}$.[2]

1.5 Isomerisation of the icosahedral cage

As previously discussed, dicarba-dodecaborane ($C_2B_{10}H_{12}$) can exist in three common isomeric forms 1,2- (*ortho*), 1,7- (*meta*) and 1,12- (*para*) (**Figure 1.4**). 1,7- and 1,12- isomers are accessible through thermal rearrangement with temperatures of 450 and 700 °C required to convert 1,2- to 1,7-,[20] and 1,7- to 1,12 respectively.[21] The precise mechanism of isomerisation has never been fully understood due to the high temperatures required preventing isolation of intermediates. Moreover, there is evidence for the scrambling of not only the carbon atoms but also the boron atoms indicating the reaction may proceed *via* more than one mechanism.[22] Nonetheless, this hasn't stopped mechanisms from being proposed. The first was reported by Lipscomb and termed the 'diamond-square-diamond' mechanism (**Scheme 1.6**).[23] This describes the breaking of an edge shared between two adjacent vertices, and formation of a new edge between two vertices perpendicular to the break. This theory applied well to the isomerisation of 1,2- to 1,7- with a proposed 'cuboctahedral intermediate', however, this mechanism was quickly rejected when the mechanism failed to conclude the formation of the *para*-isomer. The revised mechanism reported by Dvorak quite simply describes the rotation of a facet about 120° (**Scheme 1.6**).[20]

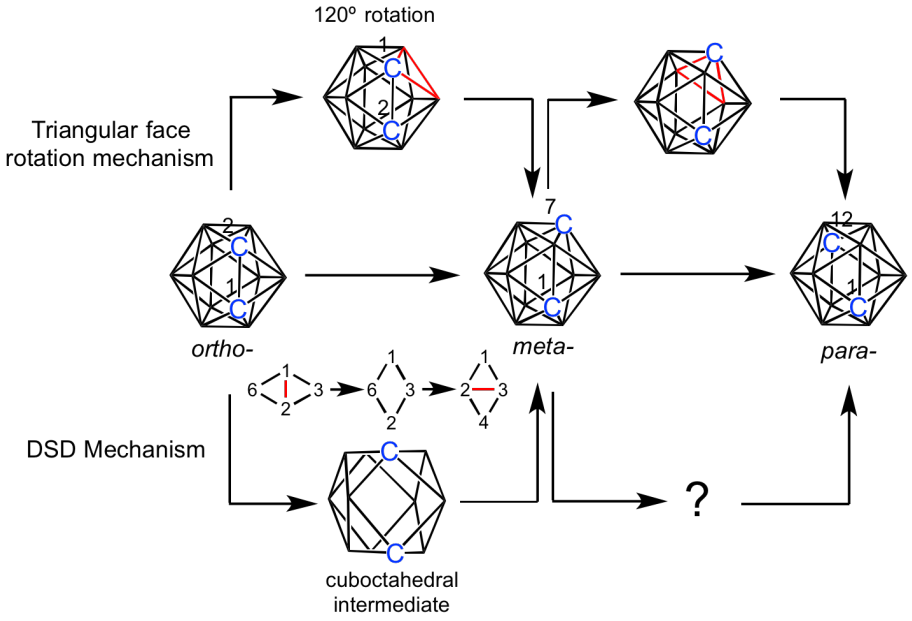

Scheme 1.6 Proposed isomerisation mechanisms of *o*-carborane.[20,22]

Although this mechanism arrives at the 1,12- isomer, computational studies rule it out due to the large energy barriers required to break the large number of connectivities to allow the facet to rotate.[24]

The first progresses towards understanding the polyhedral rearrangement mechanism was upon the realisation that replacement of a boron vertex with a metal lowered the rearrangement barrier, allowing experimental investigations to be carried out at lower temperatures. Hawthorne pioneered this field and published the first examples of metallacarboranes, which thermally isomerise at 200 °C (**Figure 1.7**).[25] Over the course of the next 5 years, the isomerisation of cyclopentadienyl-π-dicarbollyl derivatives of cobalt became well established but required much higher temperatures to isomerise (400-700 °C).[26,27] The isomerisation of other metallacarboranes was not so well-known and it was a decade later that Hawthorne published an iridium metallacarborane ($3,3\text{-}(PPh_3)_2\text{-}3\text{-}H\text{-}3,1,2\text{-}IrC_2B_9H_{11}$) that was capable of isomerisation at reflux in toluene.[28]

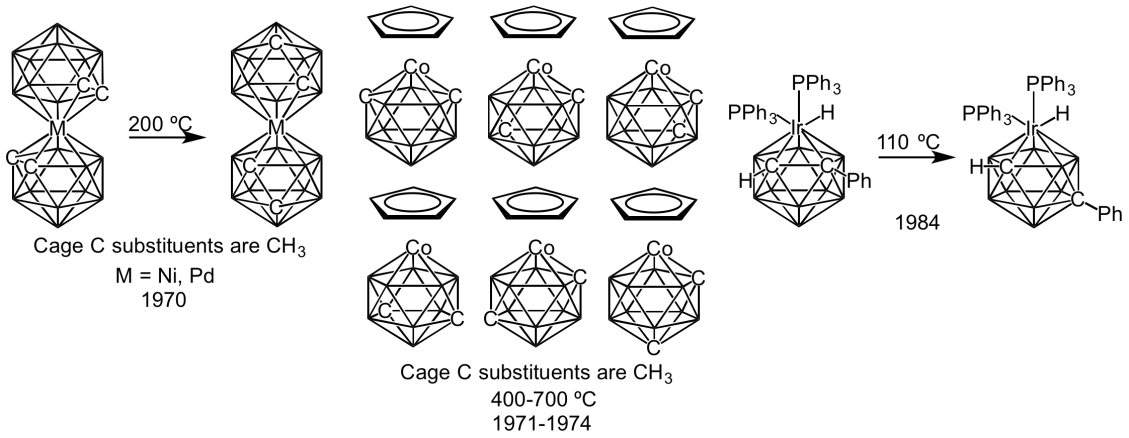

Figure 1.7 Examples of metallacarboranes that thermally isomerise.[25,26,27,28]

This chemistry then became stagnant until the mid 1990s when Welch *et al.* revolutionised the field with reports on isomerisation of sterically crowded metallacarboranes at room temperature.[29] Welch went on to identify a key intermediate in the isomerisation reaction of a molybdenum metallacarborane, which had previously only been identified theoretically (**Scheme 1.7**).[30] Over the course of the next twenty years, more examples of complexes which exhibit low temperature polytopal rearrangement have been reported.[31–34] These low temperature isomerisation complexes give chemists the opportunity to study the mechanism experimentally, which was previously inaccessible due to the high temperatures required.

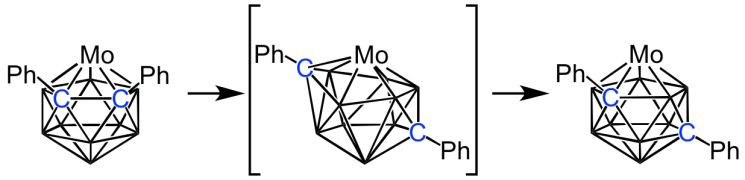

Scheme 1.7 Isolation of an intermediate in the isomerisation reaction of a molybdenum metallacarborane.[30]

1.6 Carbenes, singlet or triplet?

A carbene is a divalent carbon centre that has six valence electrons and no formal charge. The carbene can adopt either a linear or bent geometry, which governs the hybridisation of the carbon centre as either sp or sp^2-hybridised (**Figure 1.8**). The former consists of two degenerate non-bonding p-orbitals (p_x and p_y) each containing one unpaired electron. This gives linear carbenes triplet multiplicity. Carbenes which adopt a bent geometry break this degeneracy as a result of the stabilisation of the p_x orbital as it acquires some s-orbital character, thus is renamed the σ-orbital. The p_y orbital remains essentially unchanged and is referred to as the p_π-orbital. The vast majority of carbenes adopt a bent geometry, therefore their frontier orbitals are assigned σ and p_π-orbitals. Carbenes which possess a bent geometry have the possibility to have either singlet or triplet multiplicity.

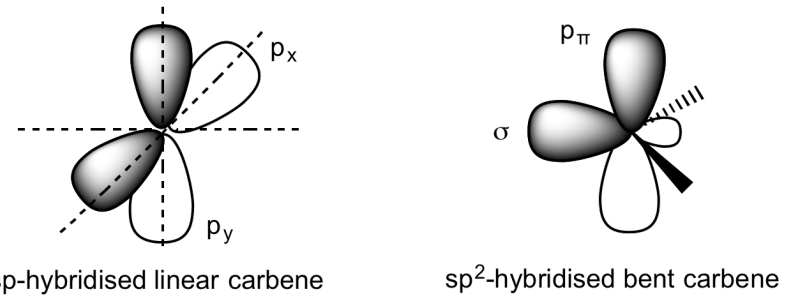

Figure 1.8 Schematic representation of the geometry and hybridisation states of carbenes.

The multiplicity of a bent carbene is dictated by the energy difference between the σ and p_π-orbitals. Hoffman and Gleiter illustrated computationally that the singlet ground state is bound to a large energy separation between the σ and p_π-orbitals, whilst the triplet ground state favours smaller energy separations.[35] The energy separation is influenced significantly by the steric and electronic nature of the α-substituents neighbouring the carbene centre (**Figure 1.9**).[36] For example, bulky α-substituents can be used to obtain carbenes which adopt triplet multiplicity through increasing the carbene bond angle. The carbene bond angle approaches linearity to minimise steric repulsion between the two α-substituents, whilst also stabilising the triplet state as the σ and p_π-orbitals approach degeneracy. Carbenes, which possess triplet multiplicity, are known for their high reactivity and are commonly termed 'di-radicals'.

The electronic influence of the α-substituents consist of a combination of both inductive and mesomeric effects, though the later dominates. The mesomeric effect describes the movement of π-electrons within a conjugated system, and π-donating groups such as F, Cl, NR_2, PR_2 and OR can donate electron density into the p_π-orbital. This increases the p_π-orbital energy, which leads to a larger σ and p_π-orbital separation favouring a carbene with singlet multiplicity and a bent geometry.

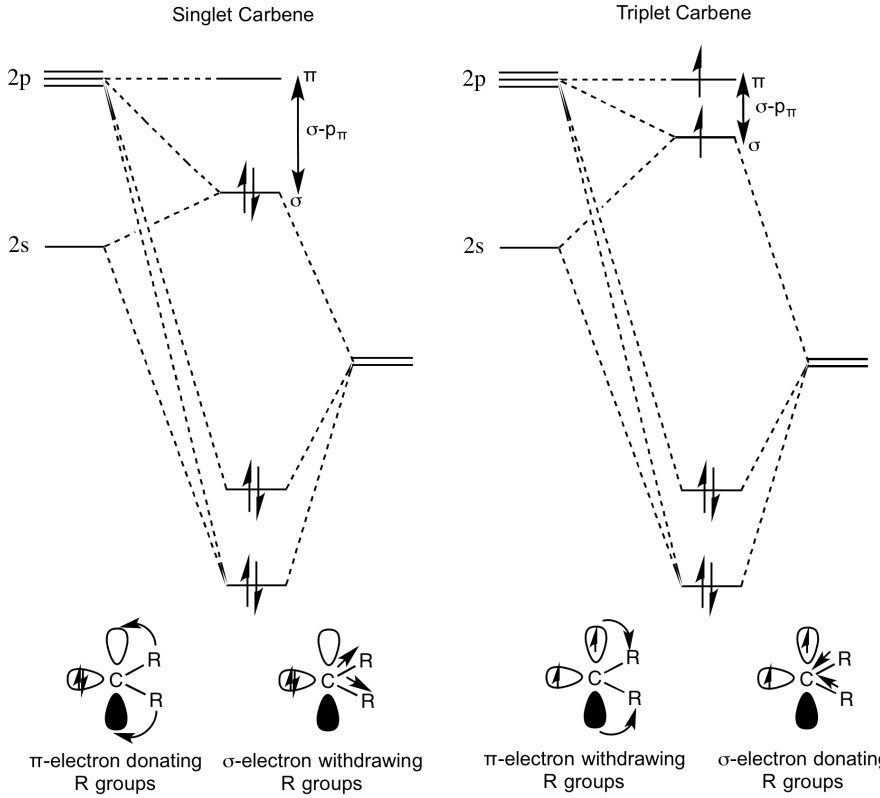

Figure 1.9 Orbital energy diagrams illustrating how the electronic and steric nature of the α-substituents influences the energy separation between the σ and p_π-orbitals.[36]

1.7 N-Heterocyclic Carbenes (NHCs)

NHCs primarily consist of a constrained 5-membered ring with diamino α-substituents. They are often termed persistent carbenes, and their inherent stability arises from mesomeric interactions of both nitrogen lone pairs with the empty p_π-orbital of the carbene. Inductive stability is also provided through the electron withdrawing nature of the diamino α-substituents. These strong interactions lead to carbene centres being sp^2-hybridised with singlet multiplicity, therefore acting as a highly nucleophilic species. As a result they are considered very strong Lewis base donors.

Carbenes were first proposed theoretically in 1958 by Breslow, who was studying the role of a coenzyme thiamine, and suggested that the enzyme is activate upon deprotonation of the thiazolium (**Scheme 1.8**, **A**).[37] In 1962, Wanzlick attempted to isolate a free carbene species (1,3-diphenylimidazolidin-2-ylidene) by thermal elimination of chloroform (**Scheme 1.8**, **B**).[38] However, due to the reactive nature of such species only the dimer was observed. The first example of isolating a crystalline NHC came through the independent research of Arduengo in 1991 (**Scheme 1.8**, **C**).[39] Arduengo utilised an imidazolium salt bearing bulky adamantane groups and deprotonated the salt with a strong base (NaH) to give the persistent carbene.

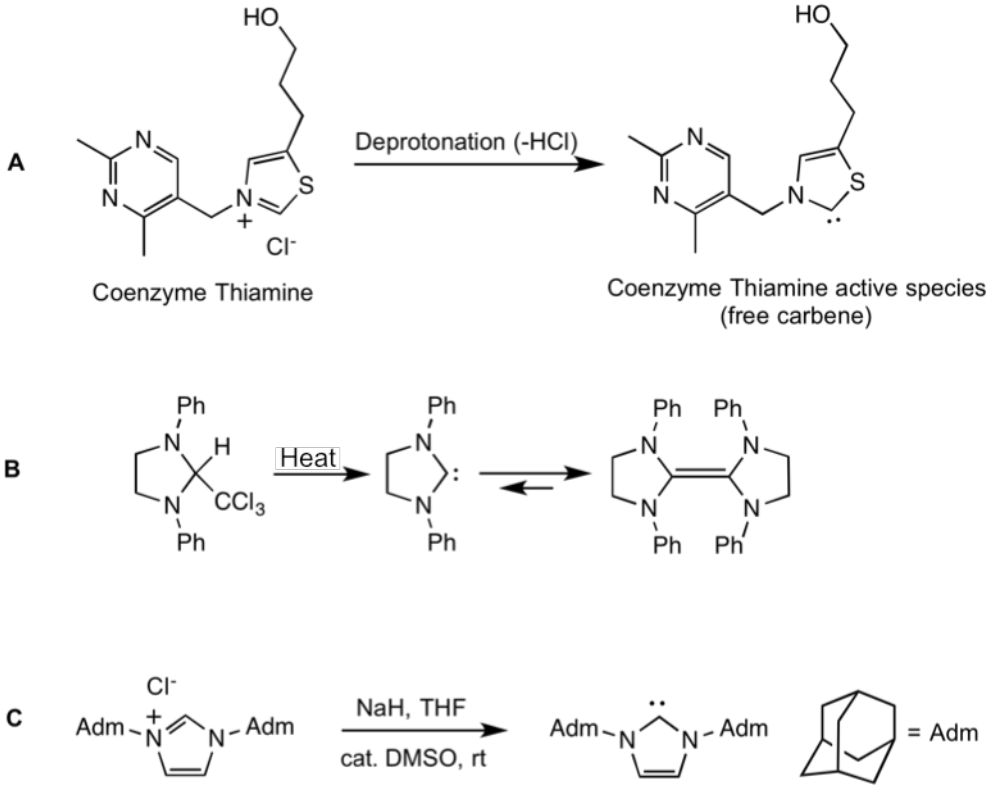

Scheme 1.8 Deprotonation of coenzyme thiamine generating active species (**A**),[37] attempted synthesis of 1,3-diphenylimidazolidin-2-ylidene (**B**),[38] and preparation of the first crystalline NHC (**C**).[39]

1.8 Synthesis of imidazolium salts

The isolation of the first stable NHC by Arduengo gave rise to a new class of ligand precursor, imidazolium salts. One of the most popular synthetic routes to symmetrical imidazolium salts involves the condensation of glyoxal with a substituted amine (2 eq) and paraformaldehyde in the presence of hydrochloric acid. This is a modification to the Debus-Radziszewski reaction and was patented by Arduengo in 1991 (**Scheme 1.9**, **A**).[40] Although this reaction is relatively facile the workup can often be tedious due to the number of by-products, and for the sterically bulky IPr.HCl this reaction is ineffective. In this case, Arduengo and co-workers found that starting from a diimine and reacting with chloromethyl-ethyl ether gave IPr.HCl in respectable yields (**Scheme 1.9**, **B**).[41] These synthetic routes remain the most commonly employed methods for forming symmetrical imidazolium salts to date. When asymmetrical salts are required a two-step synthesis can be employed involving reaction of a substituted imidazole with an appropriate electrophile, usually an alkyl halide (**Scheme 1.9**, **C**).

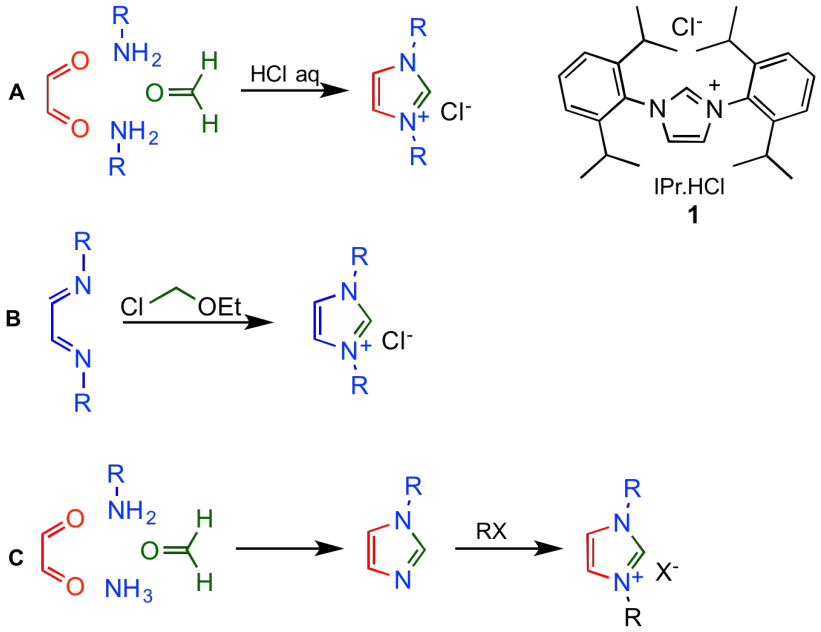

Scheme 1.9 Synthetic routes to imidazolium salts.[42]

1.9 N-heterocyclic carbene (NHC) complex synthesis

1.9.1 Transmetallation from silver[I]

Without question, transmetallation from Ag^{I} is one of the most widely adopted methods for forming transition metal-NHC complexes. The low bond strength of the Ag-$C_{carbene}$ bond coupled with the precipitation of a silver halide, which possesses a high lattice enthalpy, gives rise to a strong driving force for the transmetallation reaction to occur. The first reported Ag^{I}-NHC complex was reported by Arduengo and co-workers in 1993.[43] Yet the use of Ag^{I}-NHCs as carbene transfer agents was not realised until 1998 when Lin and co-workers isolated Au^{I} and Pd^{II} complexes by reacting the corresponding Ag^{I}-NHC complex with $Au(SMe)_2Cl$ and $Pd(MeCN)_2Cl_2$ respectively (**Scheme 1.10**).[44]

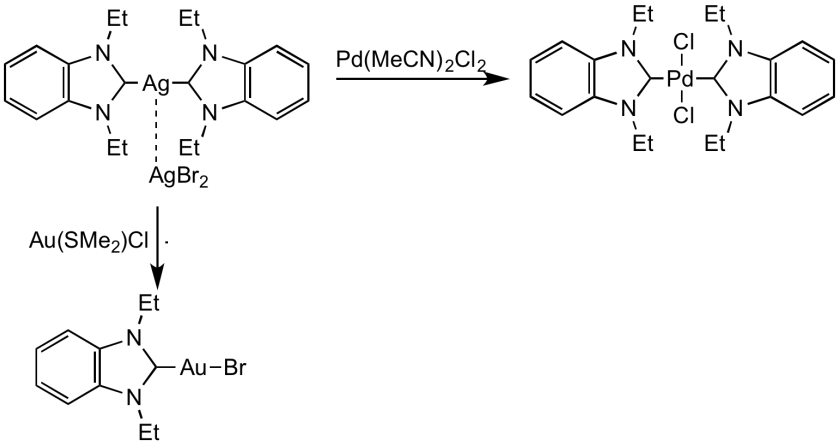

Scheme 1.10 Synthesis of Au^{I}- and Pd^{II}-NHC complexes *via* Ag^{I} transmetallation.[44]

It is noteworthy that transmetallation from other transition metals has been reported and these include Cu^{I} [45,46] and Ni^{II} [47] with the same general concept that the resulting complex forms a stronger metal-$C_{carbene}$ bond.

1.9.2 Formation of a free NHC and subsequent metallation

Generation of the free NHC generally requires the use of a strong base, with Arduengo's synthesis being the principle synthetic strategy employed. The free carbene is subsequently reacted with a metal salt (**Scheme 1.11**, **A**), or used to replace a labile phosphine as reported by Nolan and co-workers (**Scheme 1.11**, **B**).[48,49] The choice of base can lead to variations in the reaction products or undesired activation of the ligand.[50]

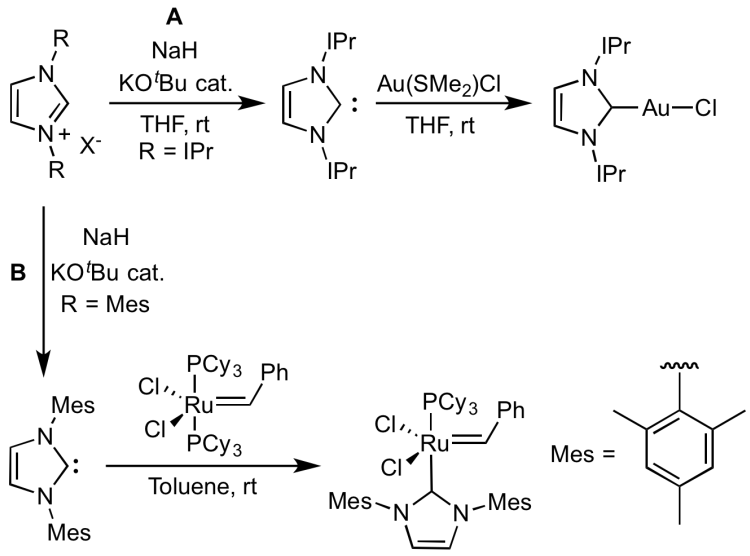

Scheme 1.11 Synthesis of a Au^{I}-NHC complex (**A**) and a Ru-NHC complex (Grubbs, 2nd generation catalyst) *via* the free carbene (**B**).[48,49]

1.9.3 *In situ* deprotonation and metallation

A related method to the formation of a free NHC is the *in situ* deprotonation of the imidazolium salt and metallation. This method does not require such a strong base with NaOAc,[51–53] and K_2CO_3[54] amongst the most popular bases employed. As an example, Richeter *et al.* utilised an imidazolium based porphyrin with K_2CO_3 and $[Rh(COD)Cl]_2$ in toluene at room temperature to form the corresponding Rh^{I}-NHC complex (**Scheme 1.12**).

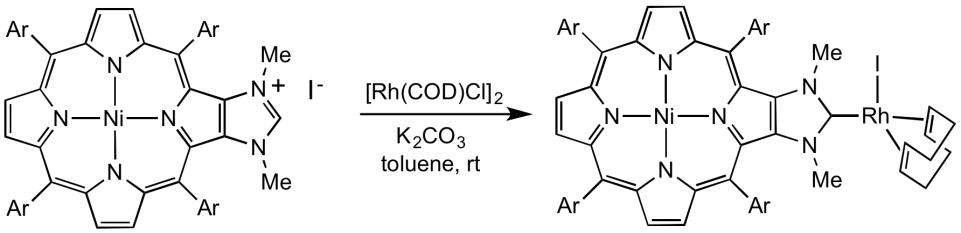

Scheme 1.12 Synthesis of a Rh^{I}-NHC porphyrin complex.[54]

1.9.4 *In situ* metallation with a basic metal precursor

This synthetic method was in fact the first utilised to synthesise a transition metal-NHC complexes with Öfele and Wanzlick both independently reporting the method in 1968.[55,56] Similarly to transmetallation *via* silver, this route takes advantage of the relatively acidic nature of the NC*H*N proton and the reagents utilised tend to be acetates,[57] oxides,[58] alkoxides[59] or amides (**Scheme 1.13**).[60]

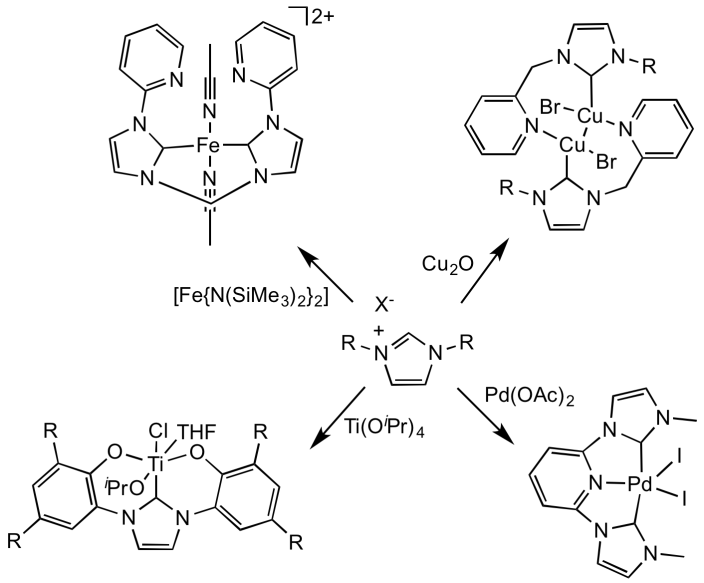

Scheme 1.13 Examples of transition metal complexes synthesised from basic metal precursors.[57–60]

1.9.5 Electrochemical method

The first example of an electrochemical synthesis to preparing metal-NHCs was reported by Chen and co-workers in 2011.[61] During the electrochemical reaction, an imidazolium ion is reduced at the cathode, releasing H_2 forming the free NHC. This is accompanied by the oxidation of the anode generating M^+ ions in solution. These two species then combine to produce a metal-NHC complex (**Scheme 1.14**, **A**). The Willans group reported a valuable extension to this work by preparing both neutral and cationic Cu^I-NHC complexes selectively (**Scheme 1.14**, **B**).[62] The major advantage of this synthetic route is basic conditions are not necessary, with base-sensitive substituents being compatible, thus significantly widening the range of metal-NHC complexes that may be developed. The diversity of this synthetic method was later demonstrated with the preparation of a range of metal-salen/salan complexes (**Scheme 1.14**, **C**).[63] Willans and co-workers then translated this batch process into flow, with the development a highly efficient electrochemical flow-cell capable of generating Cu^I-NHC complexes under neutral and ambient conditions.[64]

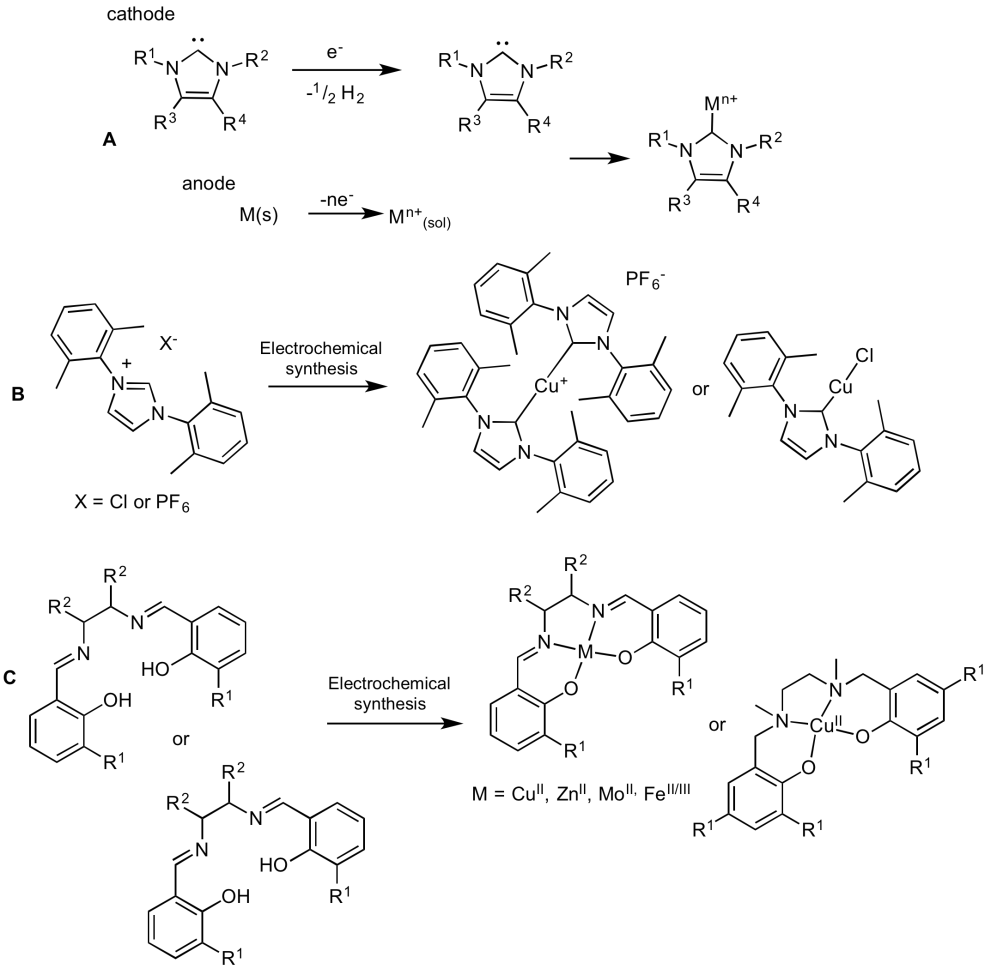

Scheme 1.14 Electrochemical synthesis of metal-NHC complexes (**A**), an example of Cu-NHC complexes (**B**) and metal-salen/salan complexes (**C**) prepared by Willans and co-workers using the electrochemical method.[62–64]

1.10 Fusion of NHCs and carboranes

Although both NHCs and carboranes are two very well established fields, the idea of fusing the two to create a brand new ligand class has only very recently been developed. In parallel to our work, Lavallo and co-workers reported an anionic imidazolium salt bearing two carba-*closo*-dodecaborate *N*-substituents (**12**), which was prepared by reacting the corresponding diimine (**11**) with paraformaldehyde and HCl (**Scheme 1.15**).[65] Deprotonation of **2** with bases of varying sterics led to isolation of three very different carbene species; employing LDA led to isolation of an abnormal carbene (**13**), the sterically less demanding amide of LiHMDS selectively deprotonates the C2 position (**14**), whilst ^{n}BuLi deprotonates both sites when used in excess to give **15**. In a follow up report Lavallo reported the synthesis of unsymmetrical N-carboranyl NHCs,[66] and went on to publish anionic and zwitterionic Au^{I} complexes (**Figure 1.10**).[67] Future reports look to utilise these $Au^{(I)}$ complexes in catalysis and look into preparing polyhalogenated carboranyl NHCs which posses even larger steric profiles.

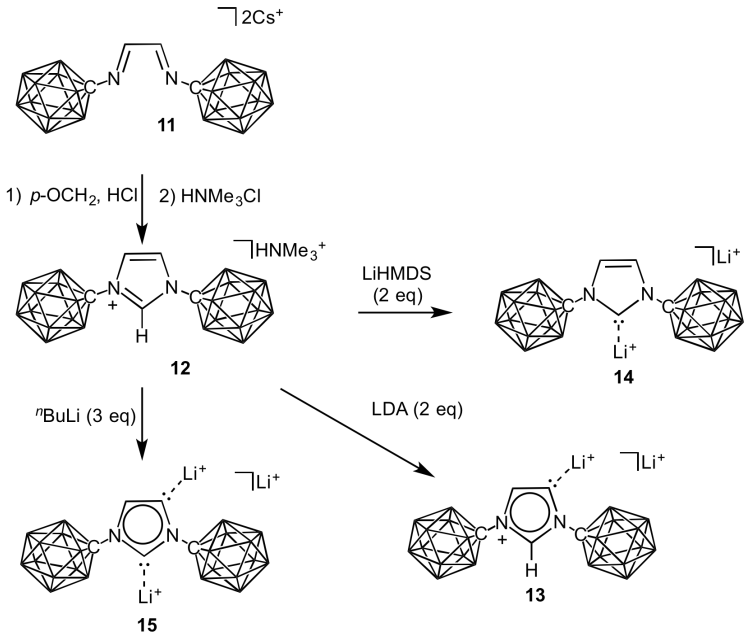

Scheme 1.15 An anionic imidazolium salt bearing two carba-*closo*-dodecaborate *N*-substituents with site specific deprotonation depending on the base used.[65]

Figure 1.10 Au^{I} complexes bearing N-carboranyl NHCs ligands.[67]

1.11 Preliminary work and project aims

Willans and co-workers reported the reaction of the free carbenes 1,3-dimethylimidazol-2-ylidene (**1**) and 1-methyl,3-ethylimidazol-2-ylidene (**2**) with *ortho*-carborane in a 3:1 ratio to give stable 1:2 carborane-NHC adducts **19** and **20** (**Scheme 1.16**).[68] The nature of the α-substituent of the NHC is crucial to its formation; when the significantly more bulky NHC (**18**) is employed an unusual imidazolium salt with a two-cage anion (**21**) is formed. The unique steric profiles of the 1:2 NHC adducts make them attractive precursors to metallacarboranes. The initial work carried out in this thesis looked at coordinating **20** to an Fe centre. Typically metallacarboranes are prepared by deprotonation of *nido*-carboranes with NaH under anhydrous conditions, and subsequently a metal salt such as $FeCl_2$ is added (Section 1.4).[69] Unfortunately, all attempts at forming a metallacarborane with **20** were unsuccessful, and through deprotonation studies of **20** with NaH it was concluded that the bridging proton of the carborane could not be selectively deprotonated.

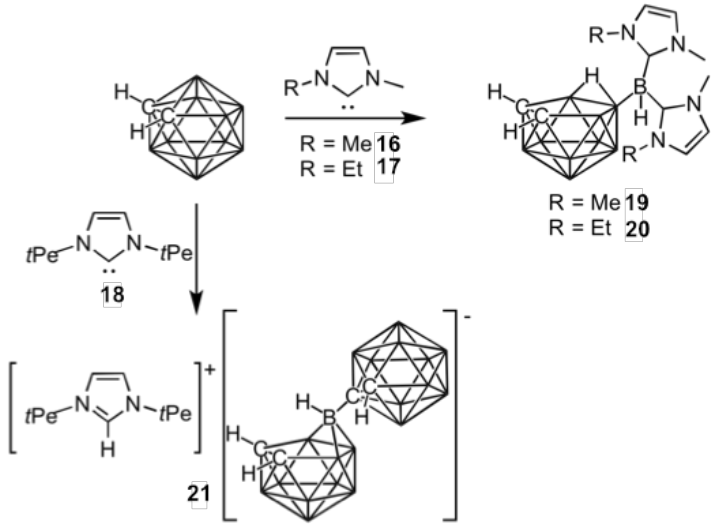

Scheme 1.16 Deprotonation and deboronation of *o*-carborane with NHCs.[68]

This work inspired the design of a brand new ligand class, with the aim of exploring the possibility of fusing NHCs with carboranes through the α-substituent of the NHC and the carboranyl carbon atoms. This would allow the carbenic carbon to be available for metal binding, with the possibility of also coordinating through a carbon or boron atom of the *ortho*-carborane, forming chelating complexes. Removal of a BH vertex should also allow for selective deprotonation of the bridging proton of a *nido*-carborane, allowing us to exploit the different properties of both moieties within one system and enabling the synthesis of mono- and bi-metallic complexes (**Figure 1.11**).

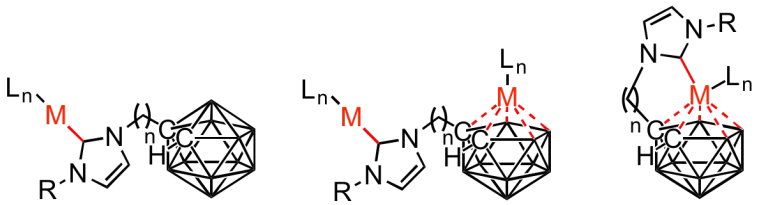

Figure 1.11 Proposed new ligand class.

The Willans group holds strong interests in the synthesis of novel organometallic complexes, and their potential as catalysts and as anticancer agents. These novel systems will be fully characterised by multinuclear NMR spectroscopy, HRMS, micro-analysis and X-ray diffraction analysis. The ultimate goal is to understand the properties of these unique complexes and evaluate their viability as catalysts in the hydrosilyation of ketones and transfer hydrogenation of acetophenone to 1-phenylethanol. In addition, selected complexes will be screened against various cancerous cell lines to evaluate their cytotoxic properties.

1.12 References

1 H. C. Longuet-Higgins and R. P. Bell, *J. Chem. Soc.*, 1943, 250–255.

2 R. N. Grimes, *Carboranes*, Academic Press, 2011.

3 W. N. Lipscomb, *New York*, 1963.

4 K. Wade, *J. Chem. Soc. D Chem. Commun.*, 1971, 792.

5 R. Schaeffer, *J. Am. Chem. Soc.*, 1957, **79**, 1006–1007.

6 T. L. Heying, J. W. Ager, S. L. Clark, R. P. Alexander, S. Papetti, J. A. Reid and S. I. Trotz, *Inorg. Chem.*, 1963, **2**, 1097–1105.

7 H. Beall, *Inorg. Chem.*, 1972, **11**, 637–638.

8 D. Grafstein, J. Bobinski, J. Dvorak, H. Smith, N. Schwartz, M. S. Cohen and M. M. Fein, *Inorg. Chem.*, 1963, **2**, 1120–1125.

9 C. R. Kutal, D. A. Owen, L. J. Todd, R. C. Stafford and N. R. Fetter, *Inorg. Synth.*, 1968, **11**, 19–24.

10 W. E. Hill, F. A. Johnson and R. W. Novak, *Inorg. Chem.*, 1975, **14**, 1244–1249.

11 B. L. Korsunskii, V. N. Kalinin, G. V. Sitonina, F. I. Dubovitskii and L. Zakharicin, *Bull. Acad. Sci. U. S. S. R. Chem. Div.*, 1971, 1712–1713.

12 U. Kusari, Y. Li, M. G. Bradley and L. G. Sneddon, *J. Am. Chem. Soc.*, 2004, **126**, 8662–8663.

13 A. Toppino, A. R. Genady, M. E. El-Zaria, J. Reeve, F. Mostofian, J. Kent and J. F. Valliant, *Inorg. Chem.*, 2013, **52**, 8743–8749.

14 M. E. El-Zaria, K. Keskar, A. R. Genady, J. A. Ioppolo, J. McNulty and J. F. Valliant, *Angew. Chemie Int. Ed.*, 2014, **53**, 5156–5160.

15 R. A. Wiesboeck and M. F. Hawthorne, *J. Am. Chem. Soc.*, 1964, **86**, 1642–1643.

16 M. F. Hawthorne, D. C. Young and P. A. Wegner, *J. Am. Chem. Soc.*, 1965, **87**, 1818–1819.

17 M. F. Hawthorne, *J. Organomet. Chem.*, 1975, **100**, 97–110.

18 M. F. Hawthorne and G. B. Dunks, *Science.*, 1972, **178**, 462–471.

19 M. F. Hawthorne, *Acc. Chem. Res.*, 1968, **1**, 281–288.

20 D. Grafstein and J. Dvorak, *Inorg. Chem.*, 1963, **2**, 1128–1133.

21 S. Papetti and T. L. Heying, *J. Am. Chem. Soc.*, 1964, **86**, 2295–2295.

22 G. M. Edvenson and D. F. Gaines, *Inorg. Chem.*, 1990, **29**, 1210–1216.

23 H. D. Kaesz, R. Bau, H. A. Beall and W. N. Lipscomb, *J. Am. Chem. Soc.*, 1967, **89**, 4218–4220.

24 M. J. S. Dewar and M. L. McKee, *Inorg. Chem.*, 1978, **17**, 1569–1581.

25 L. F. Warren and M. F. Hawthorne, *J. Am. Chem. Soc.*, 1970, **92**, 1157–1173.

26 M. F. Hawthorne, M. K. Kaloustian and R. J. Wiersemay, *J. Am. Chem. Soc.*, 1971, **93**, 4912–4913.

27 D. F. Dustin, W. J. Evans, C. J. Jones, R. J. Wiersema, H. Gong, S. Chan and M. F. Hawthorne, *J. Am. Chem. Soc.*, 1974, **96**, 3085–3090.

28 J. A. Doi, E. A. Mizusawa, C. B. Knobler and M. F. Hawthorne, *Inorg. Chem.*, 1984, **23**, 1482–1484.

29 G. O. Kyd, L. J. Yellowlees, A. J. Welch, M. U. Pilotti, F. G. A. Stone, L. J. Yellowlees, A. J. Welch, T. R. Spalding and D. O'Connell, *J. Chem. Soc. Dalt. Trans.*, 1994, **12**, 3129.

30 D. J. Wales, *J. Am. Chem. Soc.*, 1993, **115**, 1557–1567.

31 O. Tutusaus, C. Viñas, R. Kivekäs, R. Sillanpää, F. Teixidor, R. Sillanpää, R. Kivekäs and B. Stibr, *Chem. Commun.*, 2003, **62**, 2458–2459.

32 M. M. Vinogradov, M. V. Zakharova, S. V. Timofeev, D. A. Loginov, I. B. Sivaev, Y. V. Nelyubina, Z. A. Starikova, V. I. Bregadze and A. R. Kudinov, *Inorg. Chem. Commun.*, 2015, **51**, 80–82.

33 A. V. Safronov, F. M. Dolgushin, P. V. Petrovskii and I. T. Chizhevsky, *Organometallics*, 2005, **24**, 2964–2970.

34 M. M. Vinogradov, Y. V. Nelyubina, A. A. Pavlov, V. V. Novikov, N. V. Shvydkiy and A. R. Kudinov, *Organometallics*, 2017, **36**, 791–800.

35 R. Gleiter and R. Hoffmann, *J. Am. Chem. Soc.*, 1968, **90**, 5457–5460.

36 J. F. Harrison, *J. Am. Chem. Soc.*, 1971, **93**, 4112–4119.

37 R. Breslow, *J. Am. Chem. Soc.*, 1958, **80**, 3719–3726.

38 H. W. Wanzlick, *Angew. Chemie Int. Ed.*, 1962, **1**, 75–80.

39 A. J. Arduengo, R. L. Harlow and M. Kline, *J. Am. Chem. Soc.*, 1991, **113**, 361–363.

40 A. J. Arduengo, *US Pat. 5077414*, 1990.

41 A. J. Arduengo, R. Krafczyk, R. Schmutzler, H. A. Craig, J. R. Goerlich, W. J. Marshall and M. Unverzagt, *Tetrahedron*, 1999, **55**, 14523–14534.

42 L. Hintermann, *Beilstein J. Org. Chem.*, 2007, **3**, 22.

43 A. J. Arduengo, H. V. R. Dias, J. C. Calabrese and F. Davidson, *Organometallics*, 1993, **12**, 3405–3409.

44 H. M. J. W. And and I. J. B. Lin, *Organometallics*, 1998, **17**, 972–975.

45 M. R. L. Furst and C. S. J. Cazin, *Chem. Commun.*, 2010, **46**, 6924.

46 X. Liu, R. Pattacini, P. Deglmann and P. Braunstein, *Organometallics*, 2011, **30**, 3302–3310.

47 B. Liu, X. Liu, C. Chen, C. Chen and W. Chen, *Organometallics*, 2012, **31**, 282–288.

48 P. Frémont, N. M. Scott, and E. D. Stevens and S. P. Nolan, *Organometallics*, 2005, **24**, 2411–2418.

49 X. Bantreil and S. P. Nolan, *Nat. Protoc.*, 2011, **6**, 69–77.

50 R. Fränkel, C. Birg, U. Kernbach, T. Habereder, H. Nöth and W. P. Fehlhammer, *Angew. Chemie Int. Ed.*, 2001, **40**, 1907–1910.

51 F. Aznarez, P. J. Sanz Miguel, T. T. Y. Tan and F. E. Hahn, *Organometallics*, 2016, **35**, 410–419.

52 F. Aznarez, M. Iglesias, A. Hepp, B. Veit, P. J. Sanz Miguel, L. A. Oro, G.-X. Jin and F. E. Hahn, *Eur. J. Inorg. Chem.*, 2016, **2016**, 4598–4603.

53 W. B. Cross, C. G. Daly, Y. Boutadla, K. Singh, M. Albrecht, G. W. Brudvig and R. H. Crabtree, *Dalt. Trans.*, 2011, **40**, 9722.

54 J.-F. Lefebvre, M. Lo, D. Leclercq and S. Richeter, *Chem. Commun.*, 2011, **47**, 2976.

55 K. Öfele, *1,3-Dimethyl-4-imidazolinyliden-(2)-pentacarbonylchrom ein neuer übergangsmetall-carben-komplex*, 1968, vol. 12.

56 H.-W. Wanzlick and H.-J. Schönherr, *Angew. Chemie Int. Ed.*, 1968, **7**, 141–142.

57 E. Peris, J. Mata, J. A. Loch and R. H. Crabtree, *Chem. Commun.*, 2001, **81**, 201–202.

58 A. A. D. Tulloch, A. A. Danopoulos, S. Kleinhenz, M. E. Light, and M. B. Hursthouse and G. Eastham, *Organometallics*, 2001, **20**, 2027–2031.

59 C. Romain, L. Brelot, S. Bellemin-Laponnaz and S. Dagorne, *Organometallics*, 2010, **29**, 1191–1198.

60 A. Raba, M. Cokoja, S. Ewald, K. Riener, E. Herdtweck, A. Pöthig, W. A. Herrmann and F. E. Kühn, *Organometallics*, 2012, **31**, 2793–2800.

61 B. Liu, Y. Zhang, D. Xu, W. Chen, W. S. Hwang, I. J. B. Lin and Y. Zhang, *Chem. Commun.*, 2011, **47**, 2883.

62 B. R. M. Lake, E. K. Bullough, T. J. Williams, A. C. Whitwood, M. A. Little, C. E. Willans, A. H. White, C. C. Williams, D. Boyer, R. Mahiou and A. Gautier, *Chem. Commun.*, 2012, **48**, 4887.

63 M. R. Chapman, S. E. Henkelis, N. Kapur, B. N. Nguyen and C. E. Willans, *ChemistryOpen*, 2016, **5**, 351–356.

64 M. R. Chapman, Y. M. Shafi, N. Kapur, B. N. Nguyen, C. E. Willans and C. E. Willans, *Chem. Commun.*, 2015, **51**, 1282–1284.

65 A. El-Hellani and V. Lavallo, *Angew. Chemie Int. Ed.*, 2014, **53**, 4489–93.

66 M. J. Asay, S. P. Fisher, S. E. Lee, F. S. Tham, D. Borchardt, V. Lavallo, J. A. K. Howard, A. Mackinnon, R. J. Peace and K. Wade, *Chem. Commun.*, 2015, **51**, 5359–5362.

67 S. P. Fisher, A. El-Hellani, F. S. Tham, V. Lavallo, S. Mallet-Ladeira, G. Bouhadir, J. C. Slootweg, W. Uhl and D. Bourissou, *Dalt. Trans.*, 2016, **45**, 9762–9765.

68 C. E. Willans, C. A. Kilner and M. A. Fox, *Chem. - A Eur. J.*, 2010, **16**, 10644–10648.

69 H. C. Kang, S. S. Lee, C. B. Knobler and M. F. Hawthorne, *Inorg. Chem.*, 1991, **30**, 2024–2031.

Chapter 2

Dicarba-dodecaboranes bearing imidazolium tethers

*This chapter discusses the synthetic strategies explored towards a new hybrid ligand scaffold that fuses N-heterocyclic carbenes and dicarba-dodecaborane, also known as o-*carborane*. A focal point of this work was to demonstrate the tailorability of this novel ligand system. A detailed account of the techniques employed for the characterisation of these novel ligands is given.*

2.1 New hybrid ligand scaffold

2.1.1 Ligand synthesis

A variety of routes are known for the preparation of imidazolium salts, including nucleophilic substitution of an *N*-substituted imidazole with an alkyl halide. Haloalkyl-substituted *o*-carboranyl compounds can be synthesised *via* a two step procedure that is used to prepare C-substituted carboranes. Treatment of decaborane (**1**) with MeCN yields the considerably more stable Lewis base (**2**), which is subsequently reacted with the corresponding commercially available alkyne to give **P1.1** in high yield (70 %) (**Scheme 2.1**). In practice, the Lewis base adducts are usually not isolated. However, decaborane slowly forms polymeric materials overtime, so it is therefore more cost effective to store decaborane as one of its Lewis base adducts if the compound is going to be stored for a prolonged period of time.

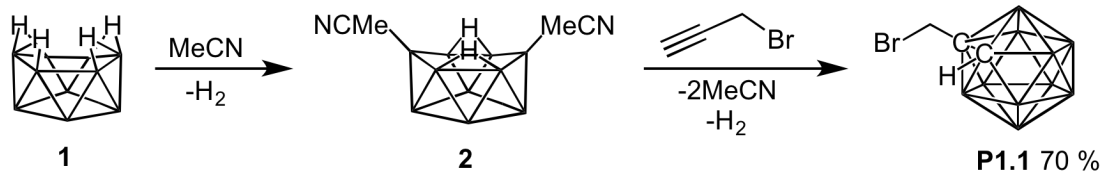

Scheme 2.1 Preparation of C-substituted *o*-carborane precursor **P1.1**.

^{t}Bu-imidazole (**I1**), which is prepared from a modification to the Debus-Radziszewski[1,2] synthesis for imidazole, is reacted with **P1.1** in a 1:1 ratio under hydrous conditions, and induces deboronation to give the zwitterionic ligand precursor **L1.2** in excellent yield (82 %) (**Scheme 2.2**). Theoretical calculations[3–5] and isolation of key intermediates experimentally (**Adduct I**[6,7] and **Adduct II**[8]) have allowed a widely accepted mechanism for deboronation of *o*-carborane to be proposed (**Scheme 2.3**). Deboronation by alkoxides,[9,10] amines[11] and fluorides[12–15] is well documented and typically a carborane/base ratio of 1:2 is required for complete deboronation.

The unusual course of reacting **I1** with **P1.1** is due to the introduction of a strongly electron withdrawing substituent (*i.e.* an imidazolium) into the cage. This increases the susceptibility of the most electropositive boron atoms to nucleophilic attack by **I1**, and based on the accepted mechanism for deboronation, affords **Adduct I'** (**Scheme 2.4**). This then reacts with another molecule of **I1** forming **Adduct II'**, which results in deboronation and then protonation to afford **L1.2** and regenerate the nucleophile.

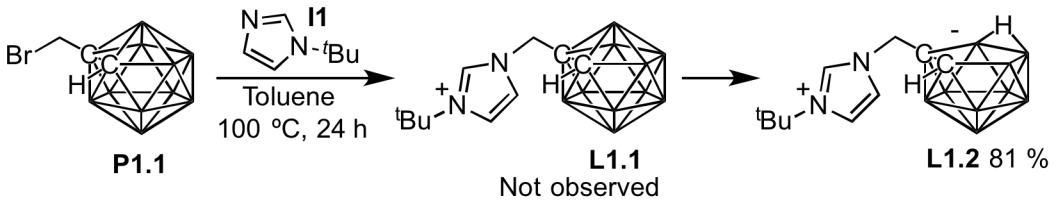

Scheme 2.2 Preparation of a zwitterionic ligand **L1.2**.

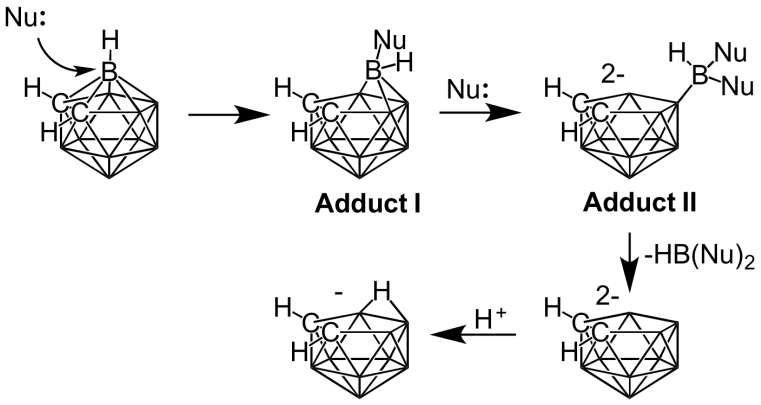

Scheme 2.3 General mechanism for deboronation of *o*-carborane.[8]

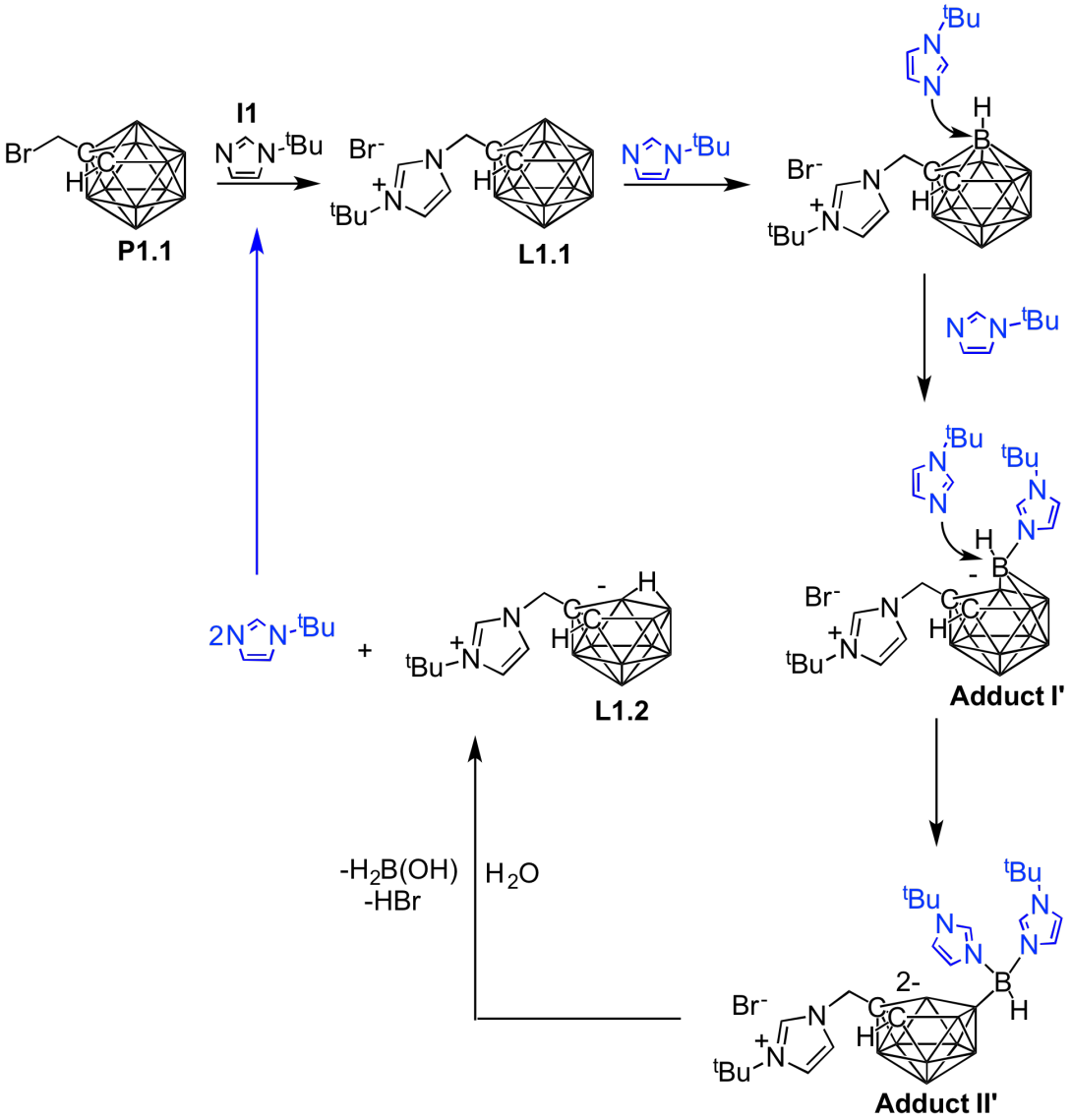

Scheme 2.4 Proposed deboronation mechanism of **L1.1** leading to formation of **L1.2**.

From the mechanism proposed; if two molecules of **I1** are required for deboronation of **L1.1**, it is surprising that **L1.2** is obtained in such high yields when a 1:1 ratio of **P1.1**:**I1** is used, as **I1** is consumed during the reaction on formation of **L1.1**. This suggests that the rate of deboronation is faster than nucleophilic substitution or that deboronation is facilitated by H_2O, for which there is literature precedent when the α-substituent of the cage is strongly electron withdrawing.[16–18] However, when repeating the reaction under strict anhydrous conditions the zwitterionic product is still isolated. There is literature precedent for deboronation of *o*-carborane promoted by a fluoride anion, but to the best of our knowledge there is no evidence of this occurring *via* the softer bromide nucleophile. To investigate the bromide anion as a possible promoter of deboronation an alternative synthetic strategy was employed. To eradicate the use of the basic imidazole in the formation of **L1.1**, the alkyne substituted imidazolium salt **P1.2** was prepared from literature procedure,[19] and subsequently reacted with $B_{10}H_{12}(MeCN)_2$ under anhydrous conditions (**Scheme 2.5**).

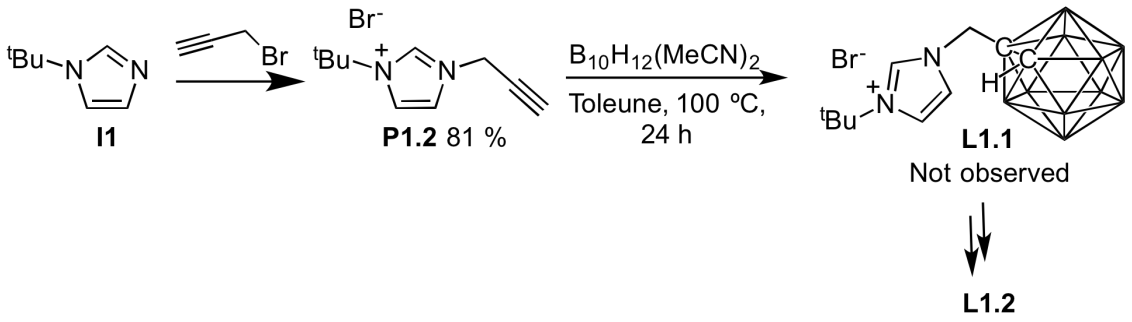

Scheme 2.5 Attempted synthesis of **L1.1**.

Analysis of the crude product indicated **L1.1** was not present and only the deboronated product **L1.2** was observed suggesting that the bromide counterion partakes in deboronation, and illustrates the instability of the cage in the presence of a bromide anion.

As a means to increase the stability of the cage in **L1.1** towards deboronation, the length of the alkyl linker was increased. As mentioned previously, one of the longstanding problems in carborane synthesis is the dramatic drop in yield when reacting longer chain alkynes with $B_{10}H_{12}(MeCN)_2$ (Chapter 1, Section 1.3.1). As a consequence, 1-bromoethyl-*o*-carborane (**P2.2**) was prepared in 35 % yield using this method. In order to form the desired product in higher yields *via* this synthetic route, the Lewis basicity of the alkyne needs to be low enough for hydroboration to be unfavourable. Valliant *et al*. reported that adding a catalytic amount of $AgNO_3$ (0.02 mmol) to the reaction significantly increases the yield, and it was proposed that the silver coordinates to the alkyne lowering both its Lewis basicity and the activation energy to formation of the desired product.[20] However, in this report these reactions were conducted on a very small scale ($B_{10}H_{12}(MeCN)_2$ = 0.27 mmol), and it was found in our laboratory that these reactions are scale sensitive with no improvement on yield observed when 4.9 mmol of $B_{10}H_{12}(MeCN)_2$ was employed.

An alternative synthetic approach to **P2.2**, which was obtained in high yields, has recently been reported by Oldfield and co-workers (**Scheme 2.6**).[21] The synthesis requires the use of ^{n}BuLi to deprotonate the acidic carboranyl proton in *o*-carborane, followed by the addition of ethylene oxide to form hydroxyethyl-*o*-carborane (**P2.1**). This can be converted to the alkyl bromide **P2.2** by reacting with triphenyl phosphine and *N*-bromosuccinimide (NBS) in anhydrous DCM, at 0 °C for 3 hours. Reaction of **P2.2** with ^{t}Bu-imidazole in a 1:1 ratio gives the *closo*-carboranyl imidazolium bromide salt **L2.1** in high yield (71 %), whereas an excess of imidazole gives the zwitterionic ligand precursor **L2.2** in good yield (65 %).

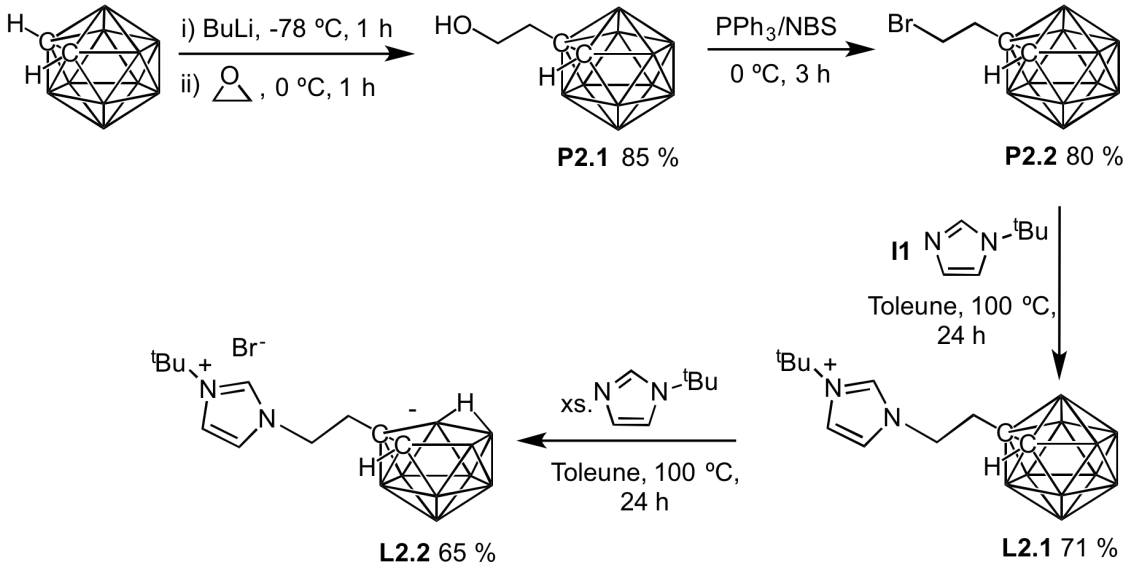

Scheme **2.6** Preparation of C-substituted *o*-carborane compounds **L2.1** and **L2.2**.[21]

2.2 Characterisation of ligand precursors

Successful formation of the *closo*-carboranyl imidazolium bromide salt **L2.1** and zwitterionic ligand precursors **L1.2** and **L2.2** was confirmed using ^{1}H, ^{11}B, and ^{13}C NMR spectroscopy, HRMS, micro-analysis and X-ray diffraction analysis.

2.2.1 ^{1}H and $^{13}C\{^{1}H\}$ NMR spectroscopy

Comparison of the multinuclear NMR spectroscopic analysis of **L2.1** and **L2.2** shows the diagnostic differences between *closo*- and *nido*-carboranyl compounds. The ^{1}H NMR spectrum of **L2.1** exhibits a broad resonance in the baseline between 3 and 0 ppm arising from the BH protons of the cage (**Figure 2.1**, **B**). This B-H region appears less resolved in comparison to the spectrum of *o*-carborane, which possess more defined peaks (**Figure 2.1**, **A**). The broadening of these peaks is a result of the protons being bound to a nucleus with a high quadrupole moment.

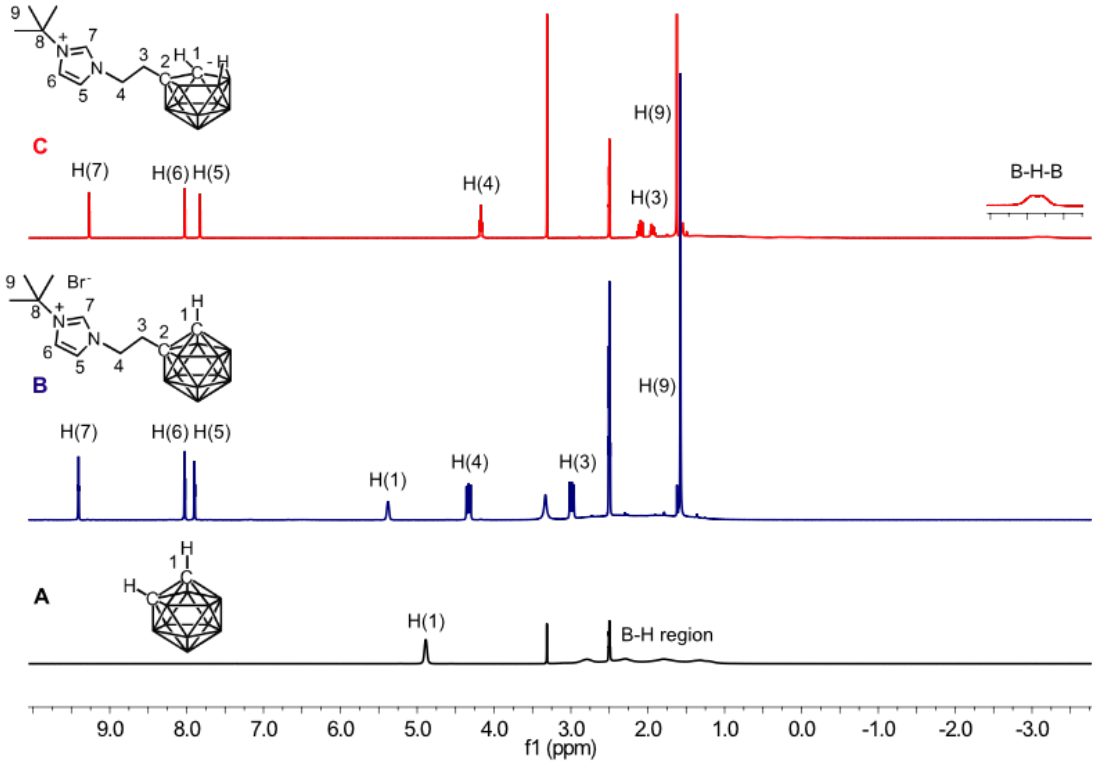

Figure 2.1 ^{1}H NMR spectra (500 MHz, DMSO-d_6) of *o*-carborane (**A**) ligand precursors **L2.1** (**B**) and **L2.2** (**C**). *Residual H_2O resonance at 3.33 ppm*.

The most notable difference between the two carborane species **L2.1** and **L2.2** is the appearance of a broad singlet at -2.98 ppm in the ^{1}H NMR spectrum of **L2.2**, which corresponds to the bridging proton of the open face of the carborane cage. The cage CH proton in *closo*-carboranyl compounds such as **L2.1** appears as a broad singlet due to the electron acceptor effect of the cage and resonates at 5.39 ppm for **L2.1**, whereas this proton is highly shielded in **L2.2**, resonating at 1.83 ppm masked by the ^{t}Bu resonance H(9). A characteristic downfield resonance attributable to the imidazolium proton H(7) at 9.41 ppm for **L2.1** and 8.98 ppm for **L2.2** confirms the formation of imidazolium salts. The imidazolium proton of **L2.1** appears more downfield due to its hydrogen bonding interaction with the bromide counterion. This H-bonding interaction causes the proton to experience a larger deshielding effect, thus resonating at a more downfield position. The ^{13}C{^{1}H} NMR spectra provide further clarification for whether the *closo*-species has been retained or deboronation has occurred. The former shows sharp resonances for each carbon vertex at 72.4 ppm for C1 and 63.1 ppm for C2, respectively (**Figure 2.2**, **bottom**). Removal of either the B3 or B6 vertex results in a high upfield shift of the carbon vertices and appear as very broad signals at 56.2 ppm and 44.7 ppm (**Figure 2.2**, **top**).

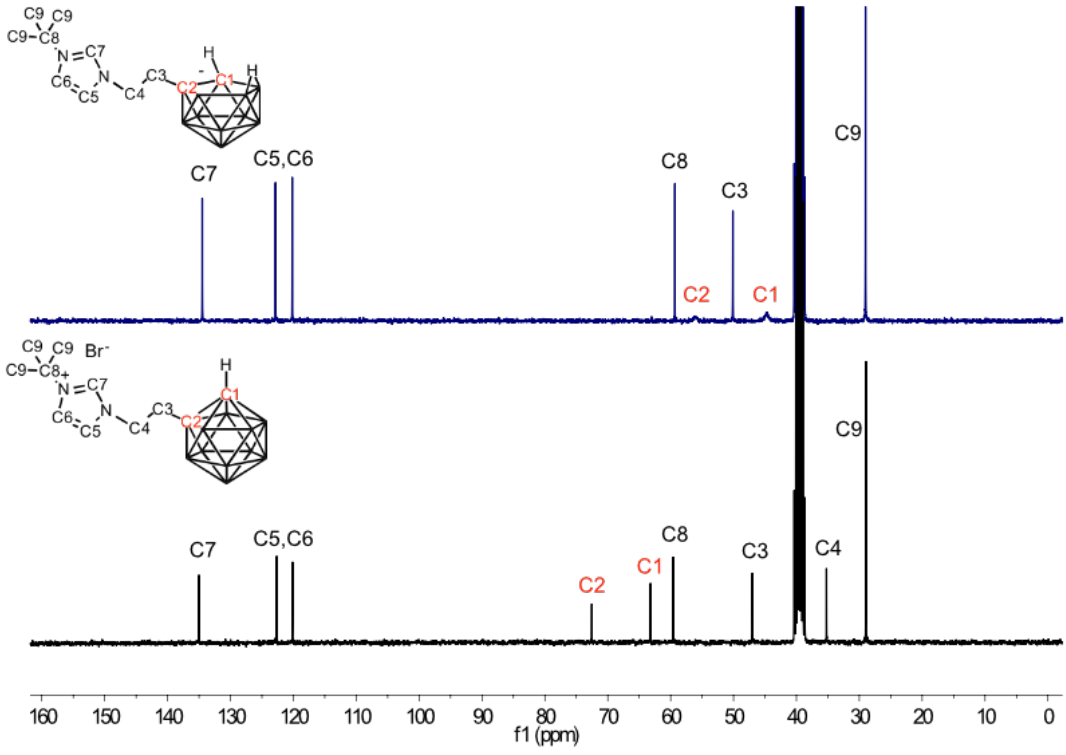

Figure 2.2 ^{13}C{^{1}H} NMR spectra (300 MHz, DMSO-d_6) of ligand precursors **L2.1** (bottom) and **L2.2** (top). *The C4 proton for **L2.2** is masked by the DMSO-d_6 signal and resonates at 38.9 ppm, which was confirmed by the ^{13}C{^{1}H} 135 DEPT spectrum.*

2.2.2 ^{11}B NMR spectroscopy

Boron has two naturally occurring isotopes, ^{10}B and ^{11}B, with relative abundances of 19.6 % and 80.4 % respectively. Both are NMR active, though ^{11}B dominates due to its higher abundance, lower quadrupole moment and higher resonance frequency, resulting in much better resolution compared to ^{10}B. Despite this ^{10}B has been found useful in thermal isomerisation mechanistic studies.[22] An underlying problem with ^{11}B NMR spectroscopy is the broadening of signals due to the large nuclear spin of the ^{11}B nucleus, even at high magnetic field strengths. This usually results in signal overlap as well as loss of coupling information, primarily ^{11}B-^{11}B coupling. ^{1}H coupling adds further complications, with each B-H nucleus possessing quartet multiplicity with relative intensities of 1:1:1:1. Therefore, ^{11}B{^{1}H} NMR experiments are most common in order to provide clearer spectra by reducing the degree of signal overlap.

^{11}B chemical shifts are dominated by paramagnetic shielding.[23] Simple geometric rules have been found to correlate well with known ^{11}B chemical shifts.[24] These rules contain antipodal (AE), butterfly (BE) and neighbour (NE) effects, with the AE effect having greatest influence on the ^{11}B chemical shift and NE having the smallest effect (**Figure 2.3**). The antipodal effect in substituted carboranes was found to be similar to the positive mesomeric effect in substituted benzenes; an increase in electron density (e.d) in the substituted atoms results in an increase in electron density in the *para*- position.[25]

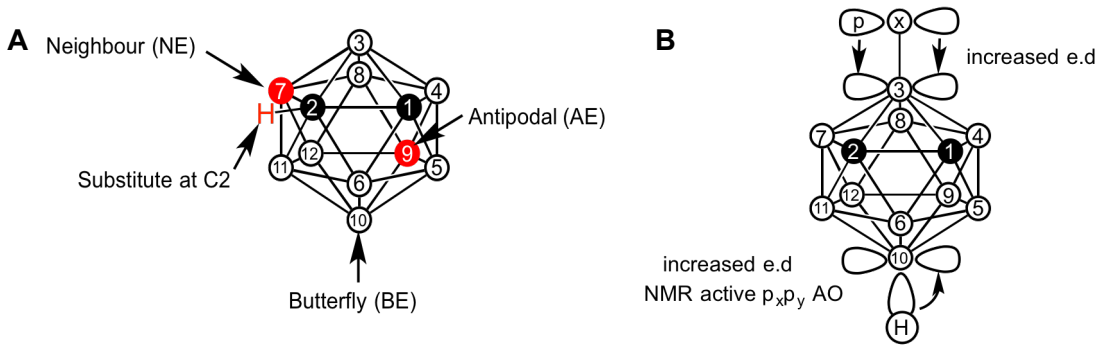

Figure 2.3 A illustrates which vertices of the cage are most effected by a substitution at the C2 vertex. **B** is a representation of the antipodal effect mechanism.

The $^{11}B\{^{1}H\}$ NMR spectra of **L2.1** and **L2.2** were fully elucidated with the aid of similar compounds in the literature, with the $^{11}B\{^{1}H\}$ NMR spectrum of **L2.1** being similar to that of *o*-carborane (**Figure 2.4**). The $^{11}B\{^{1}H\}$ NMR spectrum of *o*-carborane shows four resonances between 3 and -15 ppm, with integral values of 2:2:4:2. One may initially predict that the boron atoms *ortho* to the carbon atoms would appear most downfield if the same rules that govern ^{1}H NMR spectroscopy in most other cases are applied here. As mentioned, different effects dominate in carborane derivatives, with AE>BE>NE. Therefore, the boron atoms antipodal to the carbon atoms B9 and B12 appear most downfield, followed by the boron atoms situated in the butterfly positions B8 and B10. Upon substitution at the carboranyl carbon the antipodal boron atoms are no longer magnetically equivalent, with B9 appearing more downfield. The $^{11}B\{^{1}H\}$ NMR spectrum of **L2.2** is drastically different to that of **L2.1**. A direct result of deboronation is a more electron rich carborane skeleton and an uneven distribution of electron density, with the bulk being situated on the opposing vertex B10. As a result, a large upfield shift of this boron atom is observed. Equally, this gives rise to electropositive boron atoms antipodal to this vertex in the open pentagonal face, namely B4 and B7.

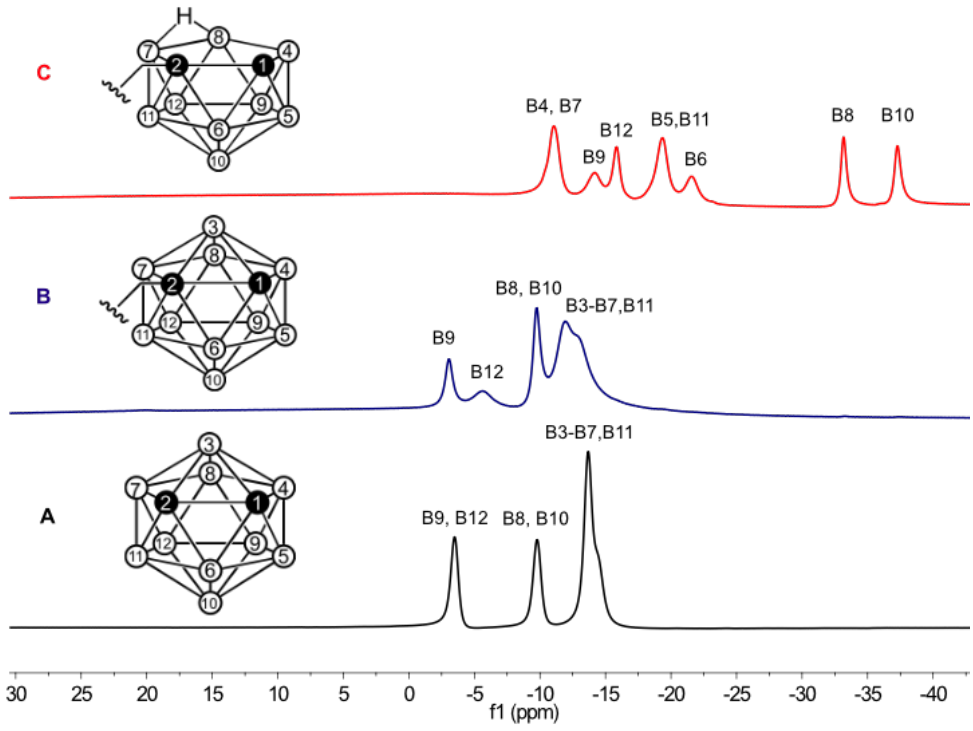

Figure 2.4 $^{11}B\{^{1}H\}$ NMR spectra (161 MHz, DMSO-d_6) of *o*-carborane (**A**), **L2.1** (**B**) and **L2.2** (**C**).

In the early 1970s, Heřmánek reported a regularity in open cage structures: 1) the direct neighbouring boron atom to that of the boron atoms in the open pentagonal face bearing the bridging proton (*i.e.* B9) resonates at the lowest frequency. It was proposed that an electron cloud exists at B9, resulting in the shielding of this vertex. A direct consequence of this is that the B12 vertex resonates at the highest frequency.[26] 2) In carborane derivatives the bridging proton on the open face is able to tautomerise and as a result an average of the signals is observed on the NMR timescale (**Scheme 2.7**).

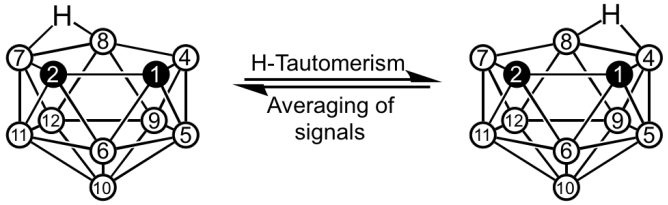

Scheme 2.7 Tautomerism of the bridging proton in *nido*-carborane.[26]

2.2.3 Mass spectrometry

As previously mentioned, boron has two naturally occurring isotopes, ^{10}B and ^{11}B, with relative abundances of 19.6 % and 80.4 % respectively. This gives rise to a distinct isotope pattern for boron rich carboranes, with a polyisotopic mass spectrum of statistically distributed ^{10}B and ^{11}B. *o*-Carborane should display an isotope distribution between *m/z* 136 and 146, with a base peak of *m/z* 144 corresponding to $^{12}C_2{}^{1}H_{12}{}^{10}B_2{}^{11}B_8$. However, the spectrum produced from the electron spray (ESI) technique in the positive ion mode does not show a peak corresponding to the parent cage. When using a very concentrated sample a molecular ion peak can be observed in the negative ion mode for $[M - H]^-$. The requirement of a concentrated sample is possibly due to the high degree of proton abstraction which destabilises the cage resulting in a low abundance of the molecular ion by the time it reaches the detector. When a charged imidazolium group is introduced into the cage the molecular ion is detectable in the positive ion mode, allowing the ligands to be characterised using mass spectrometry. Example spectra of a *closo*-imidazolium **L2.1** and a *nido*-zwitterion **L2.2** are exhibited in **Figure 2.5**.

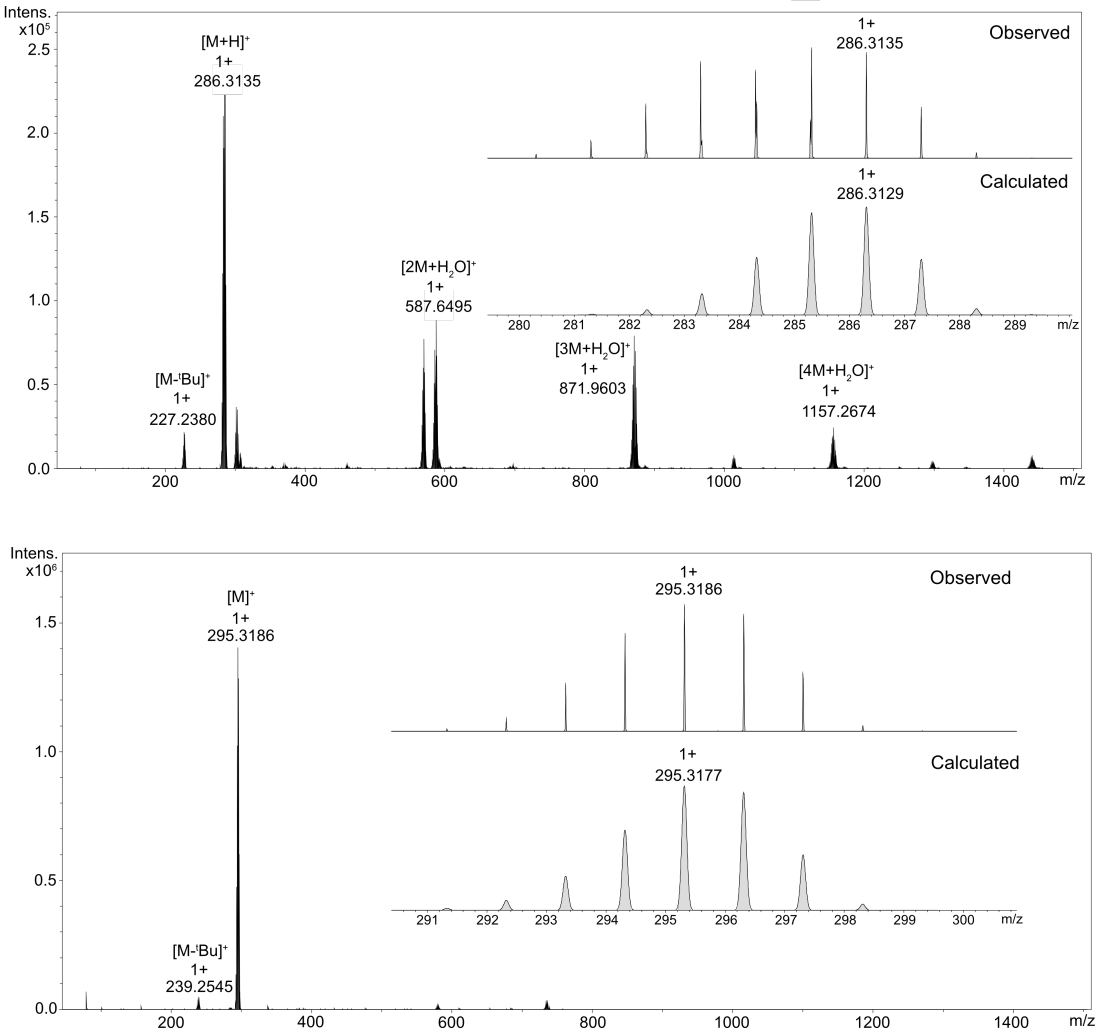

Figure 2.5 HRMS (ESI^+) of **L2.1** (bottom) and **L2.2** (top). The insets of each spectrum compares the observed molecular ion peaks $[M+H]^+$for **L2.1** and $[M]^+$ for **L2.2** against their calculated molecular masses.

2.2.4 Infrared spectroscopy

When comparing the infrared (I.R.) spectra of the three isomers of *ortho*, *meta* and *para*-carborane, one would expect the spectra to become more complex on going from the highest symmetry *para* isomer, belonging to the D_{5d} point group, to the less symmetrical *ortho* and *meta* isomers possessing C_{2v} symmetry. However, this is not the case, with all three spectra being incredibly similar as well as being much simpler than predicted. Approximately 15 bands are observed for *o*-carborane with group theory predicting 53 normal infrared vibrations.[27] This does have its advantages, with strong bands observed for characteristic environments of the cage allowing the spectrum of *o*-carborane to be easily assigned (**Figure 2.6**).[28,29]

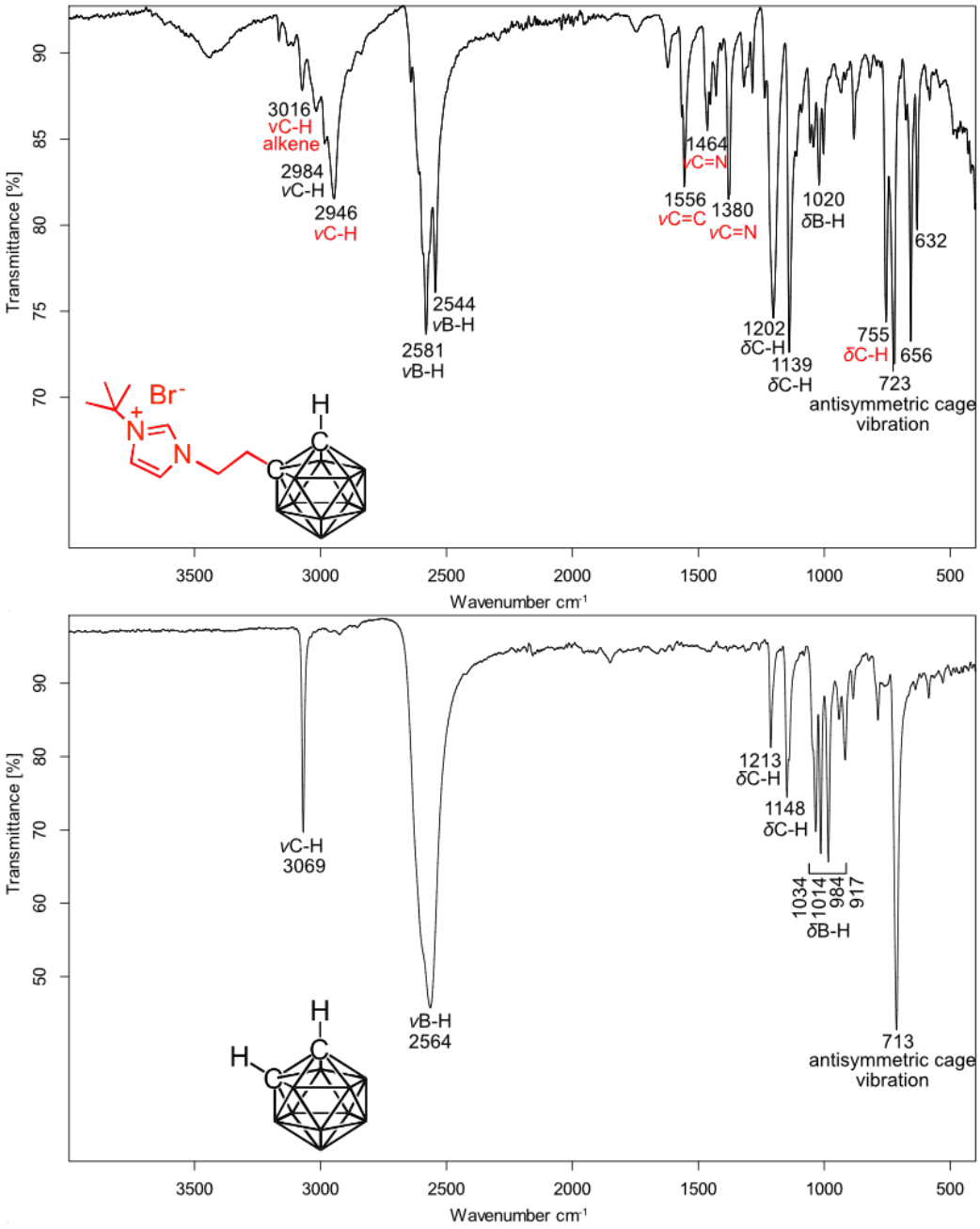

Figure 2.6 Infrared spectra of *o*-carborane (bottom) and **L2.1** (top). *The FTIR spectra were recorded as solid-state samples.*

The carboranyl CH stretching vibration in *o*-carborane is observed as a sharp band at 3069 cm^{-1} (**Figure 2.6**, **bottom**). Its high frequency arises from the strong electron acceptor effect in carboranes.[30] This band becomes difficult to assign for **L2.1**, with alkene and alkyl C-H stretches masking this region. The BH stretching vibrations in *o*-carborane appear as a strong broad band at 2564 cm^{-1} and the appearance of this band is dependent on the cage substituents, with bulky groups revealing its fine vibrational structure. This can be observed on introducing the imidazolium arm for **L2.1** (**Figure 2.6**, **top**). Other characteristic peaks in the IR spectrum of *o*-carborane include the bending bands at 1213-1148 cm^{-1} and 1034-917 cm^{-1} for C-H and B-H respectively, and a strong sharp band at 713 cm^{-1} which can be assigned to an antisymmetric cage vibration (**Figure 2.6**, **bottom**).[31]

One advantage of I.R. spectroscopy is that it can be used as a quick analytical technique for monitoring the progress of the degradation of *closo*-carboranes to their respective *nido*-species. Hawthorne and coworkers noted the *v*(B-H) band shifts to a lower frequency by approximately 50 cm^{-1}.[9,10] This can be observed when comparing the infrared spectrum of **L2.1** to that of **L2.2** (**Figure 2.7**). On loss of the B vertex, all 11 protons are retained and one of the challenges is locating the band for the bridging proton of the open pentagonal face. One proposed theory is the dynamic behaviour of this proton leads to band broadening.[32]

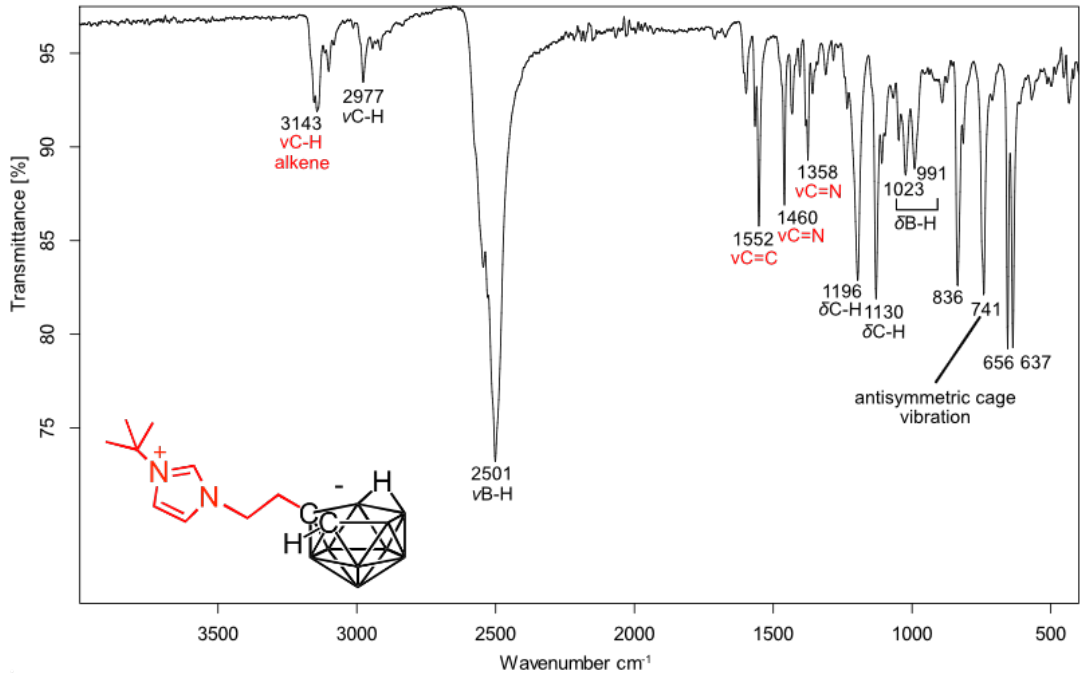

Figure 2.7 Infrared spectrum of **L2.2**. *The FTIR spectra were recorded as solid-state samples.*

2.2.5 X-ray Diffraction Analysis

X-ray crystallography is an excellent technique for unambiguously determining the molecular structure of a compound in the solid state. With advances in technology, high throughput diffractometers have revolutionised experimental methods, with processing time comparable to that of NMR spectroscopy in some instances. Crystals of **L2.1** and **L2.2** suitable for X-ray diffraction analysis were grown by vapour diffusion of Et_2O into concentrated MeCN solutions of each compound. The molecular structures are shown in Figure **2.8**, and selected bond distances and angles given in **Table 2.1**. The parameters of the imidazolium group such as the $N^{1/2}$-C^7 bond lengths and N^1-C^7-N^2 bond angle are in the expected range for imidazolium compounds.[33]

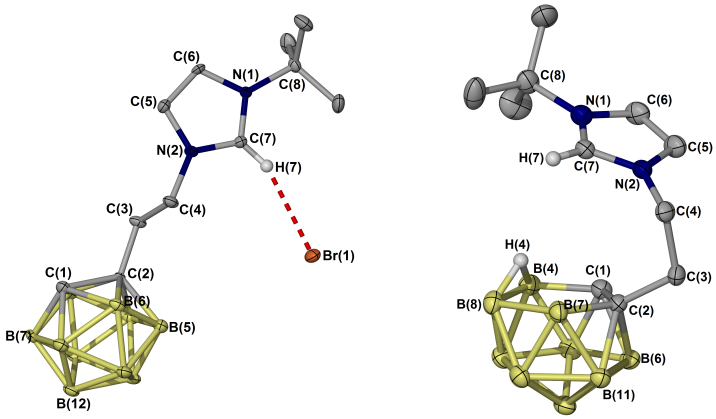

Figure 2.8 Molecular structure of **L2.1** (left) and **L2.2** (right). *Thermal ellipsoids shown at 50 % probability and hydrogen atoms are omitted for clarity.*

Table 2.1 Selected bond distances (Å) and angles (deg) for **L2.1** and **L2.2**.

Bond	**L2.1 (Å)**	**L2.2 (Å)**	Angle	**L2.1 (deg)**	**L2.2 (deg)**
N(1)-C(7)	1.331(3)	1.346(13)	N(1)-C(7)-N(2)	108.9(2)	108.8(9)
N(2)-C(7)	1.328(3)	1.341(14)			
C(5)-C(6)	1.351(3)	1.358(17)			

One of the long standing problems in single crystal X-ray diffraction analysis of carboranyl compounds is the unambiguous determination of the carbon atoms in the icosahedral cage, in particular where one or both carbon atoms are not substituted. This is due to C and B having very similar X-ray scattering powers as a simple consequence of their periodic adjacency. A common method employed for distinguishing between C and B vertices is to assign each vertex as a boron and inspect the thermal parameter (U_{eq}) values; those for C should be smaller.

However, these values can be influenced significantly by their environment, which leads to ambiguity. Often these values are coupled with the bond lengths of the cage. This can be quite effective for icosahedral cages where the carbon atoms are adjacent, as this bond length should have the shortest connectivity. Recently, Welch *et al*. reported a simple yet highly effective method for distinguishing between C and B vertices termed the Vertex-to-Centroid Distance (VCD) method.[34] This method involves measuring the distances from the topologically equivalent vertex atoms to the polyhedral centroid, where the shortest connectivity can be identified as a C vertex. In this comprehensive study a range of icosahedral and sub-icosahedral *closo*-carboranes, icosahedral metallacarboranes and supra-icosahedral metallacarboranes were employed, illustrating the generality of this method. Utilising this method allowed the unsubstituted carbon vertex of each carboranyl precursor and ligand to be unambiguously assigned in this thesis. Nonetheless, the method does have its limitations; an example of a cyclometallated complex reported in this thesis (Chapter 4, Section 4.3) where the carborane is bound through a vertex of the cage results in distortion of the icosahedral cage. As a result the VCD method fails and other analytical techniques were used in conjunction with the X-ray diffraction analysis to assign the carbon vertex.

2.3 Expansion of the ligand library

The length of the alkyl linker between the carborane and the NHC plays a crucial role in the overall stability of the cage, and consequently directs the type of ligand precursor synthesised, with an ethyl linker allowing both a *closo*-carboranyl imidazolium bromide salt **L2.1** and its *nido*- counterpart **L2.2** to be isolated in high yields (Section 2.1). Structural diversity could easily be introduced into these scaffolds through varying the N-substituent of the imidazole precursor. A range of alkyl and aryl groups with other neutral (pyridyl, amine) or anionic (alkoxide) donor functionalities were employed (**Scheme 2.8**).

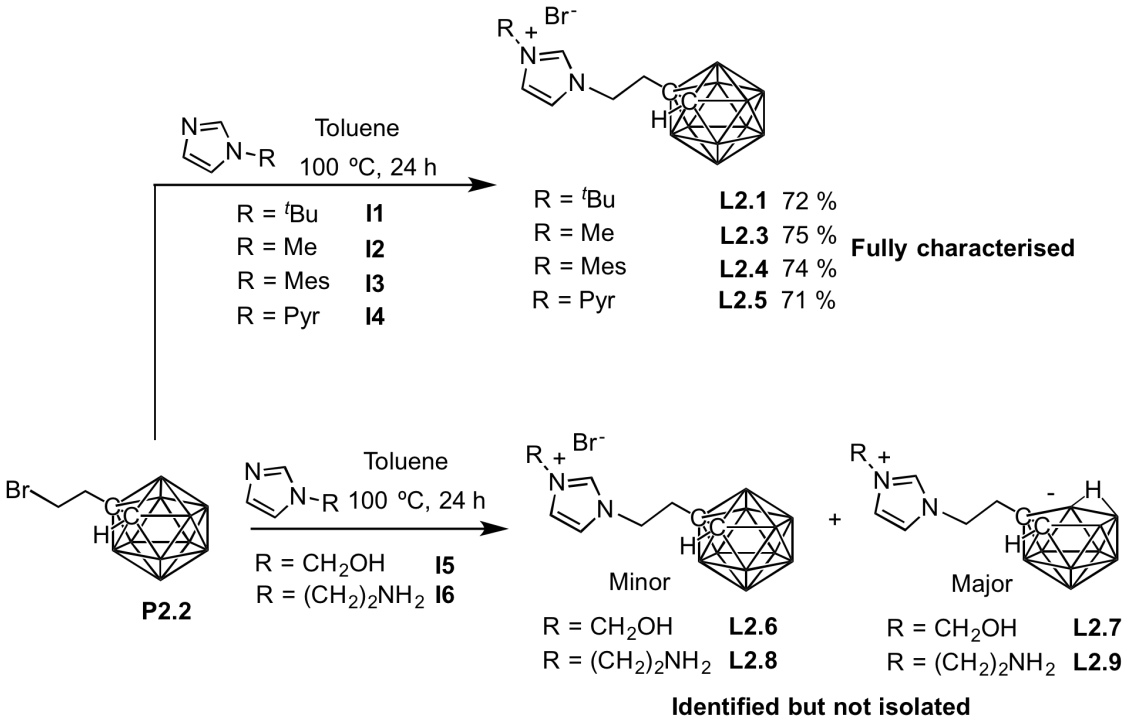

Scheme 2.8 Library of ligand precursors prepared in this work.

In the syntheses of the *closo*-carboranyl ligands (**L2.1**, **L2.3**, **L2.4**, **L2.5**) highest yields were obtained when strict anhydrous conditions were employed. All reagents were dried and stored in the glove box, and the imidazoles that exist as oils were also stored over 4 Å molecular sieves. Even under these strictly anhydrous reaction conditions the zwitterion can still form, and in some cases accounts for 10 % of the materials isolated. The majority of the *closo*-species can be selectively crystallised by the slow diffusion of Et_2O into concentrated MeOH solutions. However, as crystal formation can often require weeks this method becomes impractical as a method of isolation. Optimisation of reaction conditions found that reducing the amount of solvent in the reaction (1 mL per 200 mg of carboranyl precursor) completely eradicated the formation of the zwitterion, as it promotes the desired product to precipitate from the reaction before deboronation can occur.

o-Carborane can typically be deboronated by amines[11] and alkoxides.[9,10] Imidazoles **I4**-**I6** were employed to gage their tolerability when tethered to the base sensitive cage. When hydroxymethyl imidazole (**I5**) was reacted with **P2.2**, analysis of the crude material by $^{11}B\{^{1}H\}$ NMR spectroscopy indicated that the majority of the product was the zwitterionic species **L2.7**, with the characteristic resonances for a *nido* cage. The HRMS data supports the NMR data, with a major peak at *m/z* 228.2343 corresponding to [**L2.8** − CHOH]$^{+}$. Isolation of the **L2.6** was unsuccessful due to the highly hygroscopic nature of this compound leading to co-crystallisation with **L2.7**. Pleasingly, when pyridyl imidazole **I4** is employed, the corresponding *closo*-carboranyl ligand **L2.5** can be isolated in high yield. However, when the primary amine imidazole **I6** is employed, a mixture of the *closo*- (**L2.8**) and *nido*- (**L2.9**) species is obtained.

One of the problems encountered in this work was the synthesis of halide-mixed complexes due to utilising bromide imidazolium salts with metal chloride precursors (Chapter 5, Section 5.3). To prevent the formation of halide mixed complexes the synthesis of a chloride congener **L3.1** was attempted (**Scheme 2.9**). However, the reaction of **P3.2** with **I2** was incredibly slow and **L3.1** could only be isolated in very poor yields. The slow rate of reaction is most probably due to the chloride being a poorer leaving group when compared to bromide.

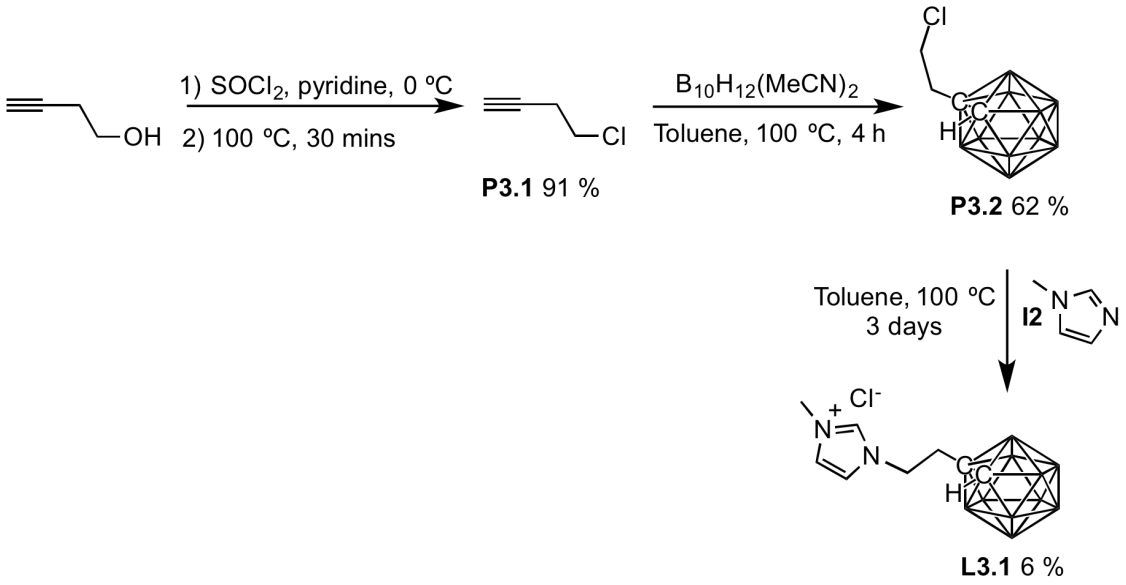

Scheme 2.9 Synthesis of *closo*-carboranyl imidazolium chloride salt **L3.1**.

A similar result was obtained when the length of the linker was extended to a propyl chain; the reaction of chloro-propyl-o-carborane **P4.1** with **I1** was incredibly slow and the expected *closo*-carboranyl ligand could not be isolated. If a *closo*-carboranyl ligand with a propyl linker is required, it would be advantageous to prepare the brominated precursor from 5-bromo-1-pentyne, which can be prepared from the corresponding alcohol, CBr_4 and PPh_3.[35]

When the zwitterionic ligand is desired, anhydrous conditions are not necessary and addition of H_2O actually facilitates the reaction. An excess of imidazole is used in the reaction to achieve full deboronation to form the zwitterionic species (**Scheme 2.10**). However, this can often make the work up of the reactions tedious; the zwitterionic ligands are recrystallised from MeOH with Et_2O, but in the majority of cases the excess imidazole employed in the reaction can 'oil-out' with the product. In these cases slow diffusion of Et_2O into concentrated MeOH solutions over the course of several days can selectively crystallise the zwitterionic ligand, but the yields vary considerably.

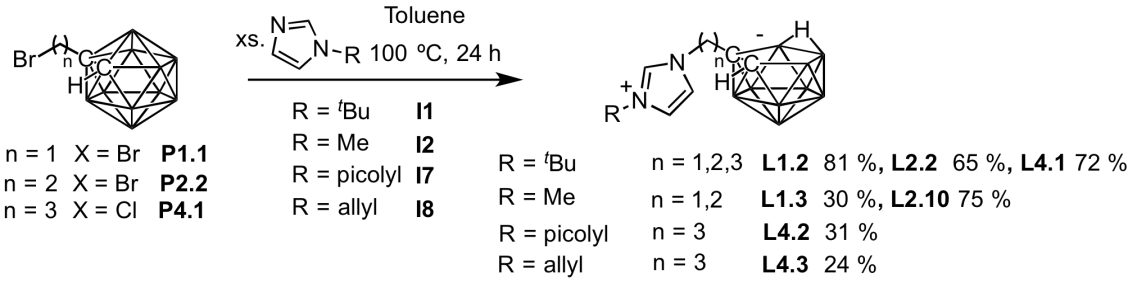

Scheme 2.10 Library of zwitterionic ligand precursors synthesised.

2.4 Di-C-substituted carborane derivatives

Whilst *o*-carborane possesses many intriguing properties, it displays chemical reactivity that in some cases is problematic when it comes to coordinating these ligands to metal centres. More specifically, the acidic cage CH proton can either react with the metal leading to decomposition of the complex, or a mixture of C and B vertex coordination at the metal centre is observed, both of which have been encountered throughout this thesis. To improve the stability of the complex, or to allow selective cyclometallation through a boron vertex, the acidic proton can be blocked through utilising a methylated carborane derivative (**P5.1**) (**Scheme 2.11**).

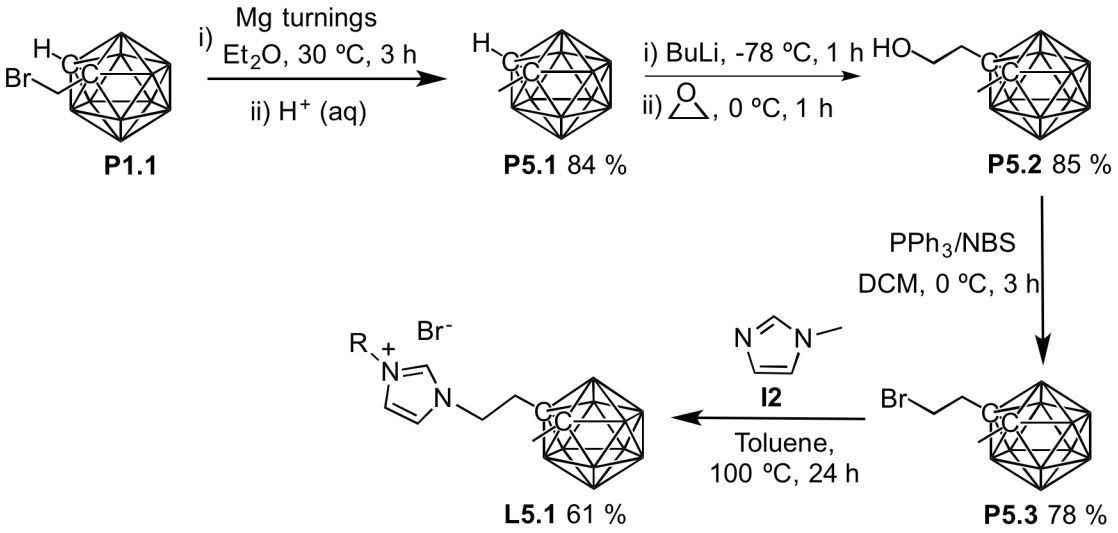

Scheme 2.11 Synthesis of ligand precursor **L5.1**.

The synthesis of Grignard reagents by activation of magnesium metal and reaction with an alkyl halide has been known since 1899.[36] Methyl-*o*-carborane (**P5.1**) can be prepared by reacting **P1.1** with magnesium turnings under anhydrous conditions, with **P5.1** being formed upon acid workup.[37] Lithiation of **P5.1** and its subsequent reaction with ethylene oxide gives **P5.2** without the requirement of further purification. **P5.2** is then brominated using NBS and PPh_3 to give **P5.3**, and subsequently reacted with **I2** to give the di-C-substituted carboranyl ligand precursor **L5.1** in good yield (**Scheme 2.11**). **L5.1** displays key differences when analysed by multinuclear NMR spectroscopy in comparison to mono-C-substituted ligands. In the ^{1}H NMR spectrum of **L5.1**, the disappearance of the characteristic broad singlet for the cage CH proton (**Figure 2.9**), and the presence of two quaternary carbon resonances in the $^{13}C\{^{1}H\}$ NMR spectrum at 77.5 and 75.6 ppm, is indicative of a di-C-substituted cage. There is little difference, however, in the $^{11}B\{^{1}H\}$ NMR spectra which is to be expected, with peaks in the range of a typical *closo*-carborane (**Figure 2.9**, **inset**). The HRMS provided the expected molecular ion peak at *m/z* 267.2877 corresponding to $[\mathbf{L5.1} - Br]^{+}$, and the X-ray diffraction analysis further clarifies the formation of **L5.1** (**Figure 2.10**).

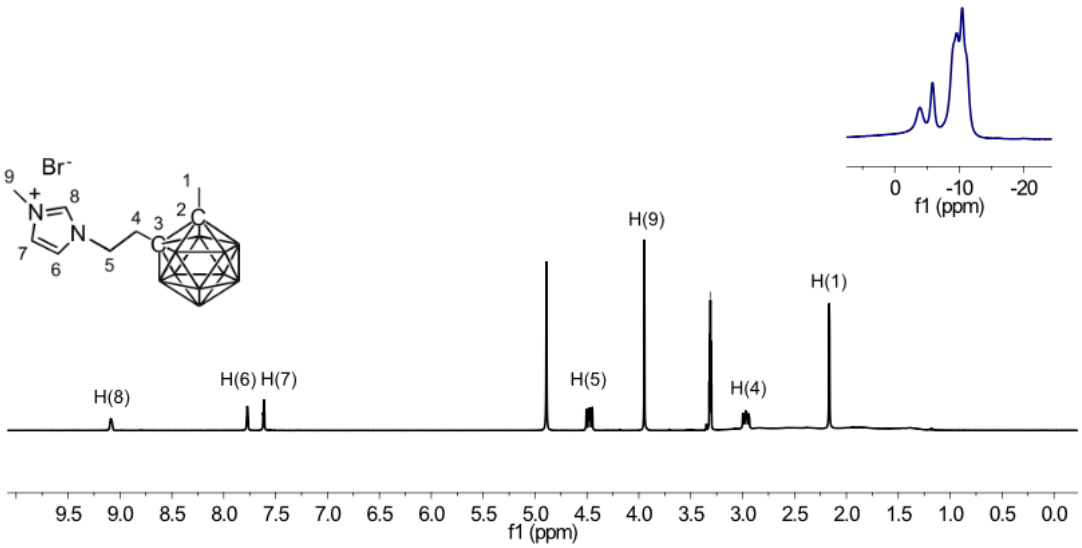

Figure 2.9 ^{1}H NMR spectrum (500 MHz, CD_3OD) and $^{11}B\{^{1}H\}$ NMR spectrum (161 MHz, CD_3OD) (inset) of **L5.1**.

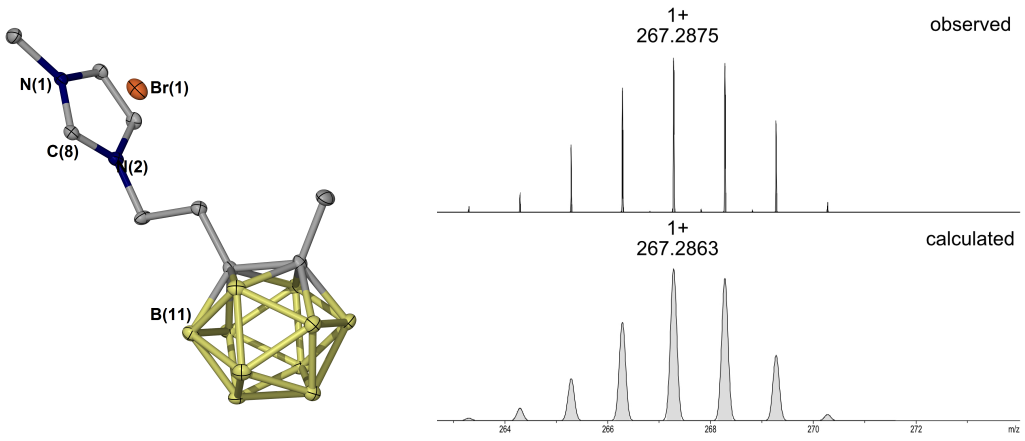

Figure 2.10 Molecular structure determined by single crystal X-ray diffraction analysis and HRMS of **L5.1** with a molecular ion peak of [**L5.1** − Br]$^{+}$.

2.5 Towards the development of CBC-type ligands

2.5.1 Background

Pincer ligands, formally known as tridentate ligands, were pioneered by Shaw, with his work on transition metals bearing a 1,3-bis(dialkylphosphinomethyl)benzene motif.[38] Pincer ligands offer great tailorability with respect to: 1) The central anchoring site, the majority of which are either carbon-based, including aliphatic and aromatic motifs, or heteroatom analogues of N, Si and P (see Reek's review and references therein),[39] 2) The metal-binding atom of the arms, with examples of P, C, N, O, S and Se donor atoms,[40,41] and 3) The auxiliary sites on the arms, which can be tuned to control the steric properties and the chirality of the ligand (**Figure 2.11**).[42]

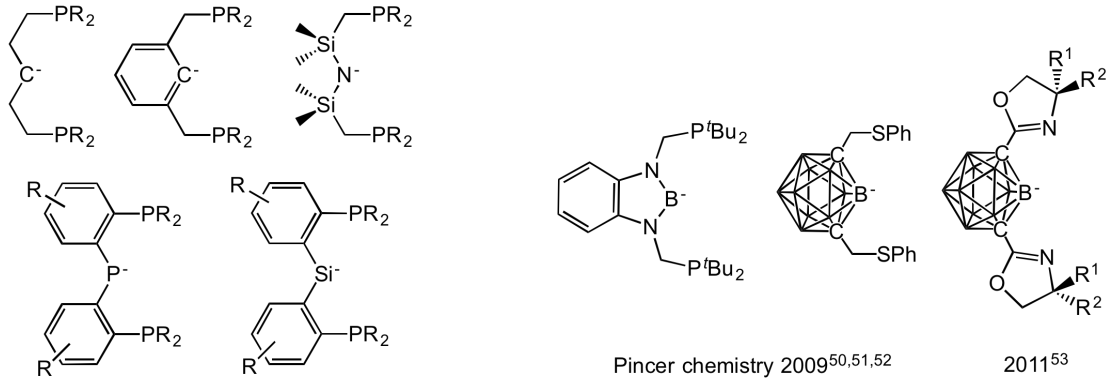

Figure 2.11 Examples of reported pincer ligands.[43]

Remarkably, boron was not considered in the design of pincer ligands until 2009, when Yamashita and Nozaki reported the first PBP ligand.[44,45] That same year Mirkin and co-workers established a new chapter in carborane chemistry, with the first example of a tridentate ligand which incorporates a carborane as the central anchoring site.[46] Surprisingly, since the establishment of this new carboranyl chemistry, only one other publication by Nakamura and co-workers on a series of NBN *m*-carborane based chiral pincer complexes has been reported.[47] This could be due to challenging synthetic methodology required to introduce functionality into the carborane. One of the most common methods used for functionalisation of *o*-carborane is deprotonation with a strong base (^{n}BuLi) and reaction with a suitable electrophile. However, due to the steric bulk of the resulting anion upon deprotonation, only reactive electrophiles are suitable which limits the range of functionality that can be introduced.

2.5.2 Synthesis of pincer ligand precursors

In the literature, one of the most popular synthetic methods to preparing imidazolium-based pincer ligand precursors involves reacting two equivalents of substituted imidazole with dibromoethylbenzene. The aim of this work was to replace the aryl ring with a carborane, which would pave the way to new carboranyl pincer ligands that possess good tailorability. 1,2-Dibromoethyl-*closo*-dodecaborane (**P6.1**) and its *m*-carborane counterpart **P7.1** were prepared *via* a modified procedure to precursor **P2.2**. Reaction of *o*- or *m*-carborane with ^{n}BuLi (2 eq) followed by addition of an excess of ethylene oxide (3 eq) gives the disubstituted hydroxyethyl carboranyl compounds (**P6.1** and **P7.1**), which are then brominated using NBS and PPh_3 to give **P6.2** and **P7.2** in excellent yields (**Scheme 2.12**).

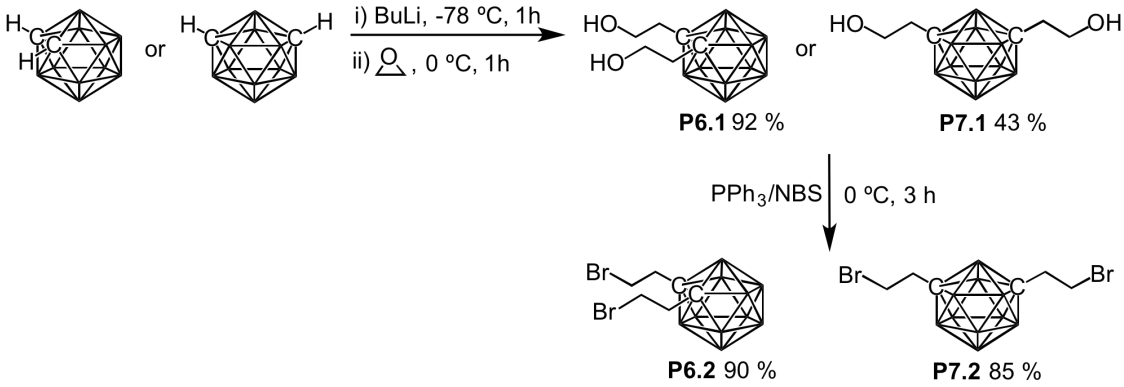

Scheme 2.12 Synthesis of 1,2- and 1,7-dibromoethyl-*closo*-dodecaborane precursors.

Our previous synthetic method for synthesising *closo*-carboranyl imidazolium salts involved using an apolar solvent to promote precipitation of the imidazolium salt and prevent further reaction to form the zwitterionic ligand (**Scheme 2.13**). In the case of **P6.2**, upon formation of the mono-substituted imidazolium salt **L6.1**, it is required to remain in solution to allow the second substitution to take place. However, upon formation of **L6.1** the cage will be highly susceptible to deboronation due to the strongly electron withdrawing imidazolium group. As a result, when **P6.2** is reacted with methyl imidazole **I2** in refluxing MeCN, a large proportion of **L6.1** and **L6.3** are deboronated to the suspected *nido* species (**L6.2** and **L6.4**), which was observed by ^{1}H and ^{11}B{^{1}H} NMR spectroscopy.

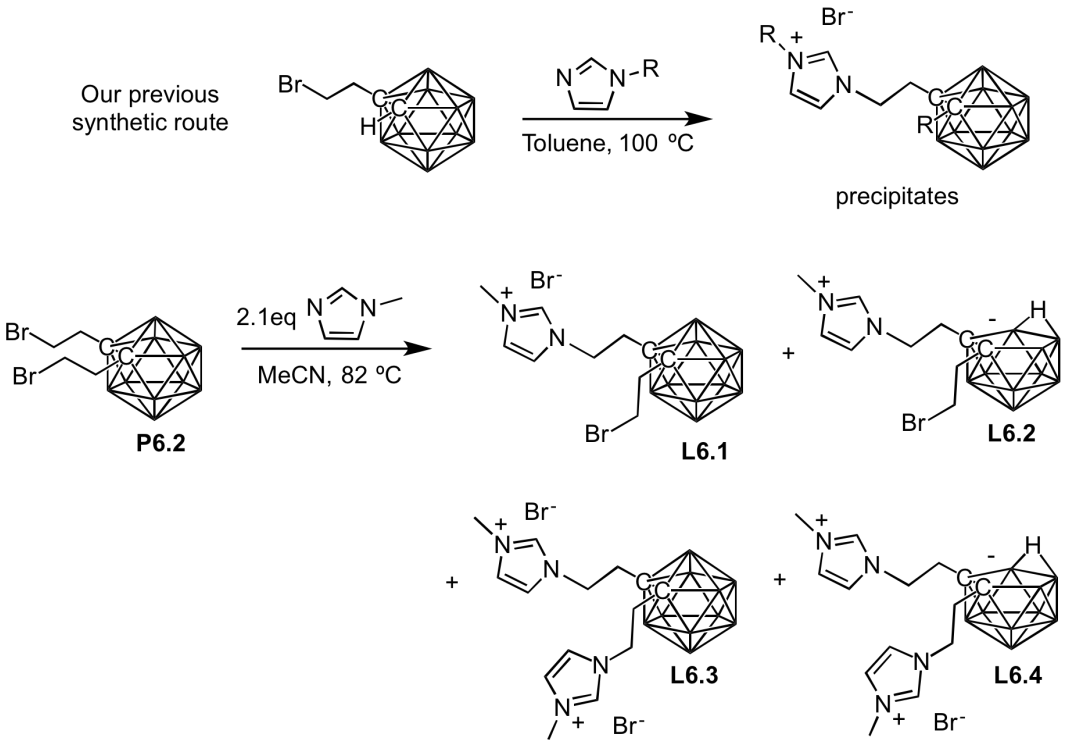

Scheme 2.13 Attempted synthesis of **L6.3**.

To overcome this problem **P7.2** was employed, as *m*-carborane derivatives are generally more stable towards basic conditions. Pleasingly, when **P7.2** is subjected to the same reaction conditions the *closo*-carborane bis-imidazolium salt **L7.2** can be isolated in high yields (**Scheme 2.14**). It is noteworthy that when toluene is used as the solvent and the imidazole is reduced to 0.9 equivalents, the mono-substituted product (**L7.1**) was the major product observed by ^{1}H NMR spectroscopy and HRMS. These reactions were screening reactions carried out on an NMR scale, and **L7.1** was not isolated. Nonetheless, this synthetic route is particularly interesting as future work should allow asymmetrical pincer ligands to be isolated, and to the best of our knowledge there are no examples of asymmetrical NHC-pincer ligands reported to date.

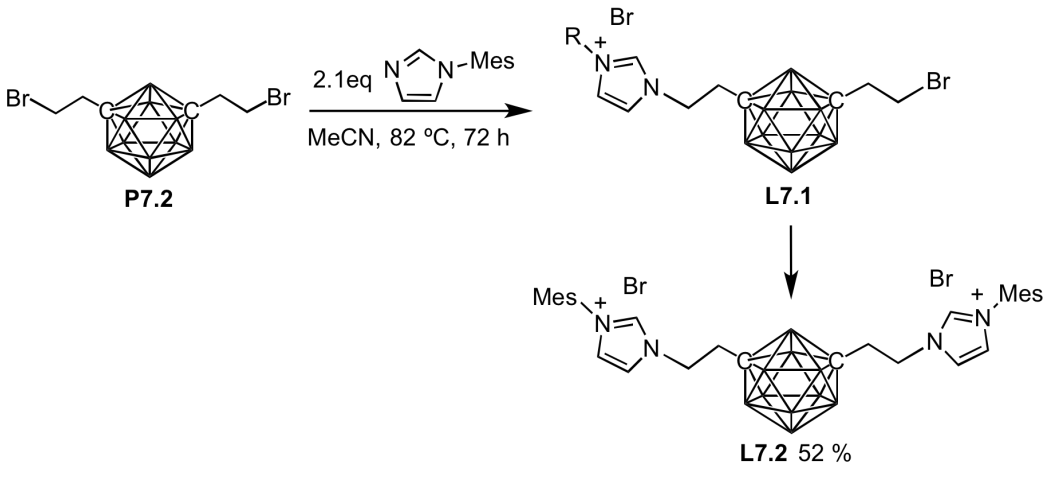

Scheme 2.14 Synthesis of the *closo*-carborane bis-imidazolium salt **L7.2**.

2.6 Conclusions

The fusion of two very different ligand families, namely NHC precursors and carboranes, has led to the synthesis of a novel ligand architecture. Various synthetic challenges to combining N-substituted basic imidazoles with the base sensitive carboranes have been overcome. The strongly electron withdrawing nature of the imidazolium group increases the susceptibility of the cage to nucleophilic attack, resulting in deboronation under very mild conditions by the action of a bromide counterion. We found that the length of the alkyl tether between the imidazolium salt and the carborane plays a crucial role in the stability of the cage, with a longer tether reducing the electron withdrawing capabilities of the imidazolium group, hence stabilising the cage and allowing stable *closo*-carboranyl imidazolium salts to be isolated.

Due to the base sensitive nature of the cage, a range of different imidazole N-substituents were employed to gauge their tolerability when tethered to *o*-carborane. Pleasingly, a range of alkyl and aryl groups, including other donor functionalities such as pyridyl, were isolated in high yields. However, functional groups such as primary amines or a hydroxyl group led to deboronation. Nonetheless, the library of *closo*-carboranyl imidazolium salts and zwitterionic ligand precursors that have been prepared illustrates the tailorability of the system. This is further demonstrated with functionalisation of both carboranyl carbon atoms leading to a Me protected and CBC type ligand precursors. The ligand precursors were fully characterised using ^{1}H, $^{11}B\{^{1}H\}$ and $^{13}C\{^{1}H\}$ NMR spectroscopy, high resolution MS and, for those which are publicised, by elemental analysis and X-ray diffraction analysis. The use of these analytical techniques to differentiate between *closo*-carborane and its *nido* counterpart was reviewed.

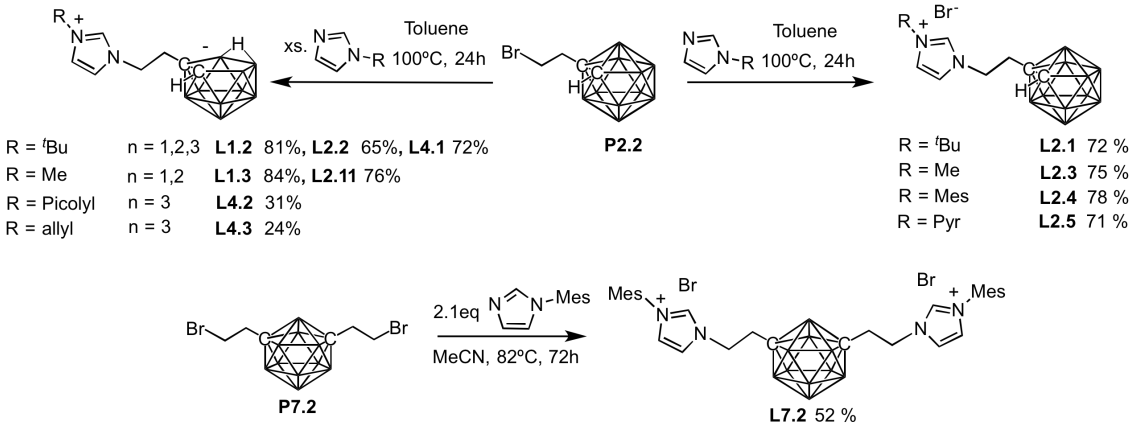

Scheme 2.15 Summary of work presented in this chapter: synthesis of mono-substituted (**A**) and disubstituted (**B**) carboranyl ligands.

2.7 Experimental

All chemicals used in this work were bought from either Sigma Aldrich or Alfa Aesar including imidazoles **I2**, **I6** and **I8**, and used without further purification. Anhydrous solvents were prepared by passing over activated alumina to remove water, copper catalyst to remove oxygen and molecular sieves to remove any remaining water, *via* the Dow–Grubbs solvent system, and then freeze–pump–thaw degassed prior to use. NMR spectra were recorded on a Bruker AV500, Bruker AV400 or a Bruker DPX300 spectrometer. ^{1}H NMR and ^{13}C{^{1}H} NMR chemical shifts were referenced against residual solvent peaks. Mass spectra were collected on a Bruker Daltonics (micro TOF) instrument operating in the electrospray mode. Elemental analyses were performed by Mr Stephen Boyer at London Metropolitan University. For compounds which have been previously reported in the literature the ^{1}H and ^{13}C{^{1}H} NMR spectroscopy and HRMS data are listed. For novel compounds all NMR spectroscopic data are fully assigned with the aid of 2D ^{1}H^{1}H COSY, ^{1}H^{13}C HMQC, ^{1}H^{13}C HMBC and ^{13}C{^{1}H} DEPT 135 experiments.

2.7.1 N-substituted imidazoles

Preparation of **I1**.[48]

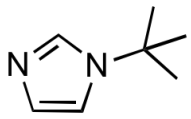

Tert-butylamine (10.50 mL, 100 mmol) was dissolved in MeOH (70 mL) at 0 °C and formaldehyde (7.45 mL, 100 mmol, 37 % in H_2O) was added followed by aqueous glyoxal (11.50 mL, 100 mmol, 40 % in H_2O) and ammonium carbonate (4.80 g, 50 mmol). The mixture was allowed to reach room temperature and stirred for 18 hours. All volatiles were removed *in vacuo*. The product was extracted from H_2O (20 mL) into DCM (4 × 20 mL). The DCM layer was washed with H_2O (20 mL), dried over $MgSO_4$, filtered and the solvent removed *in vacuo* to give an orange oil. Yield: 6.20 g, 50 mmol (50 %). ^{1}H NMR (300 MHz, $CDCl_3$): δ (ppm) 7.26 (s, 1H), δ 7.00 (d, 2H), δ 1.50 (s, 9H). ^{13}C{^{1}H} NMR (75 MHz, $CDCl_3$): δ (ppm) 157.8, 134.3, 128.9, 116.3, 30.6. HRMS (ESI^{+}): *m/z* $[C_7H_{13}N_2]^{+}$ 125.1069, calcd for $[M + H]^{+}$ 125.1079. Consistent with data previously reported.[48]

Preparation of **I3**.[49]

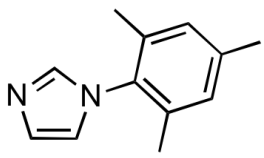

Acetic acid (10 mL), formaldehyde (3.00 mL, 40 mmol) and aqueous glyoxal (4.60 mL, 40 mmol, 40 % in H_2O) were heated at 70 °C. A solution of acetic acid (10 mL), ammonium acetate in water (3.10 g in 2 mL, 40 mmol) and 2,4,6-trimethylaniline (9.40 mL, 66.9 mmol) was added drop wise over 30 minutes. The solution was continuously stirred and heated at 70 °C for 18 hours. The reaction was then cooled to room temperature and a NaOH solution (20 g in 300 mL H_2O) was added to precipitate the product. The precipitate was filtered to obtain a

black solid. The crude product was recrystallised from acetone (30 mL) with H_2O (30 mL), filtered and repeated a further 7 times until a beige solid is obtained. Yield: 2.1 g, 11.30 mmol (28 %). ^{1}H NMR (500 MHz, $CDCl_3$): δ (ppm) 7.42 (m, 1H), 7.22 (t, *J* = 1 Hz, 1H), 6.96 (m, 2H), 6.88 (t, *J* = 1 Hz, 1H), 2.33 (s, 3H), 1.98 (s, 6H). $^{13}C\{^1H\}$ NMR (126 MHz, $CDCl_3$): δ (ppm) 138.9, 137.6, 135.5, 133.5, 129.7, 129.1, 120.2, 21.1, 17.4. HRMS (ESI^+): *m/z* $[C_{12}H_{14}N_2]^+$ 187.1249, calcd for $[M + H]^+$ 187.1291. Consistent with data previously reported.[49]

Preparation of **I4**.[50]

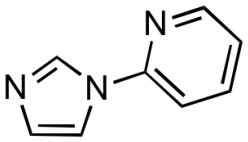

Imidazole (500 mg, 7.34 mmol), 2-bromo-pyridine (0.23 mL, 2.41 mmol) and K_2CO_3 (680 mg, 4.92 mmol) were added to an ampoule and degassed. This was heated at 190 °C under argon for 18 hours. The reaction mixture was allowed to cool then chloroform (10 mL) followed by H_2O (20 mL) was added. The product was extracted into the chloroform and was washed with a saturated solution of Na_2CO_3 (20 mL), dried over $MgSO_4$, filtered and dried *in vacuo* to give a white solid. Yield: 285 mg, 1.96 mmol (81 %). ^{1}H NMR (300 MHz, $CDCl_3$): δ (ppm) 8.49 (ddd, *J* = 4.9, 1.8, 0.8 Hz, 1H), 8.35 (s, 1H), 7.82 (ddd, *J* = 8.2, 7.5, 1.9 Hz, 1H), 7.65 (t, *J* = 1.3 Hz, 1H), 7.36 (dt, *J* = 8.2, 0.9 Hz, 1H), 7.25-7.22 (m, 1H), 7.20 (s, 1H). $^{13}C\{^1H\}$ NMR (75 MHz, $CDCl_3$): δ (ppm) 112.3, 116.1, 121.5, 122.0, 130.6, 135.0, 139.0, 149.1. HRMS (ESI^+): *m/z* $[C_8H_8N_3]^+$ 146.0730, calcd for $[M + H]^+$ 146.0718. Consistent with data previously reported.[50]

Preparation of **I5**.[51]

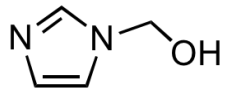

Imidazole (500 mg, 7.34 mmol) and paraformaldehyde (200 mg, 9.31 mmol) were heated in a dry melt at 110 °C for 1 hour and the liquid solidified upon cooling. The solid residue was triturated in ethyl acetate, filtered and dried *in vacuo* to give a white solid. Yield 502 mg, 5.12 mmol (70 %).^{1}H NMR (400 MHz, $CDCl_3$): δ (ppm) 7.35 (s, 1H), 7.03 (s, 1H), 6.88 (s, 1H), 5.36 (s, 2H). $^{13}C\{^1H\}$ NMR (101 MHz, $CDCl_3$): δ (ppm) 136.2, 128.3, 118.8, 70.2. HRMS (ESI^+): *m/z* $[C_4H_6N_2ONaK]^+$ 158.9636, calcd for $[M+Na+K-H]^+$ 158.9931. Consistent with data previously reported.[51]

Preparation of **I7**.

A mixture of 2-(Bromomethyl)pyridine hydrobromide (1.00 g, 3.95 mmol), imidazole (0.27 g, 3.95 mmol), and K_2CO_3 (1.64 g, 11.85 mmol) in 20 mL of MeCN was heated at 80 °C for 24 hours. The solvent was removed *in vacuo* and DCM (20 mL) and H_2O (20 mL) were added. The organic layer was separated and further washed with H_2O (2 × 20 mL). After separation,

the organic layer was dried with anhydrous $MgSO_4$. The solution was filtered, and the solvent removed *in vacuo* to give a brown oil. Yield: 364 mg, 2.29 mmol (58 %). ^{1}H NMR (400 MHz, $CDCl_3$) δ (ppm) 8.49 (d, J = 4.8 Hz, 1H), 7.57 (td, *J* = 7.7, 1.8 Hz, 1H), 7.53 (s, 1H), 7.17-7.12 (m, 1H), 7.01 (s, 1H), 6.91 (s, 1H), 6.88 (d, *J* = 7.9 Hz, 1H), 5.16 (s, 1H). ^{13}C NMR (101 MHz, $CDCl_3$) δ (ppm) 156.0, 149.6, 137.5, 137.3, 129.7, 123.0, 121.2, 119.5, 52.4. HRMS (ESI^+): *m/z* $[C_9H_{10}N_3]^+$ 160.0884, calcd for $[M + H]^+$ 160.0875. Consistent with data previously reported.[52]

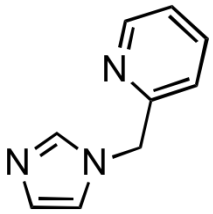

2.7.2 Carborane precursors

Preparation of **2**.[53]

A stirred solution of decaborane (5.44 g, 44.50 mmol) in acetonitrile (18 mL) was slowly heated to 80 °C. After five hours the reaction mixture was cooled to room temperature. The white precipitate was filtered off and washed with acetonitrile to give the product as a white solid. Yield: 6.48 g, 32.04 mmol (72 %). ^{1}H NMR (400 MHz, $CDCl_3$): δ (ppm) 2.70 (s, 6H). ^{13}C{^{1}H} NMR (101 MHz, DMSO-d_6): δ (ppm) 109.4, 2.8. ^{11}B{^{1}H} NMR (CD_3CN, 96 MHz): δ −4.9 (2B), −19.2 (4B), −30.5 (2B), −41.4 (2B).

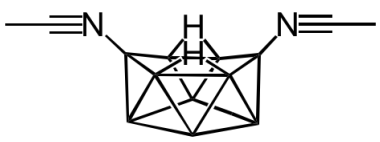

Preparation of **P1.1**.[54]

$B_{10}H_{12}(MeCN)_2$ (1.00 g, 4.94 mmol) was added to a Schlenk flask and degassed. Anhydrous toluene (8 mL) and propargyl bromide (0.52 mL, 4.94 mmol, 80 % wt. toluene) was added and slowly heated to 100 °C and kept at this temperature for 4 hours. After cooling the solvent was removed *in vacuo* and the residue was extracted with hexane (3 × 20 mL). The combined extracts were washed with a 1M NaOH solution (20 mL) then H_2O (2 × 20 mL) and dried over $MgSO_4$. This was then filtered and solvent removed *in vacuo* to give the product as a yellow oil. Yield: 811 mg, 3.42 mmol (69 %). ^{1}H NMR (400 MHz, $CDCl_3$): δ (ppm) 4.00 (br. s, 1H), 3.96 (s, 2H). ^{13}C{^{1}H} NMR (101 MHz, $CDCl_3$): δ (ppm) 71.3, 61.1, 32.3. ^{11}B{^{1}H} NMR (161 MHz, $CDCl_3$): δ (ppm) −2.4 (1B), −5.0 (1B), −8.7 (2B), −10.6 (2B), −12.4 (2B), −12.9 (2B). Anal. Calcd for $C_3H_{13}B_{10}Br$: C, 15.19; H, 5.53. Found: C, 14.95; H, 5.47. Consistent with data previously reported.[20]

Preparation of **P2.2**.

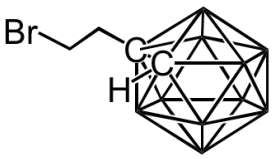

Route 1. Prepared as described for **P1.1** from 4-bromo-1-butyne (0.66 mL, 7.03 mmol), $B_{10}H_{12}(MeCN)_2$ (1.40 g, 7.03 mmol) in anhydrous toluene (10 mL). After purification the product was obtained as a white crystalline solid. Yield: 618 mg, 2.46 mmol (35 %).

Route 2.[21] *o*-Carborane (300 mg, 2.08 mmol) was added to a Schlenk flask and degassed. Anhydrous THF (10 mL) was added and cooled to -78° C. A 1.6 M solution of ^{n}BuLi in *n*-hexane (1.32 mL, 2.08 mmol) was added drop wise. This was stirred for 30 minutes at −78 °C. The temperature was then raised to 0 °C and a 2.5 M solution of ethylene oxide (1.03 mL, 2.50 mmol) was added drop wise and stirred at 0 °C for 1 hour. The reaction was quenched by adding a saturated solution of NH_4Cl (5 mL) and the aqueous phase extracted with ethyl acetate (3 × 10 mL). The organic fractions were combined and dried over $MgSO_4$, filtered and solvent removed *in vacuo* to give as a oily residue. Without further purification this was transferred to a Schlenk flask, degassed and anhydrous DCM (5 mL) was added. This was cooled to 0 °C and PPh_3 (539 mg, 2.06 mmol) and NBS (366 mg, 2.06 mmol) was added and stirred at 0 °C for 3 hours. The solvent was removed *in vacuo* and the residue was purified by chromatography (silica gel, hexane/ethyl acetate = 15/1) to give the bromide product (367 mg, 1.46 mmol, 70 %). ^{1}H NMR (DMSO-d_6, 300 MHz): δ (ppm) 5.21 (br. s, 1H), δ 3.53 (t, *J* = 7.8, 2H), δ 2.82 (t, *J* = 8.1, 2H,). $^{13}C\{^{1}H\}$ (DMSO-d_6, 75 MHz): δ (ppm) 74.2, 62.8, 38.7, 28.8. $^{11}B\{^{1}H\}$ NMR (DMSO-d_6, 96 MHz): δ (ppm) −3.2 (1B), δ −5.9 (1B), δ −9.8 (2B) δ −11.7 (4B), δ −13.1 (2B).

Preparation of **P3.1**.[55]

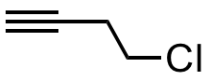

3-Butynol (3.02 mL, 40.00 mmol) and pyridine (256 µL, 4.00 mmol) were placed in a 10 mL two-necked round bottom flask and cooled to 0°C. Thionyl chloride (2.90 mL, 40.0 mmol) was added drop wise over a 10 minute period. The mixture was then heated at 100 °C for 30 minutes. The reaction was cooled to 90 °C and the product was distilled as a colourless oil. Yield: 3.20 mL, 36.36 mmol (91 %). ^{1}H NMR (300 MHz, $CDCl_3$): δ (ppm) 3.59 (t, *J* = 6.0 Hz, 2H), 2.64 (td, J = 6.0 Hz, 3 Hz, 2H), 2.07 (t, *J* = 3.0 Hz, 1H). $^{13}C\{^{1}H\}$ NMR (75 MHz, $CDCl_3$): δ (ppm) 80.3, 70.5, 42.0, 22.9. HRMS Consistent with data previously reported.[55]

Preparation of **P3.2**.[56]

Prepared as described for **P1.1** from 4-chloro-1-butyne (0.66 mL, 7.45 mmol) and $B_{10}H_{12}(MeCN)_2$ (1.00 g, 4.94 mmol) in anhydrous toluene (8 mL). After purification the product was obtained as an off white crystals. Yield: 624 mg, 3.02 mmol (61 %). ^{1}H NMR (300 MHz, DMSO-d_6): δ (ppm) 5.20 (br. s, 1H, carborane cage C*H*), 3.69 (t, *J* = 7.5 Hz, 2H, CH_2Cl),

2.75 (t, *J* = 7.5 Hz, 2H, C*H*$_2$). ^{13}C{^{1}H} NMR (75 MHz, DMSO-d$_6$): δ (ppm) 73.5 (carborane cage quaternary *C*), 62.9 (carborane cage *C*H), 41.6 (*C*H$_2$Cl), 38.6 (*C*H$_2$). ^{11}B{^{1}H} NMR (96 MHz, CDCl$_3$): δ (ppm) −3.1 (1B), −5.6 (1B), −9.7 (2B), −11.7 (4B), −13.1 (2B). Anal. Calcd for $C_4H_{15}B_{10}Cl$: C, 23.24; H, 7.31. Found: C, 23.16; H, 7.42.

Preparation **P4.1**.[57]

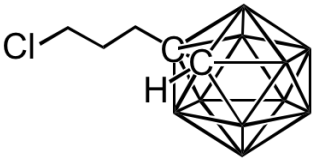

Prepared as described for **P1.1** from 5-chloro-1-pentyne (380 mg, 3.71 mmol), $B_{10}H_{12}(MeCN)_2$ (500 mg, 2.47 mmol) in anhydrous toluene (4 mL). After purification the product was obtained as a white waxy solid. Yield: 390 mg, 1.77 mmol (72 %). ^{1}H NMR (CD$_3$CN, 500 MHz): δ (ppm) 4.21 (s, 1H), 3.56-3.50 (m, 2H), 2.44-2.36 (m, 2H), 2.15-2.13 (m, 2H). ^{11}B{^{1}H} NMR (DMSO-d$_6$, 96 MHz): δ (ppm) −3.0 (1B), −6.2 (1B), −9.7 (2B), −11.8 (4B), −13.1 (2B). Consistent with data previously reported.[57]

Preparation of **P5.1**.[58]

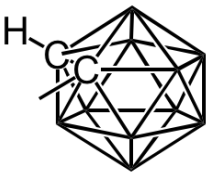

To a RBF was added magnesium turnings (0.41 g, 0.02 mmol) and anhydrous Et$_2$O (20 mL). This was heated to 30 °C and a solution of **P1.1** (3.34 g, 14.00 mmol) in anhydrous Et$_2$O (20 mL) was added drop wise via a dropping funnel. After three hours refluxing the solution was cooled and poured over 100 mL ice-cold water. The mixture was acidified with 1:1 hydrochloric acid : water and the aqueous phase was extracted with Et$_2$O (3 × 20 mL). The organic fractions were combined and dried over MgSO$_4$, filtered and the solvent removed *in vacuo*. The resulting residue was recrystallised from cold hexane (5 mL) to give the product as a white crystalline solid. Yield: 1.89 g, 11.80 mmol (84 %). ^{1}H NMR (300 MHz, CDCl$_3$): δ (ppm) 3.57 (br. s, 1H), 2.03 (s, 3H). ^{13}C{^{1}H} NMR (75 MHz, CDCl$_3$): δ (ppm) 70.5, 61.7, 26.0. ^{11}B{^{1}H} NMR (96 MHz, CDCl$_3$): δ (ppm) −1.8 (1B), −6.7 (1B), −9.2 (2B), −10.6 (2B), −11.3 (2B), −12.7 (2B). Anal. Calcd for $C_3H_{14}B_{10}$: C, 22.77; H, 8.92. Found: C, 22.72; H, 9.05.

Preparation of **P5.2**.

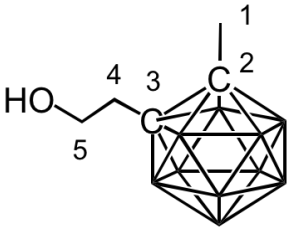

P5.1 (300 mg, 1.90 mmol) was added to a Schlenk flask and degassed. Anhydrous THF (10 mL) was added and cooled to -78°C. A 1. 6M solution of ^{n}BuLi in *n*-hexane (1.19 mL, 1.90 mmol) was added drop wise. This was stirred for 30 minutes at −78 °C. The temperature was then raised to 0 °C and a 2.5 M solution of ethylene oxide in anhydrous THF (1.13 mL, 2.81 mmol) was added

drop wise and stirred at 0 °C for 1 hour. The reaction was quenched by adding a saturated solution of NH_4Cl (5 mL) and the aqueous phase extracted with ethyl acetate (3 × 10 mL). The organic fractions were combined and dried over $MgSO_4$, filtered and solvent removed *in vacuo*. Hexane (3 mL) was added and cooled to −15 °C for 3 hours. The white crystals were filtered, washed with ice-cold hexane (5 mL) and dried *in vacuo.* Yield: 326 mg, 1.61 mmol (85 %). ^{1}H NMR (500 MHz, DMSO-d_6): δ (ppm) 4.87 (s, 1H, OH), 3.56 (t, J = 5 Hz, 2H, H^4), 2.44 (t, J = 5 Hz, 2H, H^3), 2.09 (s, 3H, H^1). ^{13}C NMR (126 MHz, DMSO-d_6): δ (ppm) 77.2 ($C^{2/3}$), 76.0 ($C^{2/3}$), 59.5 (C^5), 36.9 (C^4), 22.6 (C^1). ^{11}B{^{1}H} NMR (161 MHz, DMSO-d_6): δ (ppm) −4.9 (1B), −6.4 (1B), −8.9 (2B), −10.0 (2B), −10.9 (4B). Anal. Calcd for $C_5H_{18}B_{10}O$: C, 29.69; H, 8.97. Found: C, 29.77; H, 9.02.

Preparation of **P5.3**.

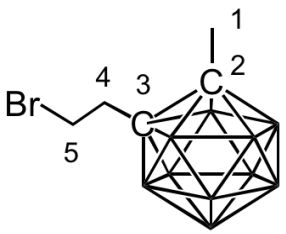

To a Schlenk flask was added **P5.1** (360 mg, 1.78 mmol) and anhydrous DCM (5 mL). This was cooled to 0 °C and PPh_3 (543 mg, 2.07 mmol) and NBS (368 mg, 2.07 mmol) was added and stirred at 0 °C for 3 hours. The organic phase was then washed with H_2O (4 × 10 mL), dried over $MgSO_4$, filtered and solvent removed *in vacuo*. Et_2O (10 mL) was added and filtered through a 5 cm silica plug and flushed with Et_2O (2 × 10 mL). The solvent was removed *in vacuo* to give the product as a white crystalline solid. Yield: 366 mg, 1.38 mmol (78 %). ^{1}H NMR (500 MHz, DMSO-d_6): δ (ppm) 3.60 (t, J = 10 Hz, 2H, H^4), 2.86 (t, J = 10 Hz, 2H, H^3), 2.12 (s, 3H, H^1). ^{13}C NMR (126 MHz, DMSO-d_6): δ (ppm) 76.9 ($C^{2/3}$), 76.2 ($C^{2/3}$), 36.5 (C^5), 28.9 (C^4), 22.4 (C^1). ^{11}B{^{1}H} NMR (161 MHz, DMSO-d_6): δ (ppm) −4.4 (1B), −6.3 (1B), −9.0 (2B), −9.9 (2B), −10.9 (4B). Anal. Calcd for $C_5H_{17}B_{10}Br$: C, 22.65; H, 6.46. Found: C, 22.77; H, 6.48.

Preparation of **P6.1**.[59]

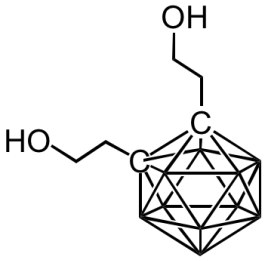

A 1.60 M solution of ^{n}BuLi in *n*-hexane (2.60 mL, 4.10 mmol) was added dropwise to a solution of *o*-carborane (300 mg, 2.08 mmol) in a dry toluene/Et_2O mixture (2:1, 30 mL) with stirring at 0 °C. The mixture was allowed to warm to room temperature and stirred for 30 minutes. The solution was then cooled to 0 °C, and a 2.5 M solution of ethylene oxide in anhydrous THF (2.46 mL, 6.00 mmol) was added. The reaction mixture was stirred at room temperature overnight and then quenched with 50 mL of water. The organic layer was separated, and the aqueous layer was extracted with Et_2O (2 × 30 mL). The combined organic portions were dried over anhydrous Na_2SO_4. Removal of the solvents gave a white solid that was washed with *n*-hexane (2 × 10 mL) and dried under vacuum to afford the product as a white powder. Yield: 445 mg,

1.91 mmol (92 %). Recrystallisation from dichloromethane yielded colourless crystals. ^{1}H NMR (500 MHz, DMSO-d_6): δ (ppm) 4.87 (br. s, 2H, OH), 3.54 (m, 4H, H^3), 2.45 (t, J = 7.5 Hz, 4H, H^2). ^{13}C{^{1}H} NMR (126 MHz, DMSO-d_6): δ (ppm) 78.5 (C^1), 59.6 (C^3), 36.7 (C^2). ^{11}B{^{1}H} NMR (161 MHz, DMSO-d_6): δ (ppm) −5.3 (2B), −10.8 (8B). Consistent with data previously reported.[59]

Preparation of **P6.2**.

Prepared as described for **P5.3** from **P6.1** (200 mg, 0.86 mmol), PPh_3 (262 mg, 1.00 mmol) and NBS (178 mg, 1.00 mmol) in anhydrous DCM (5 mL). After purification the product was obtained as a white crystalline solid. Yield: 276 mg, 0.77 mmol (90 %). ^{1}H NMR (300 MHz, DMSO-d_6): δ (ppm) 3.59 (m, 4H, H^3), 2.90 (m, 4H, H^2). ^{13}C{^{1}H} NMR (75 MHz, DMSO-d_6): δ (ppm) 78.8 (C^1), 36.1 (C^3), 29.0 (C^2). ^{11}B{^{1}H} NMR (96 MHz, DMSO-d_6): δ (ppm) −4.8 (2B), −10.5 (8B).

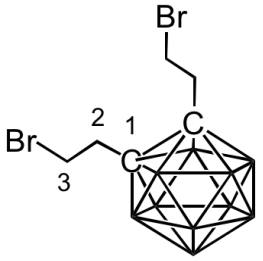

Preparation of **P7.1**.

A 1.60 M solution of ^{n}BuLi in *n*-hexane (2.64 mL, 4.3 mmol) was added dropwise to a solution of *m*-carborane (300 mg, 2.08 mmol) in anhydrous THF (5 mL) with stirring at 0 °C. The mixture was allowed to warm to room temperature and stirred for 30 minutes. The solution was then cooled to 0 °C, and an anhydrous THF solution of ethylene oxide (1.72 mL, 4.3 mmol). The reaction mixture was stirred at room temperature overnight and then quenched with water (50 mL). The organic layer was separated, and the aqueous layer was extracted with Et_2O (2 × 30 mL). The combined organic portions were dried over anhydrous Na_2SO_4. Removal of the solvents gave a white solid that was washed with *n*-hexane (2 × 10 mL) and dried under vacuum to afford the product as a white powder (207 mg, 0.89 mmol (43 %). ^{1}H NMR (300 MHz, DMSO-d_6) δ (ppm) 4.68 (t, J = 5.2 Hz, 2H, OH), 3.36 (m, 4H, H^3), 2.07 (t, J = 7.1 Hz, 4H, H^2). ^{13}C{^{1}H} NMR (75 MHz, DMSO-d_6): δ (ppm) 73.6 (C^1), 59.8 (C^3), 38.7 (C^2). ^{11}B{^{1}H} NMR (96 MHz, DMSO-d_6): δ −7.2 (2B), −11.4 (6B), −12.8 (2B).

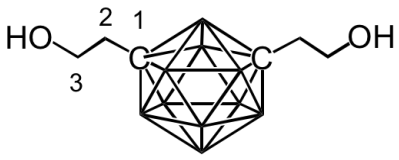

Preparation of **P7.2**.

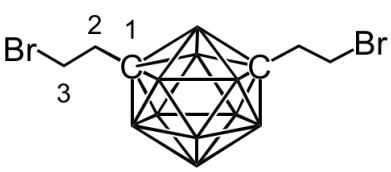

Prepared as described for **P5.3** from **P7.1** (200 mg, 0.86 mmol), PPh_3 (269 mg, 1.03 mmol) and NBS (182 mg, 1.03 mmol) in anhydrous DCM (5 mL). After purification the product was obtained as a white crystalline solid. Yield: 262 mg, 0.73 mmol (85 %). ^{1}H NMR (300 MHz, DMSO-d_6) δ (ppm) 3.42 (m, 4H, H^3), 2.52 (m, 4H, H^2). $^{13}C\{^{1}H\}$ NMR (75 MHz, DMSO-d_6): δ (ppm) 38.4 (C^3), 29.7 (C^2). $^{11}B\{^{1}H\}$ NMR (96 MHz, DMSO-d_6): δ (ppm) −7.1 (2B), −11.2 (6B), −13.4 (2B). Note: quaternary carboranyl carbon resonance not observed.

2.7.3 Imidazolium salts

Preparation of **P1.2**.[19]

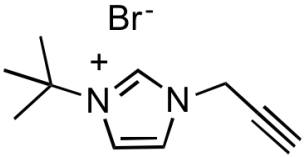

To a RBF was added MeCN (10 mL), ^{t}Bu-imidazole (4.10 g, 33.0 mmol) and propargyl bromide (7.30 mL, 66 mmol, 80 % wt. toluene). The resulting solution was stirred for 24 hours at 80 ºC and cooled to room temperature. The solvent was removed *in vacuo* and the residue washed with Et_2O (5 × 20 mL) then dried *in vacuo* to give a brown viscous oil. Yield: 6.50 g, 26.70 mmol (81 %). ^{1}H NMR (400 MHz, $CDCl_3$): δ (ppm) 10.65 (s, 1H), 7.62 (t, J = 1.8 Hz, 1H), 7.49 (t, J = 1.9 Hz, 1H), 5.52 (d, J = 2.6 Hz, 2H), 2.69 (t, J = 2.6 Hz, 1H), 1.73 (s, 9H). ^{13}C NMR (100 MHz, $CDCl_3$): δ (ppm) 136.0, 121.9, 119.4, 77.6, 74.6, 61.0, 40.0, 30.2. HRMS (ESI^+): *m/z* $[C_9H_{13}N_3]^+$ 163.1232, calcd for $[M + MeCN + H]^+$ 163.1109.

Preparation of **L2.1**.

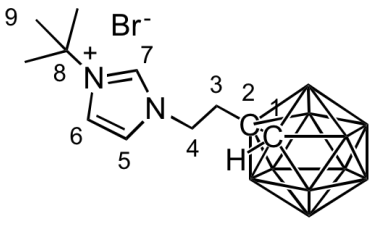

P2.1 (500 mg, 1.99 mmol), ^{t}Bu imidazole (246 mg, 1.98 mmol) and anhydrous toluene (3 mL) were added to an ampoule and heated at 100 °C for 18 hours. The reaction was cooled to room temperature, filtered, and the solid washed with toluene (3 × 10 mL) to give an off white crystalline solid. This was recrystallised from MeOH (3 mL) / Et_2O (30 mL), filtered and dried *in vacuo* to give the product as a white crystalline solid. Yield: 529 mg, 1.41 mmol (71 %). ^{1}H NMR (500 MHz, DMSO-d_6): δ (ppm) 9.41 (s, 1H, H^7), 8.03 (t, J = 1.9 Hz, 1H, H^5), 7.90 (t, J = 1.9 Hz, 1H, H^6), 5.38 (br. s, 1H, H^1), 4.33 (m, 2H, H^4), 2.99 (m, 2H, H^3), 1.57 (s, 9H, H^9). $^{13}C\{^{1}H\}$ NMR (126 MHz, DMSO-d_6): δ (ppm) 135.0 (C^7), 122.7 (C^6), 120.1 (C^5), 72.5 (C^2), 63.2 (C^1), 59.6 (C^8), 47.0 (C^4), 35.2 (C^3), 28.9 (C^9). $^{11}B\{^{1}H\}$ NMR (161 MHz, DMSO-d_6): δ (ppm) −2.8 (1B), −5.5 (1B), −9.6 (2B), −11.8 (6B). HRMS (ESI^+): *m/z* $[C_{11}H_{27}B_{10}N_2]^+$ 295.3188, calcd for $[M - Br]^+$ 295.3177. Anal. Calcd for $C_{11}H_{27}B_{10}N_2Br$: C,

35.20; H, 7.25; N, 7.46. Found: C, 34.90; H, 7.30; N, 7.10. Crystals suitable for X-ray diffraction analysis were grown by the slow diffusion of Et_2O into a concentrated solution of the product in MeCN.

Preparation of **L2.3**.

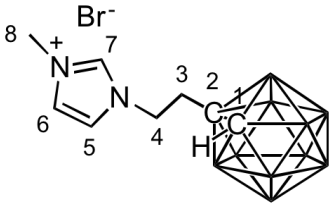

Prepared as described from **L2.1** from **P2.1** (500 mg, 1.99 mmol) and methyl imidazole (162 mg, 1.97 mmol) in anhydrous toluene (3 mL). Following purification the product was isolated as a fluffy crystalline white solid. Yield: 490 mg, 1.47 mmol (75 %). ^{1}H NMR (500 MHz, DMSO-d_6): δ (ppm) 9.21 (s, 1H, H^7), 7.84 (t, J = 1.7 Hz, 1H, H^5), 7.71 (t, *J* = 1.7 Hz, 1H, H^6), 5.37 (br. s, 1H, H^1), 4.35 (m, 2H, H^4), 3.86 (s, 3H, H^8), 2.94 (m, 2H, H^3). ^{13}C{^{1}H} NMR (126 MHz, DMSO-d_6): δ (ppm) 137.0 (C^7), 123.6 (C^6), 122.3 (C^5), 72.5 (C^2), 63.1 (C^1), 46.9 (C^4), 35.8 (C^8), 35.3 (C^3). ^{11}B{^{1}H} NMR (161 MHz, DMSO-d_6): δ (ppm) −3.0 (1B), −5.6 (1B), −9.7 (2B), −11.8 (4B), −12.9 (2B). HRMS (ESI$^+$): *m/z* $[C_8H_{21}B_{10}N_2]^+$ 253.2714, calcd for $[M - Br]^+$ 253.2706. Anal. Calcd for $C_8H_{21}B_{10}N_2Br$: C, 28.83; H, 6.35; N, 8.41. Found: C, 28.72; H, 6.41; N, 8.27.

Preparation of **L2.4**.

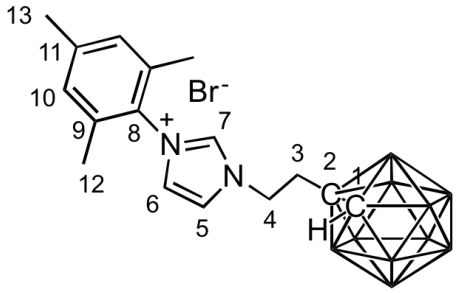

Prepared as described for **L2.1** from mesityl imidazole (445 mg, 2.39 mmol) and **P2.1** (600 mg, 2.39 mmol) in anhydrous toluene (3 mL). After purification the product is obtained as a white crystalline solid. Yield: 774 mg, 1.77 mmol (74 %). ^{1}H NMR (500 MHz, DMSO-d_6): δ (ppm) 9.53 (t, J = 1.4 Hz, 1H, H^7), 8.18 (t, *J* = 1.7 Hz, 1H, H^5), 7.95 (t, *J* = 1.8 Hz, 1H, H^6), 7.15 (s, 2H, H^{10}), 5.38 (s, 1H, H^1), 4.46 (t, *J* = 7.6 Hz, 2H, H^4), 3.12 (t, *J* = 7.6 Hz, 2H, H^3), 2.33 (s, 3H, H^{13}), 2.02 (s, 6H, H^{12}). ^{13}C NMR (126 MHz, DMSO-d_6): δ (ppm) 140.3 (C^{11}), 137.9 (C^7), 134.2 (C^9), 131.0 (C^8), 129.3 (C^{10}), 123.9 (C^6), 123.1 (C^5), 72.7 (C^2), 63.4 (C^1), 47.7 (C^4), 34.8 (C^3), 20.6 (C^{13}), 16.9 (C^{12}). ^{11}B{^{1}H} NMR (161 MHz, DMSO-d_6): δ (ppm) −3.0 (1B), −5.5 (1B), −9.7 (2B), −12.1 (6B). HRMS (ESI$^+$): *m/z* $[C_{16}H_{29}B_{10}N_2]^+$ 357.3343, calcd for $[M - Br]^+$ 357.3336.

Preparation of **L2.5**

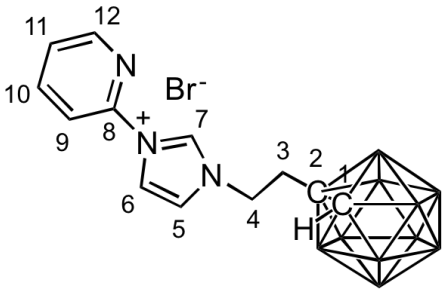

Prepared as described for **L2.1** from pyridyl imidazole (371 mg, 2.56 mmol) and **P2.1** (500 mg, 2.56 mmol) in anhydrous toluene (3 mL). After purification the product is obtained as a white crystalline solid. Yield: 699 mg, 1.82 mmol, (71 %). ^{1}H NMR (500 MHz, DMSO-d$_6$): δ (ppm) 10.21 (s, 1H, H^{7}), 8.67 (m, 1H, H^{Aryl}), 8.54 (t, *J* = 1.7 Hz, 1H, H^{6}), 8.23 (td, *J* = 8.1, 1.7 Hz, 1H, H^{Aryl}), 8.11 (s, 1H, H^{5}), 8.04 (m, 1H, H^{Aryl}), 7.66 (m, 1H, H^{Aryl}), 5.38 (br. s, 1H, H^{1}), 4.48 (m, 2H, H^{4}), 3.07 (m, 2H, H^{3}).^{13}C NMR (126 MHz, DMSO-d$_6$): δ (ppm) 149.3 (C^{Aryl}), 146.2 (C^{8}), 140.7 (C^{Aryl}), 135.6 (C^{7}), 125.3 (C^{Aryl}), 123.6 (C^{5}), 119.1 (C^{6}), 114.1 (C^{Aryl}), 72.5 (C^{2}), 63.1 (C^{1}), 47.6 (C^{4}), 35.1 (C^{3}). ^{11}B{^{1}H} NMR (161 MHz, DMSO-d$_6$): δ (ppm) −2.9 (1B), −5.6 (1B), −9.7 (2B), −11.8 (6B). HRMS (ESI^{+}): *m/z* [C$_{11}$H$_{22}$B$_{10}$N$_3$]$^{+}$ 317.2784, calcd for [M − Br]$^{+}$ 317.2781.

Preparation of **L3.1**.

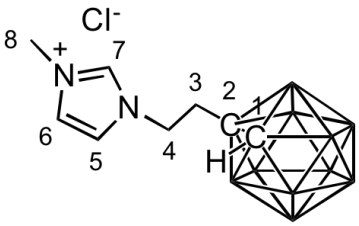

P3.2 (200 mg, 0.96 mmol), 1-methylimidazole (79 mg, 0.96 mmol) and anhydrous toluene (2 mL) was added to an ampoule and heated at 100 °C for 72 hours. The reaction was then cooled to rt and solvent removed *in vacuo*. Methanol (3 mL) was added and insoluble white precipitate filtered and dried *in vacuo*. The product was obtained as colourless crystals by slow diffusion of Et$_2$O into the concentrated methanol filtrate. Yield: 20 mg, 0.07 mmol, (7 %). ^{1}H NMR (300 MHz, DMSO-d$_6$): δ 9.34 (s, 1H, imidazolium H^{7}), 7.90 (s, 1H, imidazolium H^{6}), 7.72 (s, 1H, imidazolium H^{5}), 5.62 (br. s, 1H, H^{1}), 4.37 (t, *J* = 9 Hz, 2H, H^{4}), 3.86 (s, 3H, H^{8}), 2.97 (m, 2H, H^{3}). ^{13}C NMR (75 MHz, DMSO-d$_6$): δ 137.0 (C^{7}), 123.5 (C^{6}), 122.3 (C^{5}), 72.6 (C^{2}), 63.2 (C^{1}), 47.0 (C^{4}), 35.8 (C^{8}), 35.4 (C^{3}). ^{11}B{^{1}H} NMR (96 MHz, DMSO-d$_6$): δ −3.2 (1B), −5.6 (1B), −9.8 (2B), −12.1 (6B). HRMS (ESI^{+}): *m/z* [C$_8$H$_{21}$B$_{10}$N$_2$]$^{+}$ 253.2714, Calcd for [M − Cl]$^{+}$ 253.2706.

Preparation of **L5.1**.

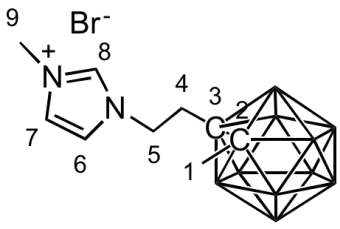

Prepared as described for **L2.1** from **P5.3** (100 mg, 0.38 mmol) and 1-methylimidazole (31 mg, 0.38 mmol) in anhydrous toluene (1 mL), with a reaction time of 6 hours. After purification the product was obtained as a fluffy crystalline white solid. Yield: 79 mg, 0.23 mmol (60 %). ^{1}H NMR (300 MHz, CD$_3$OD): δ (ppm) 9.07 (s, 1H, H^{8}), 7.75 (m, 1H, H^{7}), 7.59

(m, 1H, H^6), 4.46 (m, 2H, H^5), 3.93 (s, 3H, H^9), 2.95 (m, 2H, H^4), 2.15 (s, 3H, H^1). $^{13}C\{^1H\}$ NMR (75 MHz, CD_3OD): δ (ppm) 138.5 (C^8), 125.1 (C^7), 123.8 (C^6), 77.5 (C^3), 75.6 (C^2), 48.9 (C^5), 36.6 (C^4), 35.2 (C^9), 23.6 (C^1). $^{11}B\{^1H\}$ NMR (96 MHz, CD_3OD): δ (ppm) −3.9 (1B), −5.9 (1B), −9.6 (4B), −10.5 (4B). HRMS (ESI^+): m/z $[C_9H_{23}B_{10}N_2]^+$ 267.2875, calcd for $[M - Br]^+$ 267.2863. Anal. Calcd for $C_9H_{23}B_{10}N_2Br$: C, 31.13; H, 6.68; N, 8.07. Found: C, 31.02; H, 6.79; N, 8.12.

Preparation of **L7.1**.

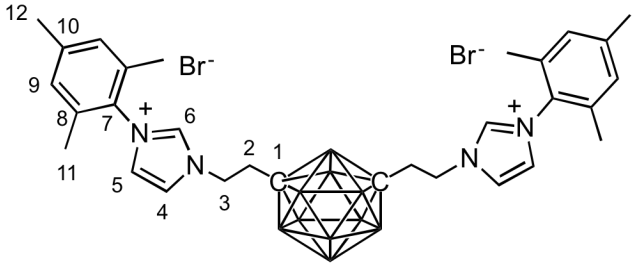

P7.2 (50 mg, 0.14 mmol), mesityl imidazole (52 mg, 0.28 mmol) and anhydrous CD_3CN (0.70 mL) were added to a Young's Tap NMR tube in the glove box. The reaction mixture was heated at 80 °C for 86 hours. The reaction was cooled to room temperature and the product precipitated as a white solid. This was filtered and washed with MeCN (5 mL) then Et_2O (30 mL) and dried *in vacuo* to yield a crystalline white solid. Yield: 55 mg, 0.08 mmol (54 %). ^1H NMR (300 MHz, CD_3OD): δ 9.31 (s, 1H, H^6), 8.01 (t, J = 1.8 Hz, 1H, H^5), 7.75 (t, J = 1.8 Hz, 1H, H^4), 7.14 (s, 2H, H^9), 4.46 (m, 2H, H^3), 2.84 (m, 2H, H^2), 2.37 (s, 3H, H^{12}), 2.08 (s, 6H, H^{11}). $^{11}B\{^1H\}$ NMR (96 MHz, CD_3OD): δ −10.8. Note: $^{11}B\{^1H\}$ NMR spectrum very broad with only one resonance.

2.7.4 Zwitterionic ligands

Preparation of **L1.2**

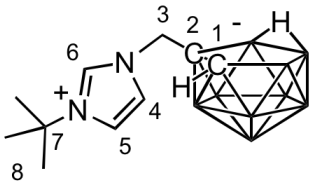

To a solution of **I1** (3.68 g, 29.60 mmol) in toluene (10 mL) was added **P1.1** (2.35 g, 9.91 mmol), and the reaction mixture was stirred at 110 ºC for 24 hours. The solvent was removed *in vacuo* to afford a brown oil. The product was obtained as a white solid by recrystallisation from MeCN (10 mL) with Et_2O (30 mL). Yield: 2.51 g, 9.27 mmol (93 %). ^1H NMR (CD_3CN, 500 MHz): δ (ppm) 8.52 (s, 1H, H^6), 7.58 (s, 1H, H^5), 7.53 (s, 1H, H^4), 4.31 (d, J = 14.0 Hz, 1H, H^3), 4.12 (d, J = 14.0 Hz, 1H, H^3), 1.64 (s, 9H, H^8). $^{13}C\{^1H\}$ NMR (75 MHz, DMSO-d_6): δ (ppm) 134.1 (C^6), 122.2 (C^5), 120.2 (C^4), 59.4 (C^7), 57.0 (C^2), 56.3 (C^3), 43.8 (C^1), 29.1 (C^8). $^{11}B\{^1H\}$ NMR (CD_3CN, 96 MHz): δ (ppm) −10.6 (2B), −14.7 (2B), −19.4 (2B), −21.1 (1B), −32.6 (1B), −36.68 (1B). HRMS (ESI^+): m/z $[C_{10}H_{26}B_9N_2]$ 273.2735, calcd for $[M + H]^+$ 273.2933.

Preparation of **L1.3**

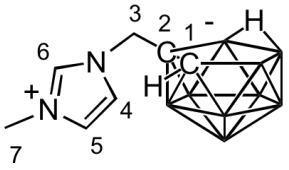

To a stirred solution of **P1.1** (320 mg, 1.35 mmol) in toluene (5 mL) was added 1-methylimidazole (550 mg, 6.70 mmol). The reaction mixture was stirred at room temperature for seven days then concentrated *in vacuo*. The solid was sonicated, filtered and washed with ^{i}PrOH to give the product as a white solid. Yield: 94 mg, 0.41 mmol (30 %) as a white powder. ^{1}H NMR (CD_3CN, 300 MHz): δ (ppm) 8.41 (s, 1H, H^6), 7.44 (s, 1H, H^5), 7.34 (s, 1H, H^4), 4.31 (d, J = 14.4 Hz, 1H, H^3), 4.11 (d, J = 14.6 Hz, 1H, H^3), 3.86 (s, 3H, H^7). ^{13}C{^{1}H} NMR (75 MHz, DMSO-d_6): δ (ppm) 136.0 (C^6), 123.4 (C^5), 122.4 (C^4), 57.0 (C^2), 56.3 (C^3), 43.7 (C^1), 35.8 (C^7). ^{11}B{^{1}H} NMR (CD_3CN, 96 MHz): δ (ppm) −10.5 (2B), −14.6 (2B), −19.1 (2B), −21.0 (1B), −32.6 (1B), −36.7 (1B). HRMS (ESI^+): m/z [$C_7H_{19}B_9N_2Na$] 253.2289, calcd for $[M + Na]^+$ 253.2283.

Preparation of **L2.2**.

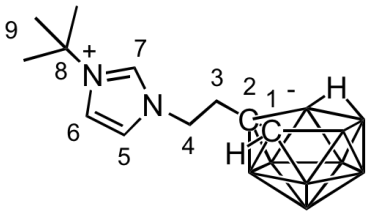

To a solution of **I1** (4.00 g, 32.20 mmol) in toluene (10 mL) was added **P2.1** (1.60 g, 6.37 mmol), and the reaction mixture was stirred at 110 ºC for 24 hours. The solvent was removed *in vacuo* to afford a brown oil to which MeOH (10 mL) was added to precipitate the product. This was filtered, washed with MeOH (3 × 10 mL) and dried *in vacuo* to afford the product as a white solid. Yield: 1.18 g, 4.14 mmol (65 %). ^{1}H NMR (501 MHz, DMSO-d_6): δ (ppm) 9.27 (t, J = 1.6 Hz, 1H, H^7), 8.03 (t, J = 1.9 Hz, 1H, H^5), 7.83 (t, J = 1.8 Hz, 1H, H^6), 4.17 (td, J = 6.8, 1.1 Hz, 2H, H^4), 2.11 (m, 1H, H^3), 1.94 (m, 1H, H^3), 1.62 (s, 9H, H^9), 1.55 (br. s, 1H, H^1). ^{13}C{^{1}H} NMR (126 MHz, DMSO-d_6): δ (ppm) 134.5 (C^7), 122.8 (C^6), 120.2 (C^5), 59.3 (C^8), 56.1 (C^2), 50.1 (C^4), 44.7 (C^1), 38.9 (C^3), 29.0 (C^9). ^{11}B{^{1}H} NMR (161 MHz, DMSO-d_6): δ (ppm) −11.1 (2B), −14.2 (1B), −15.9 (1B), −19.4 (2B), −21.6 (1B), −33.2 (1B), −37.3 (1B). HRMS (ESI^+): *m/z* $[C_{11}H_{28}B_9N_2]^+$ 286.3131, calcd for $[M + H]^+$ 286.3126. Anal. Calcd for $C_{11}H_{27}B_9N_2$: C, 46.42; H, 9.56; N, 9.84. Found: C, 46.60; H, 9.65; N, 9.80. Crystals suitable for X-ray diffraction analysis were grown by the slow diffusion of Et_2O into a concentrated solution of the product in MeCN.

Preparation of **L2.10**.

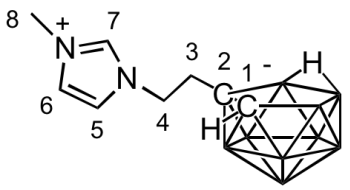

Prepared as described for **L2.2**, from **P2.1** (462 mg, 1.84 mmol) and 1-methylimidazole (205 mg, 2.5 mmol). Following purification the product was isolated as a fluffy crystalline white solid. Yield: 334 mg, 1.38 mmol (75 %). ^{1}H NMR (500 MHz, DMSO-d_6): δ (ppm) 9.12 (s, 1H, H^7), 7.73 (t, J = 1.7 Hz,

1H, H^5), 7.67 (t, *J* = 1.7 Hz, 1H, H^6), 4.15 (m, 2H, H^4), 3.84 (s, 3H, H^8), 2.05 (m, 1H, H^3), 1.89 (m, 1H, H^3), 1.57 (br. s, 1H, H^1). ^{13}C NMR (126 MHz, DMSO-d_6): δ (ppm) 136.6 (C^7), 123.4 (C^6), 122.5 (C^5), 56.2 (C^2), 50.1 (C^4), 44.8 (C^1), 39.0 (C^3) 35.6 (C^8). ^{11}B{^{1}H} NMR (161 MHz, DMSO-d_6): δ (ppm) −11.0 (1B), −11.4 (1B), −14.3 (1B), −15.8 (1B), −19.5 (2B), −21.6 (1B), −33.2 (1B), −37.3 (1B). HRMS (ESI$^+$): *m/z* $[C_8H_{21}B_9N_2Na]^+$ 266.2478, calcd for $[M + Na]^+$ 266.2476.

Preparation of **L4.1**

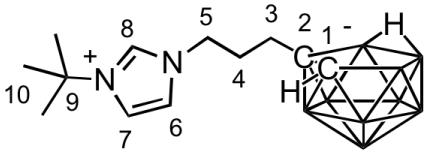

To a stirred solution of **P4.1** (150 mg, 0.68 mmol) in toluene (5mL) was added ^{t}Bu-imidazole (422 mg, 3.40 mmol). The reaction mixture was heated at reflux for seven days then concentrated *in vacuo*. The residue was recrystallised from MeCN (5 mL) with Et_2O (20 mL) to give the product as a beige powder. Yield: 147 mg, 0.49 mmol (72 %). ^{1}H NMR (DMSO-d_6, 300 MHz): δ (ppm) 9.23 (s, 1H, H^8), 7.98 (s, 1H, $H^{7/6}$), 7.83 (s, 1H, $H^{7/6}$), 4.04 (m, 2H, H^5), 1.91 (s, 9H, H^4), 1.58 (s, 9H, H^{10}), 1.44 (m, 2H, H^3). ^{13}C{^{1}H} NMR (DMSO-d_6, 75 MHz): δ (ppm) 134.8 (C^8), 124.0 ($C^{7/6}$), 120.7 ($C^{7/6}$), 59.8 (C^9), 49.5 (C^5), 35.9 (C^4), 31.7 (C^3), 29.5 (C^9). ^{11}B{^{1}H} NMR (CD_3CN, 96 MHz): δ (ppm) −11.19 (2B), −14.03 (1B), −16.63 (1B), −19.02 (2B), −21.97 (1B), −33.43 (1B), −37.29 (1B). HRMS (ESI$^+$): *m/z* $[C_{12}H_{30}B_9N_2Na]^+$ 323.3073, calcd for $[M + Na]^+$ 323.3066. Note: in the ^{1}H NMR spectrum H^1 is masked by the H^{10} and H^3 signals, and in the ^{13}C{^{1}H} NMR spectrum the C^2 and C^1 resonances are too broad to assign.

Preparation of **L4.2**

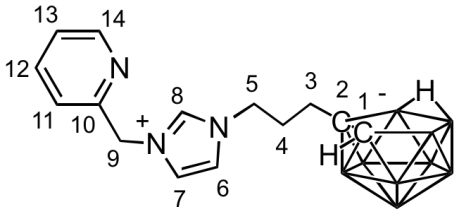

To a stirred solution of **P4.1** (150 mg, 0.68 mmol) in toluene (5 mL) was added picolylimidazole (541 mg, 3.40 mmol). The reaction mixture was heated at reflux for seven days then concentrated *in vacuo*. The residue was recrystallised from MeOH (5 mL) with H_2O (10 mL) to give the product as colourless crystals. Yield: 70 mg, 0.21 mmol (31 %). ^{1}H NMR (300 MHz, DMSO-d_6): δ (ppm) 9.28 (s, 1H, H^8), 8.54 (ddd, *J* = 4.8, 1.6, 0.9 Hz, 1H, H^{Aryl}), 7.88 (td, *J* = 7.7, 1.8, 1H, H^{Aryl}), 7.79 (t, *J* = 1.7 Hz, 1H, $H^{7/6}$), 7.76 (t, *J* = 1.7 Hz, 1H, $H^{7/6}$), 7.47 (m, *J* = 7.8 Hz, 1H, H^{Aryl}), 7.40 (ddd, *J* = 7.5, 4.9, 0.9 Hz, 1H, H^{Aryl}), 5.55 (s, 2H, H^9), 4.13 (t, *J* = 7.1 Hz, 2H, H^5), 1.88 (m, 2H, H^4), 1.64 (br. s, 1H, H^1), 1.46 (m, 2H, H^3), -2.85 (B-H-B). ^{13}C NMR (75 MHz, DMSO-d_6): δ (ppm) 153.6 (C^{10}), 149.5 (C^8), 137.5 (C^{Aryl}), 136.8 (C^{Aryl}), 123.6 (C^{Aryl}), 123.3 (C^{Aryl}), 122.4 ($C^{7/6}$), 122.3 ($C^{7/6}$), 58.5 (C^2), 53.0 (C^9), 49.0 (C^5), 45.6 (C^1), 35.2 (C^4), 31.2 (C^3). ^{11}B{^{1}H} NMR (161 MHz,

DMSO-d_6): δ (ppm) −11.2 (2B), −14.2 (1B), −17.0 (1B), −18.9 (2B), −22.2 (1B), −33.4 (1B), −37.2 (1B). HRMS (ESI^+): *m/z* $[C_{14}H_{26}B_9N_3Na]^+$ 357.2904, calcd. for $[M + Na]^+$ 357.2898.

Preparation of **L4.3**

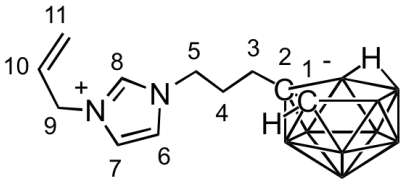

To a stirred solution of **P4.1** (150 mg, 0.68 mmol) in toluene (5 mL) was added allylimidazole (368 mg, 3.40 mmol). The reaction mixture was heated at reflux for seven days then concentrated *in vacuo*. The residue was recrystallised from MeCN (5 mL) with Et_2O (20 mL) to give the product as a white powder. Yield: 46 mg, 0.16 mmol (24 %). ^1H NMR (300 MHz, CD_3CN): δ (ppm) 8.44 (s, 1H, H^8), 7.96 (t, *J* = 1.7 Hz, 1H, $H^{7/6}$), 7.89 (t, *J* = 7.1 Hz, 1H, $H^{7/6}$), 6.03 (m, 1H, H^{10}), 5.40 (m, 2H, H^9), 4.73 (m, 2H, H^{11}), 4.09 (t, *J* = 7.3Hz, 2H, H^5), 2.01 (m, 2H, H^4), 1.69 (br. s, 1H, H^1), 1.59 (m, 2H, H^3), -2.77 (br. s, 1H, B-H-B). ^{13}C NMR (75 MHz, DMSO-d_6): δ (ppm) 149.1 (C^8), 140.5, 135.0, 125.1, 123.5, 119.2, 114.2, 58.5 (C^2), 49.7 (C^5), 45.7 (C^1), 35.3 (C^4), 31.0 (C^3). $^{11}B\{^1H\}$ NMR (96 MHz, CD_3CN): δ (ppm) −11.2 (2B), −14.1 (1B), −16.6 (1B), −19.0 (2B), −22.0 (1B), −33.4 (1B), −37.3 (1B). HRMS (ESI^+): *m/z* $[C_{11}H_{25}B_9N_2Na]^+$ 306.2794, calcd. for $[M + Na]^+$ 306.2789.

2.8 References

1 H. Debus, *Ann. der Chemie und Pharm.*, 1858, **107**, 199–208.

2 B. Radzisewski, *Berichte der Dtsch. Chem. Gesellschaft*, 1882, **15**, 2706–2708.

3 C.-C. S. Cheung, R. A. Beaudet and G. A. Segal, *J. Am. Chem. Soc.*, 1970, **92**, 4158–4164.

4 D. A. Dixon, D. A. Kleier, T. A. Halgren, J. H. Hall and W. N. Lipscomb, *J. Am. Chem. Soc.*, 1977, **99**, 6226–6237.

5 M. J. S. Dewar and M. L. McKee, *Inorg. Chem.*, 1980, **19**, 2662–2672.

6 M. G. Davidson, M. A. Fox, T. G. Hibbert, J. A. K. Howard, A. Mackinnon, I. S. Neretin and K. Wade, *Chem. Commun.*, 1999, **92**, 1649–1650.

7 A. S. Batsanov, R. C. B. Copley, M. G. Davidson, M. A. Fox, T. G. Hibbert, J. A. K. Howard and K. Wade, *J Clust. Sci*, 2006, **17**, 119–137.

8 Y. Taoda, T. Sawabe, Y. Endo, K. Yamaguchi, S. Fujii and H. Kagechika, *Chem. Commun.*, 2008, **92**, 2049–2051.

9 R. A. Wiesboeck and M. F. Hawthorne, *J. Am. Chem. Soc.*, 1964, **86**, 1642–1643.

10 M. F. Hawthorne, D. C. Young, P. M. Garrett, D. A. Owen, S. G. Schwerin, F. N. Tebbe and P. A. Wegner, *J. Am. Chem. Soc.*, 1968, **90**, 862–868.

11 L. I. Zakharkin and V. N. Kalinin, *Tetrahedron Lett.*, 1965, **6**, 407–409.

12 H. Tomita, H. Luu and T. Onak, *Inorg. Chem.*, 1991, **30**, 812–815.

13 M. A. Fox, W. R. Gill, P. L. Herbertson, J. A. H. MacBride, K. Wade and H. M. Colquhoun, *Polyhedron*, 1996, **15**, 565–571.

14 T. D. Getman, *Inorg. Chem*, 1998, **37**, 3422–3423.

15 Jeongsoo Yoo, J.-W. Hwang and Y. Do, *Inorg. Chem.*, 2001, **40**, 568–570.

16 John J. Schaeck and S. B. Kahl, *Inorg. Chem.*, 1998, **38**, 204–206.

17 L. O. Kononov, A. V. Orlova, A. I. Zinin, B. G. Kimel, I. B. Sivaev and V. I. Bregadze, *J. Organomet. Chem.*, 2005, **690**, 2769–2774.

18 C. L. Powell, M. Schulze, S. J. Black, A. S. Thompson and M. D. Threadgill, *Tetrahedron Lett.*, 2007, **48**, 1251–1254.

19 M. T. Zamora, M. J. Ferguson, R. McDonald and M. Cowie, *Organometallics*, 2012, **31**, 5463–5477.

20 A. Toppino, A. R. Genady, M. E. El-Zaria, J. Reeve, F. Mostofian, J. Kent and J. F. Valliant, *Inorg. Chem.*, 2013, **52**, 8743–8749.

21 K. Li, Y. Wang, G. Yang, S. Byun, G. Rao, C. Shoen, H. Yang, A. Gulati, D. C. Crick, M. Cynamon, G. Huang, R. Docampo, J. H. No and E. Oldfield, *ACS Infect. Dis.*, 2015, **1**, 215–221.

22 G. M. Edvenson and D. F. Gaines, *Inorg. Chem.*, 1990, **29**, 1210–1216.

23 R. A. Hegstrom, M. D. Newton, J. A. Potenza and W. N. Lipscomb, *J. Am. Chem. Soc.*, 1966, **88**, 5340–5342.

24 F. Teixidor, C. Vinas and R. W. Rudolph, *Inorg. Chem.*, 1986, **25**, 3339–3345.

25 S. Heřmánek, J. Plešek, V. Gregor and B. Štíbr, *J. Chem. Soc., Chem. Commun.*, 1977, 561–563.

26 S. Heřmánek and J. Plešek, *Allg. Chem.*, 1974, **409**, 115–120.

27 L. A. Leites, L. E. Vinogradova, S. S. Bukalov and V. I. Aleksanyan, *Bull. Acad. Sci. U. S. S. R., Chem. Div.*, 1975, 492–496.

28 R. P. Alexander and H. Schroeder, *Inorg. Chem.*, 1963, **2**, 1107–1110.

29 H. Schroeder, T. L. Heying and J. R. Reiner, *Inorg. Chem.*, 1963, **2**, 1092–1096.

30 L. A. Leites, L. E. Vinogradova, V. N. Kalinin and L. I. Zakharkin, *Bull. Acad. Sci. U. S. S. R., Chem. Div.*, 1968, 970–977.

31 L. A. Leites, L. E. Vinogradova, V. I. Aleksanyan and S. S. Bukalov, *Bull. Acad. Sci. U. S. S. R., Chem. Div.*, 1976, 2311–2317.

32 L. A. Leites, *Chem. Rev.*, 1992, **92**, 279–323.

33 F. E. Hahn and M. C. Jahnke, *Angew. Chemie Int. Ed.*, 2008, **47**, 3122–3172.

34 A. McAnaw, G. Scott, L. Elrick, G. M. Rosair and A. J. Welch, *Dalton Trans.*, 2013, **42**, 645–64.

35 J. R. Coombs, L. Zhang and J. P. Morken, *J. Am. Chem. Soc.*, 2014, **136**, 16140–16143.

36 P. Barbier, *Compt. Rend. 128:110*, 1899.

37 M. F. Hawthorne, T. D. Andrews, P. M. Garrett, F. P. Olsen, M. Reintjes, F. N. Tebbe, L. F. Warren, P. A. Wegner, D. C. Young, R. P. Alexander, R. W. Blundon, H. A. Schroeder and T. L. Heying, in *Inorg. Syntheses*, John Wiley & Sons, Inc., 1967, pp. 91–118.

38 C. J. Moulton and B. L. Shaw, *J. Chem. Soc., Dalt. Trans.*, 1976, 1020–1024.

39 J. I. van der Vlugt and J. N. H. Reek, *Angew. Chemie Int. Ed.*, 2009, **48**, 8832–8846.

40 M. E. O'Reilly and A. S. Veige, *Chem. Soc. Rev.*, 2014, **43**, 6325.

41 Q. Y. and and M. Sheets, *J. Org. Chem.*, 2006, **71**, 5384–5387.

42 D. Benito-Garagorri and K. Kirchner, *Acc. Chem. Res.*, 2008, **41**, 201–213.

43 J. I. van der Vlugt, *Angew. Chemie Int. Ed.*, 2010, **49**, 252–255.

44 Y. Segawa, M. Yamashita and K. Nozaki, *J. Am. Chem. Soc.*, 2009, **131**, 9201–9203.

45 Y. Segawa, M. Yamashita and K. Nozaki, *Organometallics*, 2009, **28**, 6234–6242.

46 A. M. Spokoyny, M. G. Reuter, C. L. Stern, M. A. Ratner, T. Seideman and C. A. Mirkin, *J. Am. Chem. Soc.*, 2009, **131**, 9482–9483.

47 M. E. El-Zaria, H. Arii and H. Nakamura, *Inorg. Chem.*, 2011, **50**, 4149–4161.

48 S. E. Howson, L. E. N. Allan, N. P. Chmel, G. J. Clarkson, R. J. Deeth, A. D. Faulkner, D. H. Simpson, P. Scott, H. A. Musallam, J. G. Vos and N. Zhu, *Dalt. Trans.*, 2011, **40**, 10416.

49 G. Occhipinti, V. R. Jensen, K. W. Törnroos, N. Å. Frøystein and H.-R. Bjørsvik, *Tetrahedron*, 2009, **65**, 7186–7194.

50 A. Raba, M. R. Anneser, D. Jantke, M. Cokoja, W. A. Herrmann and F. E. Kühn, *Tetrahedron Lett.*, 2013, **54**, 3384–3387.

51 S. Majumdar, M. M. Spaeth, S. Sivendran, J. Juntunen, J. D. Thomas and K. B. Sloan, *Tetrahedron Lett.*, 2007, **48**, 4609–4611.

52 P. L. Chiu, C-L. Lai, C-F. Chang, and C-H. Hu and H. M. Lee, *Organometallics*, 2005, **24**, 6169–6178.

53 R. Schaeffer, *J. Am. Chem. Soc.*, 1957, **79**, 1006–1007.

54 T. L. Heying, J. W. Ager, S. L. Clark, D. J. Mangold, H. L. Goldstein, M. Hillman, R. J. Polak and J. W. Szymanski, *Inorg. Chem.*, 1963, **2**, 1089–1092.

55 A. Leyva-Perez, J. R. Cabrero-Antonino, P. Rubio-Marques, S. I. Al-Resayes and A. Corma, *ACS Catal.*, 2014, **4**, 722–731.

56 M. M. Fein, D. Grafstein, J. E. Paustian, J. Bobinski, B. M. Lichstein, N. Mayes, N. N. Schwartz and M. S. Cohen, *Inorg. Chem.*, 1963, **2**, 1115–1119.

57 J. Yoo, Y. Do, M. Lamrani, C. Vinas, R. Sillanpaeae, R. Kivekaes, H. Mueller, E. Sorkau and E. Sinn, *Dalt. Trans.*, 2009, **16**, 4978.

58 M. F. Hawthorne, T. D. Andrews, P. M. Garrett, F. P. Olsen, M. Reintjes, F. N. Tebbe, L. F. Warren, P. A. Wegner, D. C. Young, R. P. Alexander, R. W. Blundon, H. A. Schroeder and T. L. Heying, in *Inorganic Syntheses*, John Wiley & Sons, Inc., 1967, pp. 91–118.

59 M-S. Cheung, A. H-S. Chan and Z. Xie, *Organometallics*, 2003, **23**, 517–526.

Chapter 3

Unique ligands that exhibit unprecedented and versatile coordination at early to mid transition metals

This chapter discusses the synthetic challenges associated with deprotonation of the zwitterionic ligand precursors reported in Chapter 2. A deprotonation study revealed that the ligand must possess an ethyl linker or longer between the imidazolium and the carborane for a free carbene to be isolated. Subsequent coordination to various metal centres, including titanium, iron and rhodium, is explored.

3.1 Introduction

3.1.1 Applications of rhodocarboranes

Hawthorne and co-workers were the first to report the utility of metallacarboranes in homogenous catalysis, by use of a rhodocarborane.[1] The complex was prepared by reacting the tris(triphenyl-phosphine)rhodium^{I} cation with [7,8-$C_2B_9H_{12}$]$^-$ in methanol at 60 °C, with formation of the product being considered to arise by oxidative addition of the bridging proton of the cage to the unsaturated Rh^{I} centre to give a η^5-coordinating Rh^{III} complex (**i**) (**Scheme 3.1**). The rhodocarborane was shown to be catalytically active in the isomerisation and hydrogenation of alkenes,[1] hydrosilyation of ketones[1] and the exchange of terminal BH bonds with deuterium gas.[2] These type of systems have been extensively studied, and in many the most catalytically active species is an *exo-nido* tautomer generated in solution (**ii**).[3,4]

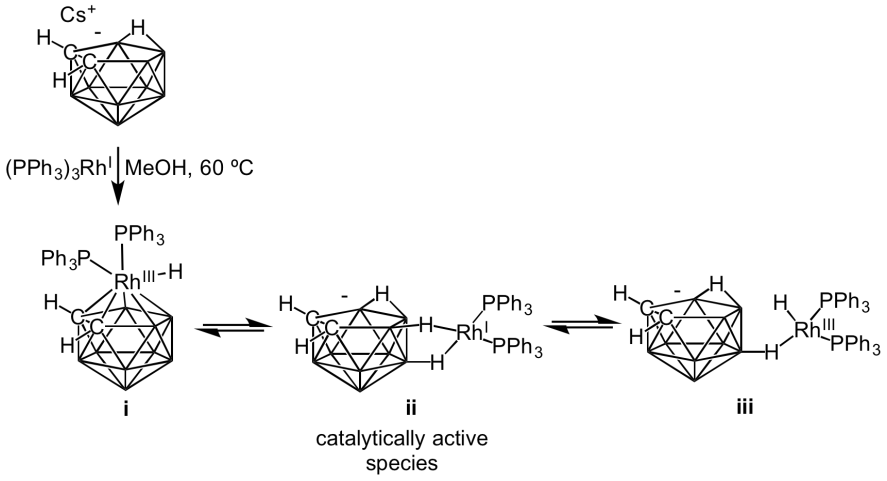

Scheme 3.1 Synthesis of rhodocarborane **i** and its respective catalytically active species.[1]

It has been reported that a second tautomer exists in which the metal centre migrates to the 'lower belt' forming a less active species (**iii**).[5] In 1996, Teixidor and co-workers reported a far superior catalyst for the hydrogenation of 1-hexene by preventing formation of the second tautomer (**Scheme 3.2**).[6] This complex houses an *exo*-monothiocarborane ligand (**iv**) with the concept that the thioether provides the necessary B-H-M interaction favouring the catalytically active species (**v**) and preventing tautomerism to the catalytically inactive *closo*-tautomer as well as preventing migration of the metal centre to the 'lower belt' to give the less active species.

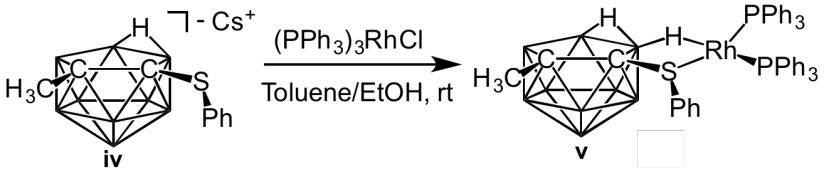

Scheme 3.2. Synthesis of Teixidor's catalysts for the hydrogenation of 1-hexene.[6]

3.1.2 Applications of rhodium-NHCs

Over the course of the last thirty years, Rh-NHCs have been utilised across a vast range of catalytic transformation, including hydrosilyation,[7,8] arylation,[9] cyclisation reactions,[10–13] and hydroformylation.[14] However, in comparison to the highly catalytically active rhodocarboranes for direct hydrogenation of alkenes, Rh-NHCs are lacklustre in this area. One of the main downfalls was that the NHC complexes decompose under hydrogenation conditions.[15] Greater success has been found in an alternative method employed for hydrogenating compounds, known as transfer hydrogenation (TH).[16–20] The TH method avoids the use of pressured H_2 gas by using a sacrificial alcohol as a hydrogen source. A more detailed account of the literature and mechanistic insights into TH is discussed in Chapter 5, Section 5.1.

Hydrosilyation is arguably the most widely studied application for Rh-NHCs.[7,8] In 1996, Herrmann reported the first NHC complex for asymmetric hydrosilylation (**Figure 3.1**).[21] Despite low enantiomeric excess (32 %), the results were promising enough to demonstrate that NHCs can be employed in asymmetric synthesis. Shortly after this report, Enders published details of (triazolinylidene)rhodium(COD) complexes, which attained yields of 60 % and ee values of up to 40 % in the hydrosilylation of various ketones (**Figure 3.1**).[22] The first break-through report was in 2003 by Shi and co-workers, with a chiral bis-carbene ligand which achieved 98 % yield with an ee of 87 % in the hydrosilylation of methyl ketones (**Figure 3.1**).[23] Shortly after, Gade *et al.* reported a bidentate oxazoline NHC ligand, which achieved 90 % ee with excellent yields employing similar substrates (**Figure 3.1**).[24] To date, this system is still one of the most active for the asymmetric hydrosilyation of ketones.[25]

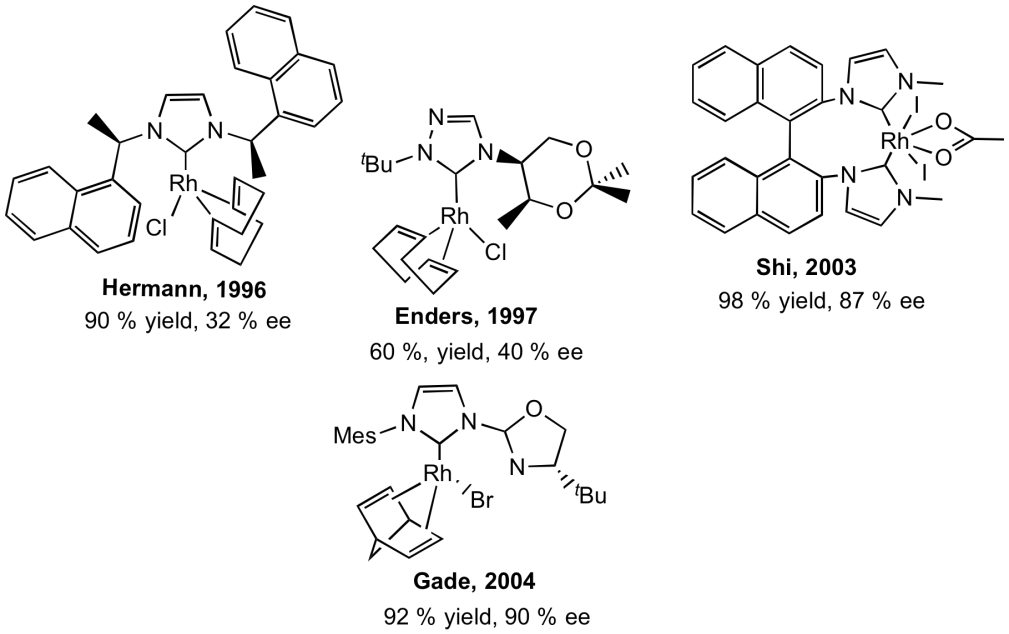

Figure 3.1 Important advances in rhodium catalysts developed for the hydrosilylation of ketones.[21–24]

3.1.3 Iron dicarbollides

Iron dicarbollides changed the course of organometallic chemistry with the synthesis of the carboranyl analogue of ferrocene in 1965.[26] However, the majority of these complexes are synthesised purely out of curiosity and to examine their structural properties. Extraction of radioactive species from nuclear waste is one of the largest fields to which metallacarboranes have been applied.[27]

3.1.4 Iron-NHC complexes

One of the most effective methods for the synthesis of Fe-NHCs was reported by Danopoulos and utilises the highly reactive Fe^{II} precursor $[Fe\{N(SiMe_3)_2\}_2]$,[28,] previously reported by Lappert and co-workers.[28,29] Conveniently, the sole by-product of this reaction is two equivalents of $HN(SiMe_3)_2$, allowing the Fe^{II}-NHC complex to be isolated cleanly by simply removing the volatile by-product *in vacuo*. A comprehensive review on Fe-NHC synthesis and their catalytic applications was recently reported by Kühn and co-workers,[30] and highlights a plethora of ligand scaffolds. By mass, Fe is the most common element on earth making it also the cheapest metal element, around 10,000 times cheaper than Pd.[31] It is also much less toxic so 'allowed' levels of trace metal in final products can be much higher for Fe than for Pd.[32] As a result, Fe-NHCs have seen a surge of interest in catalysis.[30] More specifically, Cp*Fe-NHCs have been found to be highly efficient in the hydrosilyation of ketones, and the reduction of ketones *via* hydrosilylation and transfer hydrogenation reactions, respectively (**Figure 3.2**).[33,34]

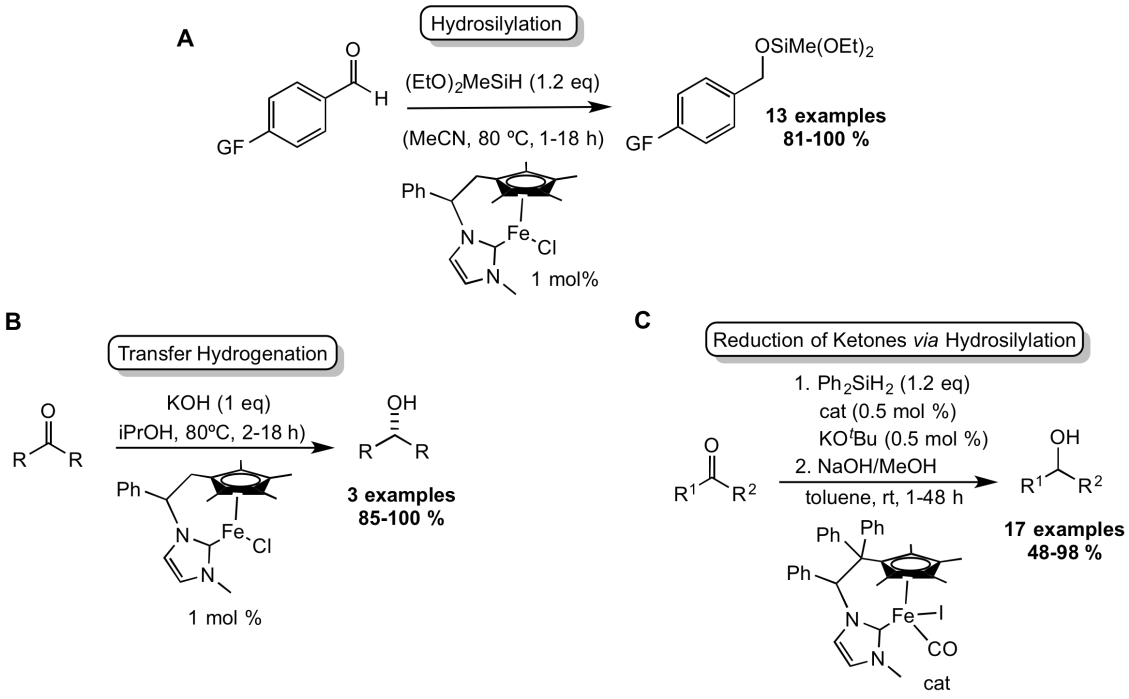

Figure 3.2 Catalytic hydrosilyation (**A**), transfer hydrogenation (**B**) and reduction of ketones (**C**) of some Fe-NHC complexes using substituted acetophenone substrates.[33,34]

3.1.5 Titanium complexes in the polymerisation of alkenes

The chemistry of NHCs bound to early transition metals, especially higher oxidation state metals, is relatively under-developed when compared to the late transition metals. There is a tendency of the NHC to dissociate from early transition metals due to the weak M^{IV}-NHC bond. To enhance the binding of the NHC one can utilise tridentate ligands, such as the bis(carbene)pyridyl ligand scaffold as reported by Gibson *et al.*, which was found to have moderate activity in the polymerisation of ethylene.[35] Alternatively, incorporation of chelating anionic groups, which act as anchor points, is a popular synthetic strategy for stabilising Ti-NHC complexes. One of the earliest examples of an anionic-tethered NHC was reported by Kawaguchi in 2003 (**Figure 3.3**).[36] There are numerous examples of CpTi-NHC type complexes but the catalytic activity of these complexes in the polymerisation of ethylene have not been reported.[37] The use of the dicarbollide ligand ($C_2B_9H_{11}$) as an anchoring point in half sandwiched Ti complexes is largely unexplored, even though the first reports of such complexes were reported over a decade ago by Kang and co-workers (**Figure 3.3**).[38,39]

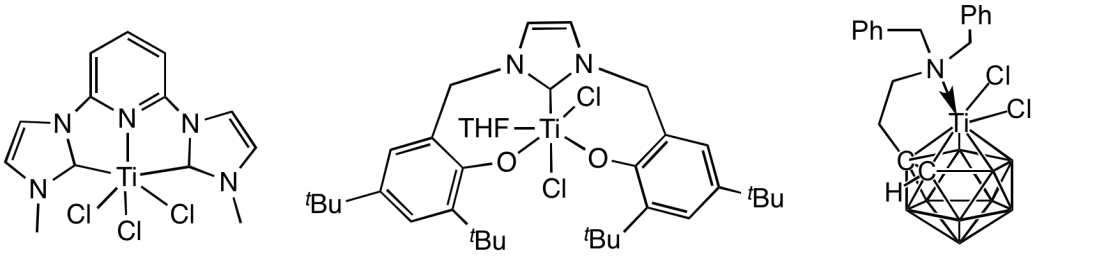

Figure 3.3 Examples of Ti-NHCs and Ti-dicarbollides used in ethylene polymerisation.[35,36,39]

3.2 Aims

A plethora of NHC and carborane complexes have been discussed, with an emphasis on the catalytic applications of these complexes. NHC ligands with anionic tethers have been described, and have carborane ligands linked to other neutral donors such as amines. The aim of this work was to prepare complexes of fused NHC-carborane ligands *i.e.* in which the NHC is the neutral donor and the carborane acts as the anionic tether. The zwitterionic compounds presented in Chapter 2 were found to be excellent precursors to a range of interesting new products.

3.3 Initial attempts at deprotonation and metallation of the zwitterionic ligand precursors

The zwitterionic ligand precursors **L1.2** and **L2.2** prepared in Chapter 2 possess two acidic protons, which require deprotonation in order to coordinate to a metal centre. These are the imidazolium NC*H*N proton and the bridging proton of the C_2B_3 face of the carborane (**Scheme 3.3**). Initial attempts at deprotonation and metallation involved using three of the most effective synthetic methods for synthesising NHC complexes; i) reaction with an inorganic base ($CsCO_3$ or KO^{t}Bu) in the presence of a metal halide salt, ii) reaction with a basic metal precursor, with $Pd(OAc)_2$ and Ag_2O being employed, and iii) deprotonation and transmetallation using Ag_2O in combination with metal halide salts.

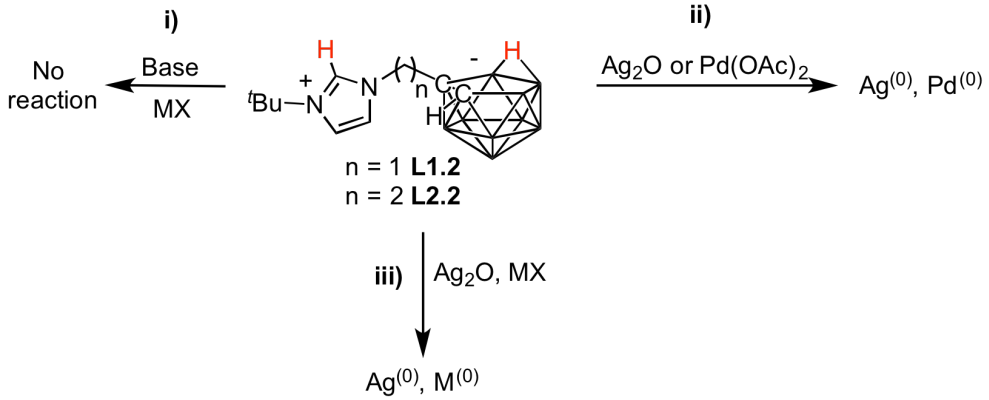

Scheme 3.3 Synthetic methods employed for the attempted synthesis of NHC-carborane complexes. i) ($CsCO_3$ or KO^{t}Bu) with a metal halide salt, ii) $Pd(OAc)_2$ or Ag_2O, and iii) Ag_2O with metal halide salts.

With **L1.2** and **L2.2** possessing diagnostic resonances in the ^{1}H NMR spectra for the acidic protons, the loss of these signals would strongly indicate coordination to a metal, making ^{1}H NMR spectroscopy a powerful tool for monitoring the progress of reactions. HRMS is another useful technique, which goes in hand with NMR spectroscopy. An extensive number of reactions were conducted, and with respect to the reactions involving an inorganic base and metal salt, no reaction occurred. The crude ^{1}H NMR spectra still possessed the diagnostic signals for the acidic protons and the major peaks in the HRMS at *m/z* 271.2892 and *m/z* 286.3131 correspond to the zwitterionic ligand precursors **L1.2** and **L2.2**, respectively. Likewise, for the other two synthetic methods, the metal salts employed formed a black precipitate (presumably M^0) irrespective of the reaction temperature and solvent used in the reaction.

3.4 Deprotonation studies

In an attempt to understand the unsuccessful deprotonation and metallation reactions (Section 3.3), the transition metals were removed from the reactions. The aim was to deprotonate the zwitterion and isolate the doubly deprotonated species *i.e.* the free carbene and the dianion. The most common base employed for deprotonation of *nido*-carboranes is NaH in anhydrous THF.[40] Since NHCs can also be deprotonated by NaH,[41] deprotonation studies with zwitterionic ligands bearing a ^{t}Bu *N*-substituent with varying tether lengths (**L1.2**, **L2.2** and **L4.1**) were conducted (**Scheme 3.4**).

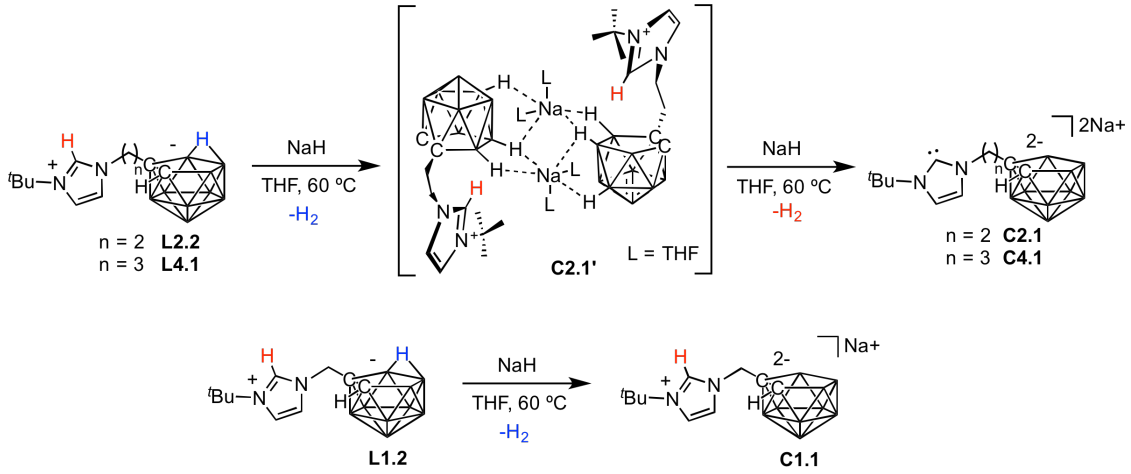

Scheme 3.4 Deprotonation reactions of the zwitterionic ligands with NaH.

After reacting **L1.2** with NaH (2 eq., 40 °C, 120 hours, d_8-THF), the resonance attributable to the bridging proton of the carborane cage at -3.01 ppm was absent from the ^{1}H NMR spectrum (**Figure 3.4**, **top**). However, the NC*H*N proton (H6) is still present, which has shifted upfield from 8.89 to 7.82 ppm, a direct consequence of forming a more charge dense cage. Surprisingly, even at elevated temperatures (up to 60 °C) or employing a stronger base (^{n}BuLi), the H6 proton still resists deprotonation. This is a very unusual observation for imidazolium protons, which are usually deprotonated under these conditions. On increasing the tether length to an ethyl (**L2.2**) or propyl (**L4.1**), both the bridging proton of the carborane cage and the imidazolium NC*H*N protons were successfully deprotonated to give **C2.1** and **C4.1** under the same reaction conditions (2 eq., 40 °C, 120 hours, d_8-THF). Increasing the temperature to 60 °C reduced the reaction times considerably, with full deprotonation achieved after 18 hours, with both diagnostic resonances (H7 and B*H*B) being absent in the ^{1}H NMR spectrum of **C2.1** (**Figure 3.5**, **top**).

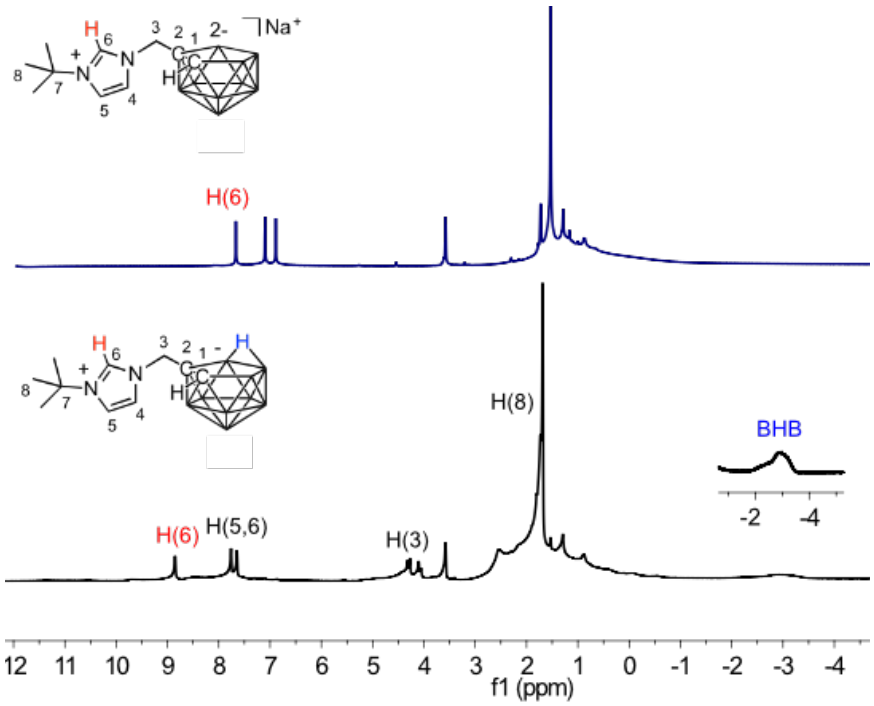

Figure 3.4 ^{1}H NMR spectra (300 MHz, d_8-THF) of **L1.2** (bottom) and after reacting with NaH at 60 °C for 14 hours (top). *The broadness of the spectrum of **L1.1** is a result of its poor solubility.*

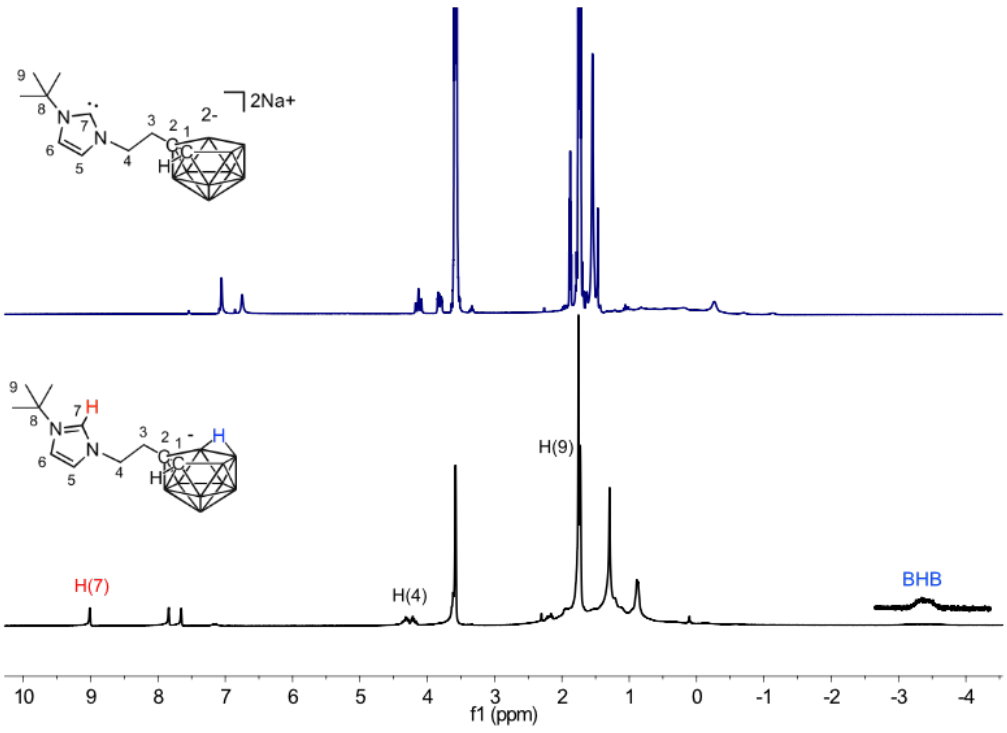

Figure 3.5 ^{1}H NMR spectra (300 MHz, d_8-THF) of **L2.2** (bottom) and the free carbene **C2.1** (top).

Comparing the $^{11}B\{^{1}H\}$ NMR spectra of **L2.2** and **C2.1**; that of **L2.2** contains peaks in the region −10 to −40 ppm, whilst that of **C2.1** are in the region −15 to −50 ppm (**Figure 3.6**). The spectrum of **C2.1** is more symmetrical than that of **L2.2** and is shifted more upfield due to an increase in electron density of the cage upon formation of **C2.1**. A large upfield shift of the B10 resonance is due to the majority of the electron density delocalising about this vertex. A detailed discussion on ^{11}B NMR assignment of the other vertices is given in Chapter 2, Section 2.2.2.

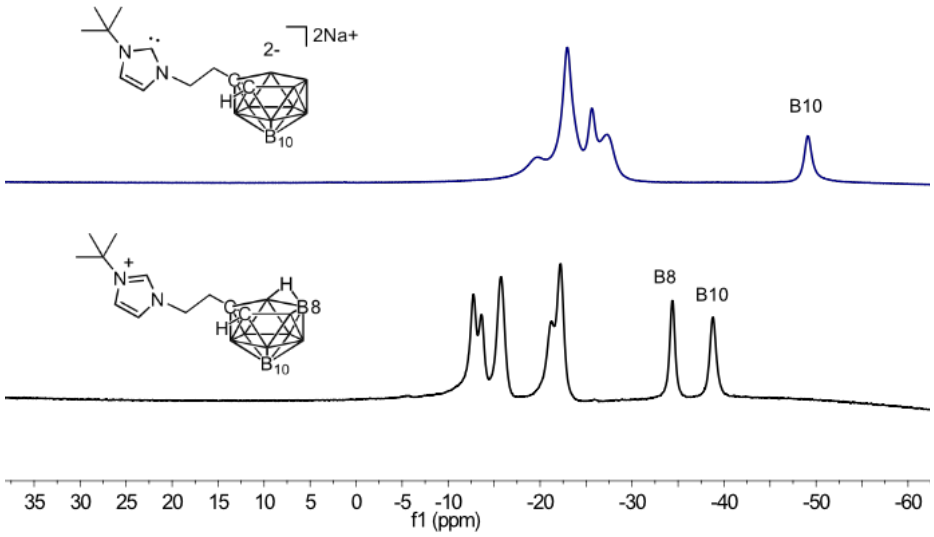

Figure 3.6 $^{11}B\{^{1}H\}$ NMR spectra (98 MHz, d_8-THF) of **L2.2** (bottom) and free carbene **C2.1** (top).

During the reaction between **L2.2** and NaH a crystalline solid precipitates from the reaction after 4-8 hours of heating at 40 °C. X-ray diffraction analysis of these crystals identified it as a possible intermediate of the reaction, where the bridging proton of the carborane has been deprotonated but the NC*H*N proton is still present (**C2.1'**) (**Figure 3.7**). The structure was solved in the monoclinic $P2_{1/n}$ space group with the selected metric parameters given in **Table 3.1**. The asymmetric unit possesses one carborane ligand with a THF-solvated Na atom *exo*-polyhedrally attached to the B(8)-B(7) edge of the carborane, which is achieved through Na-H-B bridges. It became apparent that the structure exists as a dimer possessing a centrosymmetric centre on growing out the structure from the asymmetric unit.

This interesting motif is common amongst carborane dianions, and the first reported crystal structures were reported by Meshcheryakov and co-workers in 2003.[42] The report highlighted that carboranyl dianions such as $[Na_2(THF)_3(7,8\text{-}C_2B_9H_{11})]_n$ exist as polymeric structures (**Figure 3.8**). For charge compensated cages such as $[Na_2(THF)_3(9\text{-L-}7,8\text{-}C_2B_9H_{11})]_2$, where L = SMe_2 or NMe_3, the structures exist as dimers with both Na atoms being *exo*-polyhedral with interactions to both of the carborane ligands.

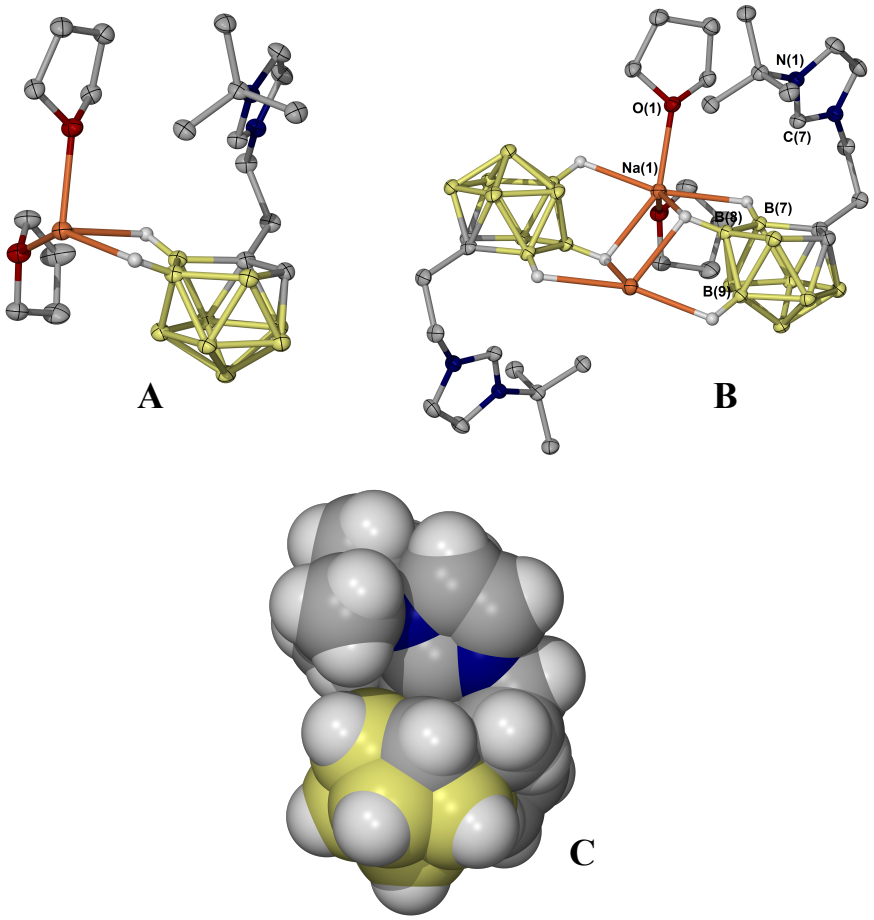

Figure 3.7 The asymmetric unit (**A**), molecular structure (**B**) and space-filling model (**C**) of **C2.1'**. *Ellipsoids are shown at 40 % probability and the hydrogen atoms, excluding those involved in Na-H-B bridges, are omitted for clarity. The THF molecules of the Na(2) atom are also omitted for clarity.*

Table 3.1 Selected bond distances (Å) for **C2.1'**.

Bond	Distance (Å)	Bond	Distance (Å)
Na(1)-O(1)	2.355(18)	C(2)-B(7)	1.631(3)
Na(1)-O(2)	2.363(18)	B(7)-B(8)	1.749(3)
Na(1)-H(7)	2.415(7)	B(4)-B(8)	1.737(3)
Na(1)-H(8)	2.329(7)		
C(1)-C(2)	1.551(3)		
C(1)-B(4)	1.621(3)		

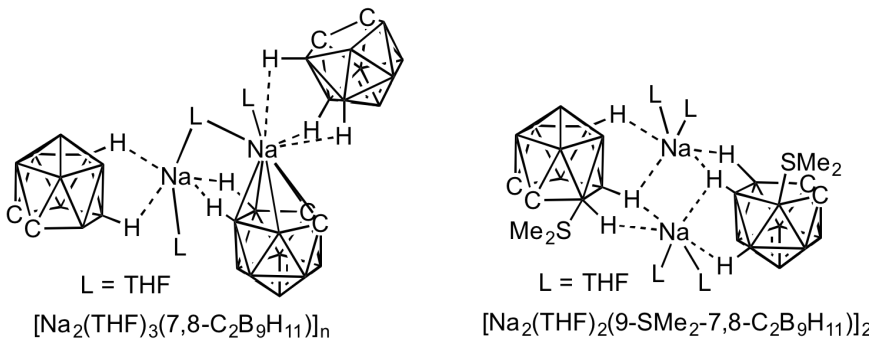

Figure 3.8 Structures of the first dianion and charge compensated anion.[43]

In the case of **C2.1'**, the positively charged imidazolium group occupies the open face of the carborane, which prevents coordination of the Na atom to the C_2B_3 face, leading to formation of the dimeric structure similar to the findings of Meshcheryakov and co-workers. The space-fill model of **C2.1'** may show why the imidazolium N*H*CN proton of **L1.2** does not deprotonate (Section 3.3). The shorter linker of **L1.2** will allow for a stronger interaction between the positively charged imidazolium and the C_2B_3 face making the proton inaccessible. However, obtaining ^{1}H and $^{11}B\{^{1}H\}$ NMR data on **C2.1'** was not possible, as analysis of the crystalline material by NMR spectroscopy revealed the bulk was in fact the free carbene (**C2.1**). In an attempt to observe **C2.1'** in solution; the amount of NaH used in the reaction was reduced from two to one equivalent. However, the ^{1}H NMR spectrum revealed just a mixture of the zwitterion **L2.2** and the free carbene **C2.1**. This suggests **C2.1'** is a crystallisation effect and in solution is to likely exist as a 1:1 ratio of **L2.2** and **C2.1**.

A comprehensive kinetic study by Hawthorne and co-workers illustrated how the substituents of C-substituted carboranes exert primarily stereochemical rather than electronic influence on the rate of deprotonation of the bridging proton of the carborane.[44] This study shows that substituents that posses a CH_2 spacer deprotonate more readily than those bound directly to the cage such as a phenyl group. This is due to their ability to 'swing out of the way' allowing the metal hydride to approach the cage surface. Temperature also has a strong influence, with elevated temperatures reducing deprotonation times considerably. Our NMR experiments are in accordance with Hawthorne's findings; the rate of deprotonation increases with the tether length from ethyl to propyl, and increasing the temperature from 40 °C to 60 °C dramatically decreases the reaction time. Most importantly, these reactions provide possible explanations for why initial attempts at forming an NHC complex with **L1.2** and **L2.2** were unsuccessful (Section 3.3).

3.5 Formation of a Rh^I bimetallic NHC-carborane complex: An example of low temperature polytopal rearrangement

All reactions discussed herein were conducted on an NMR scale, with one of the challenging aspects of this chemistry being the handling of the dianion **C2.1** (**Scheme 3.5**). Before addition of a metal salt, **C2.1** must first be isolated from the excess NaH used in its formation, which can be achieved by removing the solution from the particulate *via* syringe in the glove box. Initial attempts at removing the NaH involved filtering over glass wool or Celite, which had been pre-treated with anhydrous THF, dried *in vacuo* and stored over argon, but even under these strict anhydrous conditions each filtration led to reprotonation of *ca.* 10-20 % of the material.

Following removal from NaH *via* syringe, the treatment of **C2.1** with $[Rh^I(COD)Cl]_2$ in MeCN at room temperature produced an isomeric mixture of bimetallic complexes **C2.2** and **C2.3** (**Scheme 3.5**). The formation of **C2.3** is a consequence of isomerisation of the cage known as the 3,1,2 (*ortho*-) to 2,1,8 (*meta*-) rearrangement, with the numbers simply indicating the position of the carbons atoms in the cage. Thermal isomerisation of *o*-carborane to its respective isomers *meta*- and *para*- at high temperatures (ca. 470 °C and 700 °C) has been well established for over 50 years.[45,46] In the case of **C2.2** isomerisation occurs at room temperature, a phenomenon known to occur in metallacarboranes decorated with bulky substituents, with isomerisation relieving steric stress at the metal centre.[47–50]

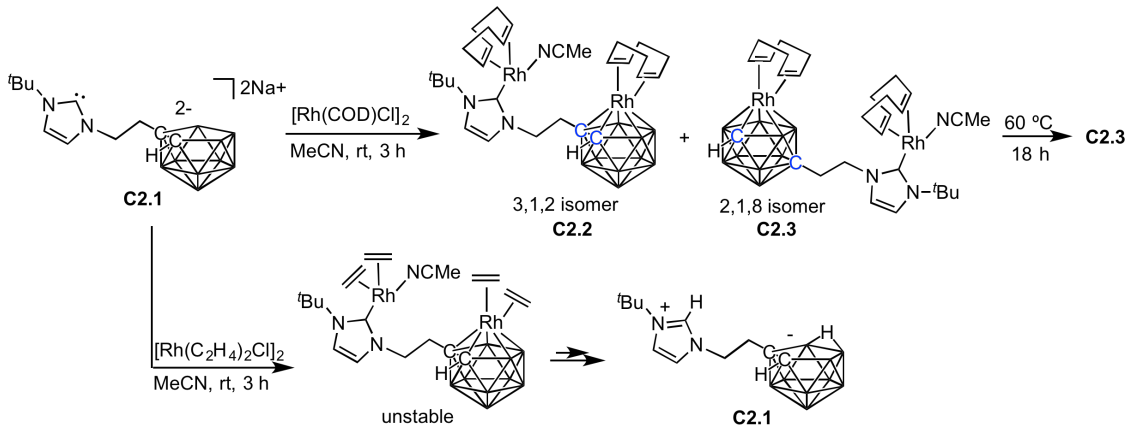

Scheme 3.5 Synthesis of a bimetallic Rh^I NHC-carborane COD complex **C2.3** and attempted synthesis of an ethylene derivative.

Work by Stone and co-workers demonstrated that low temperature isomerisation at Pd can be influenced by electronic effects of the *exo*-polyhedral ligands (**Figure 3.9**).[51] Compounds of type 1,2-Me_2-L_2-PdC_2B_9 undergo low temperature isomerisation when L_2 = COD (**A**), but not when L_2 = tmeda (**B**).

This behaviour can be rationalised by the magnitude of slipping distortion (Δ) induced by the different *exo*-polyhedral ligands. Ligands that possess the ability to accept π-electron density

from the metal result in stronger metal-to-cage bonding, with little to no ring slippage, retaining an η^5-bonding mode. As a result, these complexes are sterically crowded and susceptible to isomerisation. As the electron accepting ability of the *exo*-polyhedral ligands decreases, the metal-to-cage bonding becomes weaker allowing for ring slippage. This reduces the steric stress at the metal centre and as a consequence isomerisation is not observed. This provides a good rationale for why we observe low temperature isomerisation in **C2.2**, which was examined by attempting to exchange the COD ligand for a weaker π-acceptor by using the $[Rh(C_2H_4)_2Cl]_2$ precursor. Unfortunately this resulted in formation of a black precipitate when added to **C2.1**, presumably Rh^0, with the ^1H NMR spectrum indicating reformation of an imidazolium species (**Scheme 3.5**).

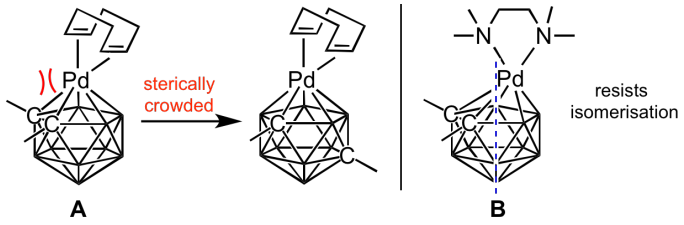

Figure 3.9 Complexes reported by Stone and co-workers that isomerise at room temperature.[51]

Complexes **C2.2** and **C2.3** were determined as structural isomers by X-ray diffraction analysis. The slow evaporation of a concentrated MeCN solution produced single crystals of **C2.2** and **C2.3** within the same sample, with each producing crystals of different morphology. Examination of the molecular structures unambiguously determined that the two complexes are structural isomers (**Figure 3.10**). In **C2.2**, the Rh(2) centre is almost equidistant from the three boron and two carbon atoms [2.217-2.306 Å] indicating symmetrical bonding and an η^5-bonding mode.

Likewise for **C2.3**, almost equidistant bonding is observed for four of the atoms in the CB_4 face, with the exception of B11, which is considerably shorter at 2.250(3) Å. This is due to the CB_4 face being puckered into an 'envelope' conformation, which arises from the carbon atoms being held closer to the centre of the cluster than the boron atoms, and is typical of rearranged 2,1,8-complexes in the literature (**Figure 3.10**).[50–52] In the rearranged product (**C2.3**), the Rh(2) and CB_4 face bond lengths are on average shorter than in **C2.2**, indicating stronger bonding between the carborane and metal centre. This is married with the reduction in π-backbonding to the COD ligand, with the Rh(2)-COD alkenyl bond length in C6 averaging 2.157 Å, which is longer than in the parent complex **C2.2** at 2.127 Å.

The Rh(1) centres of both complexes display a distorted square planar geometry, with Rh-$C_{carbene}$ bond lengths of 2.061(4) and 2.048(3) for **C2.2** and **C2.3** respectively, which is in the expected range for Rh^I-NHC(COD) type complexes.[53–56]

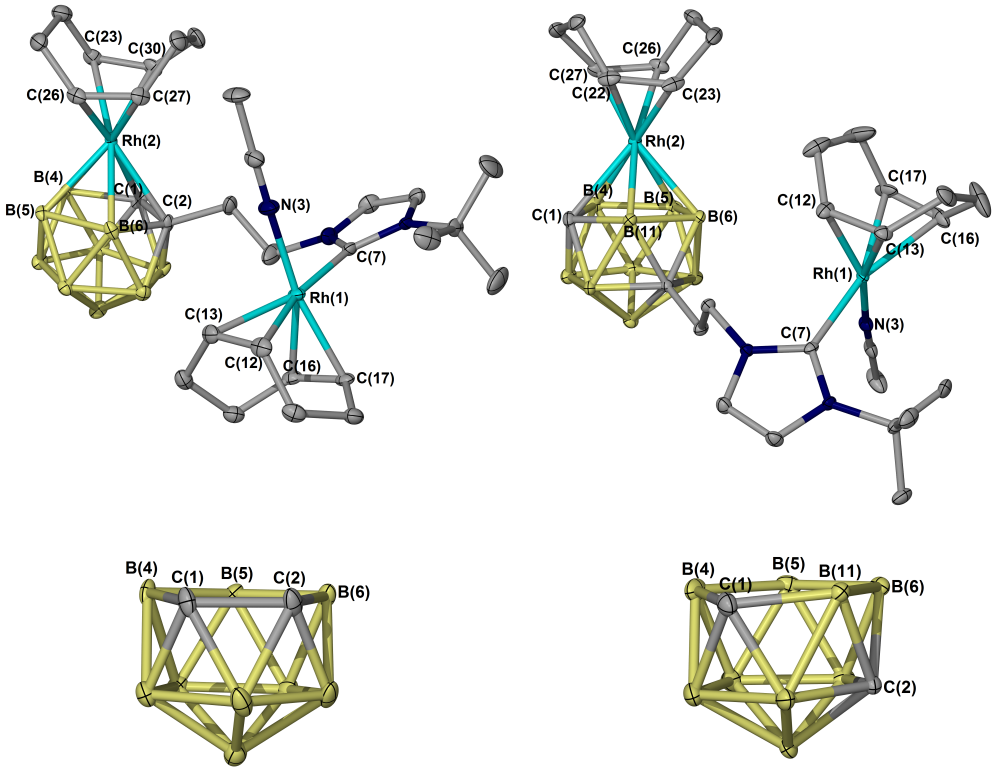

Figure 3.10 Molecular structures of **C2.2** (left) and **C2.3** (right). *Ellipsoids are shown at 40 % probability and the hydrogen atoms are omitted for clarity.*

Table 3.2 Selected bond distances (Å) for **C2.2** and **C2.3**.

Distance (Å)	**C2.2**	**C2.3**	Distance (Å)	**C2.2**	**C2.3**
C(1)-C(2)	1.608(5)	-	Rh(2)-C(23)	2.144(4)	2.158(3)
C(1)-B(11)	-	1.711(4)	Rh(2)-C(26)	2.110(3)	2.144(3)
Rh(2)-C(1)	2.231(4)	2.290(3)	Rh(2)-C(27)	2.130(4)	2.153(3)
Rh(2)-B(11)	-	2.153(3)	Rh(1)-C(12)	2.198(4)	2.118(3)
Rh(2)-C(2)	2.306(4)	-	Rh(1)-(C13)	2.189(4)	2.123(3)
Rh(2)-B(4)	2.245(4)	2.217(3)	Rh(1)-C(16)	2.126(4)	2.192(3)
Rh(2)-B(6)	2.209(4)	2.237(3)	Rh(1)-C(17)	2.118(4)	2.199(3)
Rh(2)-B(5)	2.276(4)	2.250(3)	Rh(1)-(C7)	2.061(4)	2.048(3)
Rh(2)-C(22)	2.124(4)	2.173(3)	Rh(1)-N(3)	2.056(3)	2.073(2)

The formation of **C2.2** and **C2.3** in solution was determined using NMR spectroscopic analysis. Reaction of **C2.1** with $[Rh^{I}(COD)Cl]_2$ for 3 hours at room temperature produced a spectrum containing several species, and even after leaving the sample for 3 days at room temperature, these species persist with no change to the spectrum (**Figure 3.11**, **A**). The presence of multiple species is indicated by the number of NHC backbone resonances around 7.00 to 7.50 ppm. The identity of all the species present is not known but it can be rationalised that one set of resonances belong to the 3,1,2 isomer (**C2.2**) and another belonging to the 2,1,8 isomer (**C2.3**), as both were identified crystallographically. Upon heating the sample to 60 °C for 18-24 hours the majority of the peaks subside to the baseline, whilst one set of resonances intensify belonging to **C2.3** (**Figure 3.11**, **B**). Slow evaporation of the MeCN solution allowed **C2.3** to be isolated as a pure crystalline solid in 77 % yield.

The ^{1}H NMR spectroscopic data of **C2.3** was fully assigned in acetone-d_6 (**Figure 3.11**, **C**); the absence of the downfield imidazolium NC*H*N resonance, and presence of only one set of NHC backbone resonances at 7.45 and 7.30 ppm strongly suggests the formation of one NHC species. The COD ligands appear as broad resonances at 3.56-4.98 ppm for the alkynyl and 2.91-2.03 ppm for the alkyl moieties, which are typical of similar carboranyl[51,52] and NHC complexes in the literature.[53–56] The CH_2 protons of the ethyl linker become diasterotopic due to the steric bulk exerted by the two metal centres. One of the resonances can be assigned at 5.36 ppm, whilst the others are masked under the COD alkynyl resonance at 4.22 ppm or under the alkyl COD resonances at 2.91-2.03 ppm. Similarly, the diagnostic cage CH resonance is masked by the COD alkyl resonances, all of which were determined by $^{1}H^{13}C$ 2D NMR experiments. Evidence for a coordinated MeCN is ambiguous for which we relied on the ^{13}C NMR data and X-ray diffraction analysis.

The $^{13}C\{^{1}H\}$ NMR spectrum of **C2.3** contains a resonance at 3.30 ppm characteristic of the quaternary carbon of a coordinated MeCN,[57] with its identity confirmed by its ^{2}J coupling to the Me protons of the MeCN, which are masked by the COD alkyl protons in the $^{1}H^{13}C$ HMBC spectrum (**Figure 3.12**). The doublet at 174.2 ppm ($^{1}J_{Rh\text{-}C}$ = 50.4 Hz) is attributable to the Rh^{I}-NHC carbenic carbon, and those at 75.4 ($^{1}J_{Rh\text{-}C}$ = 10.1 Hz) and 75.0 ppm ($^{1}J_{Rh\text{-}C}$ = 11.3 Hz) correspond to the Rh-COD alkenyl carbons, with the coupling being typical for similar complexes in the literature.[53–56]

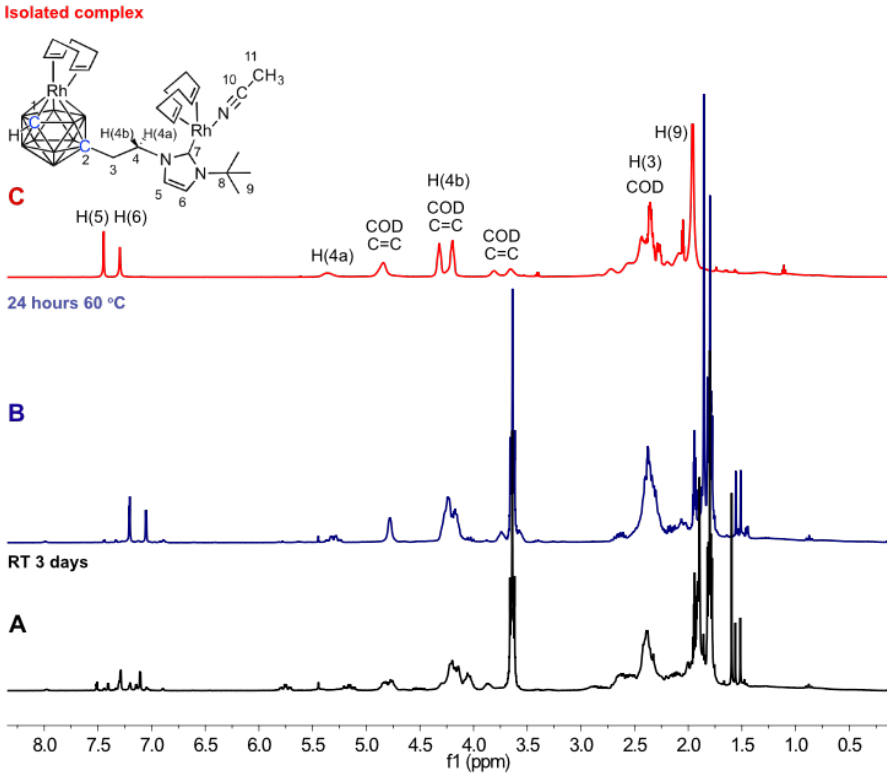

Figure 3.11 ^{1}H NMR spectra (300 MHz, CD_3CN) following reaction of free carbene **C2** with $[Rh(COD)Cl_2]_2$ for 3 days at rt (**A**) and heating of the reaction mixture at 60 °C for 24 hours (**B**) and ^{1}H NMR spectrum (500 MHz, acetone-d_6) of isolated **C2.3** (**C**).

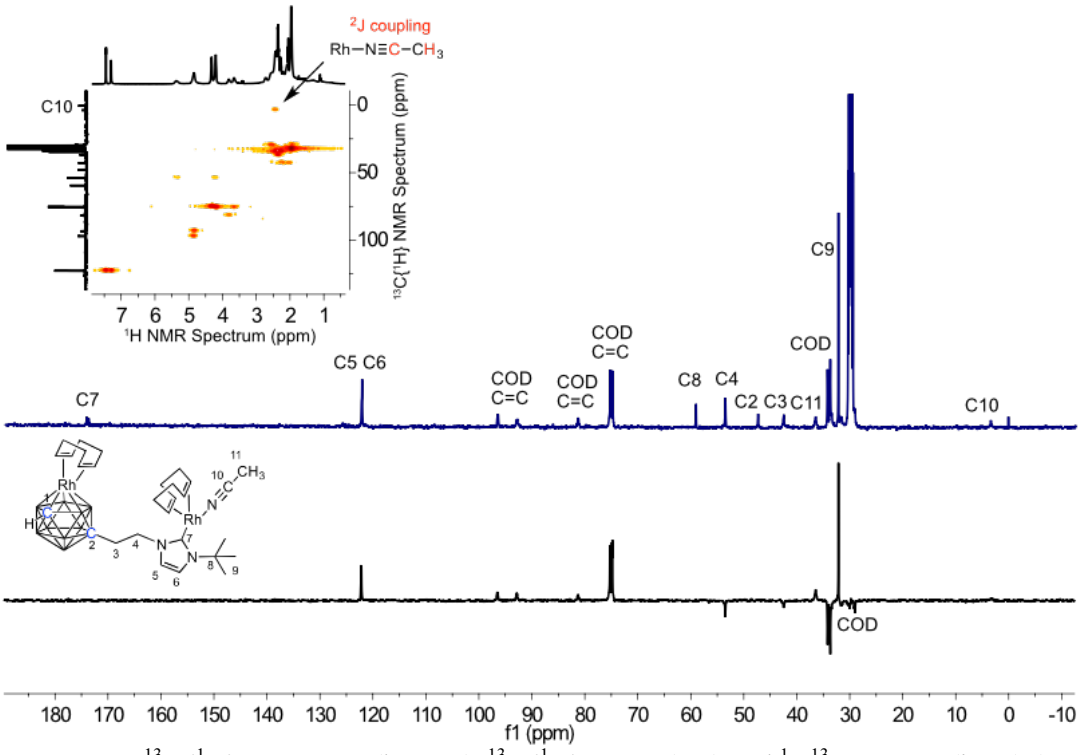

Figure 3.12 ^{13}C{^{1}H} DEPT135 (bottom), ^{13}C{^{1}H} NMR (top) and ^{1}H^{13}C HMBC (inset) (126 MHz, acetone-d_6) spectra of **C2.3**.

Comparing the $^{11}B\{^{1}H\}$ NMR spectra of the free carbene **C2.1** to that of the isomeric mixture of **C2.2** and **C2.3**; the diagnostic B(10) downfield resonance at −49.1 ppm is lost upon coordination to Rh (**Figure 3.13**). This is a result of reforming a *closo* cage with the Rh centre occupying what was once the B3/B6 vertex, with the electron density no longer being localised at the B(10) vertex, but is once again evenly delocalised across the cage. The $^{11}B\{^{1}H\}$ NMR data correlates well with the solid-state structures. The absence of a downfield resonance in the 10-30 ppm region is indicative of symmetrical bonding between the metal and the cage, hence no ring slippage. If slippage does occur it can induce strong electron deshielding at the β-boron atoms which give characteristic ^{11}B NMR spectra.[51]

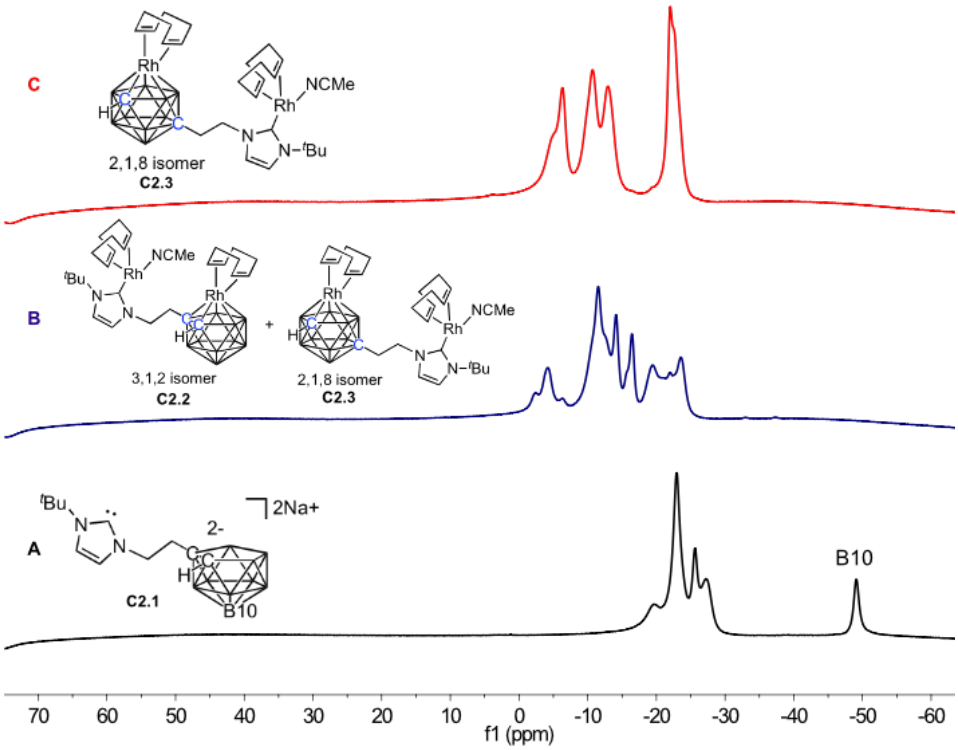

Figure 3.13 $^{11}B\{^{1}H\}$ NMR spectra (161 MHz, CD_3CN) of the free carbene **C2.1** (**A**), reaction of **C2.1** with $[Rh(COD)Cl_2]_2$ for 3 days at rt (**B**), and isolated **C2.3** (**C**).

Intriguingly, recrystallisation of **C2.3** with a mixed solvent system (MeCN/Et_2O/hexane) resulted in the formation of a dimeric solid-state structure **C2.3'**, in which the coordinated MeCN has dissociated and the resulting cationic $[Rh^I(NHC)(COD)]^+$ fragment is stabilised by an anionic $[Rh^I(carborane)(COD)]^-$ moiety of a second molecule linked by Rh-H-B bridges (**Figure 3.14**). The formation of this dimer appears to be a crystallisation effect and does not persist in solution. If **C2.3'** did exist in solution diagnostic resonances in the region of −4 to −9 ppm in the ^1H NMR spectrum, and resonances in the region of 5-20 ppm in the $^{11}B\{^1H\}$ NMR spectrum would be present. [58] Nonetheless, demonstrating the lability of this MeCN ligand and the contrasting Rh^I environments renders **C2.3'** interesting for development in catalysis.

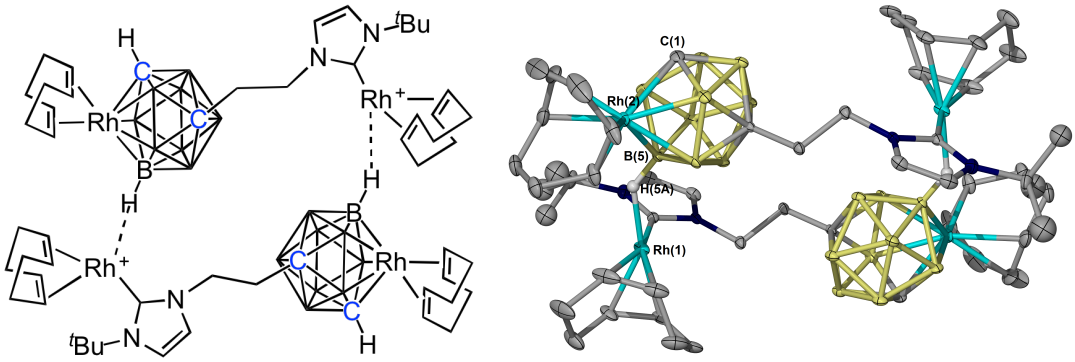

Figure 3.14 Molecular structure of **C2.3'** (right). *Ellipsoids are shown at 40 % probability and the hydrogen atoms are omitted for clarity, with the exception of the protons involved in the Rh-H-B bridges.*

3.6 Synthesis of an Fe^{III}- bis(dicarbollide) complex containing imidazolium tethers

As previously discussed (Section 3.1), chelating Fe^{II}(Cp-NHC) complexes have been reported to be highly active in hydrosilyation and transfer hydrogenation of ketones. The formation of related complexes in which the Cp is exchanged for a carborane group was investigated using ligand precursor **L2.2**. Employing a similar strategy used for the synthesis of **C2.3** (Section 3.5), **L2.2** was reacted with NaH and the reaction was monitored by ^{1}H NMR spectroscopy until both the NC*H*N and the bridging proton of the carborane had fully deprotonated to generate **C2.1**. This was isolated by transferring the solution from the particulate *via* syringe into a Young's Tap NMR tube containing a d_8-THF solution of $FeCl_2$ in the glove box. Within a few minutes of addition, a bright violet precipitate crashed out of solution, indicative of formation of a Fe^{II}-bis(dicarbollide) (**C2.4**) (**Scheme 3.6**).[40,59] A ^{1}H NMR spectrum of the reaction mixture after 3 hours showed only residual **C2.1** in solution. The violet precipitate was found to be insoluble in all organic solvents when kept under anhydrous conditions, but upon exposure to O_2 the violet precipitate instantaneously solubilises in MeCN forming a deep red solution as the complex is presumably oxidised from Fe^{II} to Fe^{III}. A salt metathesis reaction followed by recrystallisation from acetone with water gave a new charge compensated Fe^{III}-bis(dicarbollide)$(PF_6)_2$ complex **C2.5** in 34 % (**Scheme 3.6**).

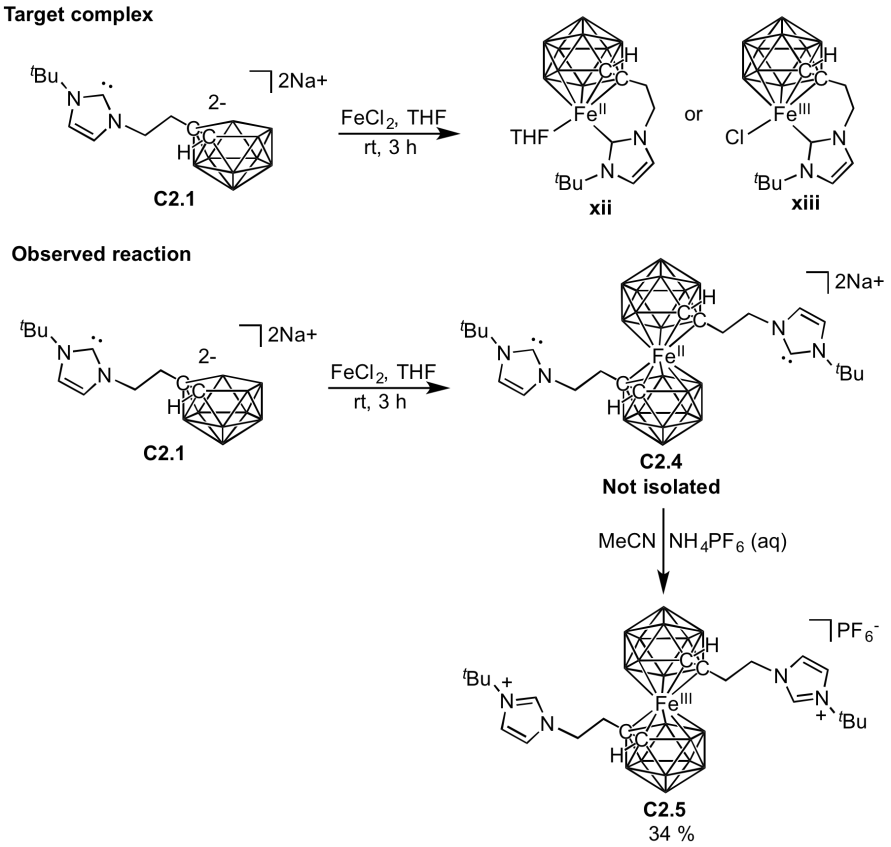

Scheme 3.6 Synthesis of a novel charge compensated Fe^{III}-bis(dicarbollide)$(PF_6)_2$ complex **C2.5**.

Due to the paramagnetic nature of **C2.5**, characterisation was limited to HRMS, X-ray diffraction analysis and micro-analysis. Crystals suitable for X-ray diffraction analysis were grown from the slow evaporation of a mixed solvent system (acetone/water 3:1). The structure was solved in the $P2_1/c$ space group with the molecular structure is shown in **Figure 3.15** with selected bond distances given in **Table 3.3**. The Fe atom is sandwiched centrally between the two cages, with the bonding faces staggered so that the pair of carbon atoms in each cage are at maximum distance apart. The Fe-C and Fe-B bond lengths range from 2.108-2.190 Å, which are typical distances for Fe-bis(dicarbollide) reported in the literature.[59,60] The Fe-C_2B_3 centroid distance of 1.55 Å is quite long in comparison to the unsubstituted Fe dicarbollide (Fe-$(C_2H_{11}B_9)_2$) which possesses a Fe-C_2B_3 centroid distance of 1.48 Å.[59] This can be rationalised by the fact that the unsubstituted dicarbollide is a dianion, hence will have a stronger metal-ligand interaction compared to **C2.5**, which is overall monoanionic. The substituents on the cage can also influence the geometry of the molecule, with the bonding faces of **C2.5** being non-parallel with a dihedral angle of 3.8°. In more sterically encumbered complexes, such as when the cage bears triethylamine substituents, the dihedral angle can be as large as 14.0°.[59]

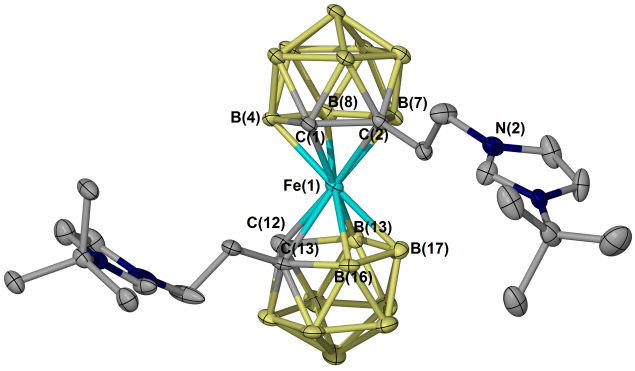

Figure 3.15 Molecular structure of **C2.5**. *Ellipsoids are shown at 40 % probability and the hydrogen atoms are omitted for clarity.*

Table 3.3 Selected bond distances (Å) for **C2.5**.

Bond	Distance (Å)	Bond	Distance (Å)
C(1)-C(2)	1.679(8)	Fe(1)-B(4)	2.118(6)
C(12)-C(13)	1.633(7)	Fe(1)-B(7)	2.149(6)
C(1)-Fe(1)	2.115(5)	Fe(1)-B(8)	2.145(7)
C(2)-Fe(1)	2.181(5)	Fe(1)-B(13)	2.131(6)
C(12)-Fe(1)	2.143(6)	Fe(1)-B(16)	2.108(6)
C(13)-Fe(1)	2.190(5)	Fe(1)-B(17)	2.118(7)

Analysis of **C2.5** by HRMS gave the expected molecular ion peak of *m/z* 623.5380 corresponding to the cationic fragment $[C_{22}H_{32}B_{18}Fe]^+$, with the calculated isotope pattern matching that of the observed (**Figure 3.16**). This, along with micro-analysis of the bulk material, confirms the presence of only one species, *i.e.* the Fe-bis(dicarbollide) complex **C2.5**. Due to the violet precipitate formed following reaction of **C2.1** with $FeCl_2$ being completely insoluble, it prevented characterisation of this material. It is presumed that this is an Fe^{II} complex **C2.4**, with the complex bearing two carbenic tethers, which will be reprotonated upon exposure to hydrous solvents (**Scheme 3.6**).

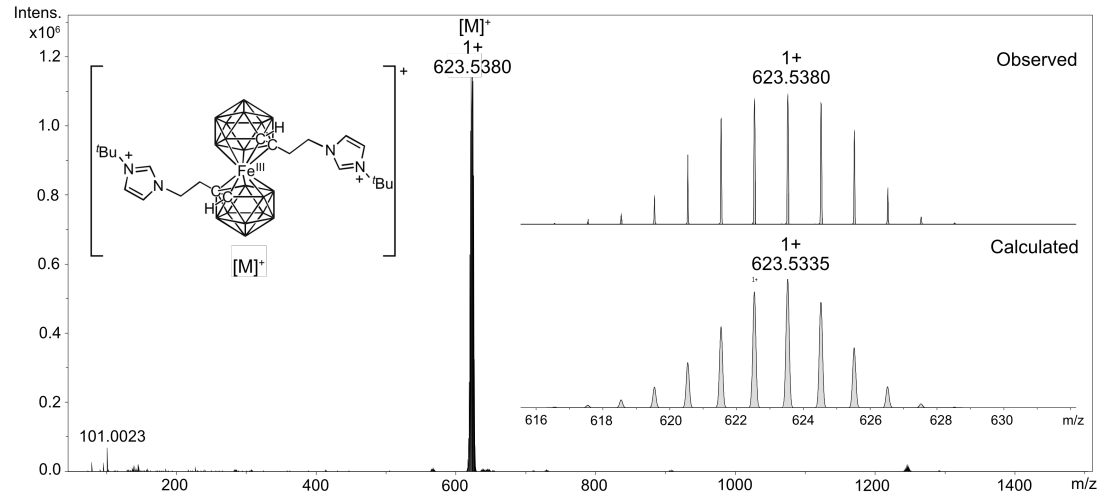

Figure 3.16 HRMS of **C2.5**. Inset shows the molecular ion peak of $[M]^+$ against the calculated mass.

Although the desired chelating complex did not form, **C2.5** has the potential to be developed into a bimetallic system (**Scheme 3.7**). Two synthetic strategies were employed in an attempt to add a M-NHC to the Fe^{II}-bis(dicarbollide): 1) **C2.5** was reacted with $CsCO_3$ in the presence of $[Rh(COD)Cl]_2$, and, 2) **C2.5** was reacted with Ag_2O in the presence of $[Rh(COD)Cl]_2$. Unfortunately both of these attempts were unsuccessful, which was confirmed using HRMS showing only the molecular ion peak for **C2.5**. It is suspected that the two-imidazolium protons are not particularly acidic due to the partially zwitterionic nature of **C2.5**. Further work using **C2.5** should employ stronger bases or electrochemical methods to deprotonate the imidazolium arms.

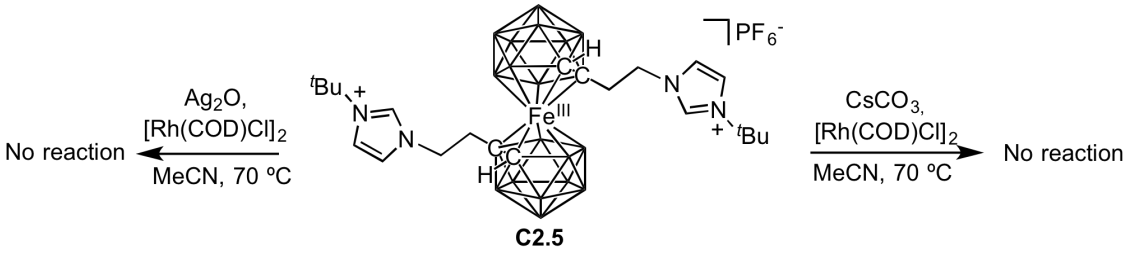

Scheme 3.7 Attempted deprotonation reactions with **C2.5**.

3.7 Synthesis of an unusual NHC-carborane adduct

Titanium tetrachloride ($TiCl_4$) is a strong Lewis acid and is an important metal precursor for the synthesis of many titanocene and titanacarborane complexes.[61–68] Similar to previously, **L2.2** was deprotonated using NaH to give **C2.1**, which was added to $TiCl_4$ at room temperature in toluene. The target complex **C2.6** was not isolated, instead an unusual NHC-carborane adduct (**C2.6.adduct**) was characterised by X-ray diffraction analysis (**Scheme 3.8**).

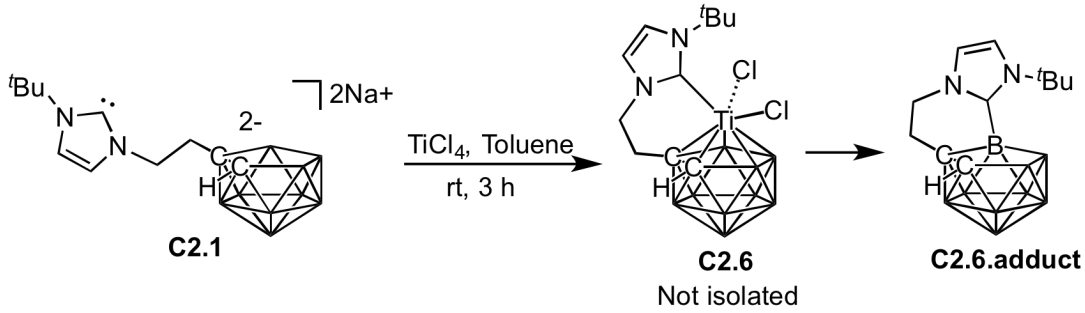

Scheme 3.8 Synthesis of an NHC-carborane adduct (**C2.6.adduct**).

Crystals of **C2.6.adduct** suitable for X-ray diffraction analysis were grown from the slow evaporation of a toluene solution. The molecular structure houses a puckered 6-membered ring with the NCN centre bound to the electrophilic B(7) vertex (**Figure 3.17**). The bridging proton of the carborane was located across the B(4)-B(8) edge, suggesting that the **C2.6.adduct** is zwitterionic with the imidazolium balancing the charge. However, upon inspection of the metric parameters of the imidazolium group it resembles the properties of a carbene. One of the striking differences in NHCs is the N^1-C^7-N^2 bond angles which are significantly smaller in comparison to the parent imidazolium salts.[69] In addition, the $N^{1/2}$-C^7 bond distances lengthen, indicative of a reduction in π-delocalisation in NHCs.[69] This is highlighted in **Table 3.4** with a comparison of the metric parameters of the **C2.6.adduct** to its parent imidazolium. Further clarification of its carbenic properties is provided by comparison to the 2:1 NHC-carborane adduct (**i**) previously reported by the Willans group, which possess an electropositive boron to which two carbenes are bound (**Figure 3.17**).[70]

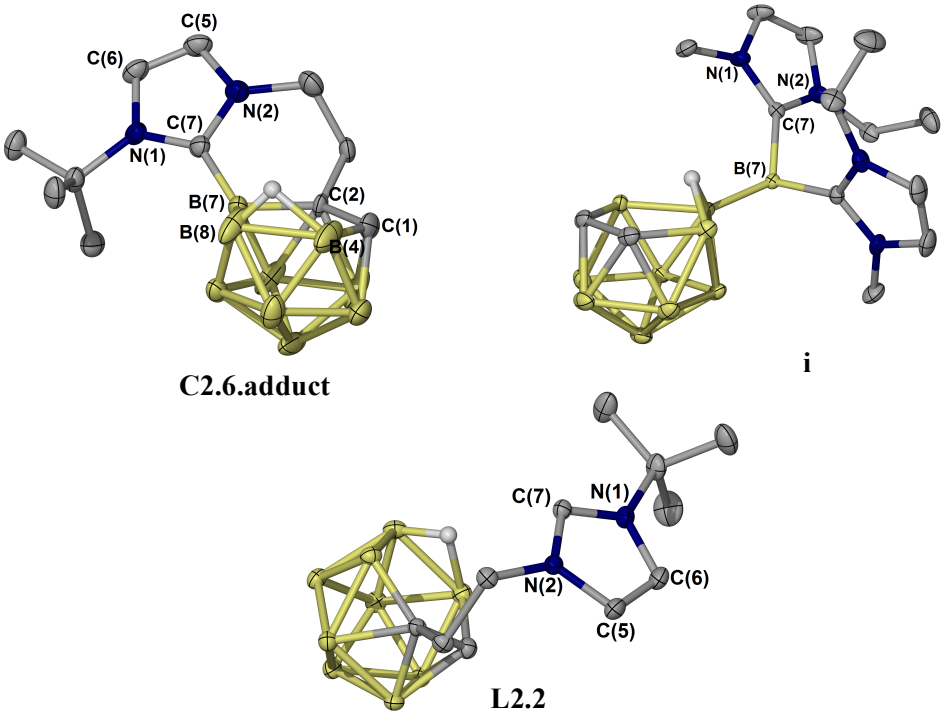

Figure 3.17 Molecular structures of **C2.6.adduct**, the 2:1 NHC-carborane adduct (**i**) reported by Willans *et al.* and our ligand **L2.2**.[70] *Ellipsoids are shown at 40% probability and the hydrogen atoms with the exception of the bridging proton are omitted for clarity. The numbering of the carbon, boron and nitrogen atoms for **L2.2** and **i** are labelled to match those of **C2.6.adduct** for clarity when comparing metric parameters.*

Table 3.4 Selected bond distances and angles for **L2.2**, **C2.6.adduct** and the 2:1 NHC-adduct (**i**).

Parameter	**L2.2**	**C2.6.adduct**	**i**
C(7)-B(7)	-	1.583(3)	1.634(19)
C(7)-N(1)	1.344(13)	1.361(3)	1.356(17)
C(7)-N(2)	1.339(13)	1.355(3)	1.362(17)
C(5)-C(6)	1.362(16)	1.336(4)	1.340(2)
C(6)-N(1)-C(7)	107.93(9)	110.74(2)	110.88(12)
N(1)-C(7)-N(2)	109.14(9)	105.50(2)	104.34(11)
C(7)-N(2)-C(5)	108.57(9)	108.84(2)	110.83(12)
N(2)-C(5)-C(6)	107.08(9)	106.65(2)	107.14(13)
C(5)-C(6)-N(1)	107.28(9)	108.27(2)	106.81(13)

The reaction of **C2.1** with $TiCl_4$ was monitored by multinuclear NMR spectroscopy from which a route to the formation of the **C2.6.adduct** was tentatively proposed (**Scheme 3.10**). The ^1H NMR spectrum of **C2.1** clearly indicates that the bridging proton of the carborane is absent, which reappears in the ^1H NMR spectrum 3 hours after addition of $TiCl_4$ at room temperature. Upon insertion of the NHC into the electrophilic B(7) vertex, a 1,2-migration of the B(7) proton (highlighted in red) occurs and bridges the B(4)-B(8) edge. It can be suggested that upon demetallation the ligand is oxidised with the titanium centre being reduced to $TiCl_2$ as a black precipitate is produced in the reaction.

As the reaction proceeds, in the $^{11}B\{^1H\}$ NMR spectrum multiple peaks are observed in the 10-20 ppm region, which is characteristic of sterically encumbered complexes and is indicative of slippage distortion. Slippage distortion is a result of the metal centre deviating from a symmetrical η^5-cooridnation mode and migration towards the β-boron atom, which in turn becomes highly shielded and experiences a large downfield shift (**Scheme 3.9**).[51] The presence of multiple downfield resonances suggests the formation of multiple species that contain a sterically encumbered titanium centre. Likewise, the ^1H NMR spectrum possesses multiple resonances attributable to the NHC backbone, suggesting that initially **C2.6** may form but is unstable in solution.

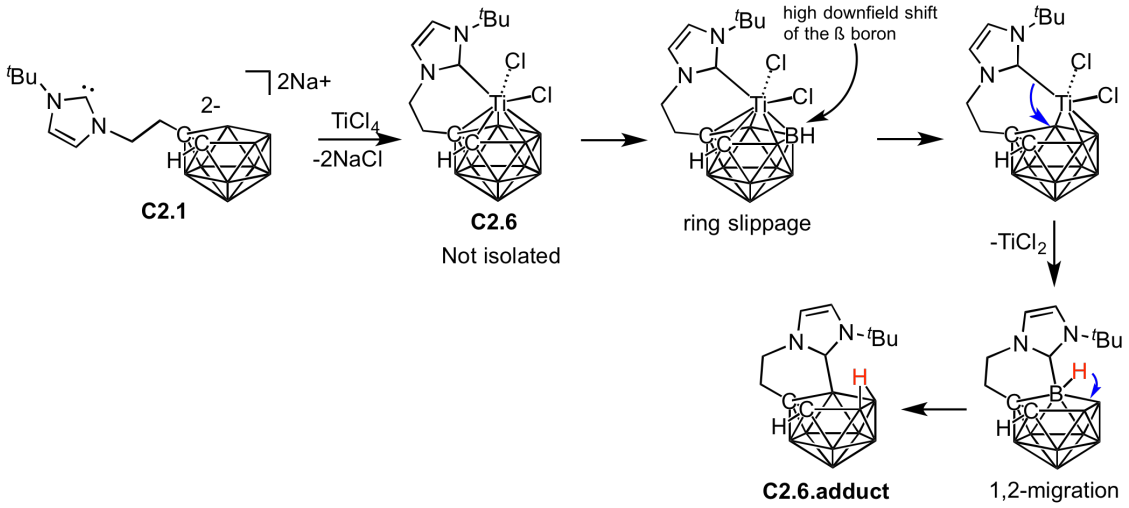

Scheme 3.9 Proposed mechanism for the formation of the **C2.6.adduct**.

Similar observations to those described above have been reported in the literature.[39,71] Kang *et al.* reported sterically protected titanium (aminoethyl)dicarbollides, which undergo demetallation and nitrogen insertion into an electrophilic boron centre of the open face yielding the zwitterion **3.adduct** (**Scheme 3.10**); however this only occurs when the complexes possess high levels of steric encumbrance.[39] **3.adduct** can be isolated in higher yields when **3** is exposed to O_2. Reducing the sterics of the amino group (**4**) allowed a stable complex to be isolated, which resisted demetallation. It is noteworthy that Kang reported a yield of 23 % for **3** when synthesised *via* deprotonation of the ligand with KH and subsequent reaction with $TiCl_4$. It was proposed that a complex redox reaction exists between the deprotonated ligand and $TiCl_4$ leading to a low yield. A respectable yield of 73 % was obtained when the basic metal precursor $Ti(NMe_2)_4$ is employed.

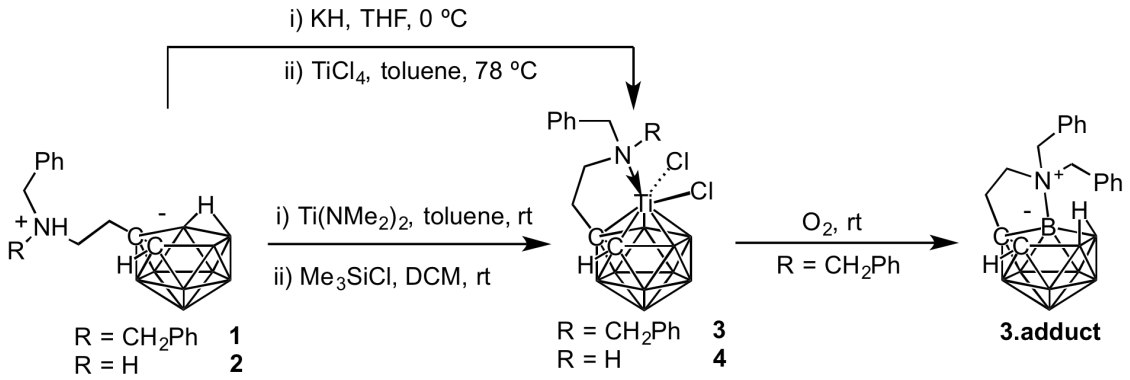

Scheme 3.10 Sterically protected titanium (aminoethyl)dicarbollides.[39]

Kang proposed that the formation of **3.adduct** is metal-mediated and that steric crowding around the metal centre, exerted by the two bulky diphenyl units, causes the facile demetallation. Since Kang found greater success when using $Ti(NMe_2)_4$, this synthetic methodology was employed with **L2.2** to investigate whether a stable Ti complex could be isolated. The reaction of **L2.2** with $Ti(NMe_2)_4$ in CD_3CN was monitored by ^1H and $^{11}B\{^1H\}$ NMR spectroscopy. No reaction takes place until the reaction is heated to 50 ºC, with the downfield imidazolium NC*H*N almost completely disappearing in the ^1H NMR spectrum after 6 hours of heating, suggesting formation of a Ti-$C_{carbene}$ bond (**Figure 3.18**). This can also be observed visually with the initial yellow solution turning deep red, which is indicative of formation of a Ti^{IV}-metallacarborane complex.[62,72] In contrast, the $^{11}B\{^1H\}$ NMR spectrum remains unchanged during reaction of **L2.2** with $Ti(NMe_2)_4$, suggesting the metal is not coordinating to the open face of the carborane. Coordination of the Ti centre to the cage would result in diagnostic shifts in the $^{11}B\{^1H\}$ NMR spectrum.[62,72]

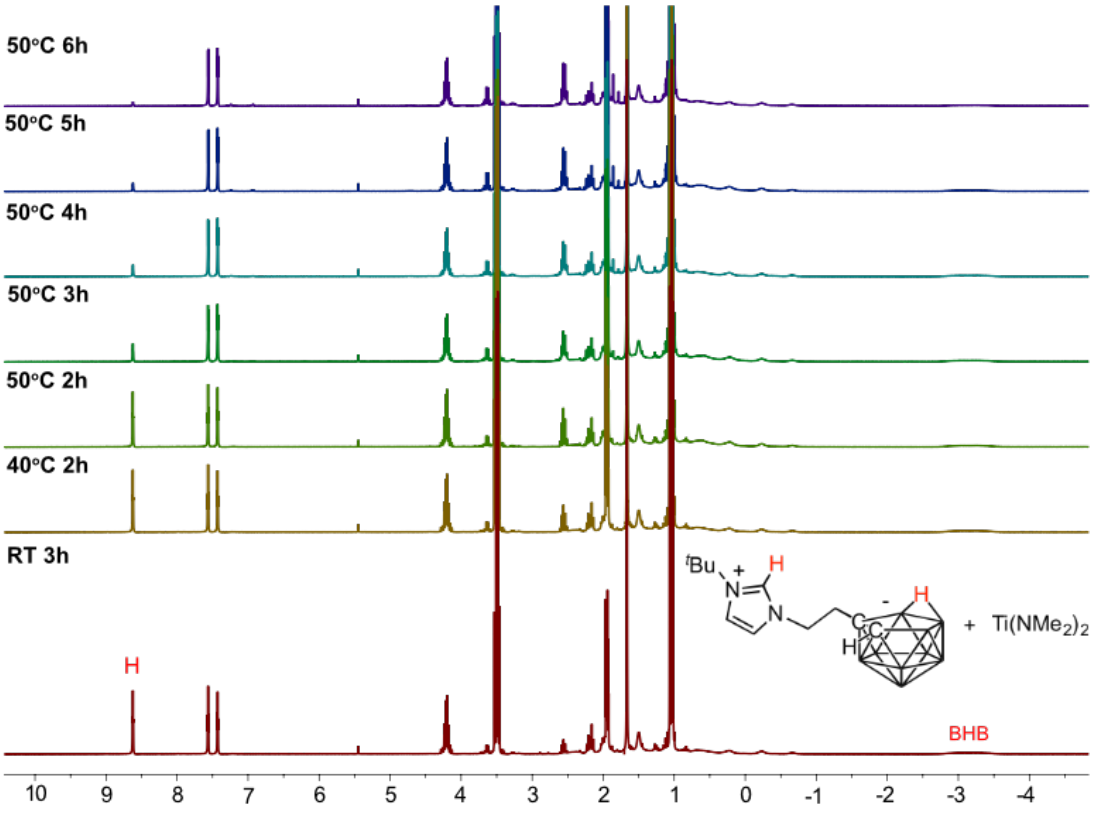

Figure 3.18 ^{1}H NMR spectra (300 MHz, CD_3CN) of the reaction of **L2.2** with $Ti(NMe_2)_4$.

Bright red single crystals suitable for X-ray diffraction analysis were grown by slow diffusion of diethyl ether into the NMR sample. However, these crystals were found to be of the starting material (**L2.2**). This reaction was repeated numerous times, each producing the same outcome. In the reaction, two equivalents of dimethylamine ($HNMe_2$) are produced as a side product. It can be proposed that a Ti^{IV} complex exists in equilibrium with the starting material; the highly basic carbene deprotonates the weakly basic $HNMe_2$ (pKa 10.7) reforming the imidazolium (**Scheme 3.11**). The coordination of Ti to the carborane remains speculative but has been included in the proposed reaction, with the dianonic cage accepting the proton from the second equivalent of $HNMe_2$ formed. Efforts were made to remove $HNMe_2$ from the reaction by employing high temperatures and regular intervals of removing volatiles *in vacuo* from the reaction mixture, but **C2.7** could not be isolated.

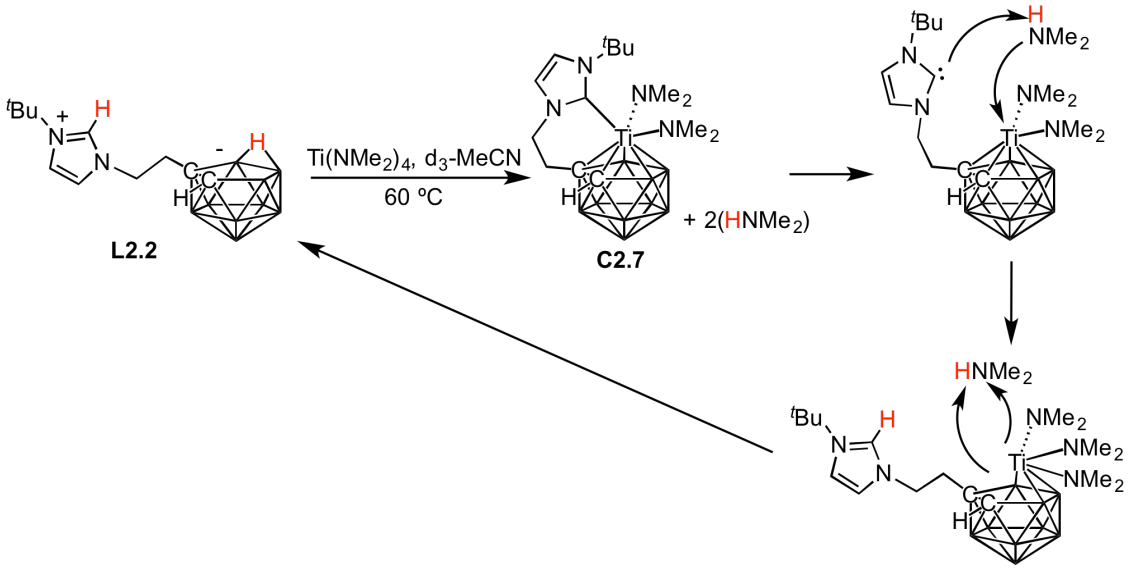

Scheme 3.11 Proposed formation and decomposition pathway of **C2.7**.

3.8 Conclusions and future work

A series of studies have been conducted to examine the deprotonation of imidazolium *nido*-carborane zwitterions **L1.2**, **L2.2** and **L4.1**. Successful deprotonation occurred at both the imidazolium NC*H*N proton and the bridging proton of the C_2B_3 face when the tether between the imidazolium and the carborane substituent is either an ethyl (**L2.2**) or propyl (**L4.1**) chain. When the shorter methyl (**L1.2**) tether is explored, deprotonation of the bridging proton of the C_2B_3 face was observed, though the imidazolium NC*H*N proton remains present.

The fully deprotonated NHC-carborane, *i.e.* the free carbene **C2.1** (with the ethyl tether), was subsequently screened with a range of metal precursors. Reaction with $[Rh(COD)Cl]_2$ led to the isolation of an unusual bimetallic complex **C2.3,** which possesses two contrasting Rh^I environments (**Scheme 3.12**). While derivatives of the $[Rh^I(carborane)(COD)]^-$ anion have been known for decades,[73,74] this is the first solid-state structural elucidation of its kind. In Chapter 4 the catalytic viability of **C2.3** is evaluated in the hydrosilylation of acetophenone.

An Fe^{III} metallacarborane **C8** was isolated through reaction of **C2.1** with $FeCl_2$. The presumed Fe^{II} complex that initially forms is completely insoluble, with the Fe^{III} charge compensated complex being obtained on exposure to air (**Scheme 3.12**). Attempts to form bimetallic complexes through deprotonation of the imidazolium NC*H*N protons using a range of basic metal precursors were unsuccessful, and it is suspected that the acidity of these protons is too low. Future efforts should look towards screening different bases in conjunction with metal halide salts to determine whether under certain reaction conditions a bimetallic metallacarborane can be isolated.

Reaction of **C2.1** with $TiCl_4$ led to formation of an unusual NHC-carborane adduct (**C2.6.adduct**) (**Scheme 3.12**). Similar observations have been reported in the literature, and it can be proposed that the steric stress that the NHC exerts at the metal centre leads reductive elimination of the metal. The question that arises from this chemistry is whether reducing the sterics of the NHC would allow a stable complex to be isolated.

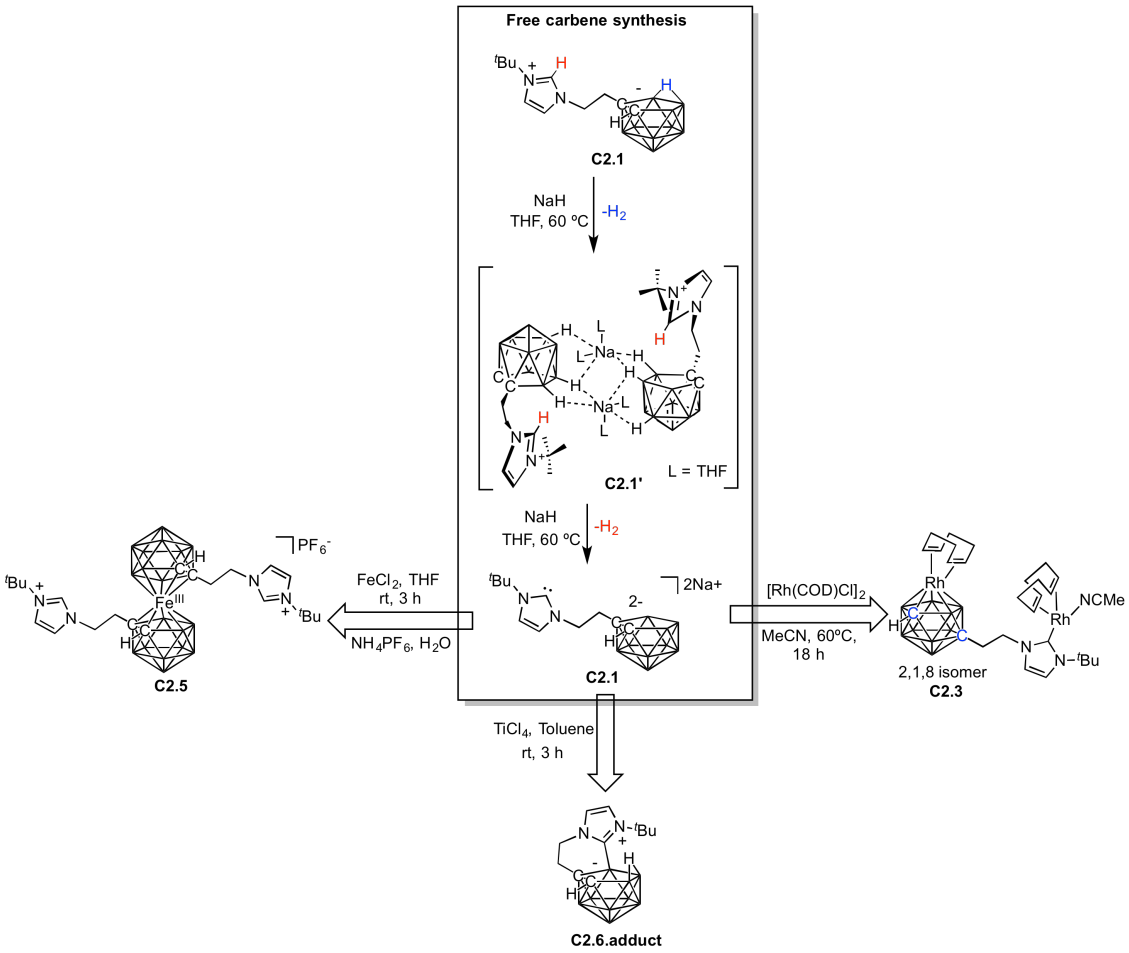

Scheme 3.12 Summary of work reported in this Chapter.

3.9 Experimental

3.9.1 General Considerations

All manipulations were carried out under an inert atmosphere by means of standard Schlenk line or glovebox techniques, unless otherwise stated. Anhydrous solvents were prepared by passing over activated alumina to remove water, copper catalyst to remove oxygen and molecular sieves to remove any remaining water, *via* the DowGrubbs solvent system, and then freeze-pump-thaw degassed prior to use. All chemicals used in this work were bought from either Sigma Aldrich or Alfa Aesar and used without further purification. NMR spectra were recorded on a Bruker AV500 or a Bruker DPX300 spectrometer. ^{1}H NMR and ^{13}C{^{1}H} NMR chemical shifts were referenced against residual solvent peaks. Assignment of ^{1}H and ^{13}C{^{1}H} NMR spectra for all complexes was aided by the use of 2D ^{1}H^{1}H COSY, ^{1}H^{13}C HMQC, ^{1}H^{13}C HMBC and ^{13}C{^{1}H} DEPT 135 experiments. Mass spectra were collected on a Bruker Daltonics (micro TOF) instrument operating in the electrospray mode. Elemental analyses were performed by Mrs Tanya Marinko-Covell at The University of Leeds. The synthesis of the ligand precursors used in this chapter can be found in Chapter 2.

3.9.2 Metal precursors

Preparation of $[Rh(COD)Cl]_2$.[75]

To a RBF was added $RhCl_{3.3}H_2O$ (2.00 g, 7.60 mmol). The system was flushed with N_2 gas and degassed H_2O (10 mL), anhydrous ethanol (50 mL) and 1,5-cyclooctadiene (2.33 mL, 19.00 mmol) was added. The solution was then refluxed at reflux under N_2 for 24 hours. The solvent was decreased to 30 mL *in vacuo* and the yellow solid was collected by filtration and washed with water (3 × 10 mL) and dried *in vacuo*. Yield: 1.44 g, 2.93 mmol (77 %). ^{1}H NMR (300 MHz, $CDCl_3$): δ 4.21 (s, 4H), 2.55-2.39 (m, 4H), 1.81-1.63 (m, 4H). ^{13}C{^{1}H} NMR (75 MHz, $CDCl_3$): δ 78.8 (d, J = 13.9 Hz), 31.0.

3.9.3 NHC-carborane complexes and adducts

Preparation of **C2.2**, **C2.3** and **C2.3'**.

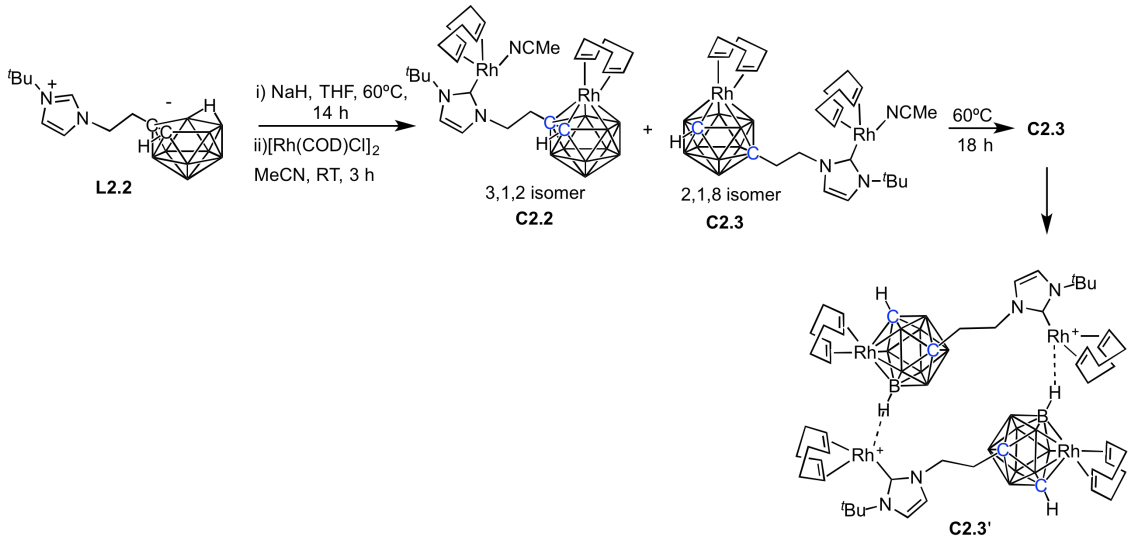

L2.2 (10 mg, 0.04 mmol), NaH (1.80 mg, 0.08 mmol) and anhydrous THF (0.5 mL) were added to a Young's Tap NMR tube. The suspension was heated at 60 ºC for 14 hours. The clear yellow solution was removed *via* syringe from the excess NaH. The solvent was removed in vacuo and $[Rh(COD)Cl]_2$ (19.10 mg, 0.04 mmol) and anhydrous MeCN (1 mL) were added. The reaction mixture was stirred at room temperature for 3 hours. Filtration of the mixture through Celite and slow diffusion of Et_2O into the MeCN solution resulted in crystals of **C2.2** and **C2.3** suitable for X-ray diffraction analysis. To obtain complex **C2.3** only, the reaction mixture was heated at 60 ºC for 18 hours instead of room temperature for 3 hours. This was subsequently filtered through Celite and slow evaporation to concentrate the solution resulted in a yellow crystalline solid. The solid was filtered, washed with anhydrous Et_2O (3 × 5 mL) and dried in vacuo to afford **C2.3** as a yellow crystalline solid. Yield: 22 mg, 0.03 mmol (75 %). Analytical data for **C2.3**; ^{1}H NMR (500 MHz, acetone-d_6): δ 7.45 (d, J = 1.9 Hz, 1H, NCH), 7.30 (s, 1H, NCH), 5.36 (br. s, 1H, CH_2), 4.84 (m, 2H, COD-CH), 4.32 (m, 2H, COD-CH), 4.22 (m, 3H, COD-CH, CH_2), 3.81 (br. s, 1H, COD-CH), 3.66 (br. s, 1H, COD-CH), 2.45 (m, 25H, CH_2, COD-CH_2, CH_3, $(CH_3)_3$, carborane cage CH). ^{13}C{^{1}H} NMR (126 MHz, acetone-d_6): δ 174.2 (d, $^1J_{Rh\text{-}C}$ = 50.4 Hz, NCN), 122.3 (NCCN), 96.6 (COD-*C*H), 93.0 (COD-*C*H), 81.5 (COD-*C*H), 75.4 (d, $^1J_{Rh\text{-}C}$ = 10.1 Hz, COD-*C*H), 75.0 (d, $^1J_{Rh\text{-}C}$ = 11.3 Hz, COD-*C*H), 59.2 (*C*$(CH_3)_3$), 53.7 (CH_2), 47.5 (carborane cage quaternary C), 42.6 (CH_2), 36.6 (NC*C*H_3), 34.3 (COD-CH_2), 33.8 (COD-CH_2, carborane cage CH), 32.3 ($(CH_3)_3$), 32.0-28.9 (COD-CH_2), 3.5 (N*C*CH_3). ^{11}B{^{1}H} NMR (161 MHz, acetone-d_6): δ −6.3 (2B), −10.7 (2B), −13.0 (2B), −22.1 (3B). HRMS (ESI$^+$): m/z $[C_{27}H_{50}B_9N_2Rh_2]^+$ 706.2982, calcd for $[M\text{-}MeCN+H]^+$ 706.2971. Anal. calcd for $C_{29}H_{52}B_9N_3Rh_2$: C, 46.70 ; H, 7.03; N, 5.63. Found: C, 46.40; H, 7.10; N, 5.70. Crystals suitable for X-ray diffraction analysis were grown by slow evaporation of a concentrated solution of **C2.3** in acetone. Crystals of **C2.3'** suitable for X-ray

diffraction analysis were grown by re-dissolving crystals of **C2.3** in the minimum amount of MeCN followed by the addition of anhydrous Et_2O and hexane in a ratio of 1:3:3.

Preparation of **C2.5**

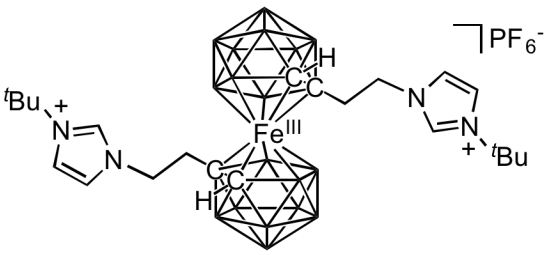

L2.2 (20 mg, 0.07 mmol), NaH (3.5 mg, 0.15 mmol) and anhydrous THF (0.5 mL) were added to a Young's Tap NMR tube. The suspension was heated at 60 ºC for 14 hours. The clear yellow solution was removed *via* syringe from the excess NaH and transferred to another Young's Tap NMR tube containing $FeCl_2$ (5.1 mg, 0.04 mmol). Within a few minutes a purple precipitate formed. After 3 hours at room temperature, the reaction mixture was exposed to air resulting in the violet precipitate resolublising with the solution becoming deep red in colour. The solvent was removed *in vacuo* and DCM (5 mL) followed by NH_4PF_6 (11.4 mg, 0.07 mmol) was added. The reaction was stirred for 10 minutes at room temperature then the organic phase was washed with H_2O (3 × 5 mL), filtered and dried *in vacuo*. The product was recrystallised from acetone (5 mL) with H_2O (5 mL) to give a red crystalline solid. Yield: 7.7 mg, 0.01 mmol (34 %). HRMS (ESI^+): m/z 623.5380 $[C_{22}H_{58}B_{18}N_4Fe]^+$, Calcd for $[M\text{-}PF_6]^+$ 623.5335. Anal. calcd. for $C_{22}H_{58}B_{18}N_4FePF_6$: C, 34.40 ; H, 6.82; N, 7.29. Found: C, 33.98; H, 6.51; N, 7.33. Crystals suitable for X-ray diffraction analysis were grown from the slow evaporation of a mixed solvent system (acetone/water 3:1).

Preparation of **C2.6.adduct**.

L2.2 (10 mg, 0.04 mmol), NaH (1.8 mg, 0.08 mmol) and anhydrous THF (0.5 mL) were added to a Young's Tap NMR tube. The suspension was heated at 60 ºC for 14 hours. The clear yellow solution was removed *via* syringe from the excess NaH. The solvent was removed in vacuo and anhydrous toluene (0.5 mL) followed by $TiCl_4$ (1eq). Crystals suitable for X-ray diffraction analysis were grown from the slow evaporation of a toluene solution. Note: Isolation of **C2.6.adduct** to obtain spectroscopic data was not possible due to the very small quantity of crystals formed.

3.10 References

1 T. E. Paxson and M. F. Hawthorne, *J. Am. Chem. Soc.*, 1974, **96**, 4674–4676.

2 E. L. Hoel and M. F. Hawthorne, *J. Am. Chem. Soc.*, 1974, **96**, 4676–4677.

3 J. A. Long, T. B. Marder and M. F. Hawthorne, *J. Am. Chem. Soc.*, 1984, **106**, 3004–3010.

4 T. B. Marder, J. A. Long and M. F. Hawthorne, *J. Chem. Soc. Chem. Commun.*, 1980, 677.

5 J. A. Belmont, J. Soto, R. E. King, A. J. Donaldson, J. D. Hewes and M. F. Hawthorne, *J. Am. Chem. Soc.*, 1989, **111**, 7475–7486.

6 F. Teixidor, M. A. Flores, C. Viñas, R. Kivekäs and R. Sillanpää, *Angew. Chemie Int. Ed.*, 1996, **35**, 2251–2253.

7 B. Marciniec, *Hydrosilylation : a comprehensive review on recent advances*, Springer, 2009.

8 S. Díez-González and S. P. Nolan, *Org. Prep. Proced. Int.*, 2007, **39**, 523–559.

9 N. Miyaura, *Bull. Chem. Soc. Jpn.*, 2008, **81**, 1535–1553.

10 L. F. R. Gomes, A. F. Trindade, N. R. Candeias, P. M. P. Gois and C. A. M. Afonso, *Tetrahedron Lett.*, 2008, **49**, 7372–7375.

11 F. J. Gómez, N. E. Kamber, N. M. Deschamps, A. P. Cole, A. A. Wender and R. M. Waymouth, *Organometallics*, 2007, **26**, 4541–4545.

12 W. Gil, T. Lis, A. M. Trzeciak and J. J. Ziółkowski, *Inorganica Chim. Acta*, 2006, **359**, 2835–2841.

13 S. I. Lee, S. Y. Park, J. H. Park, I. G. Jung, A. S. Y. Choi, Y. K. Chung and B. Y. Lee, *J. Org. Chem.*, 2006, **71**, 91–96.

14 J. M. Praetorius, C. M. Crudden, V. R. Jensen, C. Esterhuysen, H. G. Raubenheimer, V. Paquet, H. Lebel, M. W. Day and R. H. Grubbs, *Dalt. Trans.*, 2008, **129**, 4079.

15 S. Diez-Gonzalez, N. Marion and S. P. Nolan, *Chem. Rev.*, 2009, **109**, 3612–3676.

16 M. Aydemir, A. Baysal, N. Meric, C. Kayan, B. Gümgüm, S. Özkar and E. Şahin, *J. Organomet. Chem.*, 2011, **696**, 2584–2588.

17 P. Satyanarayana, G. M. Reddy, H. Maheswaran and M. L. Kantam, *Adv. Synth. Catal.*, 2013, **355**, 1859–1867.

18 A. McSkimming, B. Chan, M. M. Bhadbhade, G. E. Ball and S. B. Colbran, *Chem. - A Eur. J.*, 2015, **21**, 2821–2834.

19 M. Poyatos, W. McNamara, C. Incarvito, E. Clot, E. Peris and R. H. Crabtree, *Organometallics*, 2008, **27**, 2128–2136.

20 M. Poyatos, W. McNamara, C. Incarvito, E. Peris, R. H. Crabtree, W. Ponikwar, H. Noth, C. Moinet and W. P. Fehlhammer, *Chem. Commun.*, 2007, **124**, 2267.

21 W. A. Herrmann, L. J. Goossen, C. Köcher and G. R. J. Artus, *Angew. Chemie Int. Ed.*, 1996, **35**, 2805–2807.

22 D. Enders, H. Gielen and K. Breuer, *Tetrahedron: Asymmetry*, 1997, **8**, 3571–3574.

23 W.-L. Duan, M. Shi and G.-B. Rong, *Chem. Commun.*, 2003, 2916–2917.

24 L. H. Gade, V. César and S. Bellemin-Laponnaz, *Angew. Chemie Int. Ed.*, 2004, **43**, 1014–1017.

25 K. Riener, M. P. Högerl, P. Gigler and F. E. Kühn, *ACS Catal.*, 2012, **2**, 613–621.

26 M. F. Hawthorne, D. C. Young and P. A. Wegner, *J. Am. Chem. Soc.*, 1965, **87**, 1818–1819.

27 R. N. Grimes, *Carboranes*, Academic Press, 2011.

28 A A. Danopoulos, N. Tsoureas, A. J. A. Wright and M. E. Light, *Organometallics*, 2004, **23**, 166–168.

29 R. A. Andersen, K. Faegri, J. C. Green, A. Haaland, M. F. Lappert, W. P. Leung., *Inorg. Chem.*, 1988, **27**, 1782–1786.

30 K. Riener, S. Haslinger, A. Raba, M. P. Högerl, M. Cokoja, W. A. Herrmann and F. E. Kühn, *Chem. Rev.*, 2014, **114**, 5215–5272.

31 N. R. C. (US) C. S. Roundtable, *Replacing Critical Materials with Abundant Materials*, National Academies Press (US), 2012.

32 H. G. Seiler, H. Sigel and A. Sigel, *Handbook on toxicity of inorganic compounds*, 1988.

33 V. V. K. M. Kandepi, J. M. S. Cardoso, E. Peris and B. Royo, *Organometallics*, 2010, **29**, 2777–2782.

34 R. Lopes, J. M. S. Cardoso, L. Postigo and B. Royo, *Catal. Letters*, 2013, **143**, 1061–1066.

35 D. S. McGuinness, A. Vernon C. Gibson and J. W. Steed, *Organometallics*, 2004, **23**, 6288–6292.

36 H. Aihara, T. Matsuo, H. Kawaguchi, H. Ebeling, A. Tuchbreiter, R. Mülhaupt and M. E. Lappert, *Chem. Commun.*, 2003, **38**, 2204.

37 D. Zhang, G. Zi, K. A. Scheidt, F. Foubelo, M. Tada, V. Poirier, Y. Sarazin, A. Trifonov, M. Nitabaru, T. Nakano, H. Tanaka, N. Kashiwa, T. Fujita and T. Fujita, *Chem. Soc. Rev.*, 2015, **44**, 1898–1921.

38 D.-H. Kim, J. H. Won, S.-J. Kim, J. Ko, S. H. Kim, S. Cho and S. O. Kang, *Organometallics*, 2001, **20**, 4298–4300.

39 Y.-J. Lee, J.-D. Lee, H.-J. Jeong, K.-C. Son, J. Ko, A. M. Cheong and S. O. Kang, *Organometallics*, 2005, **24**, 3008–3019.

40 M. F. Hawthorne, D. C. Young, T. D. Andrews, D. V. Howe, R. L. Pilling, A. D. Pitts, M. Reintjes, L. F. Warren and P. A. Wegner, *J. Am. Chem. Soc.*, 1968, **90**, 879–896.

41 A. J. Arduengo, R. L. Harlow and M. Kline, *J. Am. Chem. Soc.*, 1991, **113**, 361–363.

42 A. R. Kudinov, D. S. Perekalin, S. S. Rynin, K. A. Lyssenko, G. V. G-Knyazev, P. V. Petrovskii, *Boron Chemistry at the beginning of the 21st Century*, 2003.

43 M. M. Vinogradov, M. V. Zakharova, S. V. Timofeev, D. A. Loginov, I. B. Sivaev, Y. V. Nelyubina, Z. A. Starikova, V. I. Bregadze and A. R. Kudinov, *Inorg. Chem. Commun.*, 2015, **51**, 80–82.

44 M. E. Fessler, T. Whelan, J. T. Spencer and R. N. Grimes, *J. Am. Chem. Soc.*, 1987, **109**, 7416–7420.

45 D. Grafstein and J. Dvorak, *Inorg. Chem.*, 1963, **2**, 1128–1133.

46 S. Papetti and T. L. Heying, *J. Am. Chem. Soc.*, 1964, **86**, 2295–2295.

47 L. F. Warren and M. F. Hawthorne, *J. Am. Chem. Soc.*, 1970, **92**, 1157–1173.

48 M. F. Hawthorne, M. K. Kaloustian and R. J. Wiersemay, *J. Am. Chem. Soc.*, 1971, **93**, 4912–4913.

49 D. F. Dustin, W. J. Evans, C. J. Jones, R. J. Wiersema, H. Gong, S. Chan and M. F. Hawthorne, *J. Am. Chem. Soc.*, 1974, **96**, 3085–3090.

50 J. A. Doi, E. A. Mizusawa, C. B. Knobler and M. F. Hawthorne, *Inorg. Chem.*, 1984, **23**, 1482–1484.

51 K. A. Fallis, D. F. Mullica, E. L. Sappenfield and F. G. A. Stone, *Inorg. Chem.*, 1994, **33**, 4927–4933.

52 M. M. Vinogradov, Y. V. Nelyubina, A. A. Pavlov, V. V. Novikov, N. V. Shvydkiy and A. R. Kudinov, *Organometallics*, 2017, **36**, 791–800.

53 P. S. Engl, R. Senn, E. Otth and A. Togni, *Organometallics*, 2015, **34**, 1384–1395.

54 E. Jansen, M. Lutz, B. de Bruin and C. J. Elsevier, *Organometallics*, 2014, **33**, 2853–2861.

55 B. J. Truscott, A. M. Z. Slawin and S. P. Nolan, *Dalt. Trans*, 2013, **42**, 270–276.

56 B. J. Truscott, G. C. Fortman, A. M. Z. Slawin, S. P. Nolan, F. Maseras, S. P. Nolan and V. V. Ratovelomanana-Vidal, *Org. Biomol. Chem.*, 2011, **9**, 7038.

57 L. Palacios, A. Di Giuseppe, A. Opalinska, R. Castarlenas, J. J. Pérez-Torrente, F. J. Lahoz and L. A. Oro, *Organometallics*, 2013, **32**, 2768–2774.

58 P. E. Behnken, T. B. Marder, R. T. Baker, C. B. Knobler, M. R. Thompson and M. F. Hawthorne, *J. Am. Chem. Soc.*, 1985, **107**, 932–940.

59 H. C. Kang, S. S. Lee, C. B. Knobler and M. F. Hawthorne, *Inorg. Chem.*, 1991, **30**, 2024–2031.

60 R. N. Grimes, in *Comprehensive Organometallic Chemistry*, 1982, pp. 459–542.

61 D. J. Arriola, M. Bokota, J. Richard E. Campbell, J. Klosin, R. E. LaPointe, O. D. Redwine, R. B. Shankar, A. Francis J. Timmers and K. A. Abboud, *J. Am. Chem. Soc.*, 2007, **129**, 7065–7076.

62 D.-H. Kim, J. H. Won, S.-J. Kim, J. Ko, S. H. Kim, A. S. Cho and S. O. Kang, *Organometallics*, 2001, **20**, 4298–4300.

63 J.-D. Lee, Y.-J. Lee, K.-C. Son, M. Cheong, and J. Ko and S. O. Kang, *Organometallics*, 2007, **26**, 3374–3384.

64 Z. Yinghuai, S. Lo Pei Sia, F. Kooli, K. Carpenter and R. A. Kemp, *J. Organomet. Chem.*, 2005, **690**, 6284–6291.

65 Z. Yinghuai, Z. Yulin, K. Carpenter, J. A. Maguire and N. S. Hosmane, *J. Organomet. Chem.*, 2005, **690**, 2802–2808.

66 H. Wang, Y. Wang, A. H.-W. Li and Z. Xie, *Organometallics*, 2001, **20**, 5110–5118.

67 Guofu Zi, A. Hung-Wing Li and Z. Xie, *Organometallics*, 2002, **21**, 3850–3855.

68 H. Wang, H.-S. Chan, J. Okuda and Z. Xie, *Organometallics*, 2005, **24**, 3118–3124.

69 F. E. Hahn and M. C. Jahnke, *Angew. Chemie Int. Ed.*, 2008, **47**, 3122–3172.

70 C. E. Willans, C. A. Kilner and M. A. Fox, *Chem. - A Eur. J.*, 2010, **16**, 10644–10648.

71 S. P. Downing and A. A. Danopoulos, *Organometallics*, 2006, **25**, 1337–1340.

72 M. Gao, Y. Tang, M. Xie, C. Qian and Z. Xie, *Organometallics*, 2006, **25**, 2578–2584.

73 R. Núñez, O. Tutusaus, F. Teixidor, C. Viñas, A. R. Sillanpää and R. Kivekäs, *Organometallics*, 2004, **23**, 2273–2280.

74 D. M. Speckman, C. B. Knobler and M. F. Hawthorne, *Organometallics*, 1985, **4**, 426–428.

75 R. H. Giordano, G.; Crabtree, *Inorg. Synth.*, 1990, **28**, 88.

Chapter 4

Synthesis of a chelating N-heterocyclic carbene-carborane Rh^{I} complex

The synthesis and full characterisation of Rh^{I}-NHC complexes that exhibit closo-carboranyl substituents is discussed. These complexes display unprecedented chemistry with a rare example of a Rh^{I}-metallacycle coordinating through both the NHC and the carbon vertex of the carborane. The catalytic activity of these complexes was probed in the hydrosilylation of acetophenone.

4.1 Introduction

In carborane chemistry, "cyclometallation" implies intramolecular metallation forming a bicyclic complex in which the metal is bound through a donor atom and either through the carbon or a boron vertex of the cage. In the literature, the process of cyclometallation of carboranes can be organised into two categories; 1) cyclometallation without a change in the formal oxidation state of the metal, and 2) oxidative addition to the metal. The latter mainly involves an Ir^{I} centre, which spontaneously adds across the B-H bond of the cage to form the corresponding M^{III} hydride complex, and was first reported by Hawthorne and co-workers in 1975.[1] Most recently Lavallo reported carboranyl phosphine ligands bearing either the dicarba-*closo*-dodecaborane (**i**) or the monocarba-*closo*-dodecaborate anion (**ii**), with both displaying very different chemistry (**Scheme 4.1**).[2] Carboranyl phosphine ligand **i** displayed the expected oxidative addition across the B-H bond of the B3/B6 vertex to give the Ir^{III} metallacycle. Oxidative addition involves the transfer of electrons from the metal to the B-H bond and will always take place at the vertices with the least electron density, which in the dicarba-*closo*-dodecaborane are the B3/B6 vertices. Carboranyl phosphine ligand **ii** resists spontaneous B-H cyclometallation, which is the first example reported in the literature.

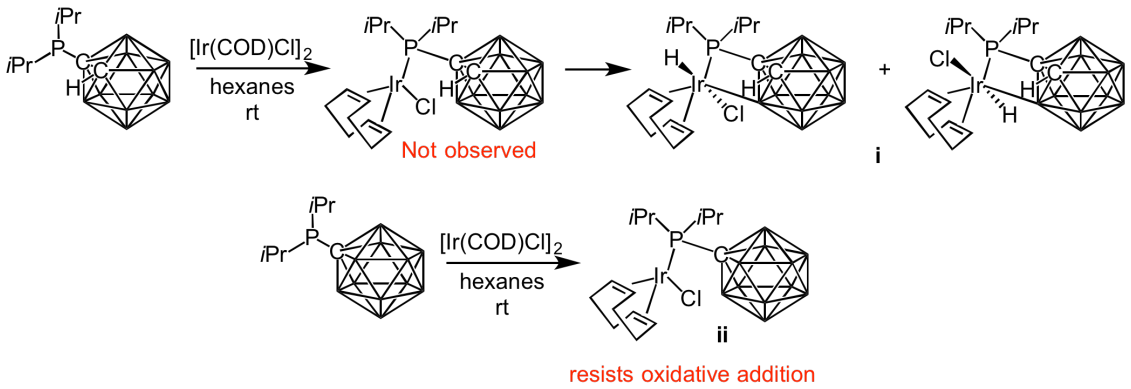

Scheme 4.1 Ir^{I}(COD) carboranyl phosphine complexes reported by Lavallo and co-workers.[2]

Lavallo suggests that **ii** has important implications for the design of future carborane catalysts, as carboranyl phosphine complexes bearing a dicarba-*closo*-dodecaborane had previously been found to be poor catalysts due to spontaneous B-H cyclometallation impeding on the catalytic activity of the complexes.[3–6]

Whilst oxidative addition across the B-H bond of the B3/B6 vertices is relatively facile, selective B-H activation of specific B-H vertices other than these electrophilic boron atoms is very difficult, though remains an active area of research. Metal mediated B-H bond functionalisation of carboranes is an important chemical transformation to provide structurally diverse carborane derivatives. B-H activation of small boranes has been successful,[7–10] but with the larger dodecaborane there are only a few examples. Half sandwich Ir^{III} complexes serve as effective reagents to induce B-H bond activation to afford metal-boryl complexes.[11–13] An exquisite example utilises three carborane (*o*-, *m*-, *p*-) dicarboxylates, which act as directing groups to allow site specific B-H activation at the B4/7 vertices of *m*-carborane and B2/10 vertices of *p*-carborane, with this being the first example of B-H activation of a *p*-carborane derivative (**Figure 4.1**, **iii**). In addition, the directing groups allow switchable reactivity between C-H and B-H bonds (**Figure 4.1**, **iv** and **v**).[14]

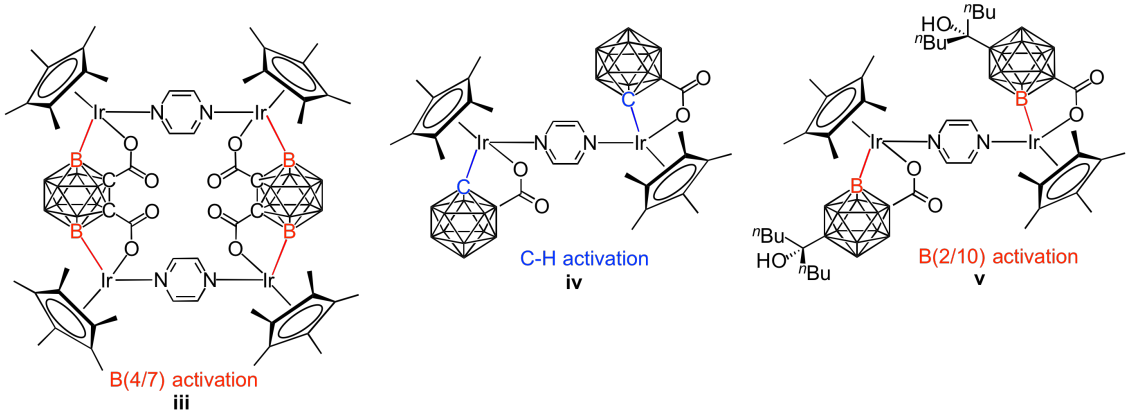

Figure 4.1 Complexes published by Jin and co-workers in which selective B-H (**iii** and **v**) and C-H (**iv**) activation is achieved.[14]

Typically, C-cyclometallated carboranes are prepared under relatively harsh conditions by employing ^{n}BuLi to generate C-lithiocarboranes, which are subsequently reacted with a metal salt. Some of the earliest examples involved metal σ-carbon bonds to Al and Ga,[15] Ni,[16] and Pt.[17] Surprisingly, there are only two examples of carboranes that possess a Rh^{I} centre bound through a C vertex of the cage, and only one of these is cyclometallated, with nearly four decades separating the two publications (**Scheme 4.2**).[18,19] Both Rh^{I} complexes are air and moisture sensitive, and complex **viii** was found to be a by-product of the reaction. It was proposed that this is formed *via* nucleophilic addition of the carboranyl anion to complex **vii**, which has previously been reported by Basato *et al*. in an analogous Ru-based system.[20]

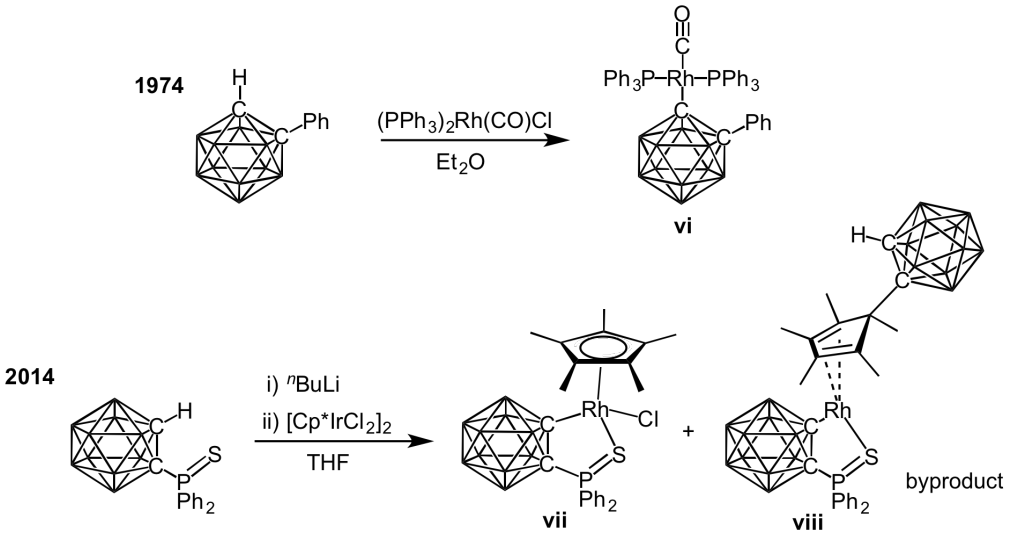

Scheme 4.2 Literature examples of complexes bearing a Rh^{I} centre σ-bound to a carboranyl carbon.[18,19]

In comparison, the literature is rich with examples of C-cyclometallated carborane complexes of the higher oxidation states of Rh^{III} and Ir^{III}.[12–14,19,21–23] Most recently, an Ir^{III} complex coordinated by an *o*-carboranyl phosphine ligand had been considered for its photophysical properties.[22] Cyclometallated Ir^{III} complexes have been widely used as colour-tuneable emitters in organic light-emitting diodes (OLEDs).[24,25] Most examples in the literature look at varying the electronic structure of a C^N ligand (typically derivatives of 2-phenylpyridine) to provide emitters with the all important sky blue or deep blue phosphorescence.[26–28] Alternatively, the choice of a strong-field ancillary ligand can provide the same effect,[28–30] and it was found that the carboranyl ligand led to a large blue shift of the emission bands (**Figure 4.2**).

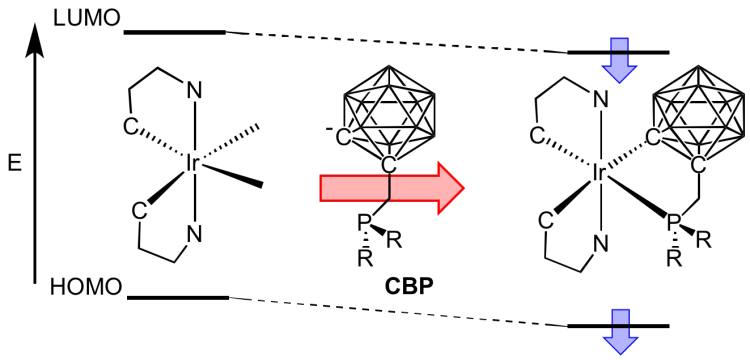

Figure 4.2 An Ir^{III} complex supported by an *o*-carboranyl phosphine reported by x et al. The strong field ancillary ligand (*o*-carborane) leds to a large shift toward blue phosphorescence.[22]

Overall, the field of Rh and Ir complexes exhibiting C- or B- coordination through the carborane is vast. The majority of these examples have been examined for their coordination chemistry, though the catalytic potential of these complexes is rarely examined. The work described in this chapter provides interesting insight into the coordination chemistry of NHC-carborane ligands, in addition to assessing the catalytic potential of the resulting complexes.

4.2 Aims

As discussed in Chapter 3, **L2.2** demonstrated interesting coordination chemistry at Rh^I, with isolation of a bimetallic complex (**C2.3**), which possesses two contrasting Rh^I environments (**Scheme 4.3**). The complex displayed low temperature isomerisation to yield the 2,1,8 isomer as a result of the high steric stress at the metal centre of the $[Rh^I(carborane)(COD)]^-$ anion. The work herein looks to extend this work and explore the coordination chemistry of the *closo*-carboranyl imidazolium salts such as **L2.1** (Chapter 2) at Rh^I. The catalytic viability of these complexes was evaluated in the hydrosilylation of acetophenone.

4.3 Complex synthesis

One of the most challenging aspects of the chemistry involving the zwitterionic ligands such as **L2.2** was achieving full deprotonation, which required a strong base (NaH). In contrast, imidazolium halide salts such as **L2.1** are known to deprotonate under much milder conditions *via in situ* transmetallation using Ag_2O, or by use of other basic metal precursors which deprotonate and form the metal carbene bond *in situ*.[31–35] Employing Ag_2O in the presence of **L2.1** and $[Rh(COD)Cl]_2$ in DCM allowed selective deprotonation of the NC*H*N proton and gave the corresponding Rh^INHC(COD)Cl complex **C2.11** in high yield (**Scheme 4.3**).

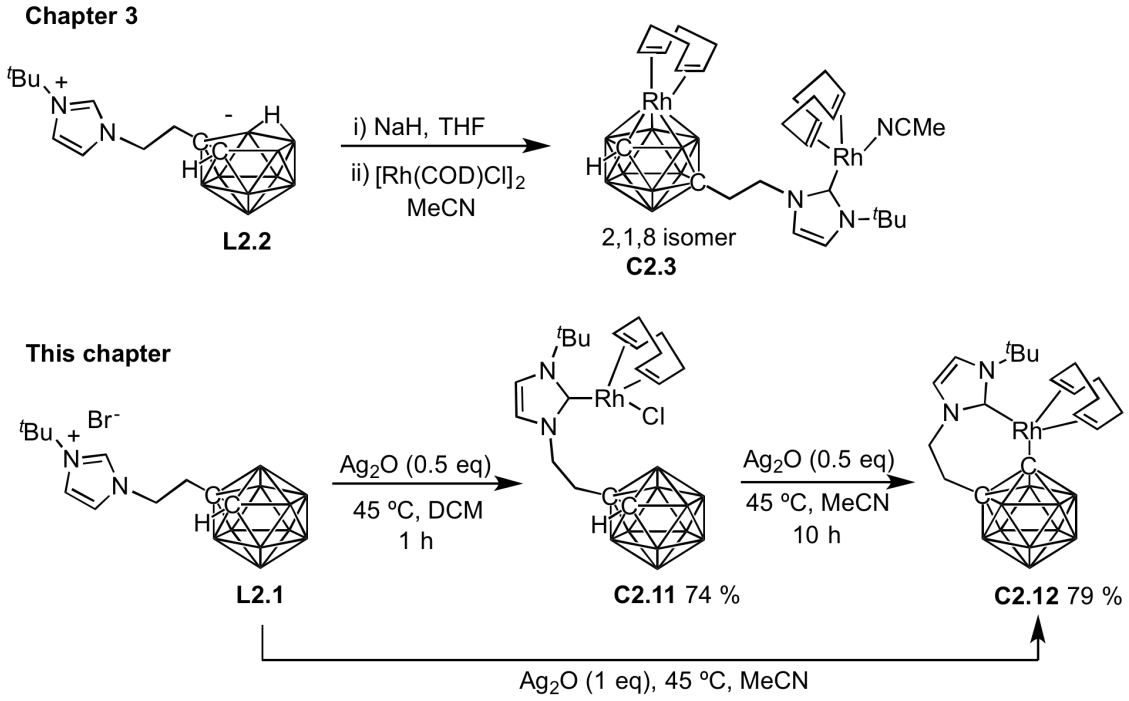

Scheme 4.3 Synthesis of a Rh^INHC(COD)Cl complex **C2.11** and Rh^I-metallacycle **C2.12**.

Surprisingly, when the same reaction was repeated in MeCN and an excess of Ag_2O was employed, the isolated product was identified as an unusual seven-membered metallacycle **C2.12**. In this case, the ligand chelates the Rh^I centre, coordinating through the carbenic carbon of the NHC and through the carbon vertex of the carborane. Deprotonation of the cage CH proton under such mild conditions is rare,[14,18] with a strong base such as ^{n}BuLi usually being used prior to addition of the metal precursor (Section 4.1).[19,22]

With different products being observed in DCM and MeCN, a range of solvents were screened to further understand the role of the solvent in this reaction. In the glove box, **C2.11** and Ag_2O (0.5 eq) were added to a Young's Tap NMR tube and dissolved in various anhydrous deuterated solvents. The reaction mixtures were heated at 45 °C and monitored over time using ^{1}H NMR spectroscopy. It was found that a coordinating solvent is necessary to promote the cyclometallation process, whereas no reaction occurs in non-coordinating solvents, and protic solvents led to complex decomposition (**Table 4.1**). A control reaction was also conducted in which **C2.11** was heated in MeCN in the absence of Ag, and monitored over the course of several days, with no cyclometallation observed. Presumably, Ag_2O is acting both as a chloride-abstracting agent and a base in this reaction.[36] The removal of the chloride must be promoted by the presence of a coordinating solvent, which stabilises the cationic Rh^I centre. Following this, the cage CH proton is deprotonated leading to M-C bond formation to yield **C2.12,** with AgOH precipitated as a brown solid from the reaction (**Scheme 4.4**).

Table 4.1 Solvent screening reaction in the cyclometallation of **C2.11** monitored by ^{1}H NMR spectroscopy.

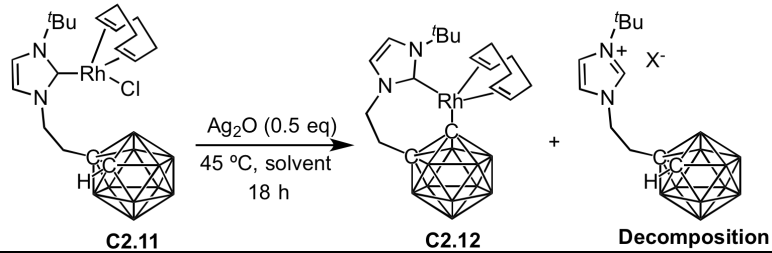

C2.11 **C2.12** **Decomposition**

	Non-Polar	Chloroform	DCM	Dioxane	Benzene	Toluene	Polar Aprotic	Acetone	DMF	DMSO	MeCN	THF	Polar Protic	Methanol
C2.11 (%)		100	100	100	100	100		92	46	47	15	89		30
C2.12 (%)		0	0	0	0	0		8	37	30	75	11		0
Decomp (%)		0	0	0	0	0		0	17	23	10	0		70

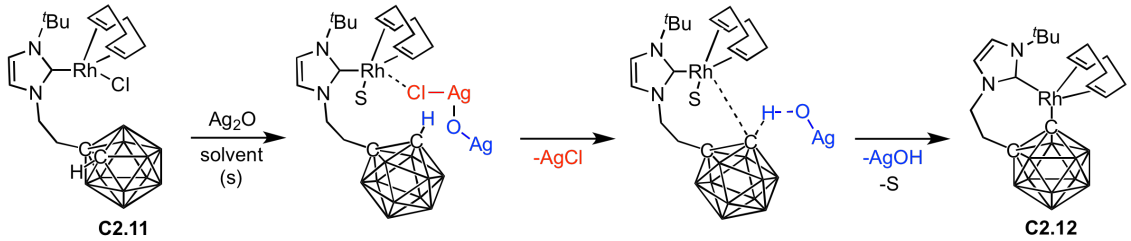

Scheme 4.4 Proposed mechanism for the formation of **C2.12** from **C2.11** using Ag_2O.

Ag_2O is not usually known for its chloride abstracting properties, so a range of different silver salts were screened to investigate whether **C2.12** could be obtained under even milder conditions (**Table 4.2**). Surprisingly, when the superior chloride-abstracting agent AgOTf was employed in the reaction, no cyclometallation occurs and around 30 % of **C2.11** decomposes. This is likely due to the ineffectiveness of AgOTf to act as a base. Jin and co-workers employ triethylamine in combination with AgOTf to isolate a C-cyclometallated complex at room temperature (Section 4.1).[23] However, employing this synthetic method still only led to decomposition of **C2.11**. The results indicated that a dimeric silver salt is required to achieve good conversion of **C2.11** to **C2.12**, with Ag_2O being most effective.

Table 4.2 The effectiveness of different silver salts in the cyclometallation of **C2.11** to form **C2.12** monitored by ^{1}H NMR spectroscopy.

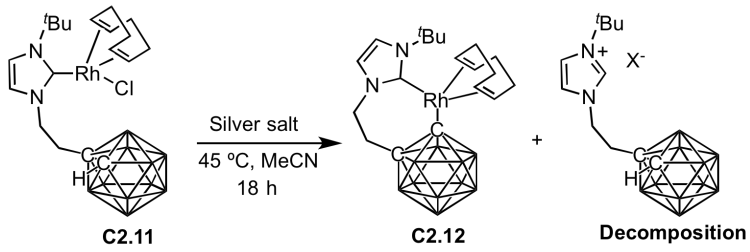

	Dimeric salts	Ag_2O	Ag_2CO_3	Ag_2SO_4	Monomeric salts	AgOAc	AgOTf
C2.11 (%)		30	41	30		55	69
C2.12 (%)		60	45	34		10	0
Decomp (%)		10	14	36		35	31

4.4 Complex characterisation

HRMS has been found to be an excellent tool for monitoring the reaction of our NHC-carborane ligands with metal precursors to ensure that the reactions have gone to completion. However, both **C2.11** and **C2.12** give the same molecular ion peak preventing their characterisation by HRMS (**Figure 4.3**).

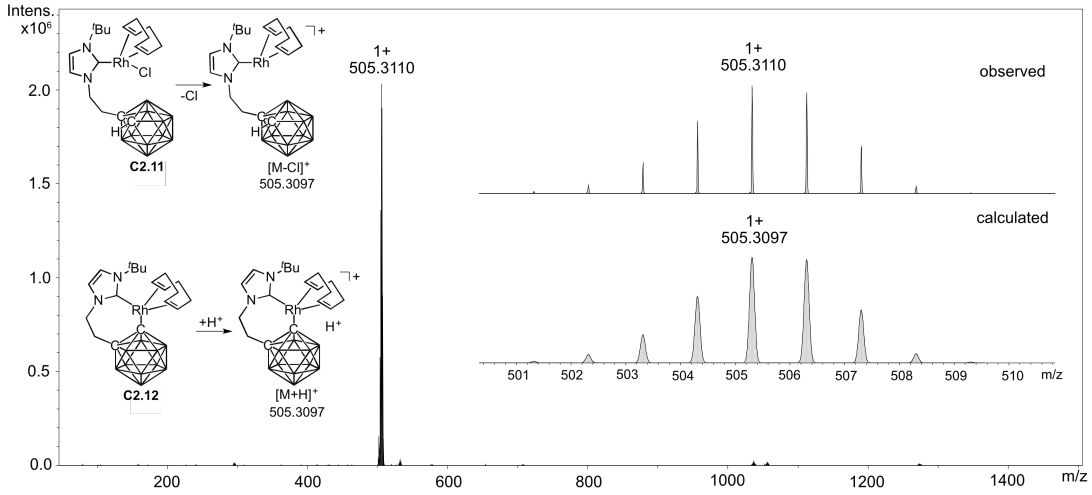

Figure 4.3 HRMS of **C2.11**, which is also the molecular ion peak for **C2.12**. Inset contains the observed molecular ion $[M-Cl]^+$ against the calculated mass.

4.4.1 Multinuclear NMR spectroscopic analysis of C2.11 and C2.12

Upon formation of **C2.11** or **C2.12**, the most downfield resonance at 9.41 ppm observed in the ^{1}H NMR spectrum of **L2.1** disappears, indicative of NHC formation (**Figure 4.4**). The $^{13}C\{^1H\}$ NMR spectra of **C2.11** and **C2.12** exhibit doublets at 181.9 ppm and 183.2 ppm respectively, which is diagnostic for M-$C_{carbene}$ bond formation (**Figure 4.5**). The $^1J_{Rh\text{-}C}$ couplings of 50.4 Hz and 52.9 Hz is in accordance with similar complexes in the literature.[37,38]

The coordination of the NHC to the metal results in the protons of the CH_2 tether becoming diasterotopic in the ^{1}H NMR spectrum of **C2.11**, with the H(4) protons splitting into two triplet of doublets, resonating at 5.97 and 4.12 ppm. Although the carboranyl unit is 5 bonds from the metal centre, there could be restricted rotation about the ethyl linkage due to the steric clash between the metal and the carborane. The sterically bulky ^{t}Bu group could also restrict rotation about the M-$C_{carbene}$ bond. Upon cyclometallation of **C2.11**, the absence of the cage CH resonance at 4.17 ppm in the ^{1}H NMR spectrum of **C2.12** along, with the $^{13}C\{^1H\}$ NMR spectrum exhibiting a doublet at 84.5 ppm, which is attributable to the Rh-coordinated carboranyl carbon with $^1J_{Rh\text{-}C}$ coupling of 52.5 Hz, confirms cyclometallation through the carbon vertex of the cage.

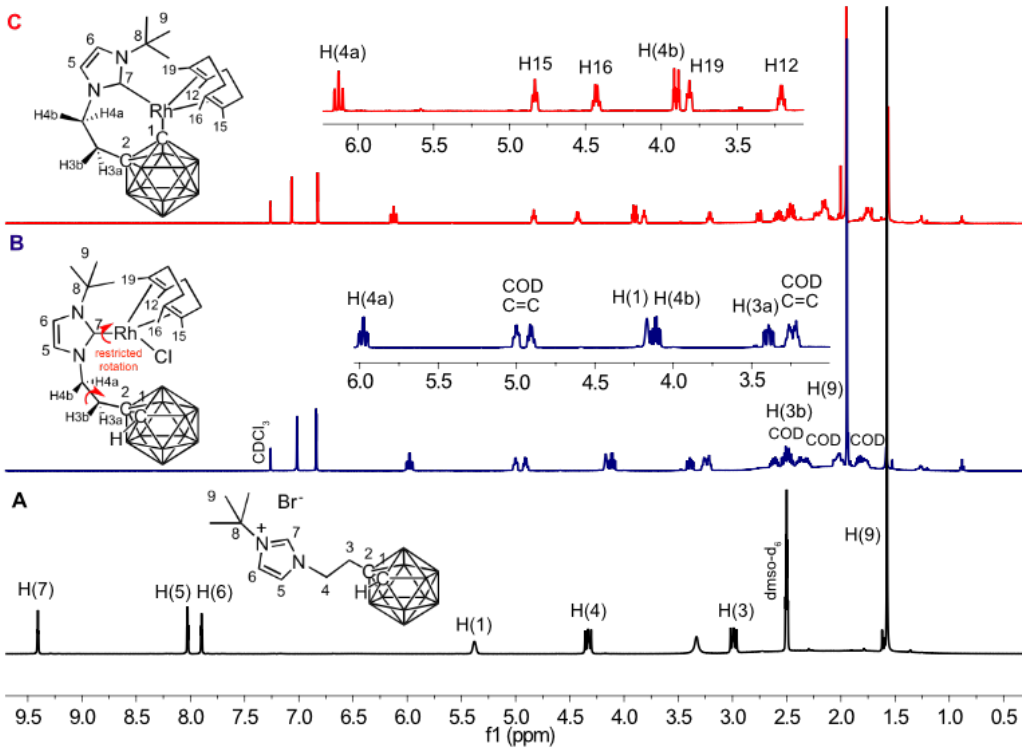

Figure 4.4 ^{1}H NMR spectrum (500 MHz, DMSO-d_6) of **L2.1** (**A**) and ^{1}H NMR spectra (500 MHz, $CDCl_3$) of **C2.11** (**B**) and **C2.12** (**C**).

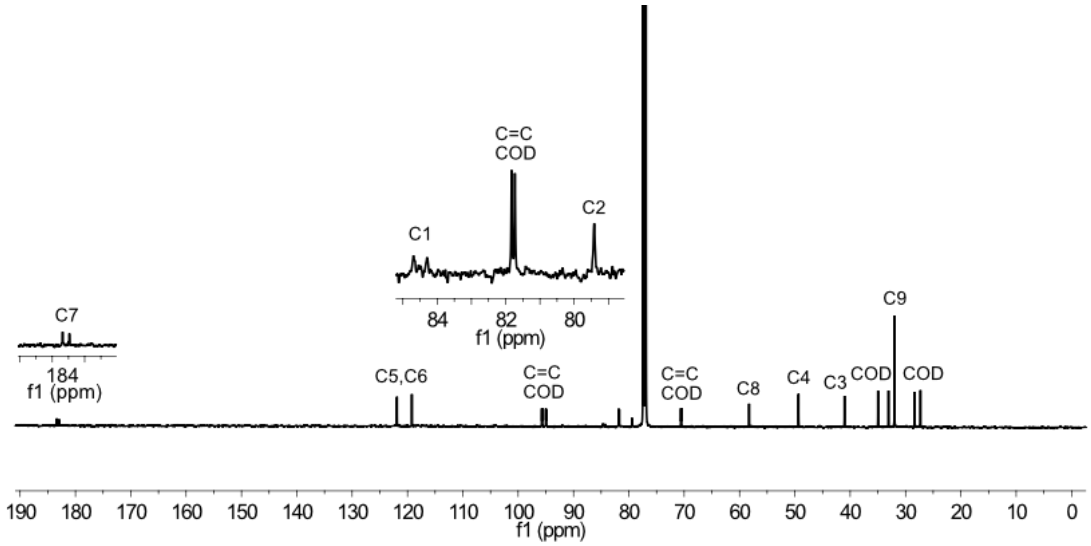

Figure 4.5 ^{13}C{^{1}H} NMR spectrum (126 MHz, $CDCl_3$) of **C2.12**.

As the ligand in **C2.12** is bound through the carbene and carboranyl carbon it is conformationally locked, and as a result the COD alkene protons are magnetically inequivalent, with each resonating at a unique chemical shift. Assignment of these resonances was made possible through use of NOESY NMR spectroscopy (**Figure 4.6**). The most upfield resonances were identified as the alkene protons axial to the carborane, with strong through-space interactions between H(19) and the diasterotopic proton (H(4a)) at 6.13 ppm, as well as interactions between H(12) and the ^{t}Bu substituent (H(9)) of the NHC. A strong interaction between the resonances attributable to H(12) and H(19) also confirmed that these are vicinal protons. Similarly, H(15) and H(16) can be assigned as the downfield resonances at 4.83 and 4.43 ppm, with a surprisingly strong interaction between H(15) and the ^{t}Bu group.

X-ray diffraction analysis was used in conjunction with the NMR data to rationalise why there is such disparity in the chemical shifts of the COD alkene protons (**Figure 4.7**). The average C_{COD}-Rh distance is 2.107 (Å) trans to the carborane whilst 2.210 (Å) *trans* to the NHC, highlighting the stronger *trans* influence of the carbene ligand, which is consistent with the literature.[39] This has a significant effect on the length of the C=C bond distances, with a short bond length of 1.385 (Å) for C(15)-C(16) in comparison to 1.405 (Å) for C(12)-C(19). This suggests that the alkene *trans* to the carbene possess more sp^2 character hence the protons will be more deshielded and appear at a high chemical shift.

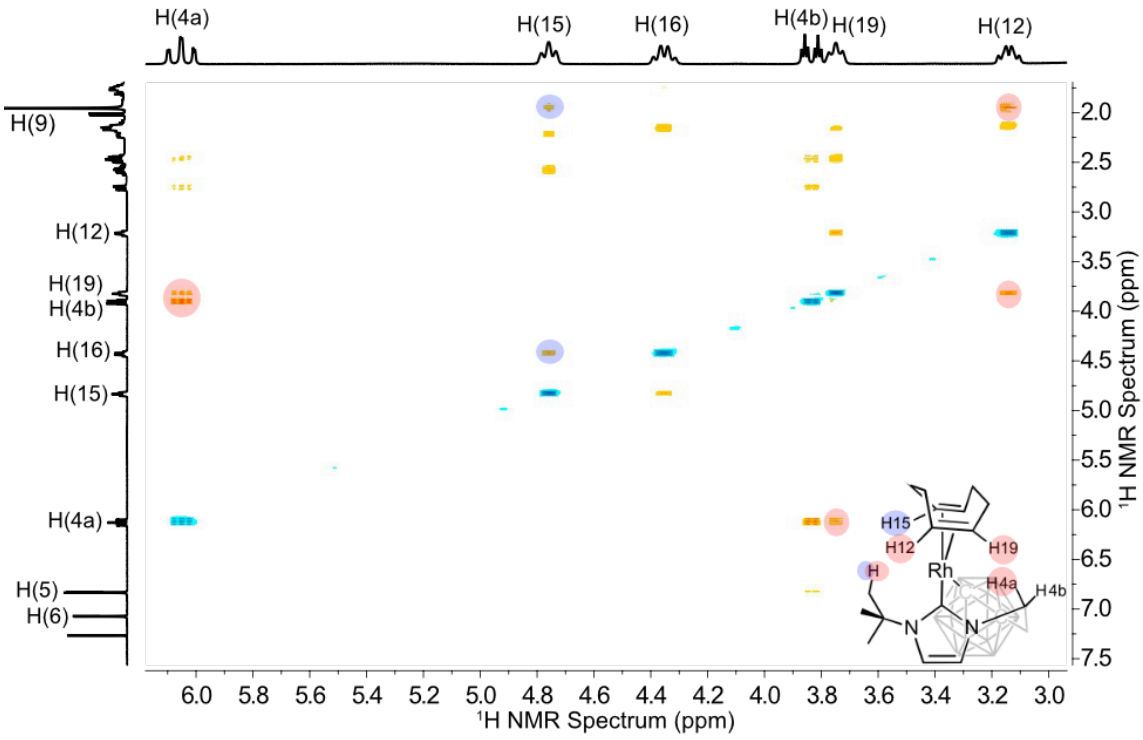

Figure 4.6 NOESY ^{1}H^{1}H NMR spectrum (500 MHz, $CDCl_3$) of **C2.12**. The cross peaks highlighted in pink and blue indicate through space interactions allowing each COD alkenyl proton to be assigned.

4.4.2 X-ray diffraction analysis

Single crystals suitable for X-ray diffraction analysis were grown from the slow evaporation of concentrated DCM solutions for both **C2.11** and **C2.12**. The solid state structure of **C2.12** shows a distorted square planar Rh^{I} centre, bearing a chelating NHC *closo*-carborane ligand coordinating in a *cis* fashion through the carbenic carbon and through the carboranyl carbon atom. The parameters highlight an elongated C(1)-C(2) bond of the carborane for **C2.12**. This elongation could be to reduce the steric stress at the metal centre, an effect observed in similar types of complexes in the literature.[22]

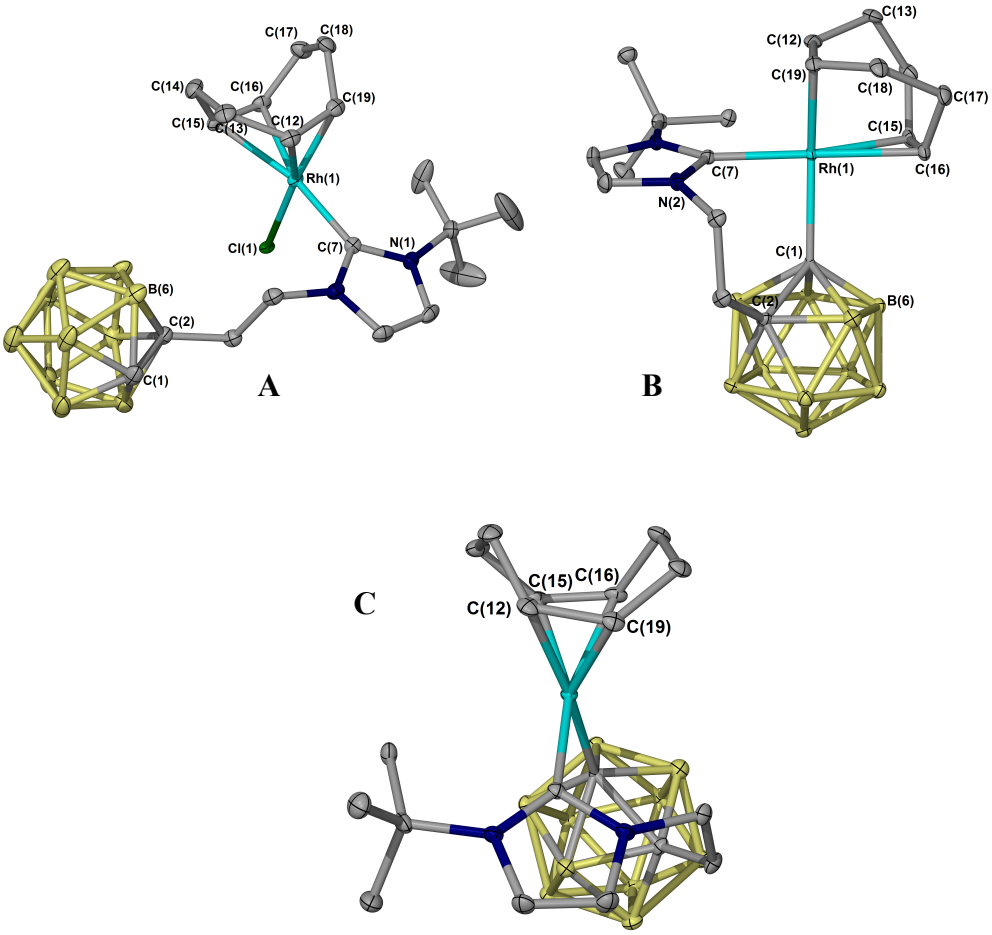

Figure 4.7 Molecular structures of **C2.11** (**A**) and **C2.12** (**B** and **C**), **C** highlights the asymmetrical binding of the COD unit. *Ellipsoids are shown at 40 % probability and the hydrogen atoms are omitted for clarity.*

Table 4.3 Selected bond distances (Å) for **C2.11** and **C2.12**.

Distance (Å)	2.11	C2.12	Distance (Å)	C2.11	C2.12
Rh(1)-C(7)	2.036(3)	2.028(3)	Rh(1)-C(19)	2.117(4)	2.146(3)
Rh(1)-Cl(1)	2.443(8)	-	C(12)-C(19)	1.407(6)	1.405(4)
Rh(1)-C(1)	-	2.158(3)	C(15)-C(16)	1.405(4)	1.385(4)
Rh(1)-C(12)	2.097(4)	2.198(3)	C(1)-C(2)	1.653(5)	1.738(4)
Rh(1)-C(15)	2.202(3)	2.189(3)	C(12)-C(19)	1.405(4)	1.405(4)
Rh(1)-C(16)	2.181(3)	2.231(3)			

As discussed in Chapter 2 (section 2.2.5), a long-standing problem in X-ray diffraction analysis of carboranyl compounds is distinguishing between C and B vertices in cases where one or both carbon atoms are not substituted. This is due to C and B having very similar X-ray scattering powers as a simple consequence of their period adjacency. It is important to be able to correctly identify the coordinating vertex, as the electronic properties of a complex will be very different depending on if the ligand is coordinated through a C or B atom, and in some literature cases the C and B vertices have been incorrectly assigned.[40] There are three methods employed for distinguishing between C and B vertices: 1) Set all vertices to be a boron atom and inspect the thermal parameter (U_{eq}) values; those for C should be significantly smaller than B; 2) Measure the bond lengths, which is an effective method when the carbon atoms are adjacent as this bond should have the shortest connectivity; 3) The VCD method developed by Welch and co-workers, an excellent method and the most effective for determining the carbon vertices in a carborane.[40] This method involves measuring the distances from topologically equivalent vertex atoms to the polyhedral centroid, where the shortest connectivities can be identified as the C vertices (**Figure 4.8**). The advantages of using the VCD method became apparent on comparing the distances in **C2.11**, allowing the C1 vertex to be easily identified with a VCD distance of 1.491 Å, compared to distances over 1.617 Å for each of the remaining vertices (**Table 4.4**). If we compare this to the thermal parameters, although consistent with the VCD method, there is very little discrepancy.

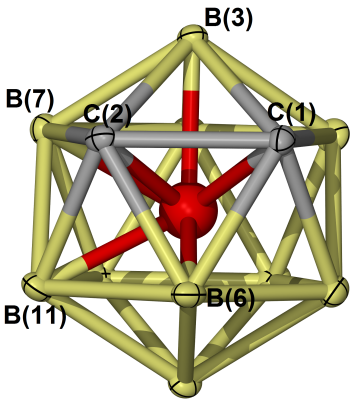

Figure 4.8 A representation of the generated centroid (red sphere) used in the VCD method.

Table 4.4 Vertex-to-Centroid Distances (Å) and thermal parameter comparisons (U_{eq}) of **C2.11** and **C2.12**.

Vertex	**C2.11**	**U_{eq}**	**C2.12**	**U_{eq}**
C(1)	1.491	0.029	1.663	0.008
C(2)	1.441	0.023	1.581	0.015
B(3)	1.636	0.032	1.686	0.021
B(6)	1.636	0.031	1.685	0.019
B(7)	1.617	0.034	1.692	0.019
B(11)	1.622	0.031	1.687	0.018

In the case of **C2.12**, the C(1) vertex could not be identified with confidence using any of the three methods. The VCD distances were very similar for each vertex. This could be attributed to the increase in steric crowding upon cyclometallation, which results in elongation of the C(1)-C(2) bond length and an increase in the VCD distance of the C(1) vertex. Similar observations have been reported by Lee *et al*.[22] Therefore, from the X-ray diffraction data we can confirm that cyclometallation has occurred, with NMR spectroscopy being used to determine which vertex the Rh centre is bound too.

4.5 Selective C-H deprotonation?

As discussed in the previous section, when ligand **L2.1** is reacted with $[Rh(COD)Cl_2]_2$ and Ag_2O in MeCN for 10 hours, a cyclometallated product (**C2.12**) in which the metal chelates through the NHC and the carboranyl carbon is isolated (**Scheme 4.3**). When the reaction time was reduced to 5 hours and the product analysed by ^{1}H NMR spectroscopy, two broad resonances were observed at 4.25 and 3.66 ppm that were not present in the ^{1}H NMR spectrum of **C2.12**. It was determined that these signals were attributable to the cage CH proton when the metal centre cyclometallates through the B3/B6 vertex of the cage. These vertices are equivalent but give rise to diasteromers resulting in the two broad resonances observed.[2] In the ^{13}C{^{1}H} NMR spectrum the double at 84.5 ppm with $^1J_{Rh\text{-}C}$ coupling of 51.7 Hz indicates that the C-cyclometallated complex (**C2.12**) is also present, suggesting a mix of C and B cyclometallation. This coincides with the ^{1}H NMR spectrum integrals of the carboranyl CH signals not totalling to 1 when compared to one of the diasterotopic CH_2 tether resonances (0.35:0.35:1).

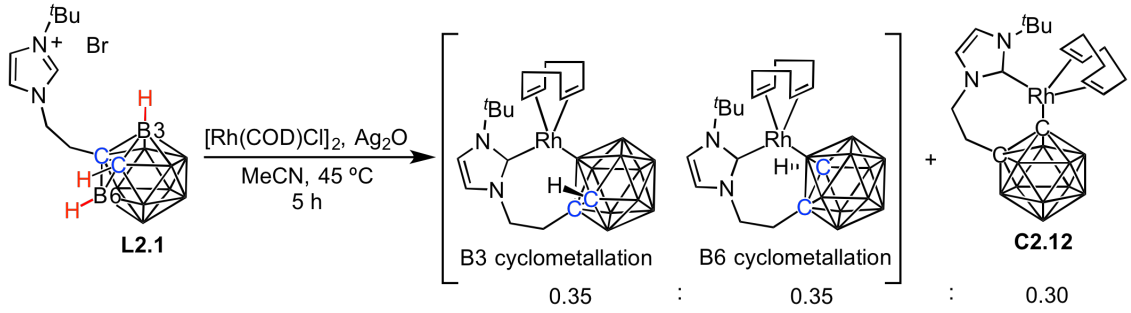

Scheme 4.5. Synthesis of a mixed C- and B-coordinated Rh^I-metallacycle.

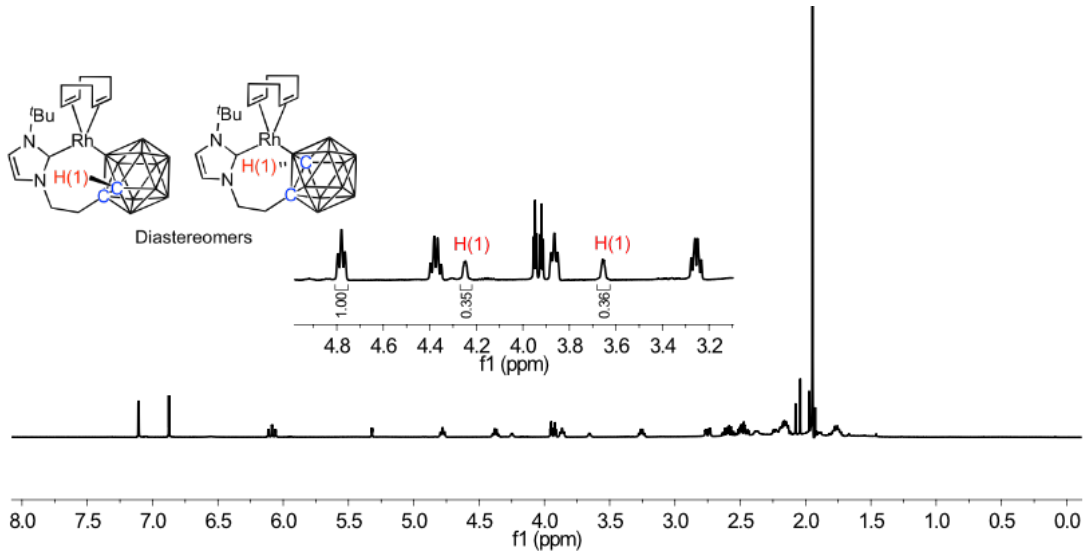

Figure 4.9 ^{1}H NMR (500 MHz, CD_2Cl_2) spectrum of isolated product after reacting **L2.1** with $[Rh(COD)Cl_2]_2$ and Ag_2O in MeCN for 5 hours. Inset highlights the diasterotopic carboranyl H(1) protons.

Interestingly, after running an NMR spectrum 12 hours later after keeping the sample at room temperature the broad resonances were absent and the NMR data coincides with that of **C2.12**, with 100 % C-cyclometallation observed. The reasoning behind the irreversible conversion of B-cyclometallation to C-cyclometallation remains unclear.

As previously discussed (Section 4.1) examples of a Rh^{I} centre bound through the carboranyl carbon are very rare.[18,19] Further to this, carboranyl phosphine complexes are notorious for oxidative addition across the B-H bond.[2] The question that arises is why does the Rh^{I} centre of **C2.11** not undergo oxidative addition across the B-H bond? The answer is likely to be due to sterics. Unlike phosphines, the steric bulk of an NHC is exerted towards the metal centre, and as a result there is inadequate space for oxidative addition across the B-H bond of the carborane, especially when the α-substituent of the NHC is a bulky ^{t}Bu group. To explore the possibility of accessing a Rh^{III} complex through oxidative addition, the sterics of the NHC was reduced to an N-Me group. Reaction of **L2.3** with $[Rh(COD)Cl_2]_2$ in the presence of Ag_2O (0.5 eq) gave the corresponding Rh^{I}NHC(COD)Cl complex **C2.13**. However, this complex is stable and oxidative addition was not observed, which was confirmed by NMR spectroscopy, as well as X-ray diffraction analysis (**Figure 4.10**). This result indicates that even the smallest NHC is too sterically bulky for oxidative addition to occur in these types of complexes.

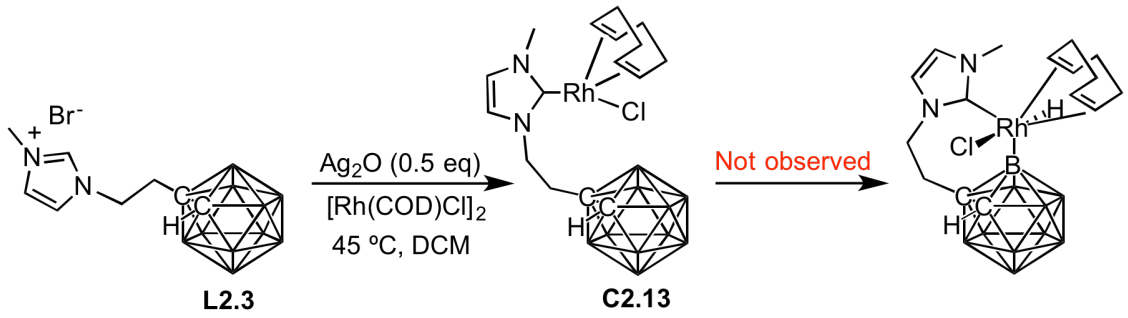

Scheme 4.6 Synthesis of **C2.13**, which resists oxidative addition across the B-H bond.

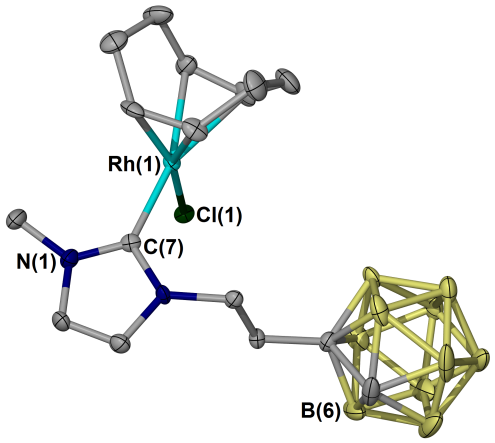

Figure 4.10 Molecular structure of **C2.13**. *Ellipsoids are shown at 50 % probability and the hydrogen atoms are omitted for clarity.*

4.6 Rhodium catalysed hydrosilylation of acetophenone

To assess the catalytic potential of the Rh^{I} complexes **C2.11** and **C2.12**, and the bimetallic complex **C2.3** (Chapter 3) they were examined in the hydrosilylation of acetophenone with diphenylsilane. $[Rh(COD)Cl]_2$ was also screened for useful comparison (**Figure 4.12**).

The hydrosilylation of acetophenone can be easily monitored by ^{1}H NMR spectroscopy, with only two possible products formed in the reaction (**Scheme 4.7**). The reactions were carried out under strict anhydrous conditions and monitored until the acetophenone was fully consumed. The yield of silyl ether **A** was calculated by comparing the integration of the CH quartet at 4.98 ppm with that of the benzylic singlet at 6.26 ppm from the internal standard, 1,3,5-trimethoxybenzene. The yield of the enol silyl ether **B** was calculated by comparing the integration of one of the vinylic CH doublets at 4.68 ppm with the internal standard. An example spectrum is shown in **Figure 4.11** and the results of the catalytic screening are presented in **Table 4.4**.

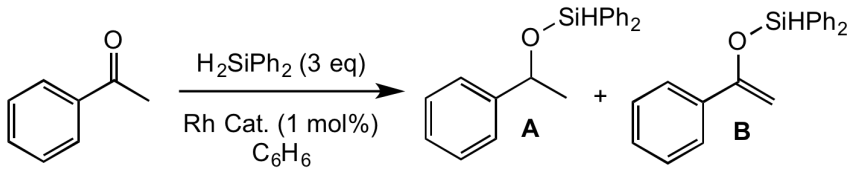

Scheme 4.7 Hydrosilylation of acetophenone.

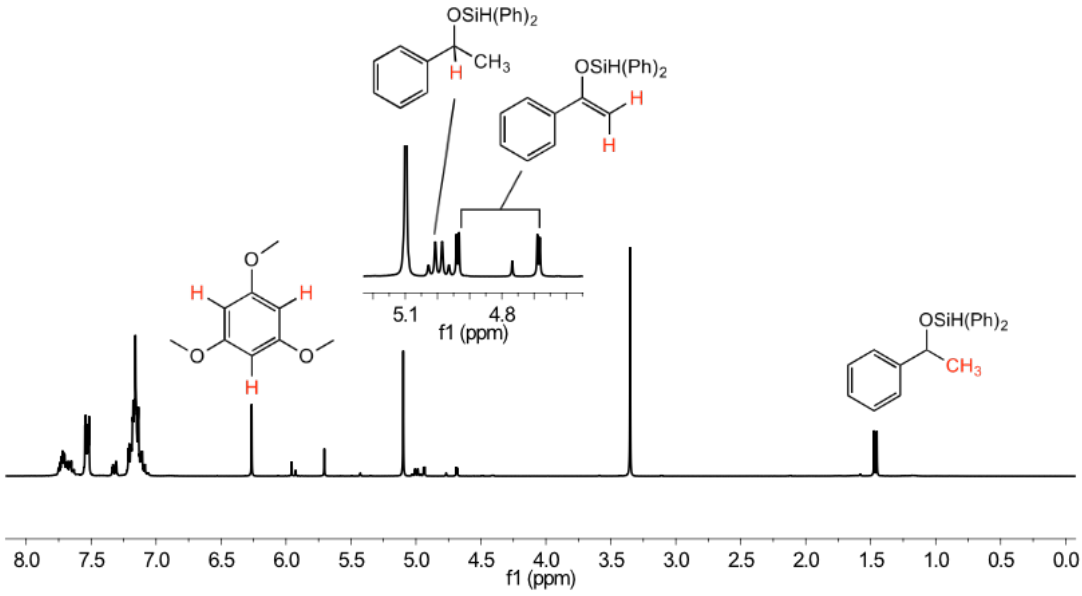

Figure 4.11 ^{1}H NMR spectrum in C_6D_6 of the hydrosilylation of acetophenone catalysed by complex **C2.12** after 12 hours at 50 °C. The labelled resonances belong to the respective highlighted red proton environments.

Table 4.5 Examination of complexes in **Figure 4.12** in the hydrosilylation of acetophenone.

Entry	Catalyst	Catalyst loading (mol %)	Solvent	Reaction time (hours)	Temp (°C)	Yield of A (%)	Yield of B (%)
1	$[Rh(COD)Cl]_2$	0.5	C_6H_6	0.5	rt	72	29
2	**C2.3**	0.5	C_6H_6	3	rt	62	38
3	**C2.11**	1.0	C_6H_6	8	rt	74	26
4	**C2.11**	1.0	THF	23	rt	69	31
5	**C2.12**	1.0	C_6H_6	8	rt	0	0
6	**C2.12**	1.0	C_6H_6	12	50*	64	36

*No reaction observed below 50 °C

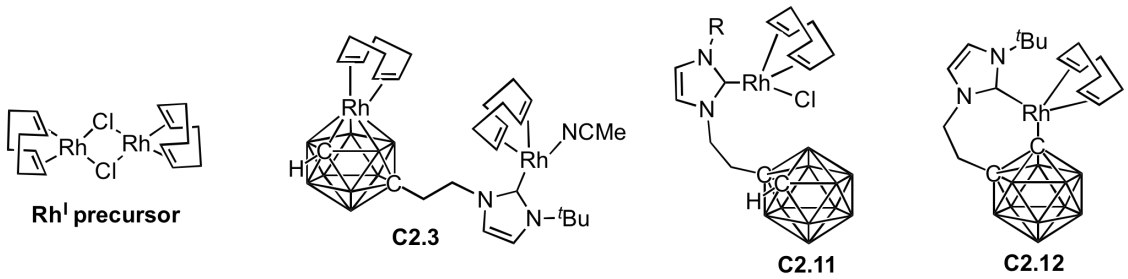

Figure 4.12 Complexes screened in the hydrosilylation reaction of acetophenone.

100 % conversion was achieved under very mild conditions using all three catalysts, with the bimetallic complex **C2.3** being the most active (full conversion in 3 hours at room temperature, 0.5 mol % catalyst (entry 2)). The RhNHC(COD) centre in **C2.3** possesses a labile MeCN, rather than a chloride as in **C2.11** and **C2.12**, which could lead to an increase in catalytic activity. Although the Rh^I precursor $[Rh(COD)Cl]_2$ out-performed **C2.3**, **C2.11** and **C2.12**, the fact that the complexes are active is encouraging for further development. In accordance with related complexes in the literature,[2–6] **C2.12** is a relatively poor catalyst and requires heating to 50 °C to become active (entry 5). This is likely due to the metal centre being co-ordinately saturated, and for catalysis to take place the COD moiety must dissociate which requires heating. It is noteworthy that when the solvent in the reaction is substituted for THF, a considerable increase in reaction time is observed, with 23 hours required to achieve full consumption of the acetophenone (entry 4).

The formation of the silyl enol ether byproduct **B** in the above hydrosilylation reactions can be explained by the extended Hofmann-Gade extended mechanism (**Figure 4.13**).[41–43] The initial step involves oxidative addition across the Si-H bond of the disubstituted-silane to yield the hydride species **I**. Next, α-hydride migration leads to formation of the dihydride species **II**, and upon coordination of the ketone to give **III** there are two possible pathways: 1) proton transfer from the metal to the ketone and subsequent reductive elimination of the desired product or 2) tautomerism of the ketone and loss of hydrogen forming the silyl enol ether **B**.

Formation of **B** requires an open coordination site on the rhodium centre, and it has been reported that the yield of **B** can be reduced by increasing the ratio of ligand to $[Rh(COD)Cl]_2$ used in the reaction as the ligand competes for this coordination site.[44] Since we are using a well-defined catalyst we cannot take advantage of this.

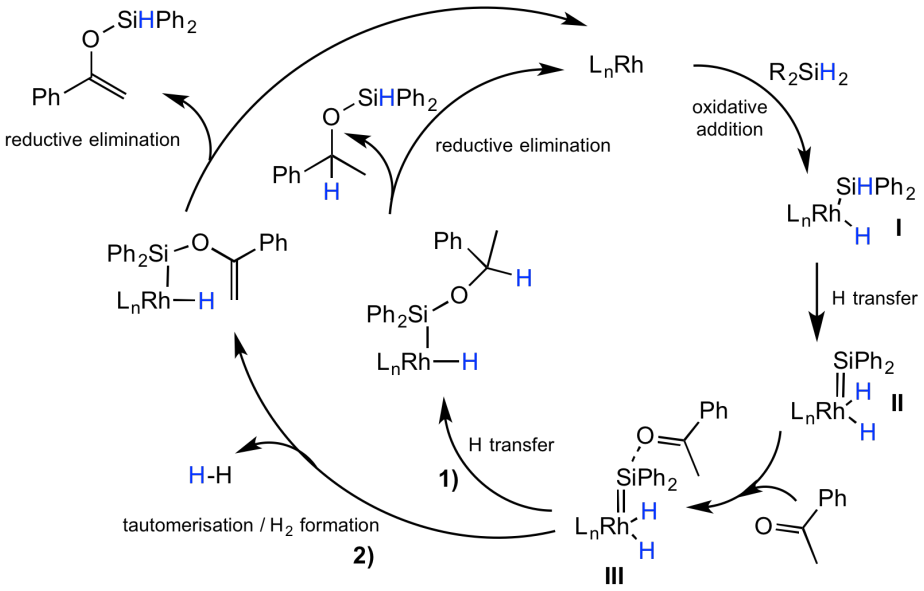

Figure 4.13 Hofmann-Gade mechanism for the hydrosilylation of ketones.[41–43]

4.7 Conclusions and future work

The reaction of *closo*-carborane imidazolium salt **L2.1** with Ag_2O in non-coordinating solvents gives **C2.11** in high yields (**Scheme 4.8**). When a coordinating solvent is employed with an excess of Ag_2O, an unusual Rh^I metallacycle exhibiting C-cyclometallation is formed (**C2.12**). Unlike its *o*-carboranyl phosphine derivatives, this ligand resists oxidative addition; it can be proposed that the steric bulk exerted at the metal centre by the NHC moiety prevents oxidative addition from occurring. This was explored further by reducing the sterics of the NHC to a Me substituent. However, the resulting Rh^INHC(COD)Cl complex (**C2.13**) was stable and oxidative addition was not observed. The catalytic viability of **C2.11** and **C2.12**, alongside bimetallic complex **C2.3** reported in Chapter 3, were screened in the catalytic hydrosilylation of acetophenone to assess their potential as catalysts. **C2.3** proved to be the most effective catalyst, although it is not clear if both Rh^I centres are catalytically active and work cooperatively. The Rh^I(COD)NHC centre in **C2.3** possesses a labile MeCN ligand which could lead to an increase in activity. The Rh^I metallacycle **C2.12** was found to be a relatively poor catalyst when compared to its non-cyclometallated counterpart **C2.11**. For catalysis to take place a ligand must dissociate, which is likely to be the COD. Future reactions should look at replacing the COD moiety with a more labile ligand such as CO, which may lead to an increase in catalytic activity. Alternatively, oxidation of the metal to Rh^{III}/Ir^{III} could allow investigation into more challenging chemical transformations, which the higher oxidation states of Rh^{III} and Ir^{III} are renowned for such as transfer hydrogenation.[45] This is a focal point of Chapter 5 in which higher oxidation state complexes have been prepared.

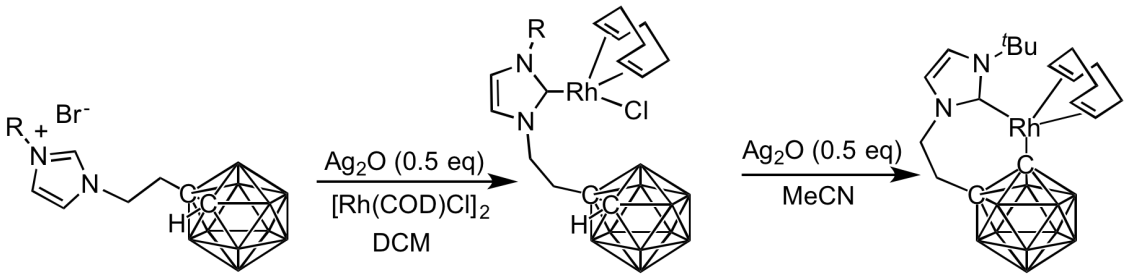

L2.1 R = ^{t}Bu
L2.3 R = Me

C2.11 R = ^{t}Bu 74 %
C2.13 R = Me 58 %

C2.12 79 %

Scheme 4.8 Summary of complexes synthesised in this work.

4.8 Experimental

4.8.1 General considerations

All manipulations were carried out under an inert atmosphere by means of standard Schlenk line or glovebox techniques unless otherwise stated. Anhydrous solvents were prepared by passing over activated alumina to remove water, copper catalyst to remove oxygen and molecular sieves to remove any remaining water, *via* the Dow–Grubbs solvent system, and then freeze–pump–thaw degassed prior to use. All chemicals used in this work were bought from either Sigma Aldrich or Alfa Aesar and used without further purification. NMR spectra were recorded on a Bruker AV500 or a Bruker DPX300 spectrometer. ^{1}H NMR and ^{13}C{^{1}H} NMR chemical shifts were referenced against residual solvent peaks. Assignment of ^{1}H and ^{13}C{^{1}H} NMR spectra for all complexes was aided by the use of 2D ^{1}H^{1}H COSY, ^{1}H^{13}C HMQC, ^{1}H^{13}C HMBC and ^{13}C{^{1}H} DEPT 135 and DOSY experiments. Mass spectra were collected on a Bruker Daltonics (micro TOF) instrument operating in the electrospray mode. Elemental analyses were performed by Elemental analyses were performed by Mrs Tanya Marinko-Covell at The University of Leeds. The preparation of the ligand precursors utilised in this work can be found in Chapter 2. The synthesis of $[Rh(COD)Cl]_2$ can be found in Chapter 3.

4.8.2 General catalytic procedure for the hydrosilylation of acetophenone

In the glove box, to a Young's tap NMR tube containing C_6D_6 (0.5 mL) was added Rh complex **C2.3**, **C2.11** or **C2.12** (1.10 μmol) and 1,3,5-trimethoxybenzene (internal standard, 3.1 mg, 18.60 μmol), followed by diphenylsilane (21 μL, 0.11 mmol) and acetophenone (12.90 μL, 11.60 μmol). The reaction was monitored by ^{1}H NMR spectroscopy until acetophenone was fully consumed.

4.8.3 Complex synthesis

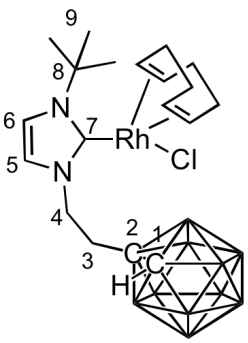

Synthesis of **C2.11**. Imidazolium-*closo*-carborane bromide salt **L2.1** (100 mg, 0.27 mmol), Ag_2O (62 mg, 0.27 mmol), $[Rh(COD)Cl]_2$ (67 mg, 0.14 mmol), several activated 4 Å molecular sieves and anhydrous DCM (5 mL) were added to an ampoule and heated at 45 °C for 1 hour. The solution was filtered through Celite and the solvent removed *in vacuo* to yield a yellow crystalline solid. The solid was washed with hexane (3 × 10 mL) and dried *in vacuo* to afford the product in 74 % yield. (108 mg, 0.20 mmol). ^{1}H NMR (500 MHz, $CDCl_3$): δ (ppm) 7.02 (d, *J* = 2.1 Hz, 1H, H^{6}), 6.84 (d, *J* = 2.1 Hz, 1H, H^{5}), 5.98 (td, *J* = 12.6, 5.0 Hz, 1H, H^{4}), 5.00 (td, *J* = 8.0, 3.4 Hz, 1H, CODCH), 4.91 (dd, *J* = 14.2, 7.4 Hz, 1H, COD-CH), 4.17 (br., 1H, H^{1}), 4.11 (td, *J* = 12.6, 5.0 Hz, 1H, H^{4}), 3.39 (m, 1H, H^{3}), 3.24 (m, 2H, COD-CH), 2.61 (m, 1H, H^{3}), 2.49 (m, 2H, COD-CH_2), 2.35 (m, 2H, COD-CH_2), 2.02 (m, 2H,

$CODCH_2$), 1.94 (s, 9H, $C(CH_3)_3$), 1.80 (m, 2H, COD-CH_2). $^{13}C\{^1H\}$ NMR (126 MHz, $CDCl_3$): δ (ppm) 181.7 (d, $^1J_{Rh-C}$ = 50.4 Hz, C^7), 120.6 (C^6), 120.0 (C^5), 97.3 (d, $^1J_{Rh-C}$ = 7.6 Hz, COD-CH), 95.5 (d, 1 $^1J_{Rh-C}$ = 7.6 Hz, COD-CH), 73.4 (C^2), 71.4 (d, $^1J_{Rh-C}$ = 15.1 Hz, COD-CH), 67.4 (d, $^1J_{Rh-C}$ = 15.1 Hz, COD-CH), 63.6 (C^1), 58.9 (C^8), 51.5 (C^4), 38.0 (C^3), 34.1 (COD-CH_2), 32.4 (C^9), 31.5 (COD-CH_2), 29.8 (COD-CH_2), 28.2 (COD-CH_2). $^{11}B\{^1H\}$ NMR (161 MHz, $CDCl_3$): δ (ppm) −2.5 (1B), −5.4 (1B), −9.2 (2B), −11.0 (2B), −12.9 (4B). HRMS (ESI^+): m/z $[C_{19}H_{38}B_{10}N_2Rh]^+$ 505.3112, calcd for $[M - Cl]^+$ 505.3097. Anal. calcd. for $C_{19}H_{38}B_{10}N_2ClRh$: C, 42.18; H, 7.08; N, 5.18. Found: C, 42.40; H, 6.90; N, 5.50. Crystals suitable for X-ray diffraction analysis were grown by the slow evaporation of a concentrated solution of the product in DCM.

Synthesis of **C2.12**. Imidazolium-*closo*-carborane bromide salt **L2.1** (200 mg, 0.53 mmol), Ag_2O (123 mg, 0.53 mmol), $[Rh(COD)Cl]_2$ (134 mg, 0.27 mmol), several activated 4 Å molecular sieves and anhydrous MeCN (10 mL) were added to an ampoule and heated at 45 °C for 10 hours. The solution was filtered through Celite and the solvent removed *in vacuo* to yield a yellow crystalline solid. The solid was washed with hexane (3 × 10 mL) and dried *in vacuo* to afford the product in 79 % yield. (213 mg, 0.42 mmol). ^1H NMR (500 MHz, $CDCl_3$): δ (ppm) 7.07 (d, J = 2.0 Hz, 1H, H^6), 6.83 (d, J = 2.0 Hz, 1H, H^5), 6.13 (td, J = 13.8, 1.85 Hz, 1H, H^{4a}), 4.83 (t, J = 7.8 Hz, 1H, H^{15}), 4.43 (dd, J = 15.3, 7.8 Hz, 1H, H^{16}), 3.90 (dt, J = 13.8, 3.45 Hz, 1H, H^{4b}), 3.82 (t, J = 7.2 Hz, 1H, H^{19}), 3.21 (m, 1H, H^{12}), 2.75 (m, 1H, H^{3a}), 2.58 (m, 1H, H^{3b}), 2.46 (m, 2H, COD-CH_2), 2.16 (m, 4H, COD-CH_2), 1.95 (s, 9H, H^9), 1.75 (m, 2H, COD-CH_2). $^{13}C\{^1H\}$ NMR (126 MHz, $CDCl_3$): δ (ppm) 183.2 (d, $^1J_{Rh-C}$ = 52.9 Hz, C^7), 121.9 (C^6), 119.2 (C^5), 95.7 (d, $^1J_{Rh-C}$ = 7.6 Hz, COD-CH), 95.0 (d, $^1J_{Rh-C}$ = 7.6 Hz, COD-CH), 84.5 (d, $^1J_{Rh-C}$ = 51.7 Hz, C^1), 81.8 (d, $^1J_{Rh-C}$ = 12.6 Hz, COD-CH), 79.4 (C^2), 70.6 (d, $^1J_{Rh-C}$ = 8.8 Hz, COD-CH), 58.3 (C^8), 49.3 (C^4), 41.0 (C^3), 35.0 (COD-CH_2), 33.1 (COD-CH_2), 32.0 (C^9), 28.4 (COD-CH_2), 27.3 (COD-CH_2). $^{11}B\{^1H\}$ NMR (161 MHz, $CDCl_3$): δ (ppm) −4.2 (1B), −5.0 (1B), −6.1 (2B), −6.6 (1B), −8.3 (1B), −9.0 (1B), −9.84 (2B), −10.8 (1B). HRMS (ESI^+): m/z $[C_{19}H_{38}B_{10}N_2Rh]^+$ 505.3089, calcd for $[M + H]^+$ 505.3097. Anal. Calcd for $C_{19}H_{37}B_{10}N_2Rh.0.3(H_2O)$: C, 44.44; H, 7.46; N, 5.46. Found: C, 44.35; H, 7.47; N, 5.10. Crystals suitable for X-ray diffraction analysis were grown by the slow evaporation of a concentrated solution of the product in DCM.

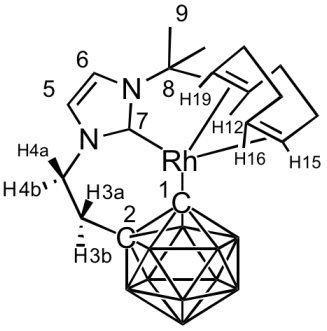

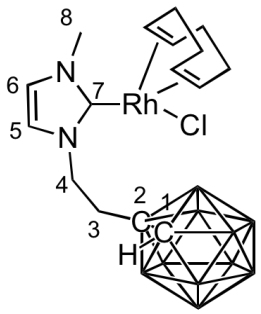

Synthesis of **C2.13**. Prepared as described for **C2.11** from **L2.3** (50 mg, 0.15 mmol), Ag_2O (70 mg, 0.075 mmol), $[Rh(COD)Cl]_2$ (37 mg, 0.075 mmol) in anhydrous DCM (5 mL). After purification the product was obtained as a yellow crystalline solid in 58 % yield. (74 mg, mmol). ^{1}H NMR (500 MHz, CD_2Cl_2): δ (ppm) 6.84 (m, 1H, H^6), 6.83 (m, 1H, H^5), 5.17 (td, J = 12.6, 3.8 Hz, 1H, H^{4a}), 4.96 (m, 2H, COD-CH), 4.27 (br. s, 1H, H^1), 4.07 (m, 1H, H^{4b}), 4.02 (s, 3H, H^8), 3.34 (m, 2H, H^{3a} + COD-CH), 3.22 (m, 1H, COD-CH), 2.69 (m, 1H, H^{3b}), 2.53-2.31 (m, 4H, COD-CH_2), 2.07-1.89 (m, 4H, COD-CH_2). ^{13}C{^{1}H} NMR (126 MHz, CD_2Cl_2): δ (ppm) 184.1 (d, $^1J_{Rh\text{-}C}$ = 50.4 Hz, C7), 123.1 (C^6), 121.2 (C^5), 99.7 (d, $^1J_{Rh\text{-}C}$ = 6.9 Hz, COD-CH), 99.5 (d, 1 $^1J_{Rh\text{-}C}$ = 6.9 Hz, COD-CH), 73.3 (C^2), 69.4 (d, $^1J_{Rh\text{-}C}$ = 14.4 Hz, COD-CH), 69.0 (d, $^1J_{Rh\text{-}C}$ = 14.7 Hz, COD-CH), 64.2 (C^1), 49.9 (C^4), 38.5 (C^3), 38.1 (C^8), 33.6 (COD-CH_2), 33.4 (COD-CH_2), 29.6 (COD-CH_2), 29.1 (COD-CH_2). ^{11}B{^{1}H} NMR (161 MHz, $CDCl_3$): δ (ppm) −2.8, −5.6, −9.5, −11.8, −12.9. HRMS (ESI^+): m/z $[C_{16}H_{32}B_{10}N_2Rh]^+$ 464.2591, calcd for $[M - Cl]^+$ 464.2587. Crystals suitable for X-ray diffraction analysis were grown by the slow evaporation of a concentrated solution of the product in DCM.

4.9 References

1 E. L. Hoel and M. F. Hawthorne, *J. Am. Chem. Soc.*, 1975, **97**, 6388–6395.

2 J. Estrada, S. E. Lee, S. G. McArthur, A. El-Hellani, F. S. Tham and V. Lavallo, *J. Organomet. Chem.*, 2015, **798**, 214–217.

3 K. Tamao, Y. Kiso, K. Sumitani and M. Kumada, *J. Am. Chem. Soc.*, 1972, **94**, 9268–9269.

4 M. Joost, L. Estévez, S. Mallet-Ladeira, K. Miqueu, A. Amgoune and D. Bourissou, *Angew. Chemie Int. Ed.*, 2014, **53**, 14512–14516.

5 M. Joost, A. Zeineddine, L. Estévez, S. Mallet−Ladeira, K. Miqueu, A. Amgoune and D. Bourissou, *J. Am. Chem. Soc.*, 2014, **136**, 14654–14657.

6 M. Joost, L. Estévez, K. Miqueu, A. Amgoune and D. Bourissou, *Angew. Chemie Int. Ed.*, 2015, **54**, 5236–5240.

7 H. Chen, S. Schlecht, T. C. Semple and J. F. Hartwig, *Science.*, 2000, **287**, 1995–1997.

8 J.-Y. Cho, M. K. Tse, D. Holmes, R. E. Maleczka and M. R. Smith, *Science.*, 2002, **295**, 305–308.

9 S. Shimada, A. S. Batsanov, J. A. K. Howard and T. B. Marder, *Angew. Chemie Int. Ed.*, 2001, **40**, 2168–2171.

10 I. A. I. Mkhalid, J. H. Barnard, T. B. Marder, J. M. Murphy and J. F. Hartwig, *Chem. Rev.*, 2010, **110**, 890–931.

11 J.-Y. Bae, Y.-J. Lee, S.-J. Kim, J. Ko, S. Cho and S. O. Kang, *Organometallics*, 2000, **19**, 1514–1521.

12 Z.-J. Yao and G.-X. Jin, *Organometallics*, 2011, **30**, 5365–5373.

13 Z.-J. Yao, G. Su and G.-X. Jin, *Chem. - A Eur. J.*, 2011, **17**, 13298–13307.

14 Z.-J. Yao, W.-B. Yu, Y.-J. Lin, S.-L. Huang, Z.-H. Li and G.-X. Jin, *J. Am. Chem. Soc.*, 2014, **136**, 2825–2832.

15 D. A. T. Young, R. J. Wiersema and M. F. Hawthorne, *J. Am. Chem. Soc.*, 1971, **93**, 5687–5694.

16 A. A. Sayler, H. Beall and J. F. Sieckhaus, *J. Am. Chem. Soc.*, 1973, **95**, 5790–5792.

17 R. Rogowski and K. Cohn, *Inorg. Chem.*, 1972, **11**, 1429–1431.

18 S. Bresadola and B. Longato, *Inorg. Chem.*, 1974, **13**, 539–542.

19 Z.-J. Yao, Y.-J. Lin, B. Xu, G.-X. Jin and M. F. Semmelhack, *Dalt. Trans.*, 2014, **43**, 4938–4940.

20 M. Basato, A. Biffis, C. Tubaro, C. Graiff, A. Tiripicchio, O. O. Sogbein and K. A. Stephenson, *Dalt. Trans.*, 2004, **248**, 4092.

21 H. J. Bae, H. Kim, K. M. Lee, T. Kim, M. Eo, Y. S. Lee, Y. Do, M. H. Lee, M. Grätzel, M. K. Nazeeruddin, M. Hoshino and K. Ueno, *Dalt. Trans.*, 2013, **42**, 8549.

22 T. Kim, J. Lee, S. U. Lee and M. H. Lee, *Organometallics*, 2015, **34**, 3455–3458.

23 B. Xu, Y.-P. Wang, Z.-J. Yao, G.-X. Jin, Y. Hong, T. B. Marder, J. J. Wilczynski, M. F. Hawthorne and M. F. Hawthorne, *Dalt. Trans.*, 2015, **44**, 1530–1533.

24 Y. Chi, P.-T. Chou, Y.-H. Hong, W.-H. Liu, T.-H. Li, C.-H. Lai, P.-T. Chou, Y. Chi, G.-H. Lee, Y.-T. Tao, C.-H. Chien, J. Leonhardt, M.-Y. Chae and S.-H. Jin, *Chem. Soc. Rev.*, 2010, **39**, 638–655.

25 H. Yersin, A. F. Rausch, R. Czerwieniec, T. Hofbeck and T. Fischer, *Coord. Chem. Rev.*, 2011, **255**, 2622–2652.

26 A. B. Tamayo, B. D. Alleyne, P.I. Djurovich, S. Lamansky, I. Tsyba, Nam N. Ho, A. R. Bau and M. E. Thompson, *J. Am. Chem. Soc.*, 2003, **125**, 7377–7387.

27 C. Fan, Y. Li, C. Yang, H. Wu, J. Qin and Y. Cao, *Chem. Mater.*, 2012, **24**, 4581–4587.

28 E. Baranoff, B. F. E. Curchod, F. Monti, F. Steimer, G. Accorsi, I. Tavernelli, U. Rothlisberger, R. Scopelliti, M. Grätzel and M. K. Nazeeruddin, *Inorg. Chem.*, 2012, **51**, 799–811.

29 V. K. Rai, M. Nishiura, M. Takimoto, Z. Hou, F. S. Ching, L. H. Mei, S. Y. Yu, T. C. Pi, S. Wang, S. Okada, M. Hoshino and K. Ueno, *Chem. Commun.*, 2011, **47**, 5726.

30 P. Coppo, E. A. Plummer, L. De Cola, H. Hughes, R. Wang, J. G. Vos, R. Bau, M. E. Thompson and M. E. Thompson, *Chem. Commun.*, 2004, **208**, 1774–1775.

31 A. J. Arduengo, H. V. R. Dias, J. C. Calabrese and F. Davidson, *Organometallics*, 1993, **12**, 3405–3409.

32 H. M. J. W. And and I. J. B. Lin, *Organometallics*, 1998, **17**, 972–975.

33 E. Peris, J. Mata, J. A. Loch and R. H. Crabtree, *Chem. Commun.*, 2001, **81**, 201–202.

34 A. A. D. Tulloch, A. A. Danopoulos, S. Kleinhenz, M. E. Light, A. M. B. Hursthouse and G. Eastham, *Organometallics*, 2001, **20**, 2027–2031.

35 A. Raba, M. Cokoja, S. Ewald, K. Riener, E. Herdtweck, A. Pöthig, W. A. Herrmann and F. E. Kühn, *Organometallics*, 2012, **31**, 2793–2800.

36 D. L. Davies, J. Fawcett, R. Krafczyk, D. R. Russell and K. Singh, *J. Chem. Soc. Dalt. Trans.*, 1998, 2349.

37 B. J. Truscott, A. M. Z. Slawin and S. P. Nolan, *Dalt. Trans*, 2013, **42**, 270–276.

38 M. Tobias Zarka, M. Bortenschlager, K. Wurst, O. Nuyken and R. Weberskirch, *Organometallics*, 2004, **23**, 4817–4820.

39 G. Lázaro, F. J. Fernández-Alvarez, M. Iglesias, C. Horna, E. Vispe, R. Sancho, F. J. Lahoz, M. Iglesias, J. J. Pérez-Torrente and L. A. Oro, *Catal. Sci. Technol.*, 2014, **4**, 62–70.

40 A. McAnaw, G. Scott, L. Elrick, G. M. Rosair and A. J. Welch, *Dalton Trans.*, 2013, **42**, 645–64.

41 L. H. Gade, V. César and S. Bellemin-Laponnaz, *Angew. Chemie Int. Ed.*, 2004, **43**, 1014–1017.

42 N. Schneider, M. Finger, C. Haferkemper, S. Bellemin-Laponnaz, P. Hofmann and L. H. Gade, *Angew. Chemie Int. Ed.*, 2009, **48**, 1609–1613.

43 P. Gigler, B. Bechlars, W. A. Herrmann and F. E. Kühn, *J. Am. Chem. Soc.*, 2011, **133**, 1589–1596.

44 C. Reyes, A. Prock and W. P. Giering, *Organometallics*, 2002, **21**, 546–554.

45 D. Wang and D. Astruc, *Chem. Rev.*, 2015, **115**, 6621–6686.

Chapter 5

Synthesis of Ir^{III}, Rh^{III} and Ru^{II} N-heterocyclic carbene-carborane complexes and evaluation of their catalytic activity in the transfer hydrogenation of acetophenone

This chapter discusses the application of our NHC-carborane ligands to the higher oxidation states of Rh^{III} and Ir^{III} as well as Ru^{II}. We have discovered that the nature of the α-substituent of the NHC, as well as reaction conditions, can determine the vertex at which cyclometallation occurs. A series of Ir^{III} complexes were successfully cyclometallated through the NHC and either a carbon atom or the B3/B6 vertex of the cage. Examination of the Ir complexes in the transfer hydrogenation of acetophenone revealed that cyclometallation through the carborane has a profound effect on the catalytic activity, indicating a bifunctional mechanism and involvement of the carborane moiety.

5.1 Introduction

5.1.1 Asymmetric hydrogenation catalysis

Transition metal-catalysed enantioselective reduction of ketones is arguably one of the most effective techniques for inducing chirality into a molecule, with industrial applications spanning agrochemicals, perfumes and pharmaceuticals.[1,2] Direct hydrogenation employs molecular hydrogen and is essentially 100 % atom efficient, providing an environmentally benign synthetic process. The first efficient transition-metal complex used for the asymmetric hydrogenation of ketones was reported in 1987 by Noyori and co-workers and was a Ru-based BINAP system (**Figure 5.1**).[3] Noyori then went on to publish the second generation catalyst [$RuCl_2$(BINAP)diimine] in 1995.[4]

In the context of this thesis, particular focus will be on the alternative method utilised for hydrogenation known as transfer hydrogenation (TH). Despite suffering from the formation of a side product (ketone), which can be easily separated and recycled, this process has advantages over direct hydrogenation: i) TH does not require pressurised H_2 gas nor an elaborate setup, as transformations can be performed at atmospheric pressure, and ii) the chemical hydrogen donors used in TH are cheap, display low toxicity and are easy to handle, with 2-propanol most commonly being employed.

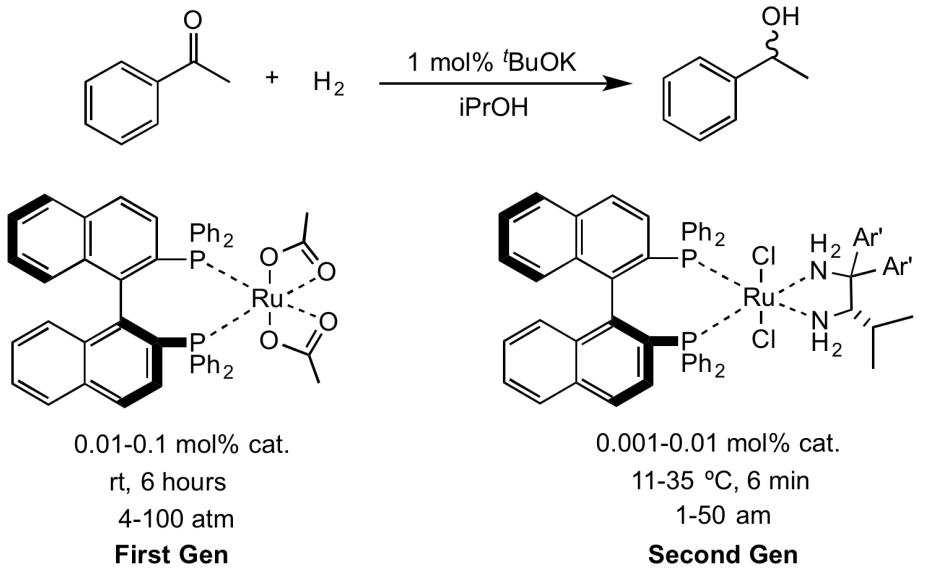

Figure 5.1 Pioneering work on direct hydrogenation by Noyori.[3,4]

TH was first reported in 1925 by the independent research of Meerwein,[5] Ponndorf,[6] and Verley[7] on the reduction of ketones and aldehydes to their corresponding alcohols, using aluminium alkoxide in the presence of a sacrificial alcohol (**Figure 5.2**). The drawback to these systems is the stoichiometric amounts of aluminium alkoxide required; this has driven the development of more efficient systems. Pioneering work by Pfaltz,[8] Genêt,[9] Lemaire,[10] and Evans[11] in the early 1990s paved the way for future catalyst design (**Figure 5.2**). However, these complexes lacked in activity and/or had insufficient enantioselectivity. Noyori revolutionised the field in 1997 with the report of the first transition-metal based system with both high activity and high ee (**Figure 5.2**).[12] Following this report, a plethora of metal complexes used in TH have been reported including Ru,[13–19] Rh,[19–24] and Ir.[19,25–30] Within these systems NHC ligands have featured heavily, ever since Nolan and co-workers reported the first example of an Ir-NHC TH catalyst in 2001 (**Figure 5.2**).[30] Efforts towards replacing precious metals with inexpensive metals such as Fe,[31,32] Co,[33] and Ni[34] have also been researched. Most recently, Morris and co-workers reported an Fe catalyst, which rivals the current Ru catalysts used in industry, with 90 % ee and 99 % yield at just 0.02 mmol catalyst loading for the reduction of acetophenone to 1-phenylethanol.[32] A drawback however is that the Fe catalyst requires an elaborate synthetic method.

It is noteworthy that some of these complexes feature a chelating proton acceptor, which was pioneered by the group of Noyori, with the initial report on a Ru complex featuring an amino tether.[12] These complexes are termed bifunctional or cooperative catalysts, as both the metal and chelating group are involved in the catalytic mechanism, which Noyori coined the "outer-sphere mechanism".[12] An alternative mechanism was proposed by Hamilton for complexes that do not possess a proton accepting group, and was termed the "inner-sphere mechanism".[35]

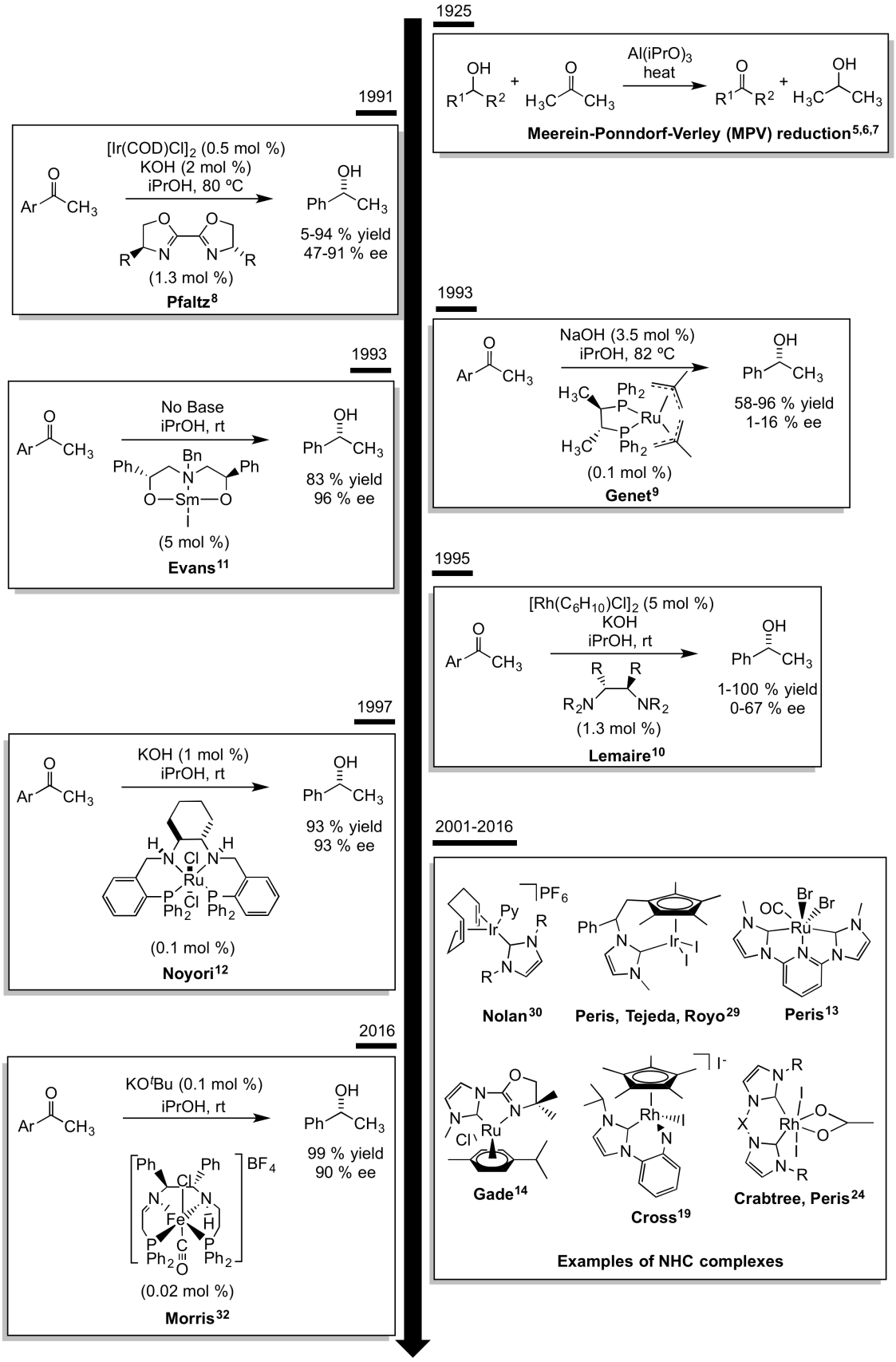

Figure 5.2 Timeline of important advances in the transfer hydrogenation of acetophenone.

5.1.2 Mechanistic pathways for asymmetric transfer hydrogenation catalysis

The inner-sphere TH mechanism proceeds *via* the alkoxide complex **I**, which is formed by deprotonation of 2-propanol in the presence of a base, which subsequently binds to the metal centre (**Scheme 5.1**). The next step involves β-hydride migration to form the metal hydride species **II** and coordinated acetone, which is released *via* ligand exchange with the substrate **III**. In the penultimate step the carbonyl is reduced by migratory insertion into the metal-hydride bond yielding the metal alkoxide **IV**. Finally, a second ligand exchange reaction yields the secondary alcohol product and the alkoxide species **I**.

In the initial step of the outer-sphere mechanism a pericyclic transition state **B** is formed. The metal and amino group accept both hydrogen atoms from 2-propanol forming acetone and the hydride complex **C**. Subsequently, interaction with the substrate leads to formation of another pericyclic transition state **D** and the two protons are donated releasing the product.

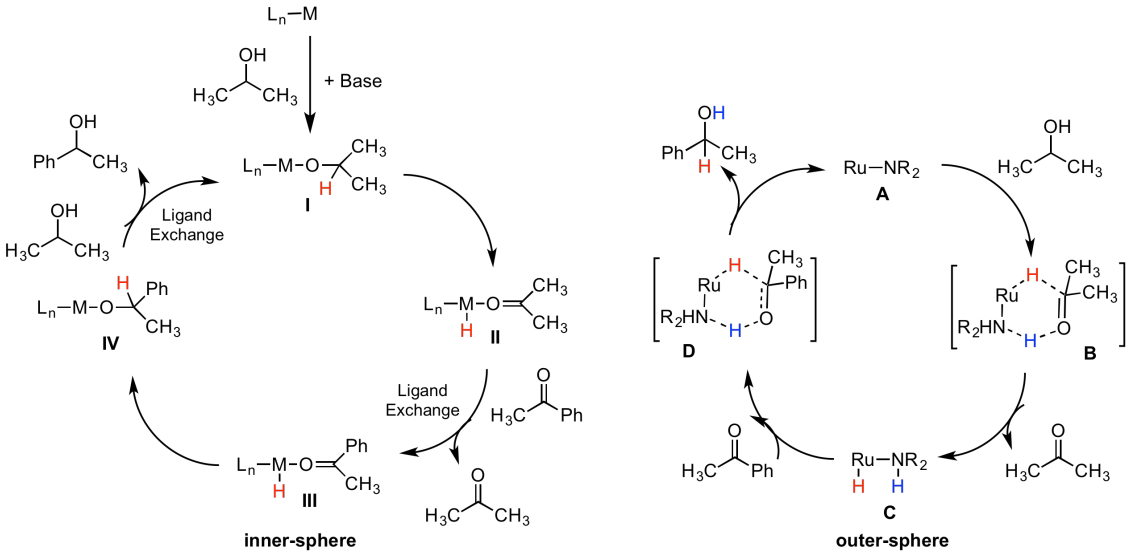

Scheme 5.1 Proposed inner sphere (left) and outer-sphere (right) mechanisms for transfer hydrogenation reaction.

5.2 Aims

Prior to our preliminary catalytic screening reaction in the hydrosilylation of acetophenone (Chapter 4, Section 4.6), no catalytic studies had been conducted on NHC complexes bearing carboranyl substituents in the literature.[36–38] To further investigate the catalytic viability of NHC-carboranyl complexes a series of Ir^{III}, Rh^{III} and Ru^{II} complexes were prepared and screened in the transfer hydrogenation of acetophenone to 1-phenylethanol. Furthermore, as the carboranyl unit is thought to be spatially equivalent to a rotating phenyl ring through 360°, NHC-phenyl complexes were prepared and examined for useful comparison against the NHC-carborane complexes.

5.3 Synthesis of an unusual (7,5)-bicyclo-metallated Cp*Ir^{III}-NHC complex

In the previous chapter, synthetic methods towards complexes of type Rh^{I}NHC(COD)Cl and a Rh^{I}-metallacycle were discussed (**Scheme 5.2**). These synthetic protocols are now applied to the higher oxidation of Ir^{III}. The reaction of **L2.1** with $[IrCp^*Cl_2]_2$ and Ag_2O in DCM gave a cyclometallated Ir^{III}-NHC complex **C2.15** in low yield (**Scheme 5.2**). In addition to NHC formation, the ^{1}H NMR spectrum revealed that intramolecular C-H activation of a Me of the ^{t}Bu group had occurred at the Ir^{III} centre. This is shown by the non-equivalent geminal proton resonances of the metallated CH_2 at 3.39 and 2.30 ppm ($^2J_{H\text{-}H}$ = 12 Hz), with the diasterotopic CH_3 groups resonating as two singlets at 1.39 and 1.09 ppm (**Figure 5.3**). The non-cyclometallated complex **C2.14** was not observed, indicating that aliphatic C-H activation is facile, as previously reported by Peris *et al.* for related Ir^{III}-NHCs.[39] Attempts were made to improve the yield by increasing the reaction time (up to 4 days), as well as carrying out the reaction at higher temperatures (70 °C) in DCE. However, no improvement on the yield was observed.

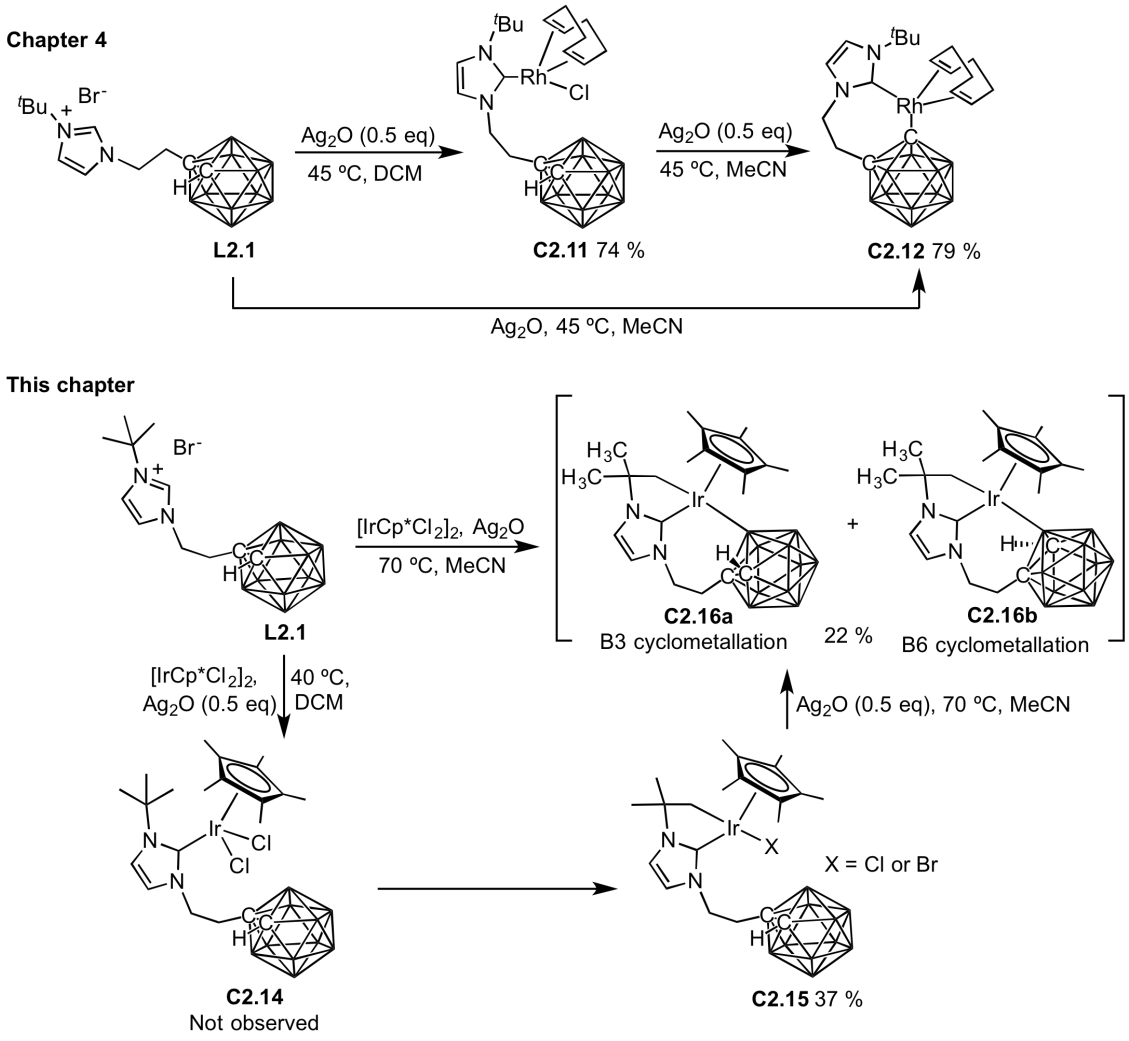

Scheme 5.2 Summary of work from Chapter 4 and reaction of **L2.1** with an Ir^{III} precursor and Ag_2O to yield cyclometallated complexes **C2.15** and **C2.16a/b**.

The ^{1}H NMR spectrum of **C2.15** suggests the presence of two complexes, with small resonances neighbouring each of the major peaks, most notably the NHC backbone and Cp*, with two Cp* resonances appearing at 1.78 and 1.74 ppm in a 1:4 ratio (**Figure 5.3**). However, micro-analysis and HRMS suggests only one species is present with a molecular ion peak of *m/z* 621.3803 corresponding to the mass of [**C2.15** − Cl]$^{+}$ (**Figure 5.4**). The X-ray diffraction analysis of **C2.15**, however, revealed the presence of an impurity. Residual electron density about the chloride suggests a halide mixed complex, and was modelled as a mixture of Cl and Br in a 4:1 ratio. Surprisingly, the micro-analysis coincides with a pure complex containing only a chloride atom, though the calculated chemical composition of C, H and N does not alter drastically when accounting for the presence of bromide. The molecular structure is presented in **Figure 5.6** along with selected bond distances in **Table 5.1**.

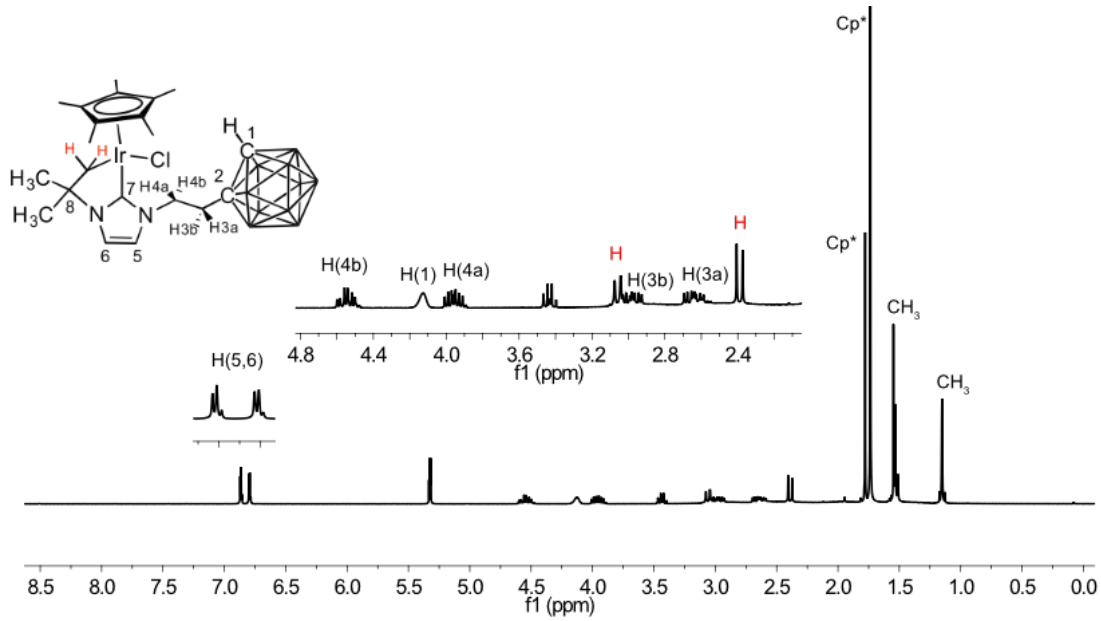

Figure 5.3 ^{1}H NMR spectrum (500 MHz, CD_2Cl_2) of **C2.15**.

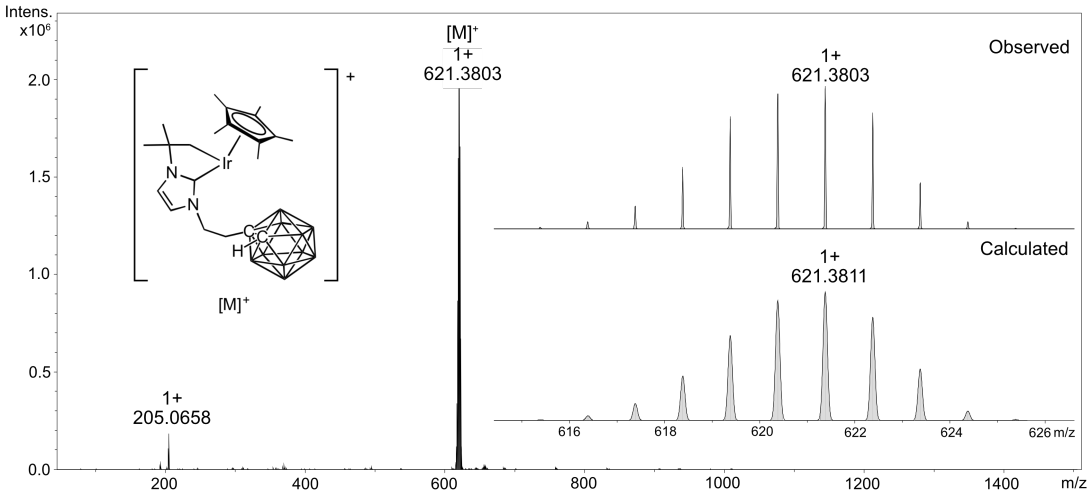

Figure 5.4 HRMS of **C2.15**. Inset shows the observed molecular ion peak of [M − Cl]$^{+}$ against the calculated molecular mass.

Our previous work with the $[Rh^{I}(COD)Cl_2]_2$ precursor has shown that solvent-assisted C-H deprotonation of the carborane moiety occurs in MeCN (Chapter 4, Section 4.3),[40] hence the reaction with **L2.1** was carried out in MeCN with an excess of Ag_2O (**Scheme 5.2**). Pleasingly, cyclometallation through the carborane did occur to give **C2.16a/b**, though in this case the cage coordinates to the metal through a boron vertex whereas in **C2.12** the complex cyclometallates through the carbon vertex of the cage (**Scheme 5.2**). Initially it was thought that cyclometallation through the cage with an Ir^{III} centre had not occurred, with only the recovery of the non-cyclometallated complex **C2.15** on workup. It was discovered that **C2.16a/b** is unstable in chlorinated solvents, which are employed during workup to remove the silver by-products. To enable **C2.16a/b** to be isolated without decomposition, the reaction mixture was passed through a short silica plug (2 cm) and eluted with MeCN to produce colourless crystals of **C2.16a/b** in 22 % yield. The ^{1}H NMR spectrum confirms the presence of diastereomers with two sets of resonances in a 2.3:1 ratio (**Figure 5.5**). This is a result of the stereogenic metal centre and a mixture of B3 and B6 metallation.[41,42] HRMS is not able to confirm the presence of **C2.16a/b** as it shares the same molecular ion peak as its non-cyclometallated counterpart **C2.15**. Nonetheless, micro-analysis and X-ray diffraction analysis were in accordance with the multinuclear NMR data. It is noteworthy that **C2.15** forms cleanly when **C2.16a/b** is dissolved in $CDCl_3$ (potential source of DCl), and the absence of the set of small resonances that were attributed to halide mixing provides further evidence that halide mixing is observed when **C2.15** is synthesised *via* the Ag_2O route.

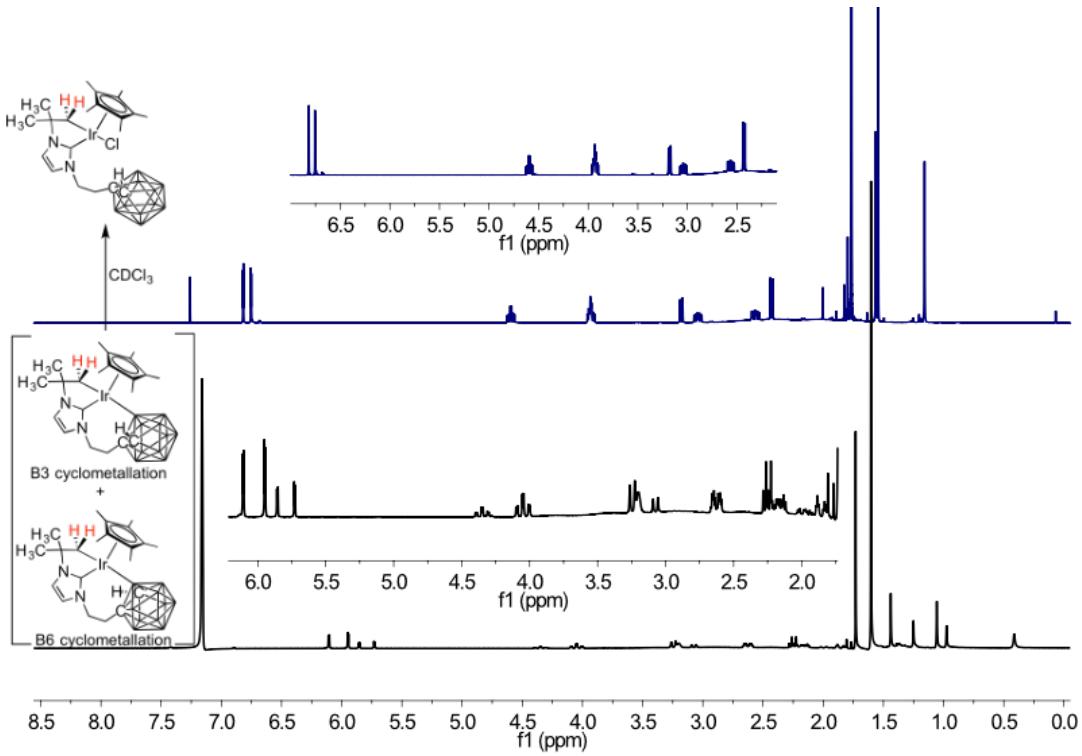

Figure 5.5 ^{1}H NMR spectrum (500 MHz, C_6H_6) of **C2.16a/b** (bottom), ^{1}H NMR spectrum (500 MHz, $CDCl_3$) of **C2.15** (top).

The molecular structures of **C2.15** and **C2.16a/b** were confirmed by X-ray diffraction analysis (**Figure 5.6**). In both cases, the coordination geometry around the metal centre can be regarded as a distorted three-legged piano stool, with a five-membered imidazolylidene-methylene metallacycle. In the molecular structure of **C2.16a/b**, HCl is lost to form a structurally distinct (7,5)-bicyclo-metallated system with a C-Ir-B bite angle of 85.65(14)°. The Ir-$C_{carbene}$ bond of **C2.15** at 2.002(5) is in the typical range for Cp*Ir-NHC complexes,[43–47] whilst that of **C2.16a/b** is comparatively short at 1.956(3) Å. The Ir-CH_2 distances for both complexes, at 2.130(6) and 2.128(3) Å for **C2.15** and **C2.16a/b** respectively, are longer than expected.[39,48] Identifying the cyclometallated vertex in **C2.16a/b** was determined by comparing the thermal parameters (U_{eq}) in conjunction with the VCD method (**Table 5.1**).[49] This allowed the cyclometallated vertex to be unambiguously assigned as the B(3/6) vertex, which are equivalent. The B6 VCD of 1.89 Å is moderately long, and are typically in the range 1.72-1.78 Å for related B-cyclometallated complexes.[41,50] It can be proposed that this vertex elongates to relieve steric encumbrance at the metal centre, similar to the Rh^{I} metallacycle (**C2.12**, Chapter 4, Section 4.3).[36]

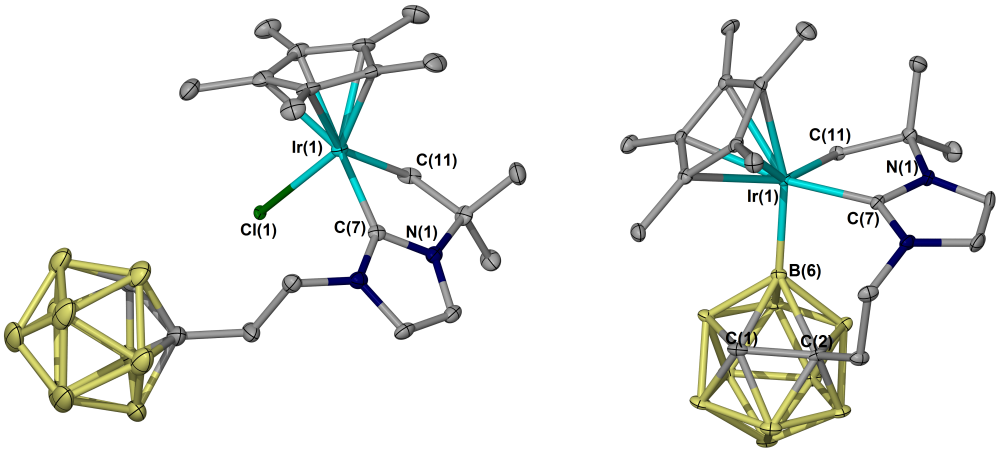

Figure 5.6 Molecular structures of **C2.15** (left) and **C2.16a/b** (right). *Thermal ellipsoids shown at 50 % probability and hydrogen atoms are omitted for clarity. The atom labelled as C1(1) in **C2.15** was found to be a mixture of Cl and Br, and could be modelled in a 4:1 ratio. Note the B(3) and B(6) vertices in **C2.16a/b** are indistinguishable.*

Table 5.1 Vertex-to-Centroid Distances (Å) and thermal parameters (U_{eq}) for **C2.16a/b**.

Vertex	**VCD (Å)**	**U_{eq}**
C(1)	1.542	0.010
C(2)	1.579	0.007
B(3)	1.712	0.021
B(6)	1.893	0.015
B(8)	1.723	0.021
B(11)	1.656	0.017

5.4 Cp*M(NHC)Cl_2 and (*p*-cymene)Ru(NHC)Cl_2 type complexes bearing a *closo*-carboranyl substituent and their phenyl congeners

5.4.1 Synthesis of complexes

Complexes **C2.15** and **C2.16a/b** were isolated in low yields (Section 5.2), and it was proposed that the steric bulk of the ^{t}Bu group was impeding the reaction. To increase the yield and enable isolation of a non-cyclometallated Cp*Ir^{III}-(NHC)Cl_2 type complex, the steric bulk was reduced by replacing the ^{t}Bu substituent of the NHC with a Me group (**L2.3**). The reaction of **L2.3** with $[IrCp^*Cl_2]_2$ under the same reaction conditions as previously gave the desired complex **C2.17** in excellent yield (**Scheme 5.3**). The corresponding Cp*Rh(NHC)Cl_2 (**C2.18**) and Ru(*p*-cymene)(NHC)Cl_2 (**C2.19**) complexes were also synthesised using analogous procedures. In addition, their phenyl congeners (**C6.1-C6.3**) were prepared in high yields, which were used for comparison in the transfer hydrogenation catalytic study (Section 5.6).

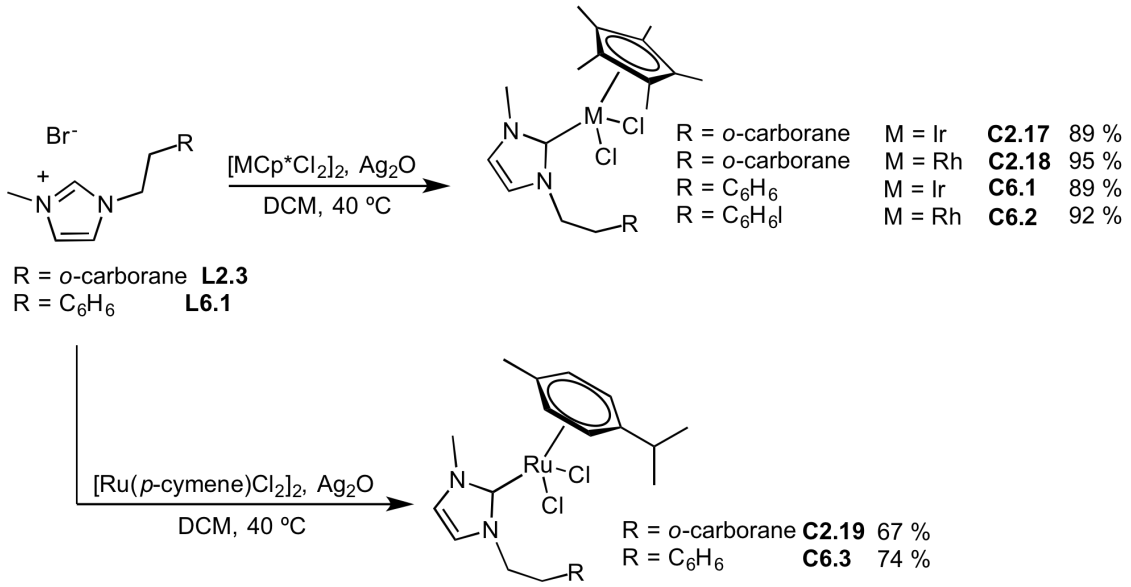

Scheme 5.3 Synthesis of Cp*M^{III}(NHC)Cl_2 and Ru(*p*-cymene)(NHC)Cl_2 type complexes bearing a carboranyl substituent (**C2.17-C2.19**) and their phenyl congeners (**C6.1-C6.3**).

5.4.2 Characterisation by multinuclear NMR and VT NMR spectroscopic studies

The ^{1}H NMR spectra of **C2.17-C2.19** and **C6.1-C6.3** confirmed formation of an NHC, with the absence of the characteristic downfield imidazolium resonance. This is further clarified by the presence of the diagnostic carbene resonances in the $^{13}C\{^1H\}$ NMR spectra typically expected for Ir^{III}-,[45,47,52] Rh^{III}-,[52–54] and Ru^{II}-NHC complexes (**Table 5.2**).[55,56] The presence of a broad singlet in the ^{1}H NMR spectra coupled with peaks in the range −2 to −13 ppm in the $^{11}B\{^1H\}$ NMR spectra confirms the presence of a tethered carboranyl substituent for **C2.17-C2.19**.

Table 5.2 Characteristic resonances in the ^{1}H and $^{13}C\{^{1}H\}$ NMR spectra (500 MHz, $CDCl_3$) for **C2.17-C2.19** and **C6.1-C6.3**.

Complex	^{1}H cage CH (ppm)	$^{13}C\{^{1}H\}$ M-$C_{carbene}$ (ppm)
C2.17	4.45	158.2
C2.18	4.62	171.9 (d, $^{1}J_{Rh-C}$ = 52.5 Hz)
C2.19	4.54	175.6
C6.1	-	157.0
C6.2	-	carbenic resonance not observed
C6.3	-	174.4

As observed for **C2.15** (Section 5.3), there is the presence of small neighbouring resonances in the ^{1}H NMR spectra for each complex for the NHC, N-Me, CH_2 linker and Cp* resonances. The relative intensities of the two sets of resonances were invariant to the purification processes employed (numerous recrystallisations from acetone with pentane and column chromatography). The micro-analysis and HRMS for each complex, contradictory to the NMR data, suggests the presence of only one species. Moreover, no halide mixing was present in the X-ray diffraction data.

A plausible explanation for the presence of the aforementioned small neighbouring peaks in the ^{1}H NMR spectra of each complex shown in **Scheme 5.3** is rotational isomers (rotamers). Rotamers can exist when a complex possesses sterically bulky ligand substituents, which hinders rotation about a M-ligand bond, in this case the M-$C_{carbene}$ bond. Variable temperature (VT) NMR spectroscopy can be an effective technique for determining the presence of rotamers,[57] hence **C2.17** was monitored by ^{1}H NMR spectroscopy over a temperature range (223 K-323 K) (**Figure 5.7**). The ^{1}H NMR spectrum of **C2.17** at 223 K reveals the presence of three species with three broad singlets for the cage CH proton (H1) at 4.52, 4.44 and 4.39 ppm in a 1.2 : 6.2 : 1.0 ratio respectively. This can also be observed for the Cp* group, with two resonances at 1.64 ppm and 1.61 ppm, with the broad minor peak at 1.64 ppm clearly splitting into a further two resonances between 233 K and 293 K.

Initially it was speculated that a B-cyclometallated species might be present at low temperature, which would give rise to diasteromers and could possibly account for the extra resonances. However, the phenyl congener **C6.1** gives rise to the same neighbouring resonances, suggesting the presence of rotamers imposed by the conformational rigidity of the bulky substituents. This is further confirmed by the spectra coalescing upon heating to 323 K, with only one set of resonances for the NHC backbone protons, cage CH proton and the diasterotopic protons observed.

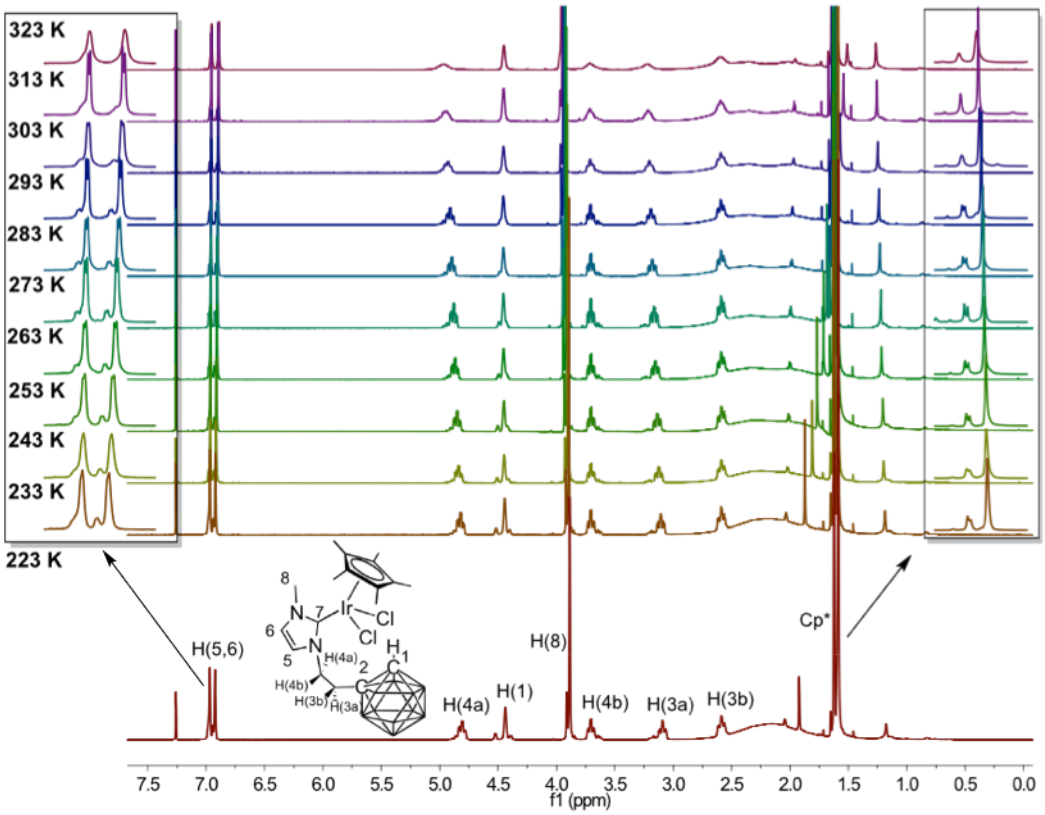

Figure 5.7 VT ^{1}H NMR spectra 500 MHz ($CDCl_3$, 223-323K) of **C2.17**.

The NMR spectra of Ru^{II} complex **C2.19** is more complex, and is quite broad at room temperature (**Figure 5.8**). Interestingly, heating the sample sharpens the majority of the peaks, whilst the diasterotopic CH_2 tether protons broaden and are absent at high temperatures. At lower temperatures (223 K) the *p*-cymene aromatic resonance at 5.48 ppm splits into two resonances. This can also be observed in the ^{1}H NMR spectrum of its phenyl derivative **C6.3** (**Figure 5.9**). These observations suggest that upon cooling the *p*-cymene ring becomes conformationally locked and each proton becomes magnetically inequivalent, indicating the presence of conformational isomers.

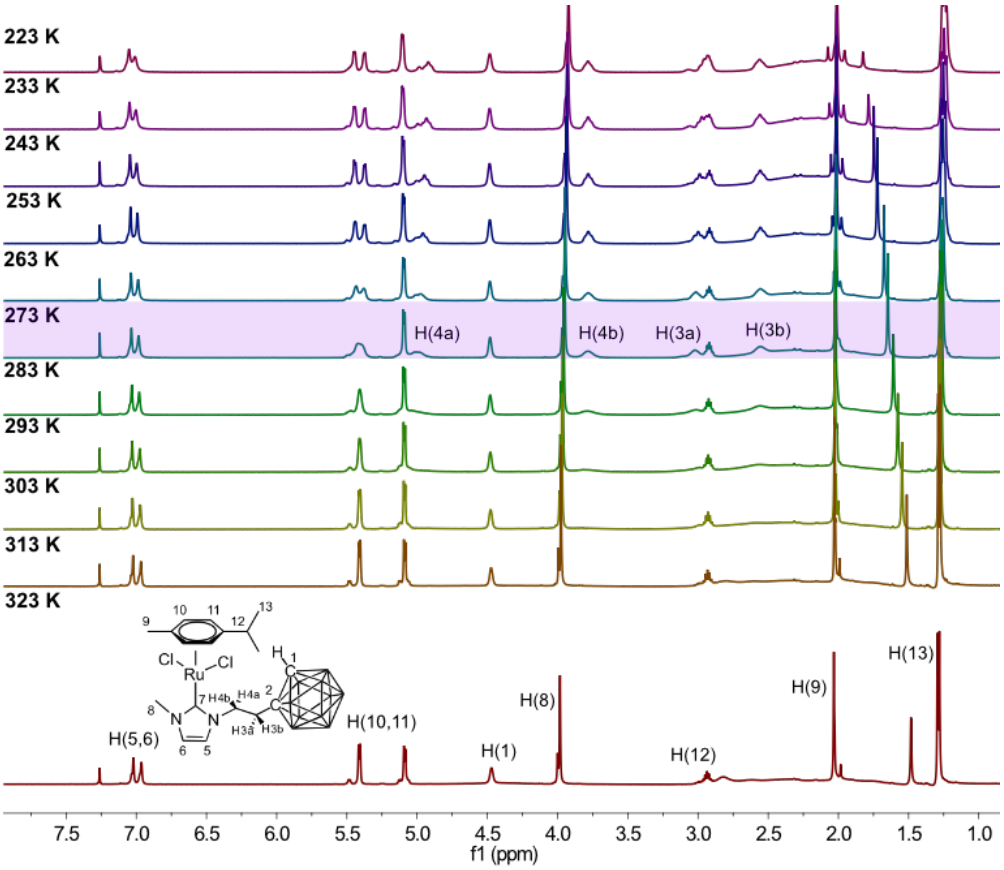

Figure 5.8 VT ^{1}H NMR spectra (500 MHz, $CDCl_3$, 223-323K) of **C2.19**. The diasterotopic CH_2 protons can be assigned at 273K (spectrum highlighted in purple).

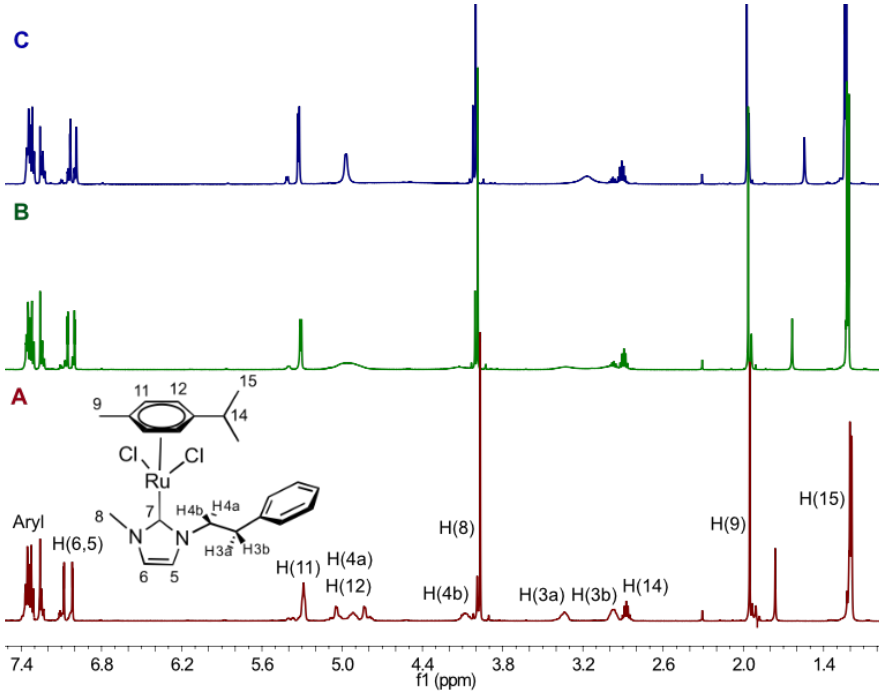

Figure 5.9 ^{1}H NMR spectrum (500 MHz, $CDCl_3$) of **C6.3** at 323K (**A**), 273K (**B**) and 253 K (**C**).

5.4.3 X-ray diffraction analysis

Crystals suitable for X-ray diffraction analysis were grown from the slow vapour diffusion of Et_2O into concentrated DCM solutions for each of the Rh^{III} and Ir^{III} complexes, with the exception of the Rh^{III} complex **C2.18**. Despite numerous efforts, a suitable crystal for X-ray diffraction analysis of **C2.18** was not obtained, and instead they form as hollow tubes consisting of multiple crystals, which is rare (**Figure 5.10**).[58] Crystals of the Ru^{II} complexes were obtained by slow evaporation of concentrated MeCN solutions.

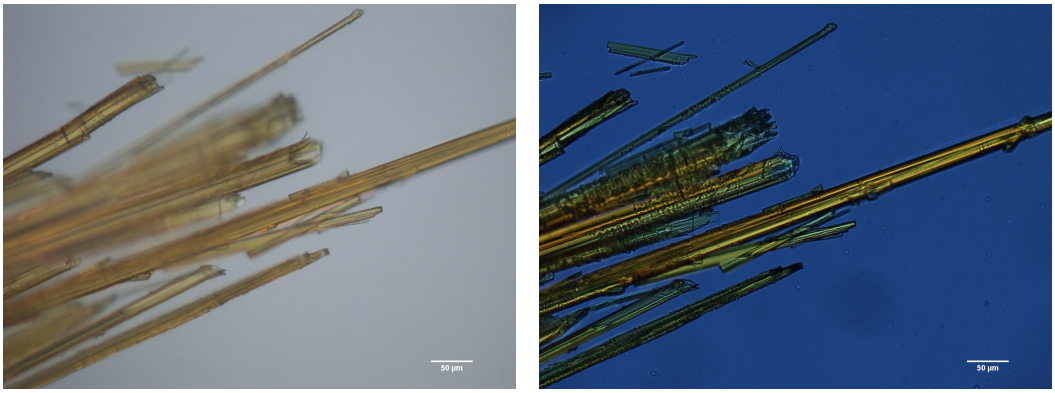

Figure 5.10 Optical microscopy images of crystals of **C2.18**.

The molecular structures of the NHC-carboranyl complexes **C2.17** and **C2.19** and the phenyl analogues **C6.1-C6.3** are all closely related and confirm the expected structures assigned by multinuclear NMR spectroscopy and HRMS data. The overall coordination geometry of each can be can be regarded as distorted three legged piano stools, with the molecular structures shown in **Figure 5.11**, along with selected bond distances provided in **Table 5.4**. The M-$C_{carbene}$ bonds are all within the expected ranges for related Ir^{III},[43–47] Rh^{III},[52,53,59] and Ru^{II}-NHC complexes.[55,61,57,58]

Comparing the average M-Cp*(centroid) distance of 1.804 (Å) to that of the average Ru-*p*-cymene (centroid); that for Ru is considerably shorter at 1.684 (Å). This may account for the more complex NMR spectra observed for **C2.19** and **C6.3**, as the *p*-cymene ring will exert greater steric encumbrance. This will restrict rotation about the *p*-cymene and the M-$C_{carbene}$ bonds leading to the *p*-cymene protons becoming magnetically inequivalent. The carboranyl carbon vertex C(1) was unambiguously determined in each case by measuring the VCD distances of the vertices vicinal to the substituted C(2) position (**Table 5.3**).

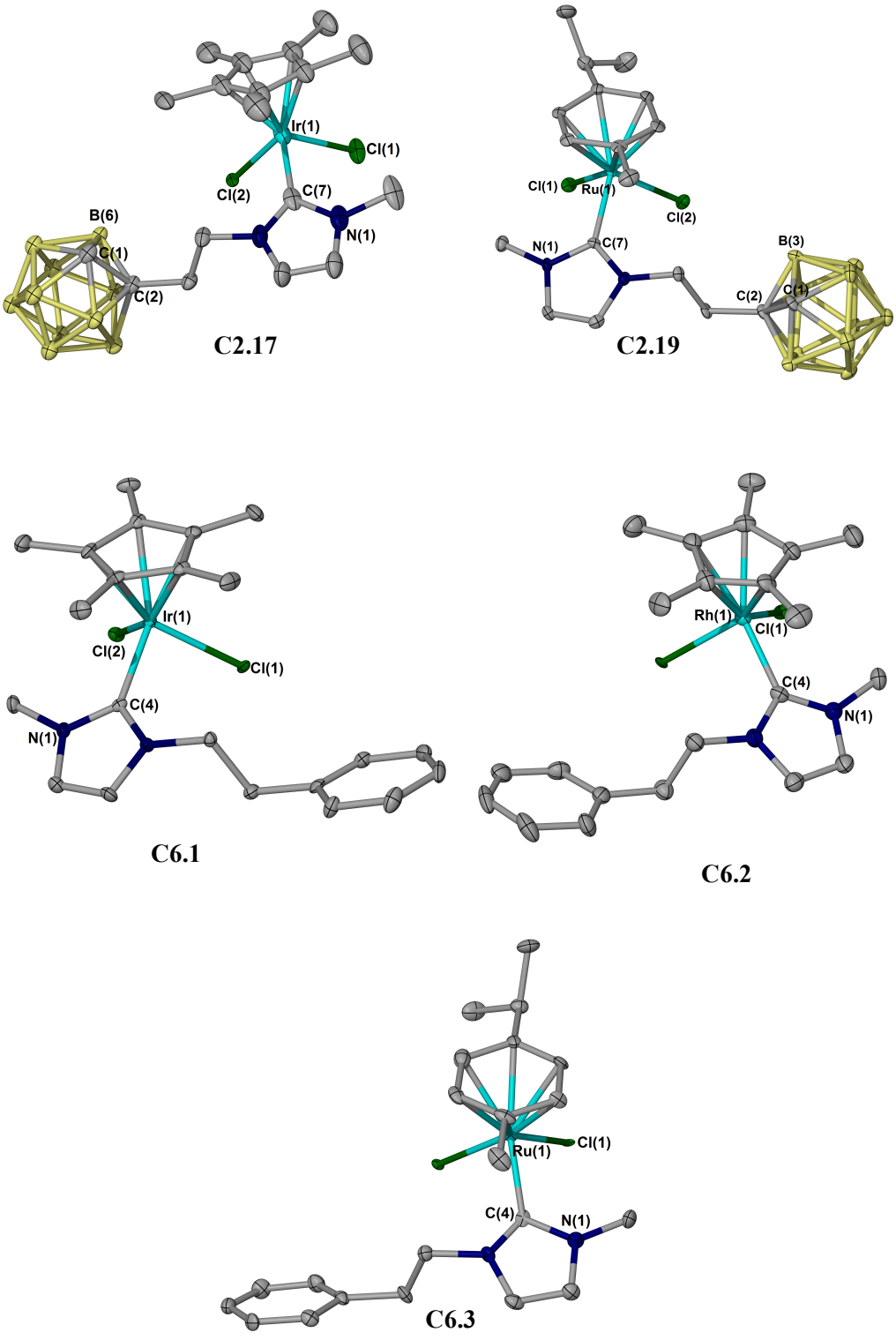

Figure 5.11 Molecular structures of complexes **C2.17**, **C2.19** and **C6.1-C6.3**. *Thermal ellipsoids shown at 50 % probability with the exception of **C2.17** (30 %), and hydrogen atoms are omitted for clarity.*

Table 5.3 Selected bond distances (Å) for complexes **C2.17**, **C2.19** and **C6.1-C6.3**.

Bond	**C2.17**	**C2.19**	**C6.1**	**C6.2**	**C6.3**
M-$C_{carbene}$	1.980(4)	2.064(7)	2.042(5)	2.058(6)	2.105(10)
M-$C_{centroid}$	1.793	1.682	1.809	1.810	1.686
M-Cl(1)	2.456(7)	2.415(18)	2.462(12)	2.467(13)	2.480(2)
M-Cl(2)	2.495(6)	2.435(2)	2.450(12)	2.483(12)	2.455(2)
VCD (C1)	1.562	1.559	-		-
VCD (B3)	1.679	1.713	-		-
VCD (B4)	1.676	1.689	-		-
VCD (B5)	1.634	1.711	-		-
VCD (B6)	1.702	1.702	-		-

5.5 Synthesis of cyclometallated NHC-carborane complexes of type Cp*Ir(NHC)Cl and a cyclometallated benzyl analogue

5.5.1 Towards site specific cyclometallation

Employing the same synthetic procedure utilised for **L2.1** (Section 5.3), the reaction of **L2.3** with $[IrCp^*Cl_2]_2$ in MeCN, with an excess of Ag_2O, gave a mixture of the B-cyclometallated (**C2.20a/b**) and the C-cyclometallated (**C2.21**) complexes (**Scheme 5.4**, **A**). This is indicative in the ^1H NMR spectrum of the product, with several overlapping NHC backbone resonances (**Figure 5.12**). When the product is dissolved in a CD_2Cl_2 the ^1H NMR spectrum is far more complex than in CD_3CN, which could indicate that an equilibrium exists between the non-cyclometallated and cyclometallated complexes in chlorinated solvents.[60] Micro-analysis of the bulk material provides evidence for the presence of only **C2.20a/b** and/or **C2.21** (all of which have the same molecular formula), along with the HRMS data revealing just one signal at *m/z* 579.3350, attributable to [complex − Cl]$^+$.

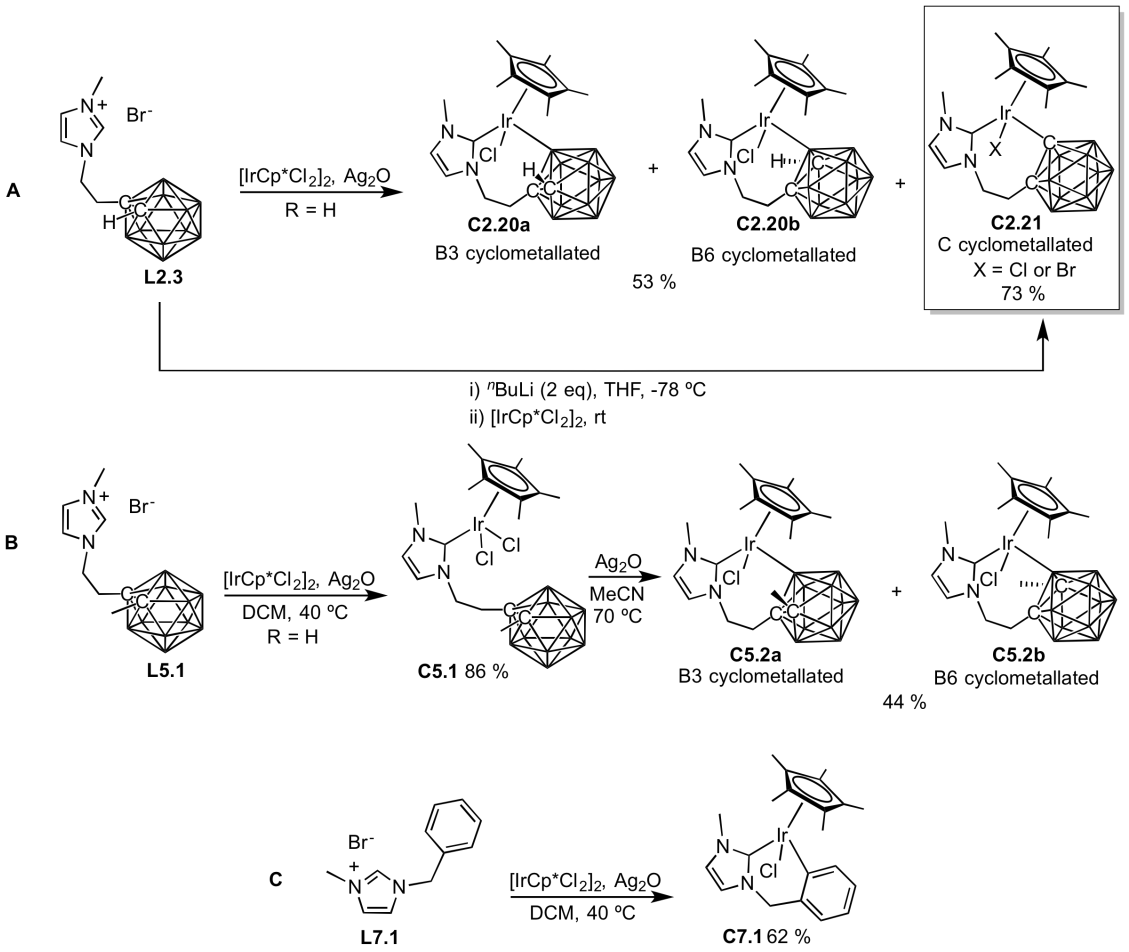

Scheme 5.4 Synthesis of C- and B-cyclometallated NHC carborane complexes (**A** and **B**) and an NHC cyclometallated benzyl complex (**C**).

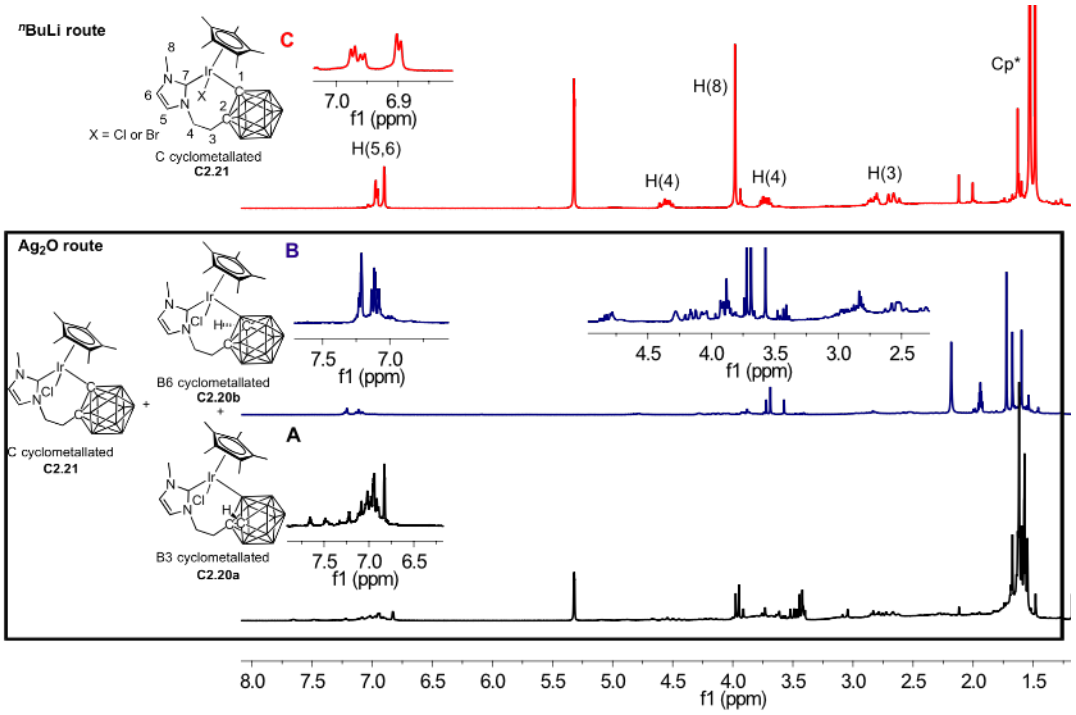

Figure 5.12 ^{1}H NMR spectrum (300 MHz, CD_2Cl_2) of mixed B- and C-cyclometallated complexes **C2.20a/b** and **C2.21** (**A**), ^{1}H NMR spectrum (300 MHz, CD_3CN) of mixed B- and C-cyclometallated complexes **C2.20a/b** and **C2.21** (**B**) and ^{1}H NMR spectrum (300 MHz, CD_2Cl_2) of C-cyclometallated complex **C2.21** (**C**).

It is intriguing that when the α-substituent of the NHC is a ^{t}Bu group, only B-cyclometallation is observed (**C2.16a/b**, section 5.3), whereas with the Me substituted ligand a mixture of B- and C-cyclometallation is obtained (**Scheme 5.4**, **A**). It can be proposed that selectivity for the B-vertex in **C2.16a/b** is due to steric stress exerted at the metal centre caused by the ^{t}Bu group. The elongation of the B-vertex reduces this steric stress, and with the C-vertices held closer to the centroid of the cage they are unable to elongate to the same extent as a B-vertex, resulting in selective cyclometallation through the equivalent B3/B6 vertices. Upon replacing ^{t}Bu with a Me substituent this steric crowding is lost and the requirement for elongation of the cyclometallated vertex is reduced resulting in a mixture of B- and C-cyclometallation.

Whether the metal is bound through a C- or B-vertex can influence the electronics of the complex, therefore it is beneficial to be able to selectively form one over the other. To negate the formation of a mixture of cyclometallated products, an alternative synthetic strategy was sought. There is literature precedent for the selective formation of C-cyclometallated complexes when ^{n}BuLi is employed as a base.[51,61] Hence, **L5.1** was reacted with ^{n}BuLi (2 eq) to deprotonate both the imidazolium NC*H*N and carboranyl C*H* protons, and subsequently reacted with $[IrCp^*Cl_2]_2$ (**Scheme 5.4**, **A**). Analysis of the resulting product revealed selective C-cyclometallation, with a much simpler ^{1}H NMR spectrum (**Figure 5.12**, **C**).

Two sets of resonances are again present in the ^{1}H NMR spectrum of **C2.21**, which in this case is a result of halide exchange to give a mixture of Ir-Cl and Ir-Br, confirmed by X-ray diffraction analysis (Section 5.5.2). Deprotonation of **L5.1** with ^{n}BuLi produces LiBr as a by-product, which is present on addition of $[IrCp^*Cl_2]_2$. It can be suggested that LiBr is responsible for the halide exchange. In an attempt to prevent the formation of a mixed halide complex, the chloride congener of **L5.1** (**L3.1**) was prepared from 1-chloro-1,2-dicarba-*closo*-dodecaborane (**P3.2**) (**Scheme 5.5**). Unfortunately, **L3.1** could not be isolated in a workable yield due to the nucleophilic substitution reaction between **P3.2** and **I2** being incredibly slow. In addition, a considerable amount of the *nido* ligand (**L3.2)** was formed making it very difficult to isolate **L3.1**. Due to this it was decided that the mixed halide system would be used in catalysis.

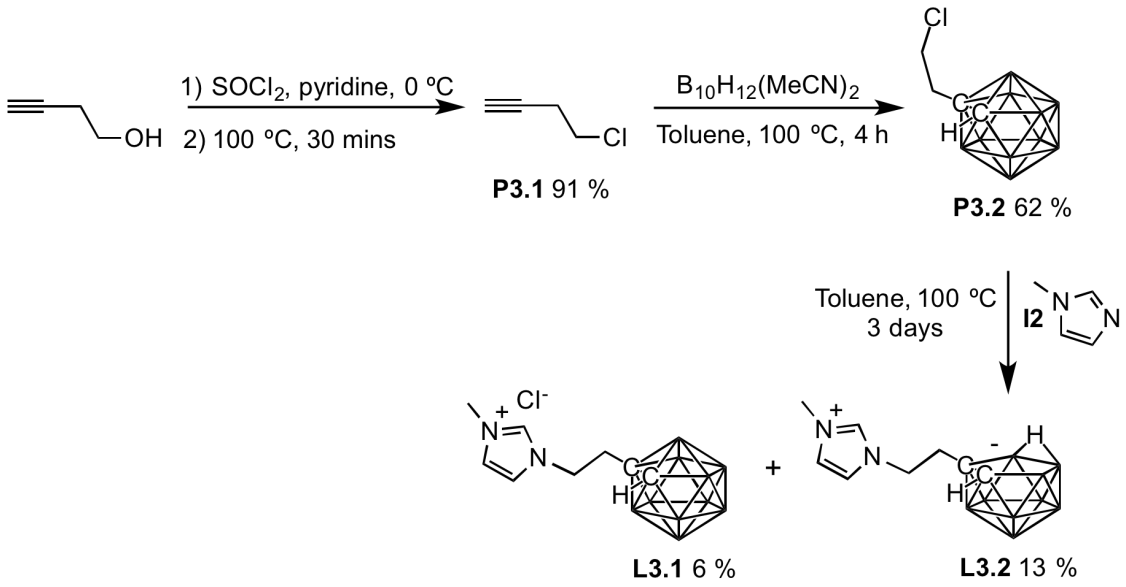

Scheme 5.5 Synthesis of a chloride imidazolium salt **L3.1**.

To allow a B-cyclometallated complex to be selectively isolated, an imidazolium salt in which the carboranyl proton was protected with a Me group (**L5.1**, Chapter 2, Section 2.4) was synthesised. **L5.1** was subjected to the same reaction conditions as **L2.3**, and gave the expected Cp*Ir-(NHC)Cl_2 type complex (**C5.1**), which was then reacted with a slight excess of Ag_2O in MeCN to give the B-cyclometallated complex **C5.2a/b** in 44 % yield (**Scheme 5.4**, **B**). Finally an Ir^{III}-NHC cyclometallated benzyl complex (**C7.1**) was prepared from literature procedure (**Scheme 5.4**, **C**),[62] and was used as a useful comparison against the complexes cyclometallated through the carborane in the catalytic transfer hydrogenation reaction of acetophenone (Section 5.6).

5.5.2 X-ray diffraction analysis

Crystals of **C2.21** suitable for X-ray diffraction analysis were grown from the slow diffusion of hexane into a concentrated DCM solution. The solid-state structure coincides with the NMR data, with the electron density of the halide being assigned as 30 % bromide to 70 % chloride. Similarly to **C2.16a/b,** a seven-membered metallacycle with a C-Ir-B bite angle of 90.58(16)° is displayed (**Figure 5.13**). Crystals of **C5.1** suitable for X-ray diffraction analysis were obtained from the slow diffusion of Et_2O into a concentrated DCM solution. Crystals of the cyclometallated derivative **C5.2a/b** could not be obtained. The Ir^{III}-$C_{carbene}$ bond lengths at 2.041(5) Å (**C2.21**) and 2.002(18) Å (**C5.1)** are in the typical range for Ir^{III}-NHC complexes. [43–47] The Ir^{III}-X bond length of **C2.21** at 2.549(7) Å is longer than a typical Ir^{III}-Cl bond and shorter than a typical Ir-Br bond, [63–65] which is to be expected with the presence of halide mixing. The assignment of the carbon vertices in the solid-state structure of **C5.1** was facile, as both C-atoms are substituted. However, like the Rh^{I} metallacycle **C2** (Chapter 4, Section 4.3), the identity of the C1 vertex in the C-cyclometallated complex **C2.21** was ambiguous using the VCD method (**Table 5.4**). The cyclometallated vertex, which was assigned as a carbon atom, possessed a very long VCD of 1.696 Å. It also has a considerably long C-C bond length at 1.741(7) Å, which is consistent with other C-cyclometallated complexes in the literature.[50,51,61]

It did, however, have the smallest thermal parameter (U_{eq}), though of the three methods (VCD, C/B-C/B bond lengths, thermal parameters) this is the most unreliable for identifying carbon atoms in *o*-carboranyl cages.[66] The elongation of the C-C bond length and VCD of the C1 vertex is expected to be a result of steric encumbrance at the metal centre. This effect was observed in the Rh^{I} C-cyclometallated complex (**C2.12**, Chapter 4, Section 4.3) and in similar complexes in the literature.[40,51] Therefore, ^{1}H NMR spectroscopy was used to confirm that the complex was cyclometallated through the C1 vertex with the absence of the characteristic broad singlet for the cage CH proton, which resonates at 4.45 ppm in the non-cyclometallated derivative (**C2.17**).

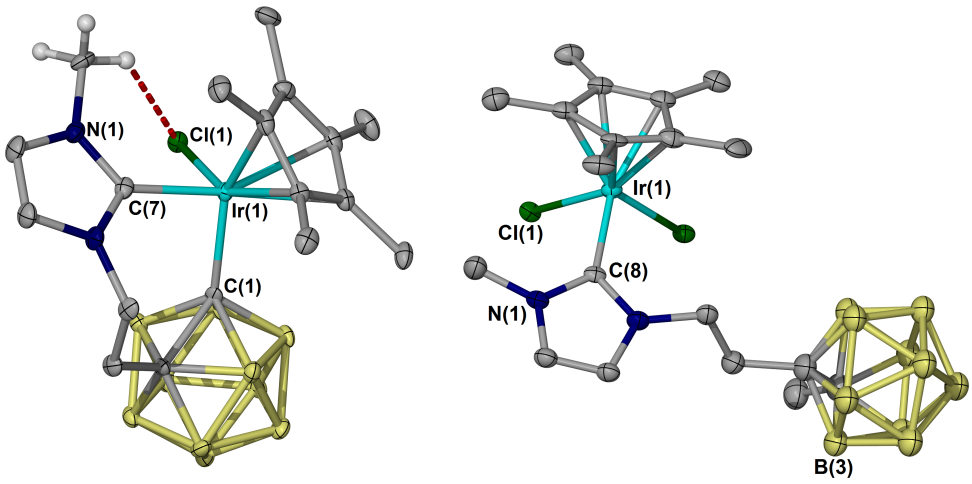

Figure 5.13 Molecular structures of complexes **C2.21** (left) and **C5.1** (right). *Thermal ellipsoids shown at 40 % probability and hydrogen atoms are omitted for clarity.*

Table 5.4 Vertex-to-Centroid Distances (Å) and thermal parameters (U_{eq}) of **C2.21** and **C5.1**.

Vertex	C2.21	U_{eq}	C5.1	U_{eq}
C(1)	1.696	0.012	1.559	0.050
C(2)	1.574	0.012	1.587	0.048
B(3)	1.690	0.024	1.672	0.054
B(6)	1.688	0.023	1.684	0.051
B(7)	1.669	0.025	1.691	0.052
B(11)	1.683	0.025	1.673	0.051

5.6 Catalysis

Transfer hydrogenation offers a mild route to secondary alcohols without the requirement of pressurised H_2 gas.[67] Several different metals have been shown to be effective in this reaction, including Ir, Rh and Ru (Section 5.1). To assess the catalytic feasibility of the complexes prepared in this work (complexes screened in catalysis are shown in **Figure 5.14**) they were examined in the transfer hydrogenation of acetophenone, alongside the Rh^{III}, Ir^{III} and Ru^{II} precursors, with the results displayed in **Table 5.5**. The reactions were carried out under anhydrous conditions and conversions were calculated using ^1H NMR spectroscopy by comparing the integration value of the Me resonance for 1-phenylethanol with that of the methoxy singlet of the internal standard, 1,3,5-trimethoxybenzene.

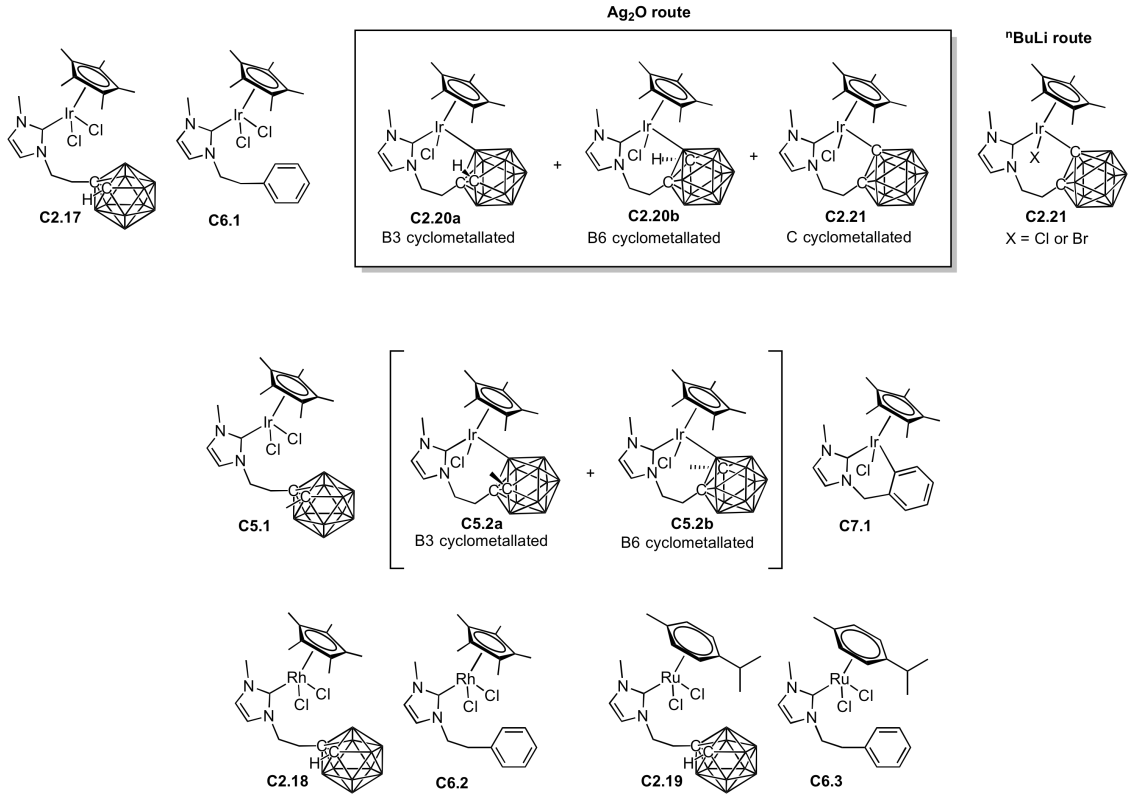

Figure 5.14 Complete series of Ir^{III}, Rh^{III} and Ru^{II} complexes synthesised and screened in the transfer hydrogenation reaction.

Table 5.5 Examination of complexes in **Figure 5.14** in the transfer hydrogenation of acetophenone to 1-phenylethanol.

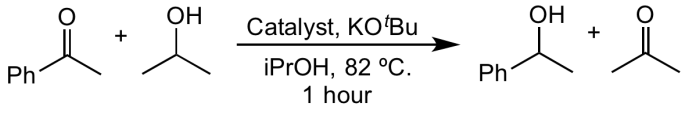

Entry	Catalyst	Catalyst Loading (mol %)	Conversion (%)
1	No catalyst	0	8
2	$[IrCp^*Cl_2]_2$	1^{Δ}	68
3	**C2.17**	1	33
4	**C6.1**	1	25
5	**C2.20a/b+C2.21**	1	>99
6	**C2.20a/+C2.21**	0.5	91
7	**C2.20a/b+C2.21**‡	1	0
8	**C2.21**	1	>99
9	**C2.21**	0.5	75
10	**C5.2a/b**	1	>99
11	**C5.2a/b**	0.5	82
12	**C7.1**	1	39
13	$[RhCp^*Cl_2]_2$	1^{Δ}	12
14	**C2.18**	1	18
15	**C6.2**	1	35
16	$[Ru(p\text{-}cymene)Cl_2]_2$	1^{Δ}	>99
17	**C2.19**	1	93
18	**C6.3**	1	94

Conditions: acetophenone (1 mmol), 2-propanol (2.3 mL, 30 mmol), ^{t}BuOK (0.1 mmol, ‡no base added), catalyst ($^{\Delta}$1.0 mol % per Ru/Rh/Ir), internal standard = 1,3,5-trimethoxybenzene (0.33 mmol), 82 °C, 1 hour.

Comparing the benchmark reactions using $[IrCp^*Cl_2]_2$, $[RhCp^*Cl_2]_2$ and $[Ru(p\text{-cymene})Cl_2]_2$, Ru is the most active catalyst with quantitative conversion after 1 hour (entry 16), and Rh^{III} is the least efficient catalyst with only 12 % conversion after 1 hour (entry 13). Incorporation of an NHC ligand saw a slight drop in yield for the Ru complexes (entries 17 and 18), with the reverse effect observed for the Rh complexes; incorporation of an NHC ligand bearing a dicarba-dodecaborane substituent (**C2.18**) saw a similar yield at 18 % (entry 14), whilst the phenyl congener **C6.2** saw an increase in conversion to 35 % after 1 hour (entry 15).

The most interesting series of results are those involving Ir^{III} complexes. $[IrCp^*Cl_2]_2$ gave good conversion of 68 % after 1 hour (entry 2). Incorporation of an NHC ligand bearing a dicarba-dodecaborane substituent (**C2.17**) deactivated the catalyst, with only 33 % conversion after 1 hour (entry 3), which decreased further to 25 % when the phenyl congener (**C6.1**) was employed (entry 4). However, upon cyclometallation of the carborane moiety a significant increase in catalytic performance is observed. The mixed C- and B-cyclometallated complex (**C2.20a/b**+**C2.21**) after 1 hour achieves quantitative conversion (entry 5), and a 91 % conversion is achieved in 1 hour upon lowering the catalyst loading to 0.5 mol % (entry 6). Intriguingly, the C-cyclometallated complex (**C2.21**) is less active than the mixed system (75 % conversion at 0.5 mol % loading (entry 9)), suggesting that either the B-cyclometallated complex is more active or that the mixed halides in **C2.21** reduce the activity. However, when the B-cyclometallated complex (**C5.2a/b**) is employed at 0.5 mol % loading only 82 % conversion is obtained (entry 11). This suggests then that halide mixing may have an effect on catalysis. If we compare these results to the cyclometallated benzyl complex (**C7.1**), only an increase to 39 % conversion is obtained upon cyclometallation (entry 12). This large disparity in catalytic activity between the dicarba-dodecaborane and phenyl substituents could suggest metal-ligand bifunctional catalysis, in which the carborane moiety becomes involved. A proposed mechanism is given in **Scheme 5.5**, which includes an inner-sphere or an outer-sphere intermediate. The catalytically active species is proposed to be an alkoxide, as no conversion is obtained in the absense of base (entry 7).[68]

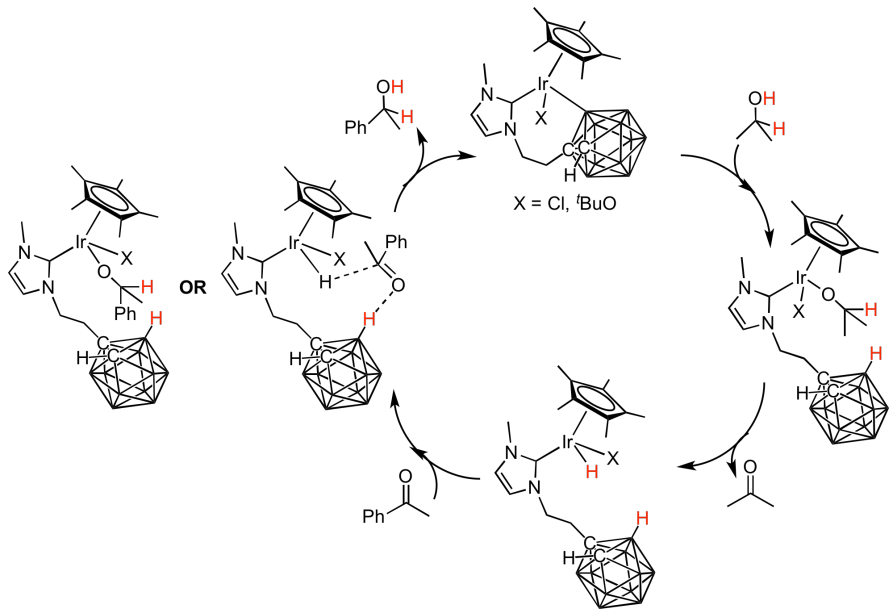

Scheme 5.6 Proposed inner-sphere or outer-sphere mechanism for the transfer hydrogenation of acetophenone by an Ir^{III} complex bearing a cyclometallated NHC-dicarbadodecaborane ligand.[68]

5.7 Conclusions and future work

5.7.1 Conclusions

A series of Rh^{III}/Ir^{III} and Ru^{II}-NHC carboranyl complexes have been prepared by reacting imidazolium salts, in the presence of Ag_2O, with the corresponding metal precursors (**Scheme 5.6**). Formation of an Ir^{III}-NHC complex, when the NHC bears the sterically bulky ^{t}Bu substituent, also results in intermolecular C-H activation of a Me of the ^{t}Bu group (**C2.16a/b**). This impedes the yield of the reaction, whereas reducing the sterics of the NHC substituent to a Me group allows a $Cp^*Ir^{III}NHC(Cl)_2$ type complex (**C2.17**) to be isolated in good yield. In addition, using analogous procedures allowed the Rh (**C2.18**) and Ru (**C2.19**) analogues to be isolated. Solvent-mediated Ag_2O cyclometallation is only applicable to the Ir^{III} complexes. The nature of the α-substituent of the NHC, as well as reaction conditions, can determine the vertex at which cyclometallation occurs. The bulky ^{t}Bu NHC substituent leads to selective B3/B6 cyclometallation (**C2.16a/b**), whilst the Me substituent leads to a mixture of C- and B-cyclometallation (**C2.20a/b**+**C2.21**).

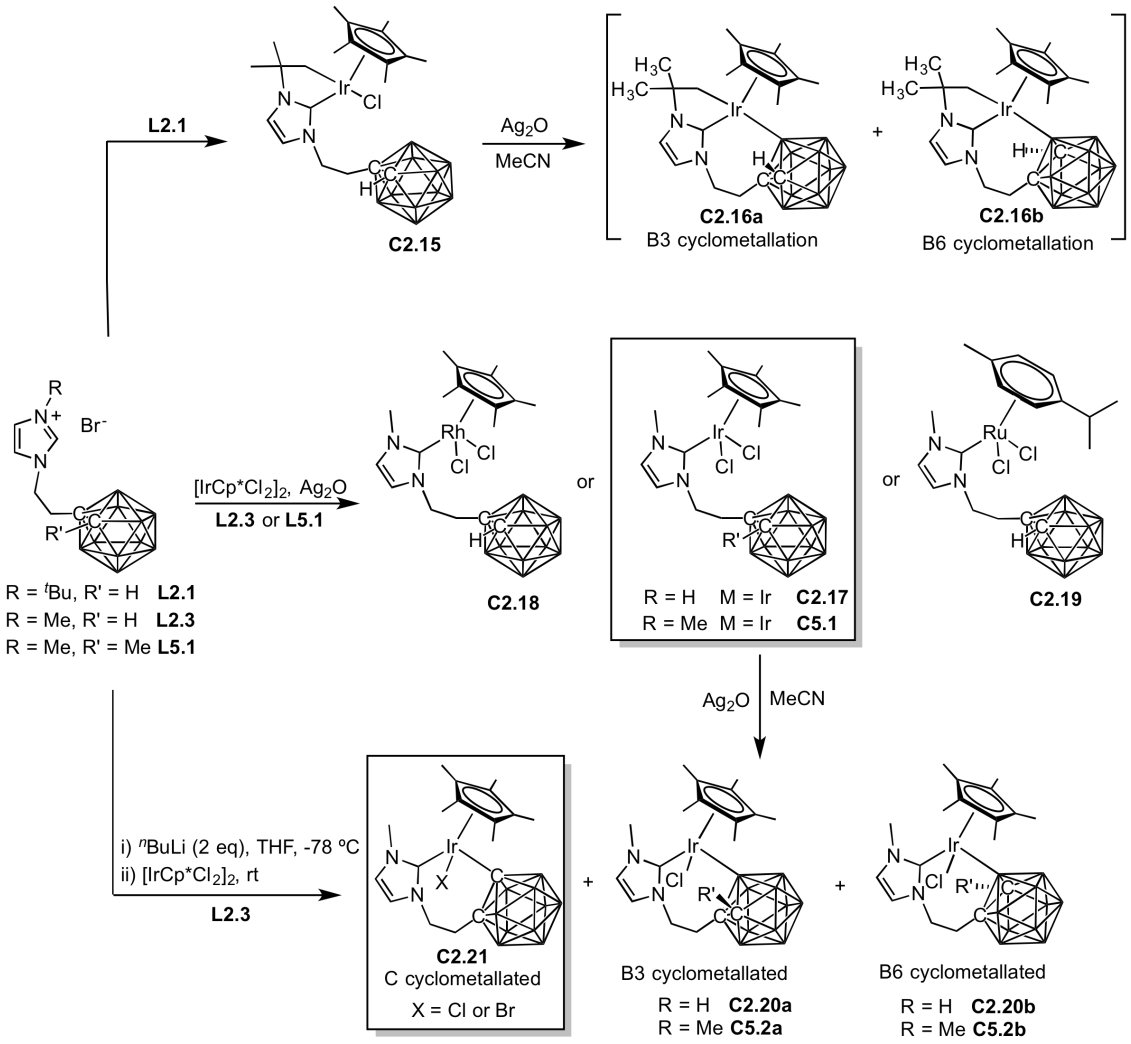

Scheme 5.6 Summary of complexes synthesised in this work.

Selective C-cyclometallation can be achieved by initially deprotonating the cage CH proton with ^{n}BuLi and then subsequently reacting with $[IrCp^{*}Cl_2]_2$. To achieve selective B-cyclometallation, the di-substituted carboranyl imidazolium salt **L3.1** is employed allowing **C5.2a/b** to be isolated in respectable yield.

The phenyl congeners of these complexes were prepared and examined for useful comparison, as the carboranyl unit is thought to be spatially equivalent to a rotating phenyl ring through 360°. The complexes were screened in the transfer hydrogenation of acetophenone, and the mixed C- and B-cyclometallated system (**C2.20a/b**+**C2.21**) was the most active (**Figure 5.15**). Initially the Ir^{III} precursor was used as a benchmark reaction, which gave a respectable conversion of 68 % after 1 hour at 1 mol % loading. Incorporation of the NHC ligands (**C2.17** and **C6.1**) deactivated the catalysts. However, upon cyclometallation of the carboranyl substituent, the mixed C- and B-cyclometallated system gave quantitative conversion after 1 hour with 91 % conversion at 0.5 mol % loading. In comparison the cyclometallated benzyl complex (**C7.1**) only saw a conversion of 39 % .

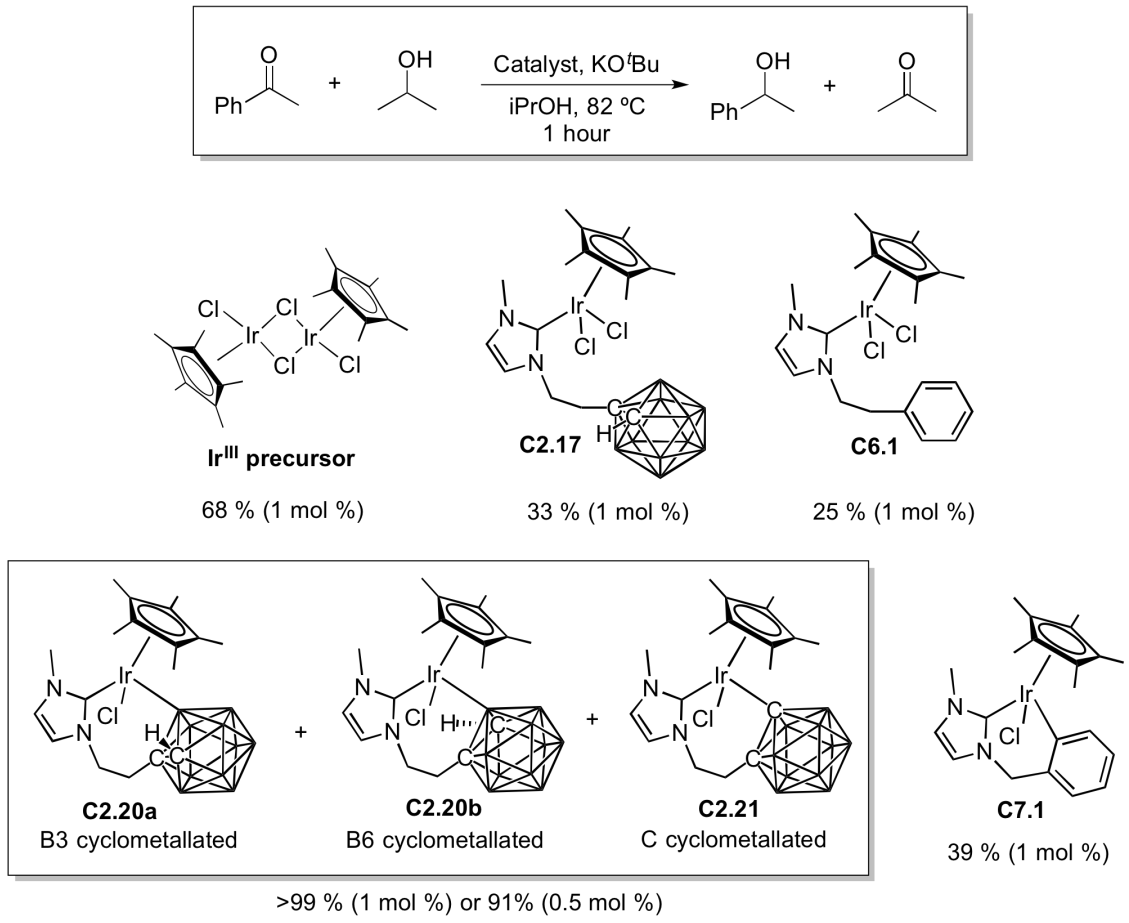

Figure 5.15 Most interesting catalytic results from the transfer hydrogenation reaction of acetophenone.

This large disparity in activity between the carboranyl cyclometallated system (**C2.20a/b**+**C2.21**) and the cyclometallated benzyl complex (**C7.1**) suggests that the carboranyl unit may be involved in the catalytic cycle and go *via* the outer-sphere mechanism associated with bifunctional catalysts. Current work on going in the Willans group involves utilising DFT to assess this reaction mechanism. More challenging substrates other than acetophenone are also being considered to determine whether **C2.20a/b**+**C2.21** are viable catalysts.

5.7.2 Towards cyclometallation of a Ru^{II}-NHC complex

It is intriguing that the Ru^{II}-NHC complex **C2.19** resists cyclometallation when Ag_2O is employed as a base. Since the non-cyclometallated Ru^{II} complexes show superior catalytic activity (**Table 5.5**, entries 17 and 18) in comparison to the analogous Ir^{III} non-cyclometallated complexes, it would be interesting to investigate whether **C2.19** can be cyclometallated under certain reaction conditions to potentially yield a superior catalyst. Jin and co-workers reported the synthesis of cyclometallated Ir^{III} carboranyl complexes by utilising a chloride-abstracting agent (AgOTf) in the presence of a base (TEA) in DCM.[50] Employing a similar synthetic approach only results in the decomposition of **C2.19**, with the characteristic resonance for the imidazolium salt appearing in the ^{1}H NMR spectrum.

Alternatively, a cyclometallated complex can be synthesised by reacting the imidazolium salt with a strong base to deprotonate both the imidazolium NC*H*N and carboranyl C*H* protons (Section 5.5), and subsequently reacted with the metal precursor $[Ru(p\text{-cymene})Cl_2]_2$. Using ^{n}BuLi was unsuccessful, though employing LiHMDS allowed the cyclometallated complex to be synthesised (**Scheme 5.7**), and the major peak in the HRMS was attributable to [**C2.19'** − Cl]$^+$ (**Figure 5.16**). Attempts at growing crystals suitable for X-ray diffraction analysis were unsuccessful. Future work should look to isolate this complex and fully characterise it by multinuclear NMR spectroscopy, X-ray diffraction and micro-analysis, and test the complex in the transfer hydrogenation of acetophenone.

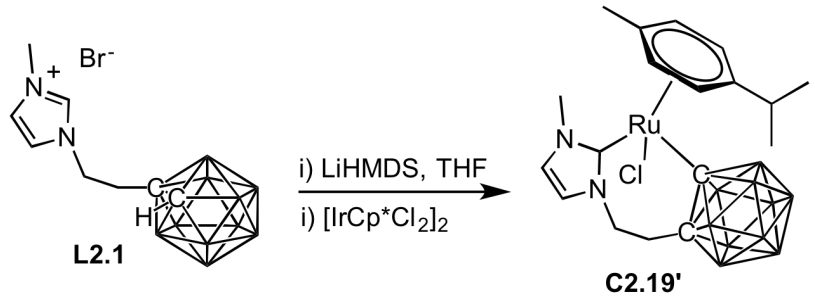

Scheme 5.7 Synthesis of a Ru^{II}-NHC carborane cyclometallated complex **C2.19'**.

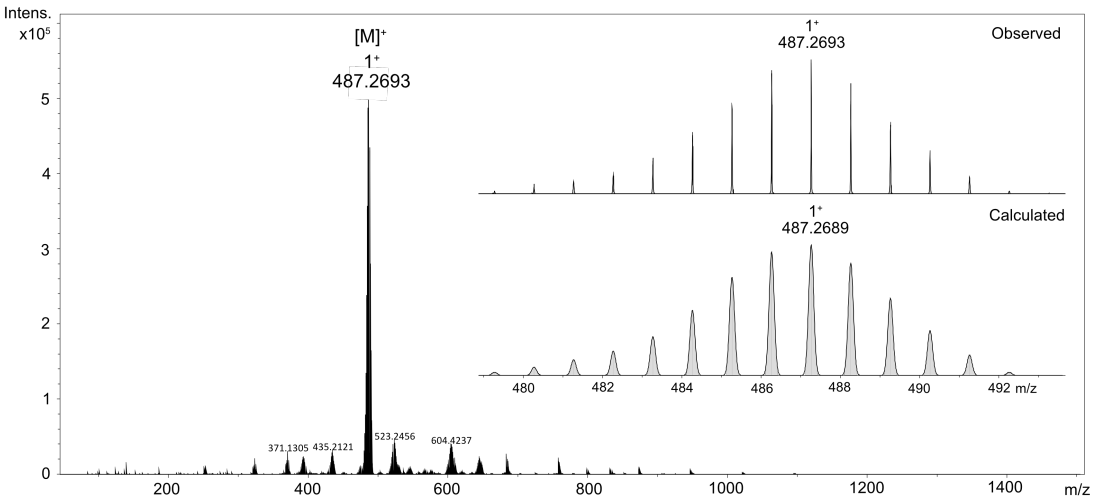

Figure 5.16 HRMS of **C2.19'**. Inset shows the observed molecular ion peak of $[M - Cl]^+$ against the calculated molecular mass.

5.8 Experimental

5.8.1 General considerations

All manipulations were carried out under an inert atmosphere by means of standard Schlenk line or glovebox techniques unless otherwise stated. Anhydrous solvents were prepared by passing over activated alumina to remove water, copper catalyst to remove oxygen and molecular sieves to remove any remaining water, *via* the Dow-Grubbs solvent system, and then freeze-pump-thaw degassed prior to use. All chemicals used in this work were bought from either Sigma Aldrich or Alfa and used without further purification. NMR spectra were recorded on a Bruker AV500 or a Bruker DPX300 spectrometer. ^{1}H NMR and $^{13}C\{^{1}H\}$ NMR chemical shifts were referenced against residual solvent peaks. Assignment of ^{1}H and $^{13}C\{^{1}H\}$ NMR spectra for all complexes was aided by the use of 2D $^{1}H^{1}H$ COSY, $^{1}H^{13}C$ HMQC, $^{1}H^{13}C$ HMBC and $^{13}C\{^{1}H\}$ DEPT 135 and DOSY experiments. Mass spectra were collected on a Bruker Daltonics (micro TOF) instrument operating in the electrospray mode. Elemental analyses were performed by Mr Stephen Boyer at London Metropolitan University. The preparation of the NHC-carborane ligand precursors (**L2.1**, **L2.3** and **L5.1**) used in this work can be found in Chapter 2, Section 2.7.

5.8.2 Metal precursors

Preparation of $[RhCp^{*}Cl_2]_2$.[69]

Hydrated $RhCl_3$ (800 mg, 3.04 mmol) was added to an RBF and degassed. Anhydrous MeOH (10 mL) and 1,2,3,4,5-pentamethylcyclopentadiene (1.43 mL, 9.13 mmol) was added and heated under reflux for 24 hours. The brown precipitate was filtered and washed with cold MeOH (10 mL) then Et_2O (3 × 10 mL). Yield: 780 mg, 1.26 mmol (83 %). ^{1}H NMR (300 MHz, $CDCl_3$): δ (ppm) 1.61 (s, 15H, Cp*). Anal. Calcd for $C_{20}H_{30}RhCl_4$: C, 38.87; H, 4.89. Found: C, 38.71; H, 4.83.

Preparation of $[IrCp^{*}Cl_2]_2$.[69]

Hydrated $IrCl_3$ (700 mg, 1.99 mmol) was added to an RBF and degassed. Anhydrous MeOH (10 mL) and 1,2,3,4,5-pentamethylcyclopentadiene (0.94 ml, 5.97 mmol) was added and heated under reflux for 48 hours. The orange precipitate was filtered and washed with cold MeOH (10 mL) then Et_2O (3 × 10 mL). Yield: 563 mg, 0.71 mmol (71 %). ^{1}H NMR (300 MHz, $CDCl_3$): δ (ppm) 1.59 (s, 15H, Cp*). Anal. Calcd for $C_{20}H_{30}IrCl_4$: C, 30.15; H, 3.80. Found: C, 30.07; H, 3.63.

Preparation of $[Ru(p\text{-}cymene)Cl_2]_2$.[70]

Hydrated $RuCl_3$ (2.00 g, 7.65 mmol) in ethanol (100 mL) was heated under reflux with α-phellandrene (10 mL, 62.0 mmol) for 4 hours. The brown precipitate was filtered off and washed with MeOH. Yield: 2.81 g, 4.59 mmol (60 %). ^{1}H NMR (300 MHz, $CDCl_3$): δ (ppm) 5.47 (d, J = 6 Hz, 2H, p-cymene benzylic H), 5.33 (d, J = 6 Hz, 2H, p-cymene benzylic H), 2.92 (septet, J = 6 Hz, 1H, CH), 2.15 (s, 3H, CH_3), 1.27 (d, J = 6 Hz, 6H, CH_3). Anal. Calcd for $C_{20}H_{28}RuCl_4$: C, 39.23; H, 4.61. Found: C, 40.46; H, 5.06 .

5.8.3 Imidazolium salts

Preparation of **L6.1**.

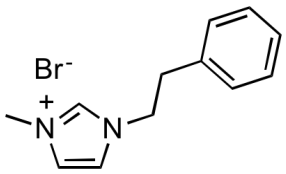

2-Phenylethylbromide (500 mg, 2.70 mmol), 1-methylimidazole (219 mg, 2.67 mmol) and MeCN (5 mL) were added to a Schlenk flask and heated at reflux for 18 hours. The reaction was then cooled to rt and the solvent removed *in vacuo*. The residue was recrystallized from DCM (5 mL) with Et_2O (30 mL) to give a pale yellow oil. This was cooled to 4°C to afford **L6.1** as an off white solid. Yield 620 mg, 2.32 mmol, (86 %). ^{1}H NMR (300 MHz, $CDCl_3$): δ (ppm) 10.08 (s, imidazolium NCN), 7.47 (t, J = 3 Hz, 1H, NCH), 7.34 (t, J = 3 Hz, 1H, NCH), 7.22-7.11 (m, 5H, Benzyl), 4.55 (t, J = 6 Hz, 2H, CH_2), 3.94 (s, 3H, CH_3), 3.18 (t, J = 6 Hz, 2H, CH_2). ^{13}C{^{1}H} NMR (75 MHz, $CDCl_3$): δ (ppm) 137.1, 135.8, 128.9, 128.8, 127.4, 123.4, 122.5, 51.0, 36.6, 36.5. HRMS (ESI^+): m/z $[C_{12}H_{15}N_2]^+$ 187.1235, calcd for $[M - Br]^+$ 187.1249. Consistent with data previously reported.[71]

Preparation of **L7.1**.[72]

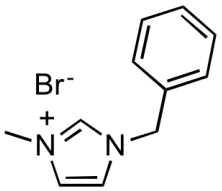

1-Methylimidazole (1.65 g, 20.10 mmol) was added to a solution of benzyl bromide (3.43 g, 20.10 mmol) dissolved in THF (20 mL). The mixture was stirred at ambient temperature overnight and the solvent removed furnishing a viscous oil. This oil was washed with Et_2O (3 × 10 mL) and dried *in vacuo* to give the product as a pale yellow oil. Yield: 4.18 g, 16.50 mmol (82 %). ^{1}H NMR (CD_3OD, 500 MHz): δ (ppm) 9.09 (s, 1H, imidazolium NCN), 7.63 (d, J = 2.0 Hz, 1H, NCH), 7.60 (d, J = 2.0 Hz, 1H, NCH), 7.48-7.39 (m, 5H, Aryl), 5.46 (s, 2H, CH_2), 3.94 (s, 3H, CH_3); ^{13}C{^{1}H} NMR (CD_3OD, 75 MHz): δ (ppm) 135.3, 130.3, 130.2, 129.8, 125.1, 123.5, 53.8, 36.9. HRMS (ESI^+): m/z $[C_{11}H_{13}N_2]^+$ 173.1095, calcd. $[M - Br]^+$ 173.1079. Consistent with data previously reported.[72]

5.8.4 NHC-carborane complexes

Preparation of Ir complex **C2.15**.

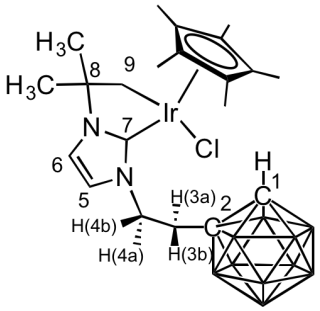

To a Schlenk flask was added **L2.1** (100 mg, 0.27 mmol), Ag_2O (34 mg, 0.15 mmol), $[Ir(Cp^*)Cl_2]_2$ (120 mg, 0.15 mmol) and anhydrous DCM (5 mL) along with some 4 Å molecular sieves. The reaction was heated at 40 °C for 16 hours, filtered through a 2 cm silica plug and flushed with DCM (3 × 10 mL). The solvent was removed from the filtrate *in vacuo* and the solid added to Et_2O (10 mL). This was filtered and removal of the solvent from the filtrate *in vacuo* gave **C2.15** as an orange powder. Yield: 63 mg, 0.10 mmol (37 %). ^{1}H NMR (300 MHz, CD_2Cl_2): δ (ppm) 6.87 (d, *J* = 3.0 Hz, 1H, H^6), 6.80 (d, *J* = 3.0 Hz, 1H, H^5), 4.56 (td, *J* = 12.0 Hz, 6.0 Hz, 1H, H^{4a}), 4.13 (br. s, 1H, H^1), 3.95 (m, 1H, H^{4b}), 3.06 (d, *J* = 12.0 Hz, 1H, H^9), 2.98 (m, 1H, H^{3a}), 2.63 (m, 1H, H^{3b}), 2.39 (d, *J* = 12.0 Hz, 1H, H^9), 1.78/1.74 (Cp*), 1.53 (s, 3H, CH_3), 1.15 (s, 3H, CH_3). $^{13}C\{^1H\}$ NMR (75 MHz, CD_2Cl_2): δ (ppm) 164.0 (C^7), 119.7 (C^6), 117.3 (C^5), 89.7/89.4 (quaternary Cp*), 73.0 (C^2), 65.9 (CH_3), 62.7 (C^1), 49.3 (C^4), 39.7 (C^3), 31.4/31.0 (CH_3), 28.3 (C^9), 10.1/10.0 (Cp*). $^{11}B\{^1H\}$ NMR (96 MHz, $CDCl_3$): δ (ppm) −2.3, −5.4, −9.5, −11.1, −12.6. HRMS (ESI^+): m/z $[C_{21}H_{40}B_{10}N_2Ir]^+$ 621.3803, calcd for $[M - Cl]^+$ 621.3811. Anal. Calcd for $C_{22}H_{42}B_{10}ClN_2Ir$: C, 38.43; H, 6.14; N, 4.27. Found: C, 38.50; H, 6.21; N, 4.35.

Preparation of Ir complex **C2.16a/b**.

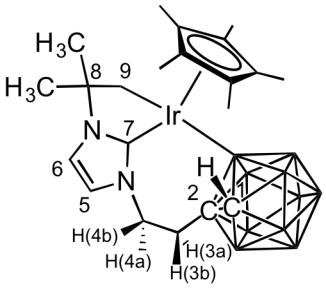

To a Schlenk flask was added **L2.1** (100 mg, 0.27 mmol), Ag_2O (94 mg, 0.41 mmol), $[Ir(Cp^*)Cl_2]_2$ (108 mg, 0.14 mmol) and anhydrous MeCN (5 mL) along with some 4 Å molecular sieves. The reaction was heated at 70 °C for 24 hours, filtered through a 2 cm silica plug and flushed with MeCN (3 × 10 mL). The solvent volume was reduced to 5 mL *in vacuo* resulting in **C2.16a/b** as colourless crystals, which were filtered, washed with pentane (5 mL) and dried *in vacuo*. Yield: 41 mg, 0.06 mmol (22 %). ^{1}H NMR (500 MHz, C_6D_6): major isomer (70 %) δ (ppm) 6.11 (d, 1H, *J* = 2.0 Hz, H^6), 5.96 (d, *J* = 2.0 Hz, 1H, H^5), 4.06 (td, *J* = 13.1 Hz, 3.0 Hz, 1H, H^{4a}), 3.24 (d, *J* = 10.0 Hz, 1H, H^9), 3.21 (br. s, 1H, H^1), 2.64 (m, 2H, H^{4b}), 2.63 (d, *J* = 10.0 Hz, 1H, H^9), 1.87 (m, 1H, H^{3a}), 1.61 (Cp*), 1.44 (s, 1H, CH_3), 1.06 (s, 1H, CH_3). Minor isomer (30 %) δ (ppm) 5.86 (d, 1H, J = 2.0 Hz, H^6), 5.74 (d, 1H, J = 2.0 Hz, H^5), 4.35 (td, J = 13.8 Hz, 3.0 Hz, 1H, H^{4a}), 3.07 (d, *J* = 10.5 Hz, 1H, H^9), 3.21 (br. s, 1H, H^1), 2.64 (m, 2H, H^{4b}), 2.63 (d, *J* = 10.5 Hz, 1H, H^9), 2.18 (m, 1H, H^{3a}), 1.98 (m, 1H, H^{3b}), 1.73 (Cp*), 1.26 (s, 1H, CH_3), 0.98 (s, 1H, CH_3). $^{13}C\{^1H\}$ NMR (75 MHz, C_6D_6): δ (ppm) 117.6/117.5 (C^6), 116.7/116.6 (C^5), 93.5/93.0 (quaternary Cp*), 65.8/65.5 (C^2), 59.9/58.3 (C^1),

45.1/44.3 (C^4), 41.3 (C^3), 31.9/31.2 (CH_3), 30.7/30.5 (CH_3), 20.6/18.4 (C^9), 9.7/9.7 (Cp*). $^{11}B\{^1H\}$ NMR (96 MHz, C_6D_6): δ (ppm) −1.4, −4.0, −7.8, −11.3, −15.3. HRMS (ESI^+): m/z $[C_{21}H_{39}B_{10}N_2Ir]^+$ 620.3766, calcd for $[M]^+$ 620.3733. Anal. Calcd for $C_{21}H_{39}B_{10}N_2Ir$: C, 40.69; H, 6.34; N, 4.52. Found: C, 40.80; H, 6.47; N, 4.30. Crystals suitable for X-ray diffraction analysis were grown by the slow evaporation of a concentrated solution of **C7a/b** in MeCN.

Preparation of Ir complex **C2.17**.

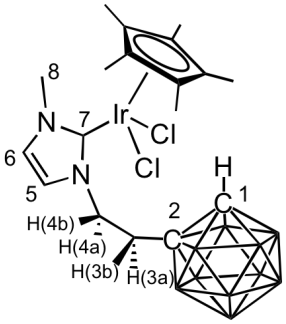

To a Schlenk flask was added **L2.3** (50 mg, 0.15 mmol), Ag_2O (17 mg, 0.075 mmol), $[Ir(Cp^*)Cl_2]_2$ (60 mg, 0.073 mmol) and anhydrous DCM (5 mL), along with some 4 Å molecular sieves. The reaction was heated at 40 °C for 16 hours, filtered through Celite and flushed with DCM (3 × 5 mL). The solvent was removed from the filtrate *in vacuo* and the residue was recrystallised from acetone (5 mL)/pentane (30 mL), filtered and dried *in vacuo* to give **C2.17** as a yellow solid. Yield: 86 mg, 0.13 mmol (89 %). ^1H NMR (300 MHz, $CDCl_3$): δ (ppm) 6.97 (d, J = 3.0 Hz, 1H, H^6), 6.90 (d, J = 3.0 Hz, 1H, H^5), 4.94 (m, 1H, H^{4a}), 4.45 (br. s, 1H, H^1), 3.97/3.95 (s, 3H, H^8), 3.71 (m, 1H, H^{4b}), 3.21 (m, 1H, H^{3a}), 2.59 (m, 1H, H^{3b}), 1.64/1.61 (s, 15H, Cp*). $^{13}C\{^1H\}$ NMR (75 MHz, $CDCl_3$): δ (ppm) 158.2 (C^7), 124.3 (C^6), 121.3 (C^5), 89.2 (quaternary Cp*), 71.9 (C^2), 60.9 (C^1), 49.7 (C^4), 39.1 (C^3), 38.8 (C^8), 9.5/9.3 (Cp*). $^{11}B\{^1H\}$ NMR (96 MHz, $CDCl_3$): δ (ppm) −2.2, −5.0, −9.6, −13.0. HRMS (ESI^+): m/z $[C_{18}H_{35}B_{10}N_2IrCl]^+$ 615.3121, calcd for $[M - Cl]^+$ 615.3106. Anal. Calcd for $C_{18}H_{35}B_{10}N_2IrCl_2$: C, 33.22; H, 5.42; N, 4.31. Found: C, 33.12; H, 5.34; N, 4.37. Crystals suitable for X-ray diffraction analysis were grown by the slow diffusion of hexane into a concentrated solution of **C2.17** in DCM.

Preparation of Rh complex **C2.18**.

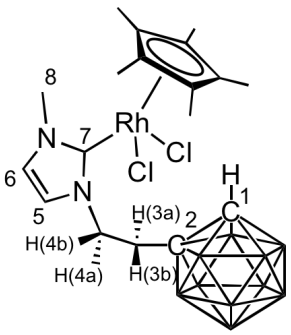

To a Schlenk flask was added **L2.3** (50 mg, 0.15 mmol), Ag_2O (17 mg, 0.075 mmol), $[Rh(Cp^*)Cl_2]_2$ (46 mg, 0.074 mmol) and anhydrous DCM (5 mL), along with some 4 Å molecular sieves. The reaction was heated at 40 °C for 16 hours, filtered through Celite and flushed with DCM (3 × 5 mL). The solvent was removed from the filtrate *in vacuo* and the residue was recrystallised from acetone (5 mL)/pentane (30 mL), filtered and dried *in vacuo* to give **C2.18** as a yellow solid. Yield: 79 mg, 0.14 mmol (95 %). ^1H NMR (300 MHz, $CDCl_3$): δ (ppm) 7.04 (d, J = 3.0 Hz, 1H, H^6), 6.99 (d, J = 3.0 Hz, 1H, H^5), 5.02 (m, 1H, H^{4a}), 4.62 (br. s, 1H, H^1), 4.00 (s, 3H, H^8), 3.76 (m, 1H, H^{4b}), 3.20 (m, 1H, H^{3a}), 2.50 (m, 1H, H^{3b}), 1.60 (s, 15H, Cp*).

$^{13}C\{^{1}H\}$ NMR (75 MHz, $CDCl_3$): δ (ppm) 171.9 (d, $^{1}J_{Rh\text{-}C}$ = 52.5 Hz, C^{7}), 125.3 (C^{6}), 122.2 (C^{5}), 96.6 (d, $^{1}J_{Rh\text{-}C}$ = 7.5 Hz, quaternary Cp*), 71.9 (C^{2}), 61.0 (C^{1}), 50.0 (C^{4}), 39.3 (C^{3}), 38.8 (C^{8}), 9.6 (Cp*). $^{11}B\{^{1}H\}$ NMR (96 MHz, $CDCl_3$): δ (ppm) −2.2, −5.1, −9.7, −12.8. HRMS (ESI^{+}): m/z 526.2550 $[C_{18}H_{35}B_{10}N_2RhCl]^{+}$, calcd for $[M - Cl]^{+}$ 526.2525. Anal. Calcd for $C_{18}H_{35}B_{10}Cl_2N_2Rh$: C, 38.51; H, 6.28; N, 4.99. Found: C, 38.63; H, 6.32; N, 5.13.

Preparation of Ru complex **C2.19**.

To a Schlenk flask was added **L2.3** (50 mg, 0.15 mmol), Ag_2O (17 mg, 0.075 mmol), $[Ru(p\text{-cymene})Cl_2]_2$ (46 mg, 0.075 mmol) and anhydrous DCM (5 mL), along with some 4 Å molecular sieves. The reaction was heated at 40 °C for 3 hours, filtered through Celite and flushed with DCM (3 × 5 mL). The solvent was removed from the filtrate *in vacuo* and the residue subjected to column chromatography on silica using a gradient elution with CH_2Cl_2/MeOH (2 %). Recrystallisation from MeCN gave **C2.19** as a microcrystalline orange solid. Yield: 58 mg, 0.10 mmol (67 %). ^{1}H NMR (500 MHz, DCM): major δ (ppm) 7.08 (d, *J* = 2.0 Hz, 1H, H^{6}), 7.03 (d, *J* = 2.0 Hz, 1H, H^{5}), 5.40 (d, *J* = 5.0 Hz, 2H, p-cymene Ar-H), 5.06 (d, *J* = 5.0 Hz, 2H, p-cymene Ar-H), 4.93 (br. s, 1H, H^{4a}), 4.54 (br. s, 1H, carboranyl H^{1}), 3.94 (s, 3H, H^{8}), 3.82 (br. s, 1H, H^{4b}), 2.93 (br. s, 1H, H^{3a}), 2.90 (septet, *J* = 10 Hz, 1H, H^{14}), 2.64 (br. s, 1H, H^{3b}), 1.93 (s, 3H, H^{9}), 1.26 (d, *J* = 10 Hz, 6H, H^{15}). $^{13}C\{^{1}H\}$ NMR (126 MHz, CD_2Cl_2): δ (ppm) 175.6 (C^{7}), 125.3 (C^{6}), 122.0 (C^{5}), 110.4 (p-cymene quaternary C), 99.4 (p-cymene quaternary C), 86.4 (p-cymene Ar), 82.4 (p-cymene Ar), 72.6 (C^{2}), 61.5 (C^{1}), 50.5 (C^{4}), 39.9 (C^{8}), 39.0 (C^{3}), 31.2 (C^{14}), 23.0 (C^{9}), 21.9/18.8 (C^{15}). $^{11}B\{^{1}H\}$ NMR (161 MHz, CD_2Cl_2): δ (ppm) −2.4, −5.4, −9.8, −12.9. HRMS (ESI^{+}): m/z $[C_{18}H_{34}B_{10}N_2RuCl]_{+}$ 523.2460, calcd for $[M - Cl]^{+}$ 523.2455. Anal. Calcd for $C_{18}H_{34}B_{10}N_2RuCl_2$: C, 38.71; H, 6.14; N, 5.02. Found: C, 38.63; H, 6.02; N, 5.12. Crystals suitable for X-ray diffraction analysis were grown by the slow evaporation of a concentrated solution of **C2.19** in MeCN.

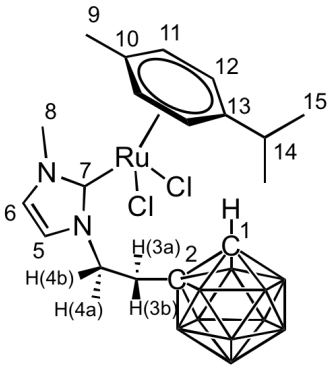

Preparation of Ir complex **C2.20a/b** and **C2.21** mixture.

To a Schlenk flask was added **C2.17** (100 mg, 0.15 mmol), Ag_2O (52 mg, 0.22 mmol) and anhydrous MeCN (5 mL) along with some 4 Å molecular sieves. The reaction was heated at 70 °C for 16 hours, filtered through a 2 cm silica plug and flushed with MeCN (2 × 10 mL). The solvent was reduced to 5 mL and the desired product was precipitated with Et2O (30 mL), filtered and the solvent removed *in vacuo* to give a mixture of **C2.20a/b** and **C2.21**. Yield: 52 mg, 0.08 mmol (53 %). HRMS (ESI^{+}): m/z $[C_{18}H_{34}B_{10}N_2Ir]^{+}$ 579.3350, calcd for $[M - Cl]^{+}$

579.3340. Anal. Calcd for $C_{18}H_{34}B_{10}N_2IrCl$: C, 35.20; H, 5.58; N, 4.56. Found: C, 35.34; H, 5.57; N, 4.63.

Preparation of Ir complex **C2.21**.

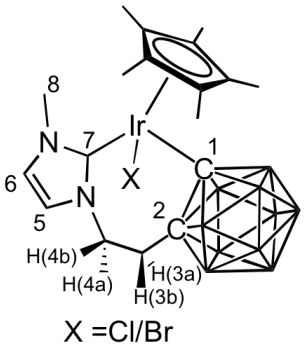

To a Schlenk flask was added **L2.3** (50 mg, 0.15 mmol) and anhydrous THF (5 mL). The solution was cooled to -78 °C and a 1.6 M solution of ^{n}BuLi in hexane (133 μL, 0.32 mmol) was added dropwise. This was stirred at -78 °C for 30 minutes, then the temperature was then raised to 0 °C and stirred for a further 1 hour. A solution of $[IrCp^*Cl_2]_2$ (60 mg, 0.073 mmol) in THF (3 mL) was added at 0 °C and the reaction was stirred at room temperature for 12 hours. The solvent was removed *in vacuo*, DCM (5 mL) added and filtered through a 2 cm silica plug which was flushed with DCM (2 × 10 mL). The solvent volume was reduced to 5 mL and the product precipitated with pentane (30 mL), filtered and dried *in vacuo* to give **C2.21** as a yellow solid. Yield: 68 mg, 0.11 mmol (73 %). ^{1}H NMR (300 MHz, CD_2Cl_2): δ (ppm) 6.97 (m, 1H, H^6), 6.90 (s, 1H, H^5), 4.54 (m, 1H, H^{4a}), 3.98/3.94 (s, 3H, H^8), 3.72 (m, 1H, H^{4b}), 2.82 (m, 1H, H^{3a}), 2.66 (m, 1H, H^{3b}), 1.53/1.48 (Cp*). ^{13}C{^{1}H} NMR (75 MHz, CD_2Cl_2): δ (ppm) carbenic C not observed, 126.0/125.9 (C^6), 121.2 (C^5), 93.8/93.5 (quaternary Cp*), 46.2 (C^4), 42.3, 41.0, 39.2 (C^8), 9.6/9.3 (Cp*). HRMS (ESI$^+$): m/z $[C_{22}H_{29}B_{10}N_2Ir]^+$ 549.1650, Calcd for $[M\text{-}X]^+$ 549.1635. Crystals suitable for X-ray diffraction analysis were grown by the slow diffusion of hexane into of a concentrated solution of **C2.21** in DCM.

Preparation of Ir complex **C5.1.**

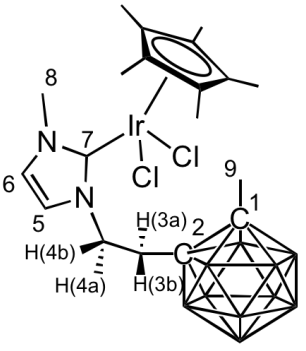

Prepared as described for **C2.17**, starting from **L5.1** (50 mg, 0.14 mmol), Ag_2O (16 mg, 0.07 mmol), $[Ir(Cp^*)Cl_2]_2$ (56 mg, 0.07 mmol) and anhydrous DCM (5 mL). After purification the product was obtained as a yellow solid. Yield: 80 mg, 0.12 mmol (86 %). ^{1}H NMR (300 MHz, $CDCl_3$): δ (ppm) 6.99 (d, J = 2.1 Hz, H^6), 6.92 (d, J = 2.1 Hz, H^5), 5.04 (m, 1H, H^{4a}), 3.99/3.97 (s, 3H, H^8), 3.84 (td, J = 12.0 Hz, 3 Hz, 1H, H^{4b}), 3.41 (m, 1H, H^{3a}), 2.48 (m, 1H, H^{3b}), 2.15 (s, 3H, H^9), 1.67/1.63 (Cp*). ^{13}C{^{1}H} NMR (75 MHz, $CDCl_3$): δ (ppm) 158.6 (C^7), 121.3 (C^6), 89.4/89.1 (quaternary Cp*), 74.9 (carboranyl quaternary C) (only one carboranyl quaternary C observed), 49.9 (C^4), 38.9 (C^8), 36.6 (C^3), 23.9 (C^9), 9.5/9.3 (Cp*). ^{11}B{^{1}H} NMR (96 MHz, $CDCl_3$): δ (ppm) −3.7, −6.1, −10.0. HRMS (ESI$^+$): m/z $[C_{19}H_{37}B_{10}N_2IrCl]^+$ 629.3283, calcd for $[M\text{-}Cl]^+$ 629.3263. Crystals suitable for

X-ray diffraction analysis were grown by the slow diffusion of hexane into a concentrated solution of **C5.1** in DCM.

Preparation of Ir complex **C5.2a/b**.

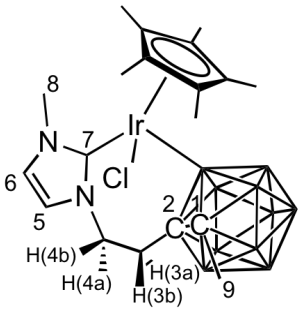

This complex was prepared as described for **C2.20a/b** and **C2.21**, starting from **C5.1** (60 mg, 0.09 mmol), Ag_2O (16 mg, 0.07 mmol) and anhydrous MeCN (5 mL). After purification the product was obtained as a yellow solid. Yield: 25 mg, 0.04 mmol (44 %). ^{1}H NMR (500 MHz, CD_3CN): δ (ppm) 7.23 (d, *J* = 2.0 Hz, 1H, NCH), 7.19 (d, *J* = 2.0 Hz, 1H, NCH), 7.14 (d, *J* = 2.0 Hz, 1H, NCH), 7.11 (d, *J* = 2.0 Hz, 1H, NCH), 5.01 (td, *J* = 12.5 Hz, 6.0 Hz, 1H, CH_2), 4.25 (m, 1H, CH_2), 4.02–3.95 (m, 1H, CH_2), 3.71/3.61 (s, 3H, CH_3), 3.17 (m, 1H, CH_2), 2.72 (m, 1H, CH_2), 2.30 (m, 1H, CH_2), 2.17 (s, 1H, CH_3), 1.72/1.68/1.63 (Cp*). ^{13}C{^{1}H} NMR (126 MHz, CD_3CN): δ (ppm) 124.4 (NCH), 122.8 (NCH), 95.5/89.6 (quaternary Cp*), 50.5 (C^4), 37.9, (C^3), 36.9 (C^8), 23.9 (C^9), 9.3, 9.2, 9.0, 8.8 (Cp* region). ^{11}B{^{1}H} NMR (161 MHz, CD_3CN): δ (ppm) −4.2, −6.3, −8.5, −9.8, −10.6. HRMS (ESI$^+$): m/z $[C_{19}H_{36}B_{10}N_2Ir]^+$ 593.3513, calcd for $[M - Cl]^+$ 593.3497. Anal. Calcd for $C_{19}H_{36}B_{10}ClN_2Ir$: C, 36.32; H, 5.78; N, 4.46. Found: C, 36.45; H, 5.77; N; 4.60.

5.8.5 NHC-Benzyl complexes

Preparation of **C6.1**.

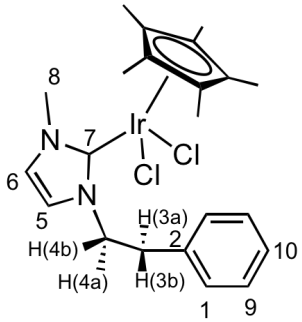

To a Schlenk flask was added **L6.1** (50 mg, 0.19 mmol), Ag_2O (22 mg, 0.095 mmol), $[Ir(Cp^*)Cl_2]_2$ (76 mg, 0.095 mmol) and anhydrous DCM (5 mL) along with some 4 Å molecular sieves. The reaction was heated at 40 °C for 16 hours and filtered over Celite, which was flushed with DCM (3 × 5 mL). The solvent was removed from the filtrate *in vacuo* and the residue was recrystallised from acetone (5 mL) with pentane (30 mL), filtered and dried *in vacuo* to give **C7.1** as a yellow solid. Yield: 97 mg, 0.17 mmol (89 %). ^{1}H NMR (300 MHz, $CDCl_3$): δ (ppm) 7.47–7.20 (m, 5H, Ar), 6.95–6.89 (m, 2H, $H^{5/6}$), 5.08 (dt, *J* = 12.0, 6.0 Hz, 1H, H^{4a}), 4.00/3.98 (s, 3H, H^8) 3.89 (dt, *J* = 12.0, 6.0 Hz, 1H, H^{4b}), 3.50 (dt, *J* = 12.0, 6.0 Hz, 1H, H^{3a}) 2.99 (dt, *J* = 12.0, 6.0 Hz, 1H, H^{3b}), 1.62/1.59 (s, 15H, Cp*). ^{13}C{^{1}H} NMR (75 MHz, $CDCl_3$): δ (ppm) 157.0 (C^7) 138.7 (Ar), 129.4 (Ar), 128.7 (Ar), 126.7 (Ar), 123.5 (C^6), 121.5 (C^5), 88.8 (quaternary Cp*), 52.2 (C^4), 38.7 (C^8), 38.4 (C^3), 9.5/9.3 (Cp*). HRMS (ESI$^+$): m/z $[C_{22}H_{29}N_2IrCl]^+$ 549.1650, Calcd for $[M - Cl]^+$ 549.1635.

Anal. Calcd for $C_{22}H_{29}N_2IrCl_2$: C, 45.20; H, 5.00; N, 4.79. Found: C, 45.06; H, 4.93; N, 4.85. Crystals suitable for X-ray diffraction analysis were grown by the slow diffusion of hexane into a concentrated solution of **C6.1** in DCM.

Preparation of Rh complex **C6.2.**

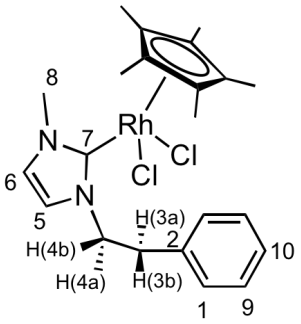

Prepared as described for **C2.18** from **L6.1** (50 mg, 0.19 mmol), Ag_2O (22 mg, 0.095 eq), $[Rh(Cp^*)Cl_2]_2$ (59 mg, 0.095 mmol) and anhydrous DCM (5 mL) After purification the product was obtained as an orange solid. Yield: 86 mg, 0.17 mmol, (92 %). ^{1}H NMR (300 MHz, $CDCl_3$): δ (ppm) 7.50-7.15 (m, 5H, benzyl), 7.02-6.97 (m, 2H, $H^{5/6}$), 5.20 (m, 1H, H^{4a}), 4.06/4.04 (s, 3H, H^8) 3.92 (m, 1H, H^{4b}), 3.51 (m, 1H, H^{3a}) 2.96 (m, 1H, H^{3b}), 1.62/1.58 (s, 15H, Cp*). $^{13}C\{^1H\}$ NMR (75 MHz, $CDCl_3$): δ (ppm) 138.7 (benzyl), 129.4 (benzyl), 128.7 (benzyl), 126.7 (benzyl), 124.5 (C^6), 122.5 (C^5), 96.3 (d, $^1J_{Rh\text{-}C}$ = Hz, quaternary Cp*), 52.5 (C^4), 39.3 (C^8), 38.2 (C^4), 9.8/9.6 (Cp*). HRMS (ESI^+): m/z $[C_{22}H_{29}N_2RhCl]^+$ 459.1074, calcd for $[M - Cl]^+$ 459.1069. Anal. Calcd for $C_{22}H_{29}N_2RhCl_2$: C, 53.35; H, 5.90; N, 5.66. Found: C, 53.18; H, 5.95; N, 5.73. (Note: the resonance for the carbenic carbon is not observable in the ^{13}C NMR spectrum.) Crystals suitable for X-ray diffraction analysis were grown by the slow diffusion of hexane into a concentrated solution of **C6.2** in DCM.

Preparation of Ru complex **C6.3**.

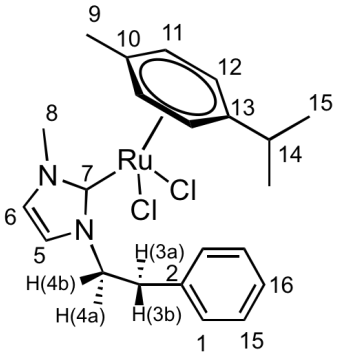

To a Schlenk flask was added **L6.1** (50 mg, 0.19 mmol), Ag_2O (22 mg, 0.095 mmol), $[Ru(p\text{-cymene})Cl_2]_2$ (58 mg, 0.095 mmol), anhydrous DCM (5 mL) and anhydrous MeOH (0.1 mL) along with a small number of 4 Å molecular sieves. The reaction was heated at 40 °C for 3 hour. The reaction was then cooled to rt, filtered over Celite and further washed with DCM (3 × 5 mL). The solvent was removed *in vacuo* and the residue subjected to column chromatography on silica using a gradient elution with DCM/MeOH (2 %) to afford an orange solid. Recrystallized from acetone (5 mL) with pentane (30 mL), afforded **C6.3** as an orange powder. Yield: 69 mg, 0.14 mmol (74 %). ^{1}H NMR (500 MHz, 273 K, $CDCl_3$): Major isomer; δ (ppm) 7.38-7.22 (m, 5H, benzyl), 7.08 (d, J = 2 Hz, 1H, H^6), 7.02 (d, J = 2 Hz, 1H, H^5), 5.29 (m, 2H, p-cymene Ar-H), 5.05 (d, J = 5 Hz, 1H, p-cymene Ar-H), 4.92 (m, 1H, H^{4a}), 4.84 (d, J = 5 Hz, 1H, p-cymene Ar-H), 4.08 (m, 1H, H^{4b}), 3.97 (s, 3H, H^8), 3.34 (m, 1H, H^{3a}), 2.97 (m, 1H, H^{3b}), 2.88 (septet, J = 10 Hz, H^{14}), 1.95 (s, 3H, H^9), 1.20 (d, J = 5 Hz, 6H, H^{15}). $^{13}C\{^1H\}$ NMR (126 MHz, $CDCl_3$): δ (ppm) 174.0 (C^7),

138.6 (benzyl), 129.3 (H^6), 128.8 (H^5), 126.8 29 (benzyl), 124.1 (benzyl), 121.8 (benzyl), 109.0 (p-cymene quaternary C), 99.2 (p-cymene quaternary C), 85.1/84.8 (p-cymene Ar), 82.7/82.4 (p-cymene Ar), 53.1 (C^4), 39.7 (C^8), 37.9 (C^3), 30.7 (C^{14}), 22.7/22.5 (C^{15}), 18.7 (C^9). HRMS (ESI^+): m/z $[C_{22}H_{28}N_2RuCl]^+$ 457.0995, calcd for $[M - Cl]^+$ 457.0982. Crystals suitable for X-ray diffraction analysis were grown by the slow diffusion of hexane into a concentrated solution of **C6.3** in DCM. (Note: complex exists as two isomers in solution with only the major isomer quoted and the resonances for the diasterotopic CH_2 protons are only visible at temperatures below room temperature).

Preparation of Ir complex **C7.1**.[62]

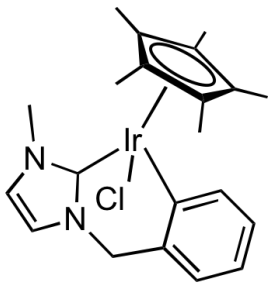

To a Schlenk flask was added **L7.1** (50 mg, 0.20 mmol), Ag_2O (23 mg, 0.10 mmol), $[Ir(Cp^*)Cl_2]_2$ (79 mg, 0.10 mmol) and anhydrous DCM (5 mL) along with some 4 Å molecular sieves. The reaction was heated at 40 °C for 18 hours and filtered over Celite, which was flushed with DCM (3 × 5 mL). The solvent was removed from the filtrate *in vacuo* and the residue was recrystallised from DCM (5 mL) with hexane (30 mL), filtered and dried *in vacuo* to give **C7.1** as a yellow solid. Yield: 65 mg, 0.17 mmol (62 %). ^1H NMR (CD_3OD, 500 MHz): δ (ppm) 7.44−7.33 (m, 5H, Aryl) 7.27 (d, J = 2.0 Hz, 1H, NCH), 6.91 (d, J = 2.0 Hz, 1H, NCH), 6.09 (d, J = 14.4 Hz, 1H, CH_2) 5.22 (d, J = 14.9 Hz, 1H, CH_2), 4.02 (s, 3H, CH_3), 1.66 (s, 15H, Cp*). $^{13}C\{^1H\}$ NMR (75 MHz, $CDCl_3$): δ (ppm) 128.8, 128.6, 128.1, 123.4, 122.0, 89.0, 54.7, 38.9, 9.4 (needs stronger carbon). HRMS (ESI^+): m/z $[C_{21}H_{26}N_2Ir]^+$ 499.1716, calcd for $[M - Cl]^+$ 499.1725. Consistent with data previously reported.[62]

Catalytic transfer hydrogenation general procedure. Catalyst (0.01 or 0.005 mmol) and 1,3,5-trimethoxybenzene (55.50 mg, 0.33 mmol) were added to an ampoule and degassed. In a Glovebox, ^{t}BuOK (14 mg, 0.10 mmol) and acetophenone (117 µL, 1.00 mmol) were added to the ampoule. Under an atmosphere of N_2, anhydrous ^{i}PrOH (2.30 mL, 30.00 mmol) was added and the reaction was heated at 82 °C for 1 hour. The reaction mixture was quenched by cooling in an ice bath and an aliquot (0.10 mL) was added to an NMR tube with $CDCl_3$ (0.40 mL). Conversion was calculated using ^1H NMR spectroscopy by comparing the integration of the Me resonance of 1-phenylethanol with the internal standard, and values are an average of two separate runs.

5.9 References

1 J. G. de Vries and C. J. Elsevier, in *The Handbook of Homogeneous Hydrogenation*, Wiley-VCH Verlag GmbH, Weinheim, Germany, 2008, pp. 1547–1568.

2 L. (Libor) Červený, *Catalytic hydrogenation*, Elsevier, 1986.

3 R. Noyori, T. Ohkuma, M. Kitamura, H. Takaya, N. Sayo, H. Kumobayashi and S. Akutagawa, *J. Am. Chem. Soc.*, 1987, **109**, 5856–5858.

4 T. Ohkuma, H. Ooka, S. Hashiguchi, T. Ikariya and R. Noyori, *J. Am. Chem. Soc.*, 1995, **117**, 2675–2676.

5 R. Meerwein, H.; Schmidt, *Ann. Chem.*, 1925, **444**, 221.

6 W. Ponndorf, *Angew. Chem.*, 1926, **39**, 138.

7 A. Verley, *Bull. Soc. Chim. Fr.*, 1925, **37**, 537.

8 D. Müller, G. Umbricht, B. Weber and A. Pfaltz, *Helv. Chim. Acta*, 1991, **74**, 232–240.

9 J.-P. Genêt, V. Ratovelomanana-Vidal and C. Pinel, *Synlett*, 1993, **7**, 478–480.

10 P. Gamez, F. Fache and M. Lemaire, *Tetrahedron: Asymmetry*, 1995, **6**, 705–718.

11 D. A. Evans, S. G. Nelson, M. R. Gagne and A. R. Muci, *J. Am. Chem. Soc.*, 1993, **115**, 9800–9801.

12 R. Noyori and S. Hashiguchi, *Acc. Chem. Res.*, 1997, **30**, 97–102.

13 M. Poyatos, J. A. Mata, E. Falomir, R. H. Crabtree and E. Peris, *Organometallics*, 2003, **22**, 1110–1114.

14 M. Poyatos, A. Maisse-François, S. Bellemin-Laponnaz, E. Peris and L. H. Gade, *J. Organomet. Chem.*, 2006, **691**, 2713–2720.

15 S. Yaşar, S. Çekirdek and İ. Özdemir, *J. Coord. Chem.*, 2014, **67**, 1236–1248.

16 T. Wdowik, C. Samojłowicz, M. Jawiczuk, M. Malińska, K. Woźniak, K. Grela, W. Danikiewicz, K. Woźniak, A. Pazio, A. Szadkowska, A. Kozłowska and K. Grela, *Chem. Commun.*, 2013, **49**, 674–676.

17 J. Witt, A. Pöthig, F. E. Kühn and W. Baratta, *Organometallics*, 2013, **32**, 4042–4045.

18 G. K. Zieliński, C. Samojłowicz, T. Wdowik, K. Grela, K. Kirchner, T.-L. Choi, S. Ding, M. W. Day and R. H. Grubbs, *Org. Biomol. Chem.*, 2015, **13**, 2684–2688.

19 W. B. Cross, C. G. Daly, Y. Boutadla, K. Singh, M. Albrecht, G. W. Brudvig and R. H. Crabtree, *Dalt. Trans.*, 2011, **40**, 9722.

20 M. Aydemir, A. Baysal, N. Meric, C. Kayan, B. Gümgüm, S. Özkar and E. Şahin, *J. Organomet. Chem.*, 2011, **696**, 2584–2588.

21 P. Satyanarayana, G. M. Reddy, H. Maheswaran and M. L. Kantam, *Adv. Synth. Catal.*, 2013, **355**, 1859–1867.

22 A. Nova, D. J. Taylor, A. J. Blacker, S. B. Duckett, R. N. Perutz and O. Eisenstein, *Organometallics*, 2014, **33**, 3433–3442.

23 A. McSkimming, B. Chan, M. M. Bhadbhade, G. E. Ball and S. B. Colbran, *Chem. - A Eur. J.*, 2015, **21**, 2821–2834.

24 M. Albrecht, R. H. Crabtree, J. Mata, E. Peris, M. B. Hursthouse, R. S. Hay-Motherwell and W. B. Motherwell, *Chem. Commun.*, 2002, **20**, 32–33.

25 A. Bartoszewicz, N. Ahlsten and B. Martín-Matute, *Chem. - A Eur. J.*, 2013, **19**, 7274–7302.

26 R. Malacea, R. Poli and E. Manoury, *Coord. Chem. Rev.*, 2010, **254**, 729–752.

27 M. V. Jiménez, J. Fernández-Tornos, J. J. Pérez-Torrente, F. J. Modrego, P. García-Orduña and L. A. Oro, *Organometallics*, 2015, **34**, 926–940.

28 D. Gülcemal, A. G. Gökçe, S. Gülcemal, B. Çetinkaya, R. Poli, S. Garcia-Granda, A. Menendez-Velazquez, M. I. Burguete, S. V. Luis and V. Gotor, *RSC Adv.*, 2014, **4**, 26222.

29 A. Pontes da Costa, M. Viciano, M. Sanaú, S. Merino, J. Tejeda, E. Peris and B. Royo, *Organometallics*, 2008, **27**, 1305–1309.

30 A. C. Hillier, H. M. Lee, A. E. D. Stevens and S. P. Nolan, *Organometallics*, 2001, **20**, 4246–4252.

31 A. A. Mikhailine and R. H. Morris, *Inorg. Chem.*, 2010, **49**, 11039–11044.

32 W. Zuo and R. H. Morris, *Nat. Protoc.*, 2015, **10**, 241–257.

33 R. V. Jagadeesh, D. Banerjee, P. B. Arockiam, H. Junge, K. Junge, M.-M. Pohl, J. Radnik, A. Brückner, M. Beller, M. Beller, A. Brückner and M. Beller, *Green Chem.*, 2015, **17**, 898–902.

34 H. Xu, P. Yang, P. Chuanprasit, H. Hirao and J. S. Zhou, *Angew. Chemie Int. Ed.*, 2015, **54**, 5112–5116.

35 D. Morton and D. J. Cole-Hamilton, *J. Chem. Soc. Chem. Commun.*, 1988, 1154.

36 A. El-Hellani and V. Lavallo, *Angew. Chemie Int. Ed.*, 2014, **53**, 4489–93.

37 M. J. Asay, S. P. Fisher, S. E. Lee, F. S. Tham, D. Borchardt, V. Lavallo, J. A. K. Howard, A. Mackinnon, R. J. Peace and K. Wade, *Chem. Commun.*, 2015, **51**, 5359–5362.

38 S. P. Fisher, A. El-Hellani, F. S. Tham, V. Lavallo, S. Mallet-Ladeira, G. Bouhadir, J. C. Slootweg, W. Uhl and D. Bourissou, *Dalt. Trans.*, 2016, **45**, 9762–9765.

39 R. Corberán, M. Sanaú and E. Peris, *Organometallics*, 2006, **25**, 4002–4008.

40 J. Holmes, C. M. Pask, M. A. Fox and C. E. Willans, *Chem. Commun.*, 2016, **52**, 6443–6446.

41 J. Estrada, S. E. Lee, S. G. McArthur, A. El-Hellani, F. S. Tham and V. Lavallo, *J. Organomet. Chem.*, 2015, **798**, 214–217.

42 N. Fey, M. F. Haddow, R. Mistry, N. C. Norman, A. G. Orpen, T. J. Reynolds and P. G. Pringle, *Organometallics*, 2012, **31**, 2907–2913.

43 F. Hanasaka, Y. Tanabe, and K.-ichi Fujita and R. Yamaguchi, *Organometallics*, 2006, **25**, 826–831.

44 F. Hanasaka, and K.-ichi Fujita and R. Yamaguchi, *Organometallics*, 2006, **25**, 4643–4647.

45 D. Iglesias, S. Sabater, A. Azua and J. A. Mata, *New J. Chem.*, 2015, **39**, 6437–6444.

46 X.-H. Zhu, L.-H. Cai, C.-X. Wang, Y.-N. Wang, X.-Q. Guo and X.-F. Hou, *J. Mol. Catal. A Chem.*, 2014, **393**, 134–141.

47 A. Bartoszewicz, R. Marcos, S. Sahoo, A. K. Inge, X. Zou and B. Martín-Matute, *Chem. - A Eur. J.*, 2012, **18**, 14510–14519.

48 N. M. Scott, R. Dorta, E. D. Stevens, A. Correa, A. Luigi Cavallo and Steven P. Nolan, *J. Am. Chem. Soc.*, 2005, **127**, 3516–3526.

49 A. McAnaw, G. Scott, L. Elrick, G. M. Rosair and A. J. Welch, *Dalton Trans.*, 2013, **42**, 645–64.

50 Z.-J. Yao, W.-B. Yu, Y.-J. Lin, S.-L. Huang, Z.-H. Li and G.-X. Jin, *J. Am. Chem. Soc.*, 2014, **136**, 2825–2832.

51 T. Kim, J. Lee, S. U. Lee and M. H. Lee, *Organometallics*, 2015, **34**, 3455–3458.

52 K. Ogata, T. Nagaya and S. Fukuzawa, *J. Organomet. Chem.*, 2010, **695**, 1675–1681.

53 A. Labande, J.-C. Daran, N. J. Long, A. J. P. White, R. Poli, A. Guagliardi, A. G. G. Moliterni, G. Polidori and R. Spagna, *New J. Chem.*, 2011, **35**, 2162.

54 J. Wolf, A. Labande, J.-C. Daran and R. Poli, *Eur. J. Inorg. Chem.*, 2007, **2007**, 5069–5079.

55 C. Gandolfi, M. Heckenroth, A. Neels, G. Laurenczy and M. Albrecht, *Organometallics*, 2009, **28**, 5112–5121.

56 W. Ghattas, H. Müller-Bunz and M. Albrecht, *Organometallics*, 2010, **29**, 6782–6789.

57 R. A. Al-Horani and U. R. Desai, *Tetrahedron*, 2012, **68**, 2027–2040.

58 F. L. Thorp-Greenwood, A. N. Kulak and M. J. Hardie, *Nat. Chem.*, 2015, **7**, 526–531.

59 R. Cariou, C. Fischmeister, A. Loïc Toupet and P. H. Dixneuf, *Organometallics*, 2006, **25**, 2126–2128.

60 H. M. Peng, R. D. Webster and X. Li, *Organometallics*, 2008, **27**, 4484–4493.

61 X. Wang and G.-X. Jin, *Chem. - A Eur. J.*, 2005, **11**, 5758–5764.

62 R. Corberán, M. Sanaú and E. Peris, *J. Am. Chem. Soc.*, 2006, **128**, 3974–3979.

63 M. Viciano, M. Feliz, R. Corberán, J. A. Mata, A. Eric Clot and E. Peris, *Organometallics*, 2007, **26**, 5304–5314.

64 R. Maity, H. Koppetz, A. Hepp and F. E. Hahn, *J. Am. Chem. Soc.*, 2013, **135**, 4966–4969.

65 N. Hellou, C. Jahier-Diallo, O. Baslé, M. Srebro-Hooper, L. Toupet, T. Roisnel, E. Caytan, C. Roussel, N. Vanthuyne, J. Autschbach, M. Mauduit, J. Crassous, M. Vallet and J. Crassous, *Chem. Commun.*, 2016, **52**, 9243–9246.

66 A. McAnaw, G. Scott, L. Elrick, G. M. Rosair and A. J. Welch, *Dalt. Trans.*, 2013, **42**, 645–664.

67 D. Wang and D. Astruc, *Chem. Rev.*, 2015, **115**, 6621–6686.

68 J. Holmes, C. M. Pask and C. E. Willans, *Dalt. Trans.*, 2016, **45**, 15818–15827.

69 C. White, A. Yates, P. M. Maitlis and D. M. Heinekey, in *Inorganic Syntheses*, John Wiley & Sons, Inc., 1992, pp. 228–234.

70 M. A. Bennett and A. K. Smith, *J. Chem. Soc. Dalt. Trans.*, 1974, 233.

71 S. V. Dzyuba and R. A. Bartsch, *J. Heterocycl. Chem.*, 2001, **38**, 265–268.

72 E. E. Alberto, A. L. Braga and M. R. Detty, *Tetrahedron*, 2012, **68**, 10476–10481.

Chapter 6

Synthesis, structure and biomedical evaluation of silver complexes bearing NHC-carborane ligands

This chapter discusses the diverse coordination modes of NHC-carborane ligands at Ag^I. The steric nature of the ligand precursor plays a crucial role in the overall stability and the type of silver complex formed, with the first structurally elucidated example of Ag^I directly bound through the carborane reported. In addition, a series of carboranyl complexes derived from the natural product theobromine were synthesised. The antiproliferative properties of these complexes against the HCT116 (colon) cancer cell line were evaluated.

6.1 Introduction

6.1.1 History of silver

Silver has been used extensively throughout history as a potent antimicrobial agent, specifically in the form of silver nitrate, with reports of its utility as early as the 17th century for the treatment of chronic ulcers and open wounds.[1] By the 19th century it had become common practice for dilute solutions of silver nitrate to be dropped into the eyes of new-born babies to prevent transmission of bacterial infections during birth.[2] The discovery of penicillin in the late 20th century, often termed the 'miracle drug', marked the decline of silver antimicrobials. However, with the discovery of antibiotics came the emergence of antibiotic resistant bacteria resulting in a resurgence in silver, with silver sulfadiazine becoming one of the most widely used topical burn treatments (**Figure 6.1**).[3] It's effectiveness as an antimicrobial agent is owed to its steady release of Ag^+ ions over a prolonged period of time, providing maximum protection against infection as the wound heals.[4] Other silver salts such as silver nitrate, which deposit large amounts of silver in one instance, would require frequent reapplication deeming them much less effective and impractical. More recently, Collins *et al.* reported that antibiotics when dosed with ionic silver can kill between 10 and 1,000 times more bacteria, and also shed some light on the mode of action of silver as an antimicrobial, as the precise mechanism is still under debate.[5] They report that ionic silver attacks bacterial cells in two main ways: i) by increasing the permeability of the cell membrane, allowing large-molecule antibiotics to bypass the protective coating of gram-negative bacteria, and ii) by disruption of the cell's metabolism leading to high levels of toxic oxygenated compounds being produced.

However, before silver can be added to our antibiotics, a major complication to overcome is that a high concentration of silver in the body can lead to the skin turning blue-grey in colour, a condition known as argyria, with the effects being irreversible.[6]

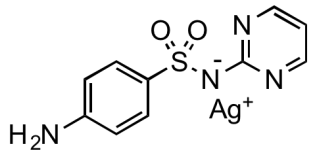

Figure 6.1. Structure of silver sulfadiazine.

6.1.2 Ag^{I}-NHCs as antimicrobials

As previously mentioned, silver sulfadiazine is a highly effective antimicrobial agent due to its steady release of Ag^{+} ions over a prolonged period of time.[4] A slow release rate of silver is affiliated with its ancillary ligands, the more stable the complex, the slower the silver is released. Currently, Ag^{I}-NHC complexes are the most widely studied type of metal-NHC in antimicrobials. Professor Wiley J. Youngs is well established in this area of chemistry, with his earliest work reporting water soluble pyridine-linked pincer Ag^{I}-NHC complexes, which were found to be much more active than silver nitrate against *E. coli*, *S. aureus* and *P. aeruginosa* (**Figure 6.2**, **1**).[7] This was attributed to the slower release of Ag^{+} ions from Ag^{I}-NHCs into the culture medium. Encapsulation of a Ag^{I}-NHC complex (**Figure 6.2**, **2**) further enhances the antimicrobial activity, demonstrating faster kill rate and increased bioavailability of Ag^{+} ions when compared to silver sulfadiazine and silver nitrate.[8] This was attributed to the polymer providing a very slow release of Ag^{+} ions, which are trapped within the polymer matrix as the silver complex decomposes. Unfortunately, the imidazolium salt formed upon decomposition of the Ag^{I}-NHC complex was found to be toxic and highlighted the importance of utilising non-toxic ancillary ligands, which was the natural progression of Youngs' research, with the synthesis of NHC complexes derived from caffeine (**Figure 6.2**, **3**).[9,10]

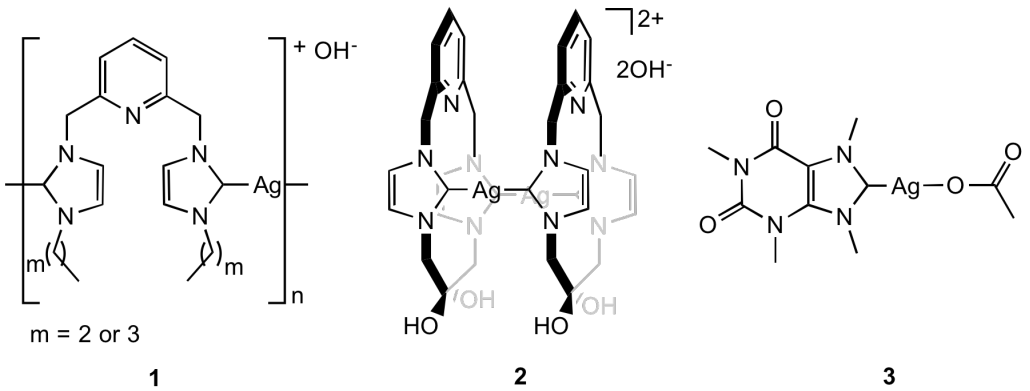

Figure 6.2 Complexes reported by Youngs *et al*.[7–10]

6.1.3 Ag^{I}-NHCs in the treatment of cancer

Cancer is one of the leading causes of death in the Western world, and it is expected that one in two people will develop cancer according to the most accurate prognosis from Cancer Research UK.[11] If we are to triumph in our interminable battle with cancer we must continue to develop more effective treatments. The development of cisplatin was a milestone in oncology and is still used in modern medicine for the treatment of cancer. However, cisplatin can have severe side effects, as well as tumours capable of building resistance to the platinum-based drug. This has driven research into finding replacement metallodrugs with complexes of titanium, iron and ruthenium going through clinical trials.[12–14] Silver is renowned for its antimicrobial properties but had been over looked with regards to its cytotoxic properties. One of the first silver compounds reported to exhibit cytotoxic properties was a silver fluorobenzoate dimer.[15] Five years later the first Ag^{I}-NHC complexes (**4-6**) were reported by Youngs (**Figure 6.3**), and were screened against OVCAR-3 (ovarian), MB157 (breast) and HeLa (cervical) cancer cell lines, and for comparison purposes cisplatin was also screened (**Table 6.1**).[16]

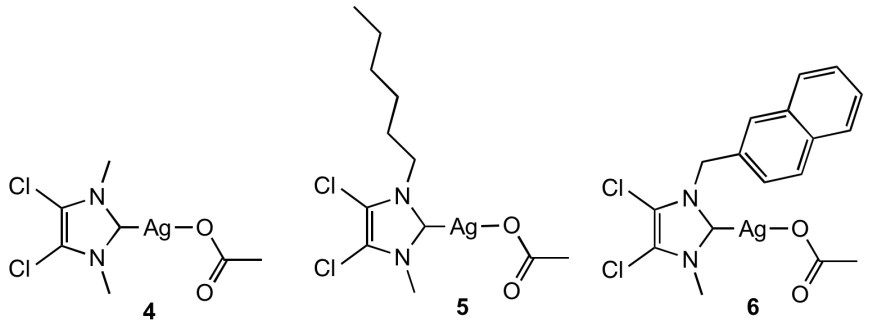

Figure 6.3 $Silver^{I}$-NHC acetate complexes reported by Youngs and co-workers.[16]

Table 6.1 $Silver^{I}$-NHC acetate complexes and their respective IC_{50} values against ovarian, breast and cervical cancer call lines.[16]

	IC_{50} (μM) OVCAR-3	IC_{50} (μM) MB157	IC_{50} (μM) HeLa
Cisplatin	12	25	25
4	35	8	>200
5	30	20	>200
6	20	10	>200

The effectiveness of a compound to induce proliferation of cancer cells can be quantified by a number of different techniques, the most effective method involves measuring the incorporation of methyl-[3H]-thymidine (radioactive derivative of the DNA precursor thymidine) into the DNA of dividing cancer cells.[17] The concentration of methyl-[3H]-thymidine is measured allowing an IC_{50} value to be derived. IC_{50} is defined as the concentration of the complex required to achieve incorporation of methyl-[3H]-thymidine into half of the cancer cells in the assay, a parameter indicative of cell death.

Complexes **4**-**6** exhibited highest cytotoxicity towards the MB157 cell line and had little effect on the HeLa cell line, highlighting the selectivity towards specific cancers for this type of complexes (**Table 6.1**). The effectiveness of complexes **4**-**6** as potential anticancer drugs was further highlighted when substantial tumour death was observed in *in vivo* studies in mice, with high selectivity towards the cancerous cells. More recently, Willans *et al.* reported a family of xanthine-derived imidazolium salts, prepared from caffeine, theophylline and theobromine.[18] $Silver^{I}$-NHC complexes were prepared and evaluated against eight cancer cell lines and hydrophobicity values sought as a means to assess the ability of each complex to cross the cell membrane (**Figure 6.4**). Although cisplatin was most active, the study highlighted that introducing a hydrophilic substituent (R = $(CH)_2OH$) increased the antiproliferative properties. It was proposed this increase in potency was due to the ability of the complex to cross the cell membrane more easily, which was determined from the hydrophobicity studies. From the remaining alkyl substituted complexes (R = Me, ^{n}Bu and Ph); the complex bearing the most sterically bulky subsistent (R = Ph) was found to the most cytotoxic. It was proposed that the sterically bulky *N*-substituents on the ligand may result in a slower release rate of silver, resulting in an increase in cytotoxicity. From these conclusions it was proposed that a Ag complex that possesses hydrophilic qualities, as well as steric bulk would lead to a more cytotoxic complex.

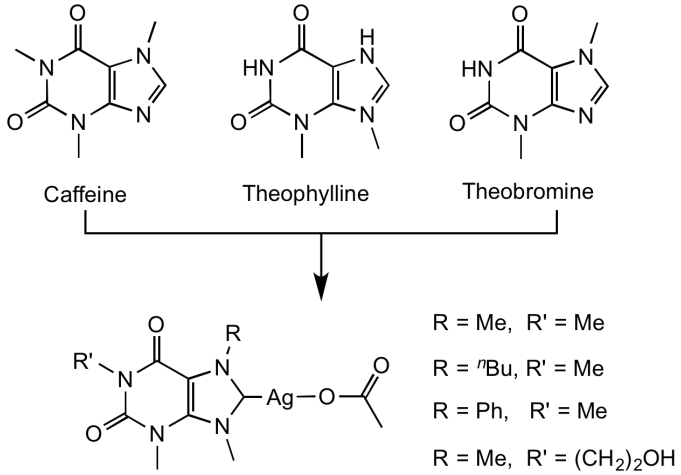

Figure 6.4 Silver(I)-NHC complexes derived from the natural xanthine products caffeine, theophylline and theobromine.[18]

This led on to further research, and in unpublished work the Willans group report a series of Ag^{I}-NHC complexes possessing a *N*-hydroxyethyl substituent whilst varying the steric bulk of the other *N*-substituent (**7**-**11**) (**Graph 6.1**). These complexes were tested against the pancreatic caner cell line (Panc 10.05), and the IC_{50} values supported their proposed theory from the previous study; that fine tuning of the hydrophilic properties of the complex to allow easier passage across the cell membrane, coupled with using sterically bulk substituents to allow for a potentially slower release of Ag from the complex, leads to an increase in cytotoxicity.

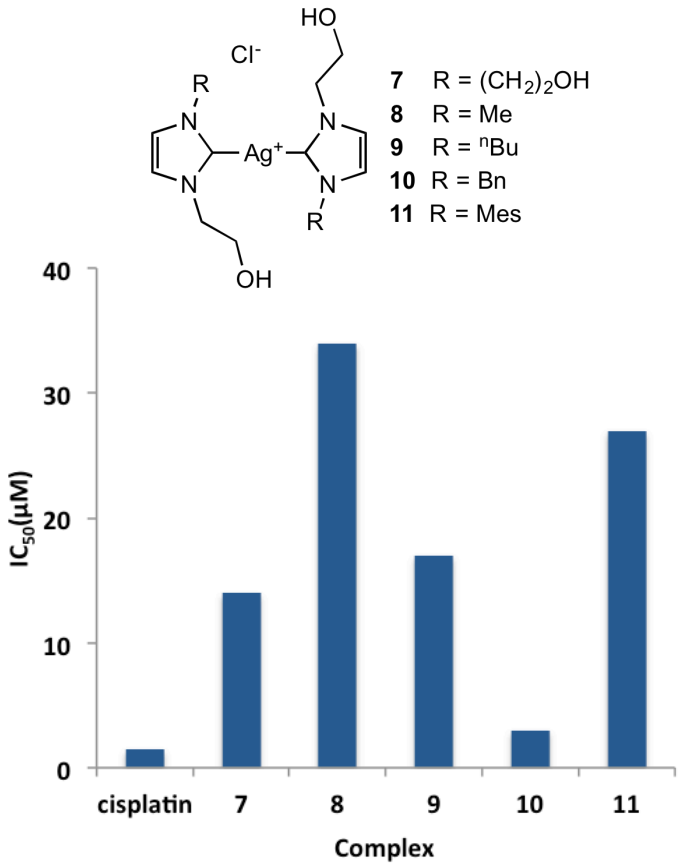

Graph 6.1 Silver(I)-NHC complexes and their respective IC_{50} values against the Panc 10.05 cancer cell line.

With the successful preparation of a Ag^{I}-NHC complex (**10**) with cytotoxicity comparable to that of cisplatin, the focus turned towards the development of a drug delivery system. Encapsulation of the Ag^{I}-NHC complexes into micelles formed from a polyethylene glycol based polymer ($mPEG_{5000}P(Phe)$). Interestingly, the anticancer activity of the micelles displayed higher potency than the non-encapsulated Ag^{I}-NHC complex against the Panc 10.05 cancer cell line. It was proposed that either the polymer may exhibit cytotoxic properties, or that the micelles stabilise the complex resulting in a slow release of Ag^{+} ions. Future work aims towards testing the micelles *in vivo* to evaluate their efficiency at delivering the complex to the tumour cells.

6.2 Aims

In Chapters 4 and 5 Rh^{I} and Ir^{III} complexes bearing **L1** were prepared *via in situ* transmetallation using Ag_2O, with examples shown in **Scheme 6.1**. In this section of work the focus was isolation of the Ag^{I}-NHC complex, which was previously prepared *in situ* in previous reactions, by employing the same reaction conditions with the exception of adding the metal precursor (**Scheme 6.1**). In addition, a series of carboranyl complexes derived from the natural product theobromine were synthesised and, similarly to the catalytic study in Chapter 5, phenyl congeners of each of the carboranyl complexes were also prepared for useful comparison when evaluating their antiproliferative properties.

6.3 Synthesis of a silver σ-bound carboranyl $Ag_2(NHC)_2$ complex

Reaction of **L2.1** with Ag_2O (0.55 eq) under anhydrous conditions in CD_2Cl_2 was monitored by ^{1}H NMR spectroscopy (**Scheme 6.1**). A visible indication that a reaction is occurring is the consumption of the sparingly soluble Ag_2O and the precipitation of a grey solid, presumably AgBr, which is easily removed by filtering the solution through Celite. Full conversion of **L2.1** was not achieved until the amount of Ag_2O added to the reaction was increased to 1 equivalent. Analysis of the ^{1}H NMR spectrum after 9 hours revealed complete disappearance of the resonance for the imidazolium proton (H7), which is strongly characteristic of the formation of a metal-NHC bond (**Figure 6.5**). The characteristic carboranyl proton (H1) is a broad singlet hidden under the CH_2 resonance at 4.31 ppm. The 2D $^{1}H^{13}C$ HMQC experiment confirms this, with strong coupling observed between this resonance and the carboranyl cage carbon at 63.3 ppm (**Figure 6.5**).

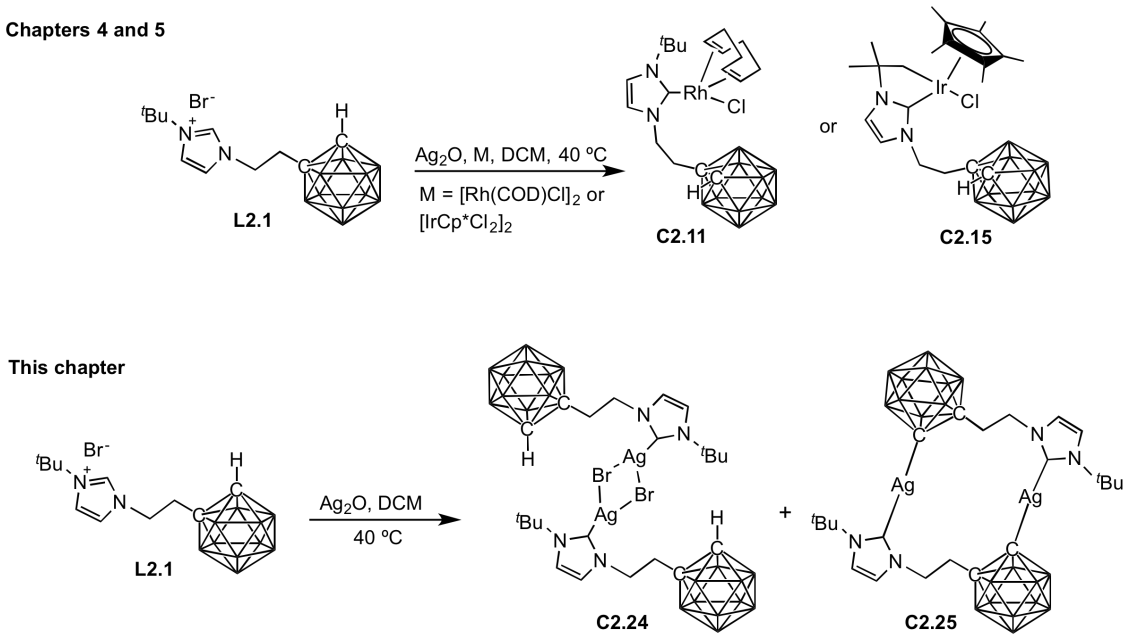

Scheme 6.1 Example reactions in which silver was used as a transmetallating agent from Chapters 4 and 5, and the Synthesis of Ag^{I}-NHC complexes **C2.24** and **C2.25**.

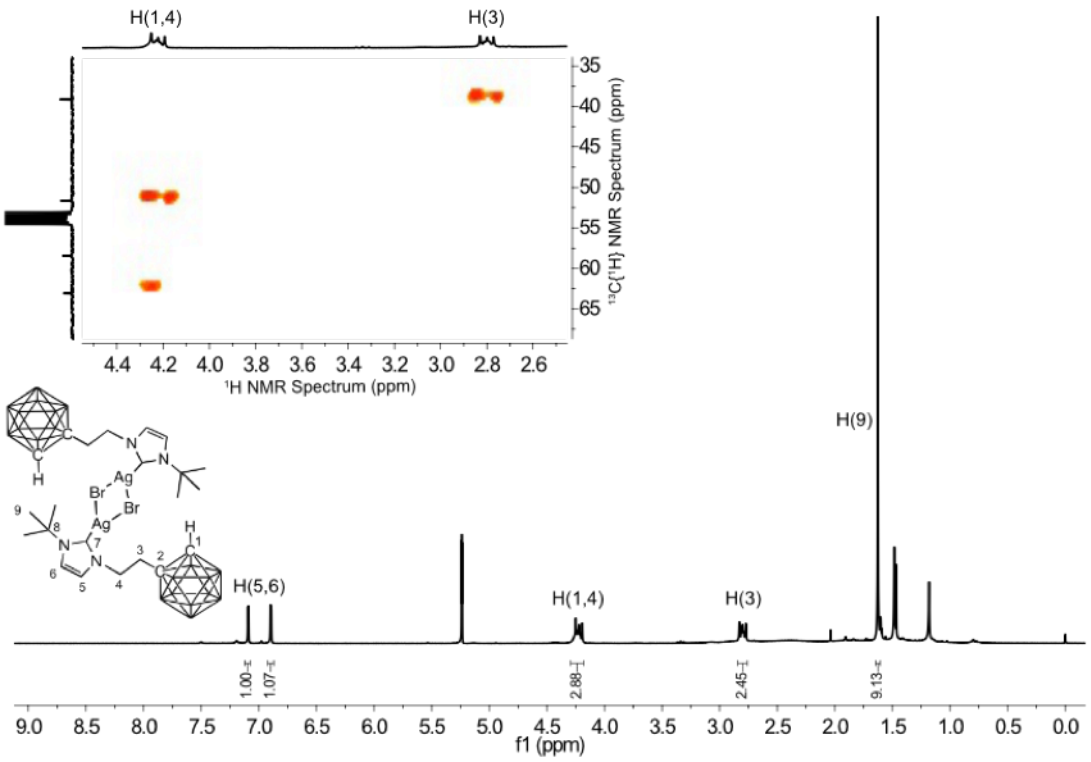

Figure 6.5 ^{1}H NMR and ^{1}H^{13}C HMQC spectra (300 MHz, CD_2Cl_2) of **C2.24**. Inset highlights the coupling between the masked H(1) resonance and the carboranyl carbon C(1).

C2.24 appears unstable, and within a few hours of forming the complex signs of decomposition are observed in anhydrous solvent, with the characteristic imidazolium H(7) proton reappearing in the ^{1}H NMR spectrum and formation of a black precipitate, presumably Ag^0. However, single crystals of **C2.24** suitable for XRD analysis can be grown within 12 hours by slow diffusion of diethyl ether into the NMR sample. The asymmetric unit of **C2.24** consists of a molecule of AgBr(NHC), which possess a centre of inversion to give the dimeric structure shown in **Figure 6.6**.

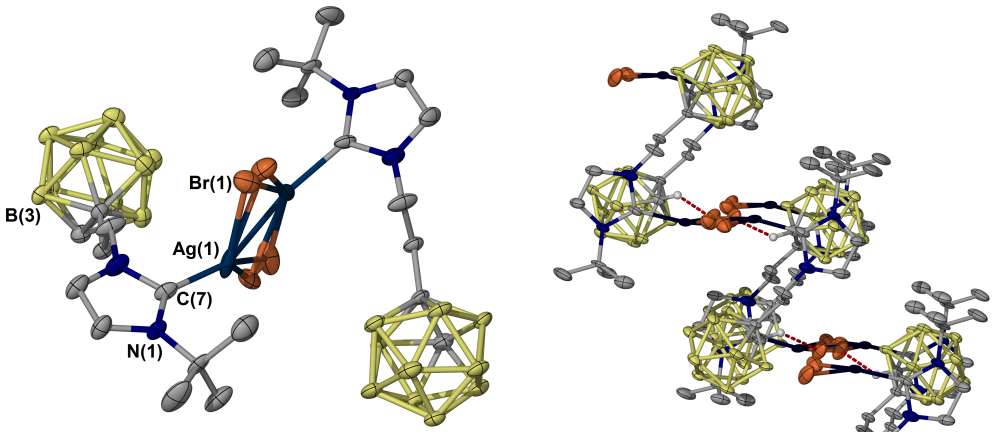

Figure 6.6 Molecular structure of **C2.24** (left) and packed structure (right) highlighting the inter-molecular hydrogen bonding between the carboranyl proton and the bromides (red dotted lines). *Thermal ellipsoids shown at 50 % probability and hydrogen atoms are omitted for clarity. Bromides are disordered over two positions with 50 % occupancy.*

The geometry about the silver centre is distorted trigonal planar, and in relation to the two NHCs can be considered bent with an Ag(2)-Ag(1)-C(7) bond angle of 157.4°, which is typical of similar $Ag_2(NHC)_2$ halide complexes in the literature.[19] With the bromides disordered over two positions, with 50 % occupancy, a centroid between each was generated to give an average distance for each of the Ag-Br bonds. The Ag-Br(1) bond at 2.628 (Å) is considerably longer than the Ag-Br(2) bond length of 2.282 (Å). Within the extended structure of **C2.24**, hydrogen bonding between H(1) and the bridging bromide atoms is observed (**Figure 6.6**).

Obtaining reproducible results from this reaction was problematic due to the instability of the complex. Crystals of a second complex were also found in the product mixture, and were characterised as an unusual macrocycle **C2.25**, in which the silver is bound to the NHC of one molecule of ligand and the carboranyl carbon of another, with the geometry about the silver being almost linear with bond angles of 176.3° for C(7)-Ag(2)-C(12) and 177.1° for C(1)-Ag(2)-C(18) (**Figure 6.7**). The formation of **C2.25** is intriguing as the ^{1}H and $^{13}C\{^{1}H\}$ NMR spectra of **C2.24** clearly indicate the carboranyl cage proton (H1) is present. This suggests that **C2.25** could be a decomposition product of **C2.24**. It is noteworthy that the crystallisation mother liquor does change colour from colourless to dark orange, which may indicate the formation of HBr and/or Br_2 upon formation of the **C2.25.** The crystals were picked by hand, and in an attempt to obtain spectroscopic data were redissolved in CD_2Cl_2, but unfortunately the complex was too unstable in solution. Although **C2.25** is unstable, this is the first structurally elucidated example of silver directly bound to *o*-carborane. The selected bond distances for **C2.24** and **C2.25** are provided in **Table 6.2**, and the Ag-$C_{carbene}$ bond lengths are in the expected range for similar complexes in the literature.[20,21]

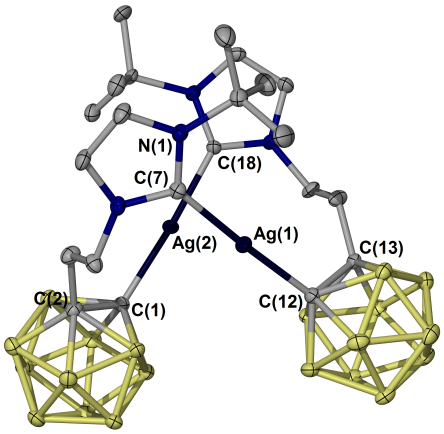

Figure 6.7 Molecular structure of **C2.25**. *Thermal ellipsoids shown at 50 % probability and hydrogen atoms are omitted for clarity.*

Table 6.2 Selected bond distances (Å) for **C2.24** and **C2.25**.

C2.24		**C2.25**	
Bond	Distance (Å)	Bond	Distance (Å)
Ag(1)-C(7)	2.034(4)	Ag(1)-C(7)	2.096(3)
Ag(1)-Br(1)$_{centroid}$	2.628	Ag(2)-C(18)	2.115(3)
Ag(1)-Br(2)$_{centroid}$	2.282	Ag(1)-C(12)	2.120(3)
		Ag(2)-C(1)	2.131(3)

6.4 Towards the synthesis of stable silver NHC carborane complexes

Complexes of type $Ag_2Br_2(NHC)_2$ such as **C2.24** are uncommon, and it can be rationalised that the sterically bulky ^{t}Bu group of **C2.24** prevents the formation of the more traditional $Ag(NHC)_2Br$ type complex (Section 6.2.1). It is important to retain some steric protection of the metal centre, as research within the Willans group has demonstrated that these out perform ligand systems containing little steric protection in anticancer studies.[22] With this in mind, a ligand precursor containing a mesityl substituent (**L2.4**) was prepared (**Scheme 6.2**). Its phenyl congener **L8.1** was also prepared for useful comparison when evaluating the complexes as potential anticancer agents.

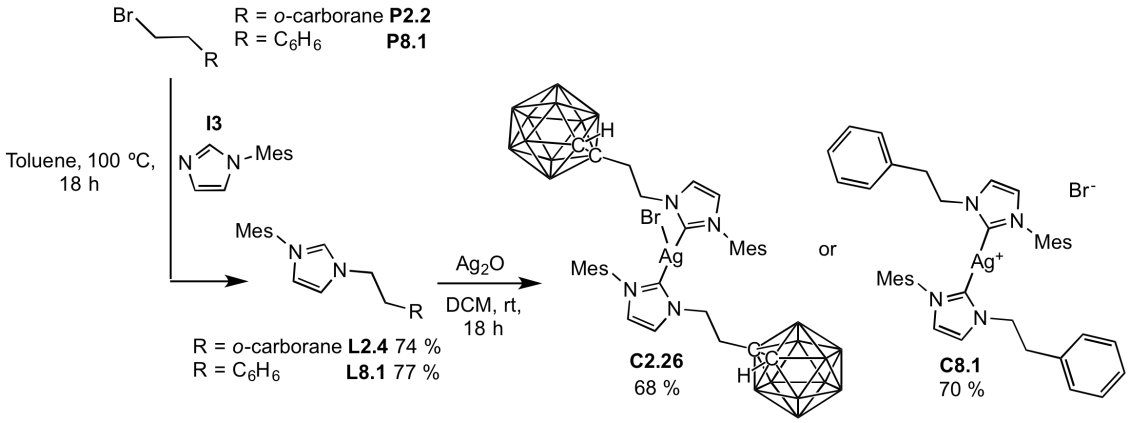

Scheme 6.2 Synthesis of $Ag(NHC)_2Br$ complexes **C2.26** and **C8.1**.

Adopting the same synthetic procedure used for the synthesis of **C2.24** allowed the corresponding $Ag(NHC)_2Br$ type complexes **C2.26** and **C8.1** to be isolated in good yields. These were fully characterised by multinuclear NMR spectroscopy, HRMS, and elemental analysis. Single crystals of each were grown from either the slow evaporation of a concentrated MeCN solution (**C2.26**), or the slow diffusion of Et_2O into a concentrated DCM solution (**C8.1**), with the molecular structures shown in **Figure 6.8** and selected bond distances given in **Table 6.3**. The molecular structures unveiled that for carboranyl complex **C2.26**, the bromide is bound to the silver centre, which exhibits a distorted T-shaped geometry to accommodate for the sterically bulky ligands. The Ag-Br bond length is rather long but is typical for these type of complexes.[19] In comparison, phenyl complex **C8.1** forms the more traditional cationic complex with essentially a planar arrangement of the ancillary ligands.

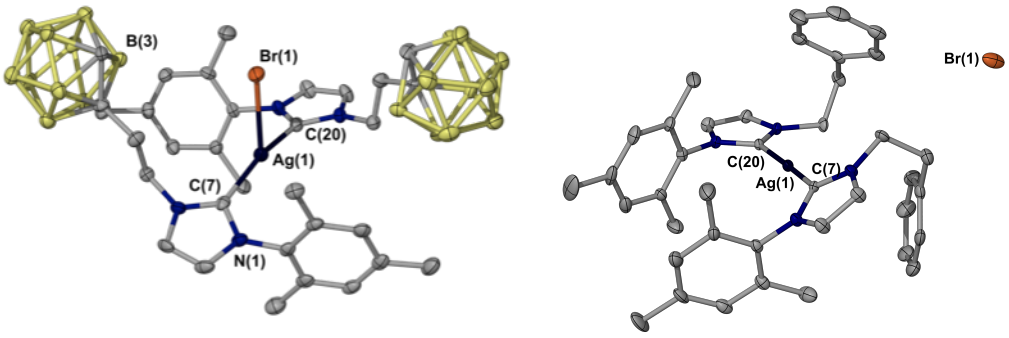

Figure 6.8 Molecular structure of **C2.26** (left) and **C8.1** (right). *Thermal ellipsoids shown at 40 % probability and hydrogen atoms are omitted for clarity.*

Table 6.3 Selected bond distances (Å) for **C2.26** and **C8.1**.

Bond	**C2.26**	**C8.1**	Angle	**C2.26**	**C8.1**
C(7)-Ag(1)	2.100(7)	2.069(4)	C(20)-Ag(1)-C(7)	159.6(8)	176.1(14)
C(20)-Ag(1)	2.106(7)	2.077(4)			
Br(1)-Ag(1)	2.906(9)	-			

Although the solid state structures revealed an abundance of structural information, in solution complexes can behave very differently. $^{13}C\{^{1}H\}$ NMR spectroscopy provides more definitive information of the nature of the silver^{I}-NHC bonding in solution. Silver has two naturally occurring isotopes, ^{107}Ag and ^{109}Ag, with a percentage abundance of 51.8 % and 48.2 % respectively. Both are NMR active with a nuclear spin of ½. Given this information, one would expect the carbenic carbon to have a splitting pattern of two doublets. This can be observed in the $^{13}C\{^{1}H\}$ NMR spectrum of **C8.1** at 182.0 ppm, with coupling constants of 209.3 and 182.0 Hz, which is in the typical range for these types of complexes.[23] It is also common for long-range coupling to be observed to the backbone carbons of the NHC ring for complexes that exhibit carbene coupling to silver, which can be observed in the $^{13}C\{^{1}H\}$ NMR spectrum of **C8.1** at around 122.5 ppm (**Figure 6.9**, **top**). The carbenic resonance for **C2.26**, however is not observed **(Figure 6.9**, **bottom**). The appearance of the carbenic resonance for some silver complexes can be concentration dependent.[24] It is also common for the resonance to appear as a singlet with all coupling information lost. Lin *et al*. proposed these characteristics are indicative of a complex that is fluxional in solution,[25] which may be expected to be the case for **C2.26**; with a rather long Ag-Br bond one would expect dissolution into separate ions in solution.

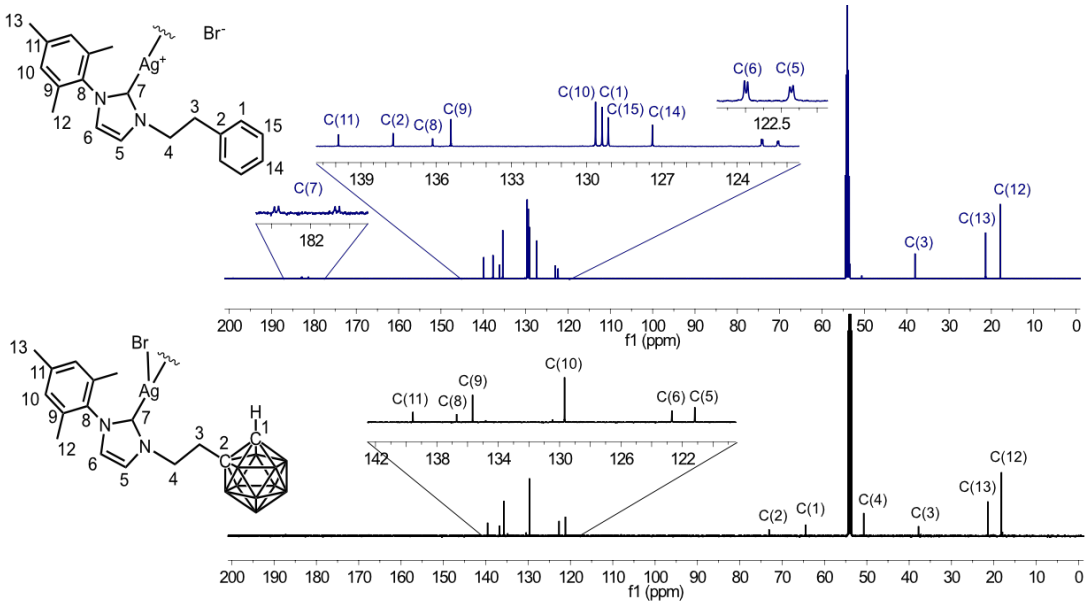

Figure 6.9 $^{13}C\{^{1}H\}$ NMR spectra (126 MHz, CD_2Cl_2) for **C2.26** (bottom) and **C8.1** (top), which were fully assigned through the aid of 2D $^{1}H^{1}H$ COSY, $^{1}H^{13}C$ HMQC, $^{1}H^{13}C$ HMBC and $^{13}C\{^{1}H\}$ DEPT 135 experiments.

6.5 Theobromine derived silver-NHC complexes

6.5.1 Synthesis of imidazolium salts

Theobromine (**1**) is a naturally occurring xanthine derivative and is the main alkaloid found in chocolate. Youngs *et al*. were the first to functionalise theobromine, through reaction with iodoethanol in refluxing DMF with a base (K_2CO_3), allowing isolation of a product substituted only at the backbone (**2**) (**Scheme 6.3**). This is due to the amine being a much stronger nucleophile when deprotonated than the imidazole nitrogen. Although the poor nucleophilicity of the imidazole nitrogen allows for excellent site selectivity, methylation of this nitrogen requires a high excess of MeI (20 eq) to form the imidazolium salt (**3**), and any attempts at introducing alternative groups other than Me have failed, limiting synthetic functionality to the first step of this synthesis.[22]

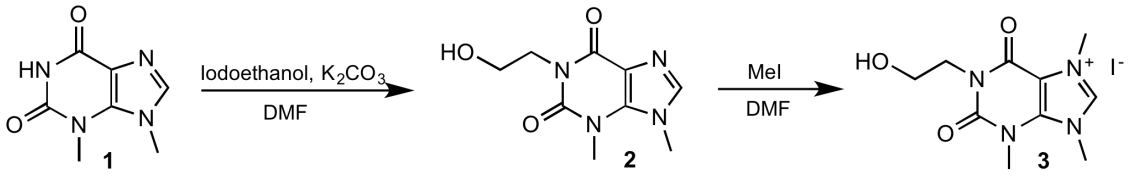

Scheme 6.3 Synthesis of a theobromine-derived imidazolium salt.

Willans *et al.* have reported various derivatives of theophylline, which were subsequently coordinated to Ag^I, and screened against a range of cancer cell lines (Section 6.1.3).[18] Derivatives of theobromine other than that reported by Youngs are yet to be explored. This work looked to compliment the previous study by preparing carboranyl derivatives of theophylline, and to evaluate the antiproliferative properties of the corresponding Ag^I complexes. Initial efforts to incorporate a carboranyl unit employed a similar synthetic strategy reported by Youngs; reaction of theobromine with bromomethyl-*o*-carborane (**P1.1**, Chapter 2, Section 2.1) in the presence of a base (Cs_2CO_3) with heating at 82 °C for 24 hours in MeCN (**Scheme 6.4**, **A**). However, analysis of the crude product indicated that no reaction had taken place. Literature findings report that S_N2 type substitution reactions on **P1.1** are very challenging,[26] and is termed a "dead" synthon due to the strong σ-accepting effect of the cage. However, Litvinov *et al.* reported the first successful nucleophilic substitution reaction at **P1.1** by replacing the inorganic base with Et_3N.[27] It was proposed that utilising Et_3N as a base "frees-up" the negative charge of the nucleophile, making substitution much easier. When the more traditional inorganic bases were used in these reactions no reaction occurs, and it was proposed that the inorganic salts form a strong ionic pair with the deprotonated substrate resulting, in no reaction taking place. This chemistry was therefore explored, and when Cs_2CO_3 was substituted for Et_3N the desired product (**L1.3**) was obtained (**Scheme 6.4**, **B**). However, the reaction is incredibly slow and **L1.3** could not be isolated in a workable yield. In addition, the product is contaminated with the *nido* species (**L1.4**), which is presumably formed by NEt_3 deboronating **L1.3**.

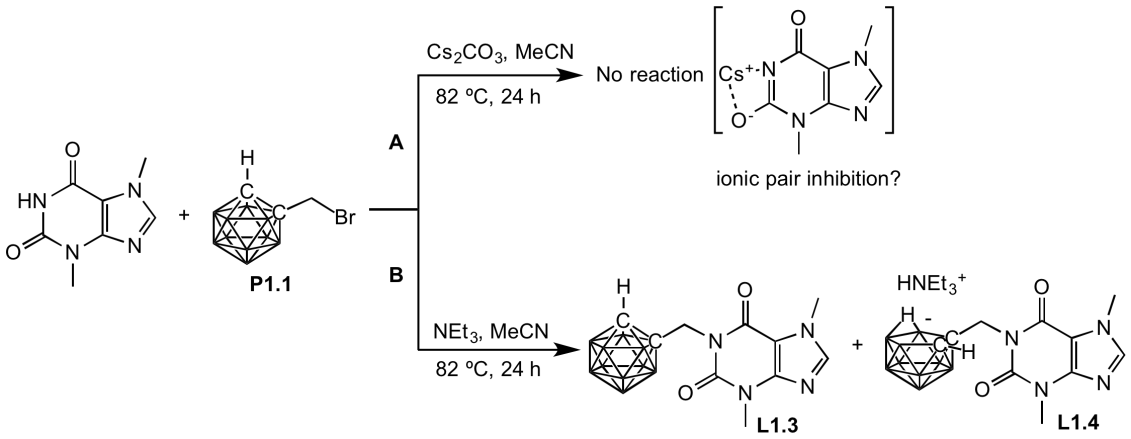

Scheme 6.4 Attempted synthesis of a theobromine-derived carboranyl compound **L1.3**.

Multi nuclear NMR spectroscopy provided evidence for formation of **L1.4**, with a broad singlet at −3.0 ppm in the ^{1}H NMR spectrum being indicative of the bridging proton at the open pentagonal face of the cage. This can also be observed in the ^{11}B{^{1}H} NMR spectrum. Removal of a BH vertex results in an uneven distribution of electron density within the cage resulting in some boron atoms becoming highly shielded and resonating at −35.2 and −37.5 ppm. Details of this phenomenon are explained in Chapter 2, Section 2.2.2.

As an alternative synthetic approach, **P9.1**-**P11.1** were prepared in acceptable to high yields by reaction of theobromine with the corresponding alkynyl halides (**Scheme 6.5**). The significant drop in yield when employing 4-bromo-1-butyne to synthesise **P11.1**, in comparison to when using the shorter alkyne (propargyl bromide) to prepare **P9.1**, can be rationalised by the fact that the S_N2 transition of 4-bromo-1-butyne is not as stable as that of propargyl bromide, which is stabilised by the π-system of the alkynyl unit. Attempts were made to prepare **P11.1** in higher yield by employing longer reaction times, and carrying the reaction out at higher temperatures (120 °C, DMF) but all were unsuccessful.

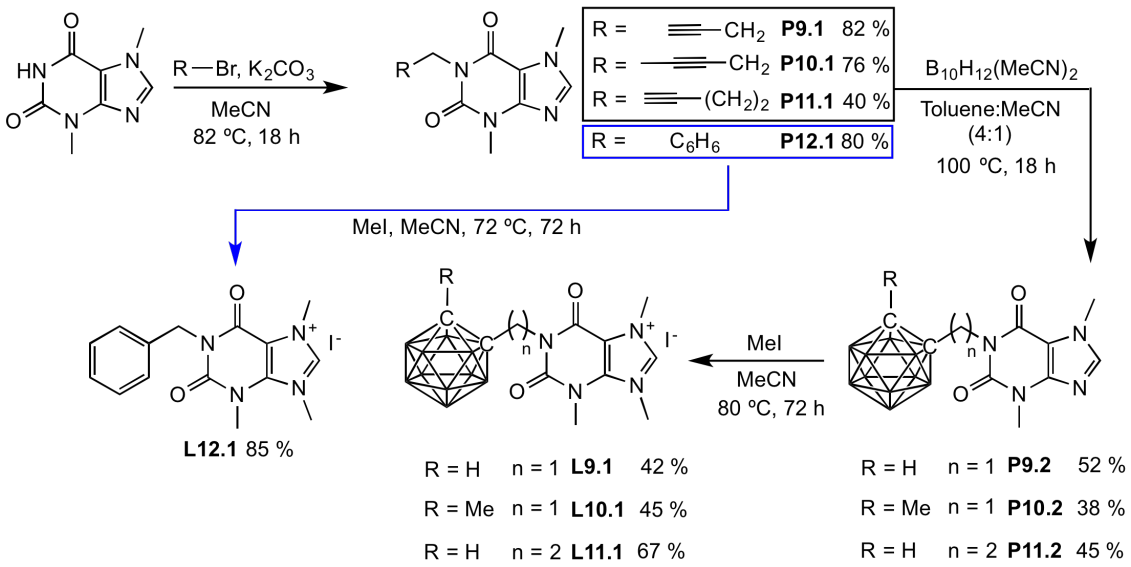

Scheme 6.5 Synthesis of theobromine-derived imidazolium salts.

Reaction of alkynyl compounds with $B_{10}H_{12}(MeCN)_2$ can be an effective route to a variety of carboranyl compounds but is often low yielding (Chapter 1, Section 1.5.1). Hence, the reaction of **P9.1**-**P11.1** with $B_{10}H_{12}(MeCN)_2$ under anhydrous conditions gave carboranyl precursors (**P9.2**-**P11.2**) in only 38-52 % yield.

Finally, each precursor (**P9.2**-**P11.2** and **P12.1**) was subsequently methylated by heating at reflux in MeCN with MeI, which required prolonged reaction times of 3 days to achieve yields between 42-85 % (**Scheme 6.5**). Shorter reaction times are possible when using DMF, which is the solvent employed in the literature, but an increase in yield is not observed. There are only two by products in this reaction; excess MeI, which can be removed *in vacuo*, and any unreacted imidazole, which unlike the product is soluble in Et_2O. This allows any unreacted imidazole to be reclaimed, which is much more difficult if DMF is employed.

Figure 6.10 provides fully assigned ^{1}H NMR spectra of each step of the synthesis of **L9.1**. Evidence for alkylation of theobromine with a 1-bromo-2-butyne substituent is provided by the loss of the amine proton at 11.09 ppm, the presence of a quartet at 4.55 ppm for the methylene linker, and a triplet at 1.73 ppm for the Me group (**Figure 6.10**, **B**). The splitting patterns observed for these resonances are a result of long range ^4J coupling (2.2 Hz) between the alkynyl proton and the methylene linker. Upon formation of the carborane in the next step, the ^{11}B{^{1}H} NMR spectrum exhibits the characteristic resonances of a *closo*-carborane with peaks ranging from -3 to -12 ppm. The ^{1}H NMR spectrum provides further clarity, with a downfield shift of the methyl group that was once an internal alkyne and is now part of a electron withdrawing icosahedral cage (**Figure 6.10**, **C**). Interestingly, the methylene bridge protons become diasterotopic and resonate as two doublets at 4.81 ppm and 4.70 ppm ($^2J_{H\text{-}H}$ = 15.2 Hz). This is observed in each of the carboranyl compounds and can be rationalised through observing **P9.2** in the space-filling model (**Figure 6.11**). The bulky *o*-carborane substituent conformationally locks the methylene bridge due to the steric hindrance of the surrounding carbonyl groups, resulting in protons being magnetically inequivalent. In comparison, alkynyl precursors **P9.1**-**P11.1** can freely rotate about the methylene bridge carbon, hence the protons are magnetically equivalent and appear as one resonance.

The ^{1}H NMR spectrum of **L10.1** provides clear evidence for methylation of the imidazole nitrogen, with a large downfield shift of the NC*H*N (H8) proton at 9.34 ppm (**Figure 6.10**, **D**). All attempts at obtaining crystals suitable for XRD analysis of imidazolium salts (**L9.1**-**L12.1**) were unsuccessful due to the highly hygroscopic nature of these compounds.

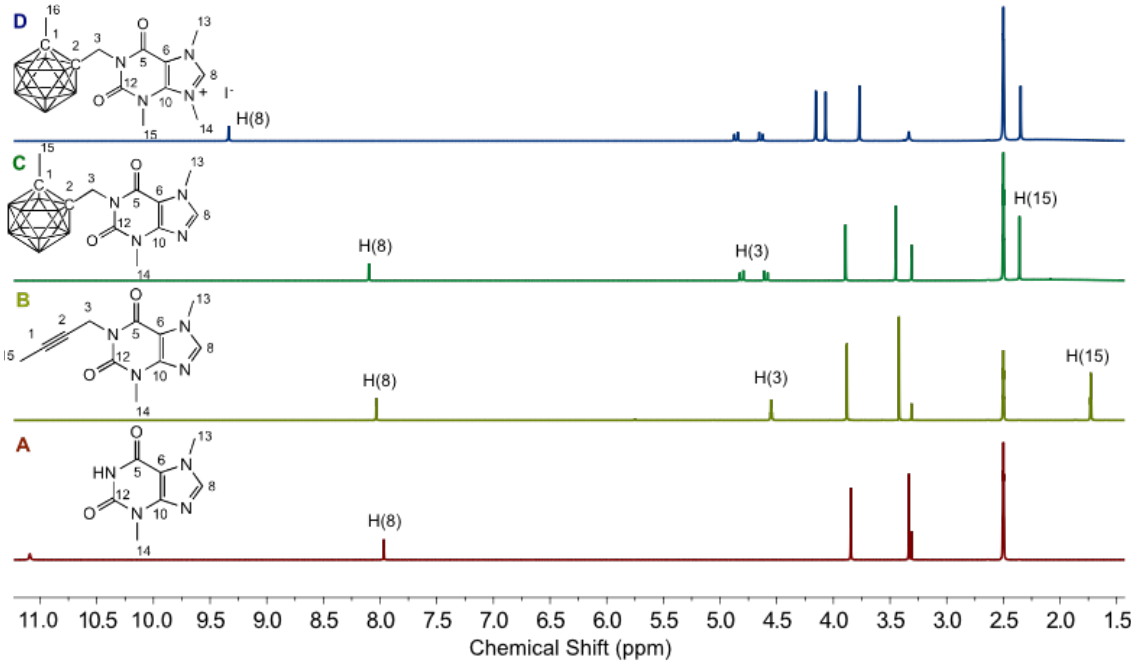

Figure 6.10 ^{1}H NMR spectra (500 MHz, 298 K, DMSO-d_6) for theobromine (**A**), alkylated theobromine compound **P10.1** (**B**), carboranyl substituted theobromine **P10.2** (**C**) and imidazolium salt **L10.1** (**D**).

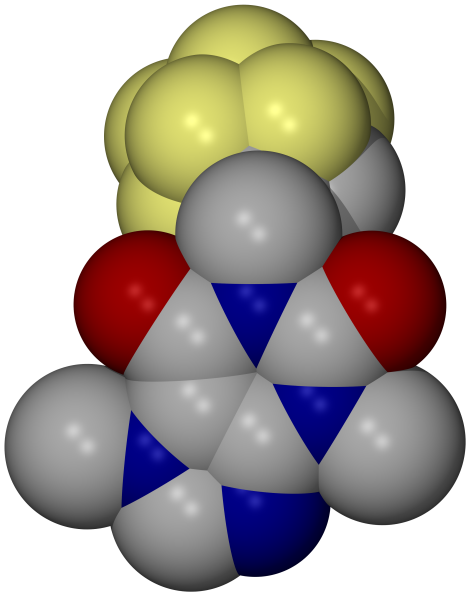

Figure 6.11 Molecular structure in the space-filling model of **P9.2**.

6.5.2 Synthesis of Ag^{I}-OAc complexes

Initial efforts looked towards synthesising complexes using Ag_2O (**Scheme 6.6**, **A**). However, due to the low acidity of the imidazolium NC*H*N proton, no reaction occurred between **L10.1** and Ag_2O. This has previously been found by the Willans group, with more success found employing AgOAc.[18] Hence, reaction of **L10.1** with AgOAc at room temperature for 48 hours allowed the corresponding Ag^{I}-OAc complex **C10.1** to be isolated in a respectable yield of 55 % (**Scheme 6.6**, **B**). Interestingly when **L9.1** or **L11.1** are employed, the corresponding complexes **C9.1** and **C11.1** could not be isolated, with the formation of a black precipitate as the reaction proceeds, presumably Ag^{0}. The benzyl derivative **C12.1** however, could be isolated in high yields (**Scheme 6.6**, **C**).

The ^{1}H NMR spectrum of **C9.1** provides evidence for NHC formation, with the absence of the imidazolium resonance and presence of a singlet at 1.95 ppm characteristic of the methyl resonance of the acetate unit (**Figure 6.12**).[18,28] The $^{13}C\{^{1}H\}$ NMR spectrum provides further clarity, exhibiting a carbene resonance at 188.4 ppm (**Figure 6.13**). The $^{11}B\{^{1}H\}$ NMR spectrum of **C10.1** shows the expected peaks for a *closo*-carboranyl compound (**Figure 6.12**, **inset**). **C10.1** could not be characterised by HRMS due to scrambling, with the major molecular ion peaks corresponding to the ligand and an $Ag(NHC)_2$ complex (**Figure 6.14**). Micro analysis confirmed that **C10.1** had formed, and not the dimeric $Ag(NHC)_2$ type complex that the HRMS suggests.

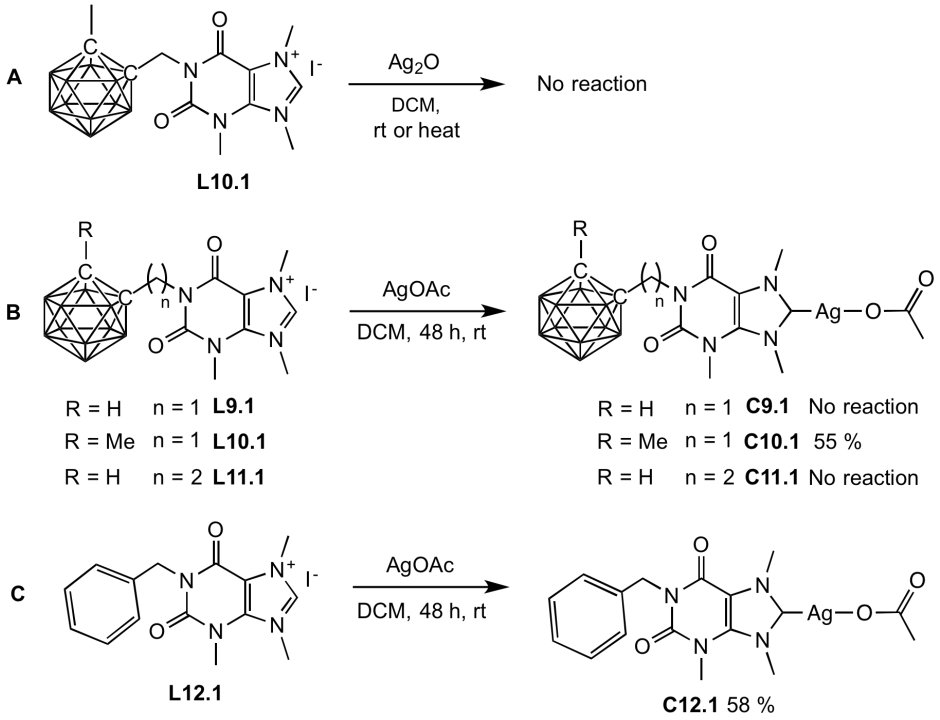

Scheme 6.6 Initial efforts towards synthesising a Ag^{I} complex (**A**), synthesis of NHC-carboranyl Ag^{I}-OAc complex **C10.1** and attempted synthesis of **C9.1** and **C11.1** (**B**) and synthesis of an NHC-benzyl Ag^{I}-OAc complex (**C**).

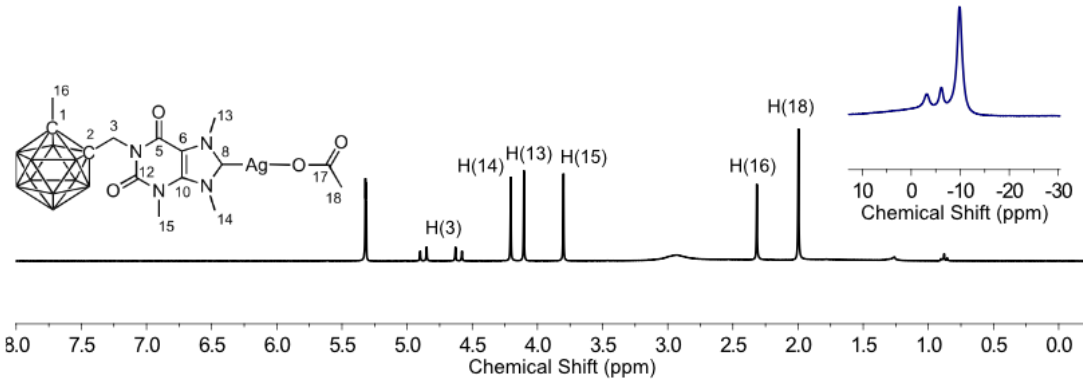

Figure 6.12 ^{1}H NMR spectrum (500 MHz, CD_2Cl_2) and $^{11}B\{^{1}H\}$ NMR spectrum (196 MHz, CD_2Cl_2) of **C10.1** (inset).

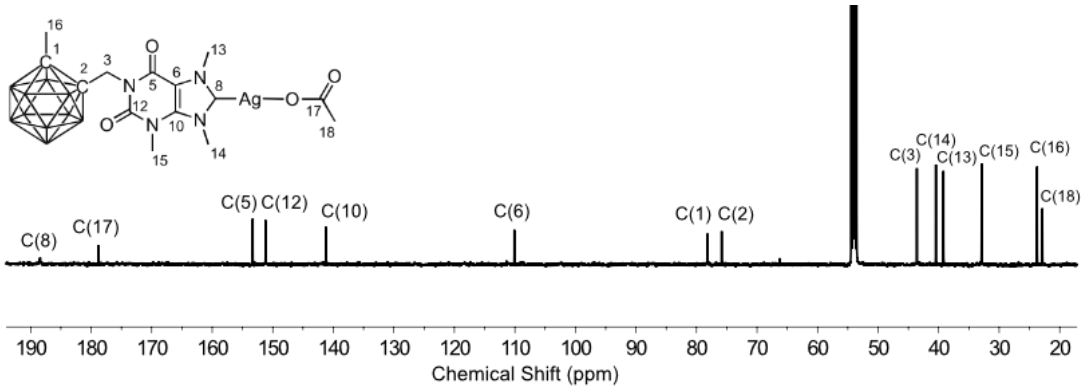

Figure 6.13 $^{13}C\{^{1}H\}$ NMR spectrum (126 MHz, CD_2Cl_2) of **C10.1**.

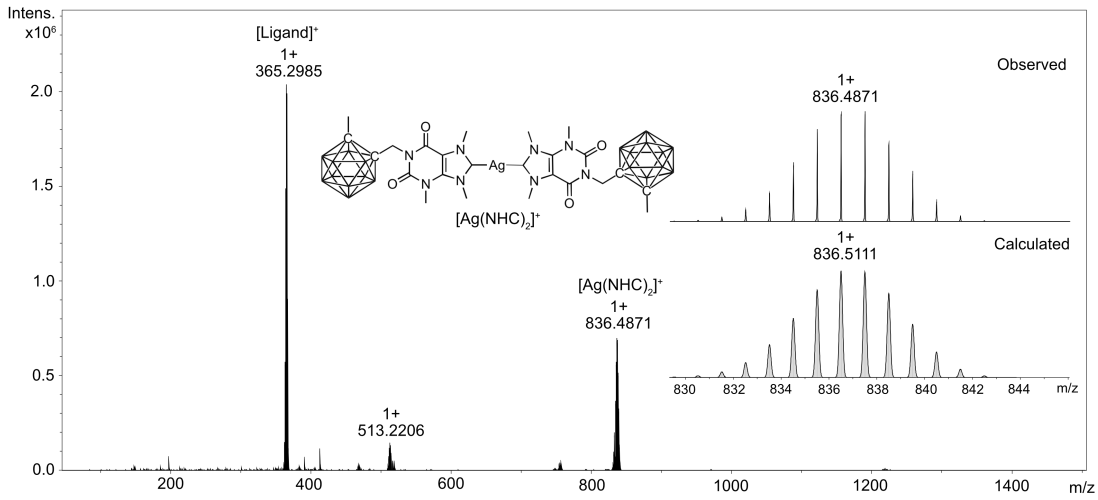

Figure 6.14 HRMS of **C10.1**. Inset shows the observed molecular ion peak of $[Ag(NHC)_2]^+$ for **C10.1** against the calculated mass.

The molecular structure of complexes **C10.1** and **C11.1** were elucidated by X-ray diffraction analysis (**Figure 6.15**). Crystals suitable for XRD analysis for both complexes were obtained from the slow diffusion of Et_2O into concentrated DCM solutions. The Ag-$C_{carbene}$ bond lengths of 2.108(3) Å (**C10.1**) and 2.134(7) Å (**C11.1**) are within the expected range of similar (NHC)AgOAc type complexes in the literature (**Table 6.4**),[18] and the geometry about the silver atoms deviate slightly from linearity, with C(8)-Ag(1)-O(3) bond angles of 171.8° and 175.9° for **C10.1** and **C11.1** respectively.

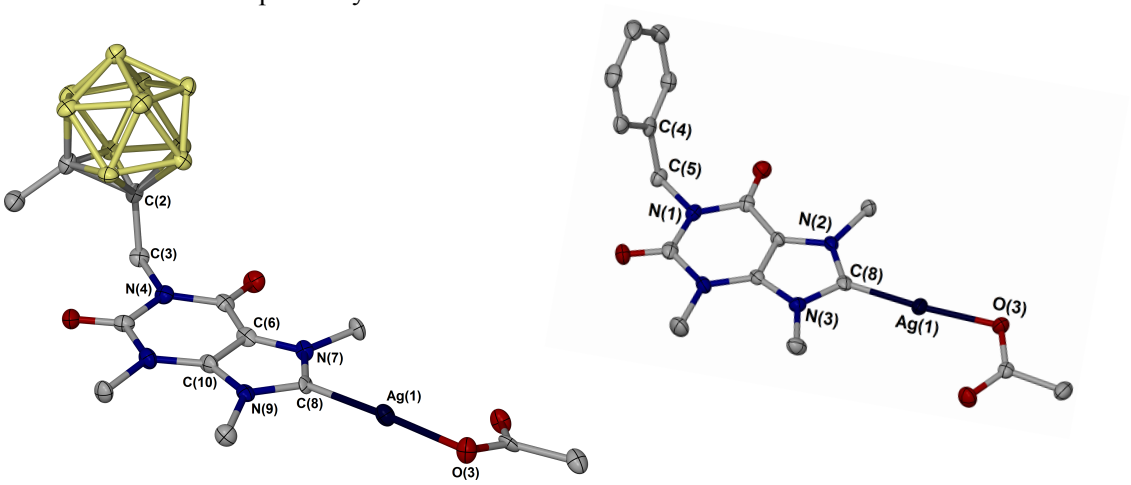

Figure 6.15 Molecular structures for **C10.1** (left) and **C11.1** (right). *Thermal ellipsoids shown at 50 % probability and hydrogen atoms are omitted for clarity.*

6.5.3 Decomposition studies of the Ag^I-OAc complexes

It is interesting that of the carboranyl complexes **C9.1-C11.1**, only **C10.1** can be isolated in good yield. Both **C9.1** and **C11.1** possess an acidic cage CH proton, and it can be suggested that this could interact with the silver leading to decomposition of the complexes. It is noteworthy however, that over the course of several weeks **C10.1** shows signs of decomposition in the solid state even when stored in a dark environment. In comparison, phenyl complex **C11.1** remains stable and even when dissolved in hydrous DMSO-d_6 no decomposition is observed, even after several weeks. When **C10.1** is dissolved in hydrous DMSO-d_6 signs of decomposition are apparent within a couple of hours. This can be observed visually with the formation of a black precipitate presumably Ag^0, and by ^{1}H NMR spectroscopy, with the presence of a small downfield resonance characteristic of the imidazolium proton in the ^{1}H NMR spectrum. After leaving the sample of **C10.1** for a further 9 days and observing the ^{1}H NMR spectrum, it was surprising to see that deboronation of the cage had occurred, with a characteristic resonance at −3.0 ppm for the bridging proton of the open face of the cage. This suggests that the theobromine unit is electron withdrawing and increases the susceptibility of the cage towards deboronation. It is unusual for deboronation to occur under such mild conditions but there are examples in the literature.[29–31]

Kahl *et al.* reported the serendipitous degradation reaction of a *closo*-carboranyl porphyrin (**A**) to the *nido*-species in hydrous DMSO (**Figure 6.16**).[29] This led to further investigation into the factors which effect the decomposition of the closo cage to the nido species, by exploring the nature of the α-substituent of the cage and solvent used in the reaction (**Figure 6.16, B-F**). It was reported that DMSO out performed various polar solvents containing 5 % water (DMF, *N*-methylpyrrolidinone, MeCN, THF and acetone) and that when anhydrous solvents were employed no degradation of the cage was observed. Rapid deboronation was observed with strongly electron withdrawing groups (**B** and **C**) but introducing a methylene linker between the cage and the electron withdrawing substituent (**D**) made the cage resilient to deboronation. Introducing groups which are not electron withdrawing (**E** and **F**) also prevents deboronation of the cage.

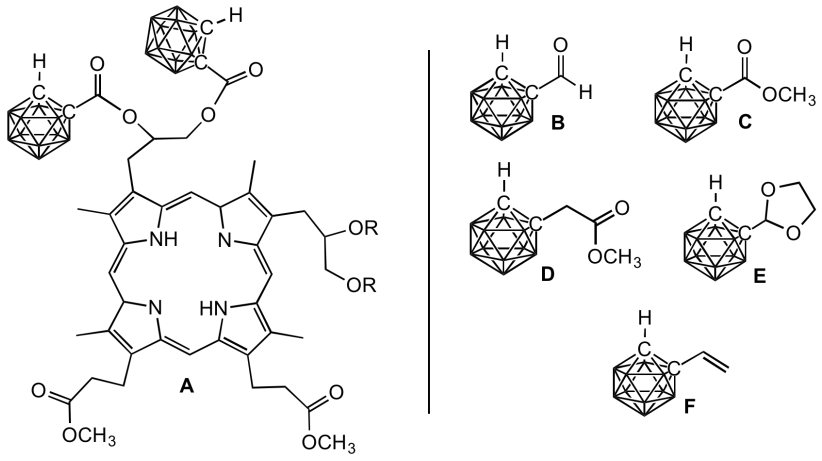

Figure 6.16 A *closo*-carboranyl porphyrin (**A**) reported by Kahl *et al.* and a series of functionalised carboranes (**B**-**F**) screened for their degradation in DMSO.[29]

It was concluded that the degradation reaction was dependent on the ability of the solvent to stabilise the nucleophilic attack by water, and that electron withdrawing α-substituents facilitate deboronation. In light of this research a series of decomposition studies were carried out to determine whether the theobromine moiety promotes deboronation. Each of the theobromine derived carboranyl compounds (**P9.2**, **P10.2**, **P11.2**, **L9.1**, **L10.1**, **L11.1** and **C10.1**) were placed in an NMR tube and dissolved in DMSO-d_6 (<0.02% H_2O) and monitored by ^{1}H and $^{11}B\{^{1}H\}$ NMR spectroscopy. In accordance with Kahl's findings, no deboronation occurs in the absence of water. To each sample was then added 5 % D_2O, and it was found that **P9.2** and **L9.1** are deboronated by D_2O, with **L9.1** deboronating the fastest (**Table 6.4**). It can be proposed that **L9.1** is more prone to deboronation due to formation of a stable zwitterionic compound (**L9.2**). In comparison, the deboronated product of **P9.2** is presumably stabilised by a hydronium cation (**P9.3**). The disubstituted carboranyl compounds **P10.1** and **L10.1** are resilient towards deboronation. The electron density induced onto the cage by the methyl group reduces the electropositive nature of the boron atoms, hence providing stability towards

degradation of the cage. Similarly, the compounds possessing a longer tether between the theobromine unit and the cage (**P11.1** and **L11.1**) also resist deboronation.

Table 6.4 Deboronation screening reactions involving the reaction of each of the theobromine derived carboranyl compounds **P9.2**, **P10.2**, **P11.2**, **L9.1**, **L10.1**, **L11.1** and **C10.1** with D_2O (5%) in DMSO-d_6. Inset schemes highlight the suspected decomposition products.

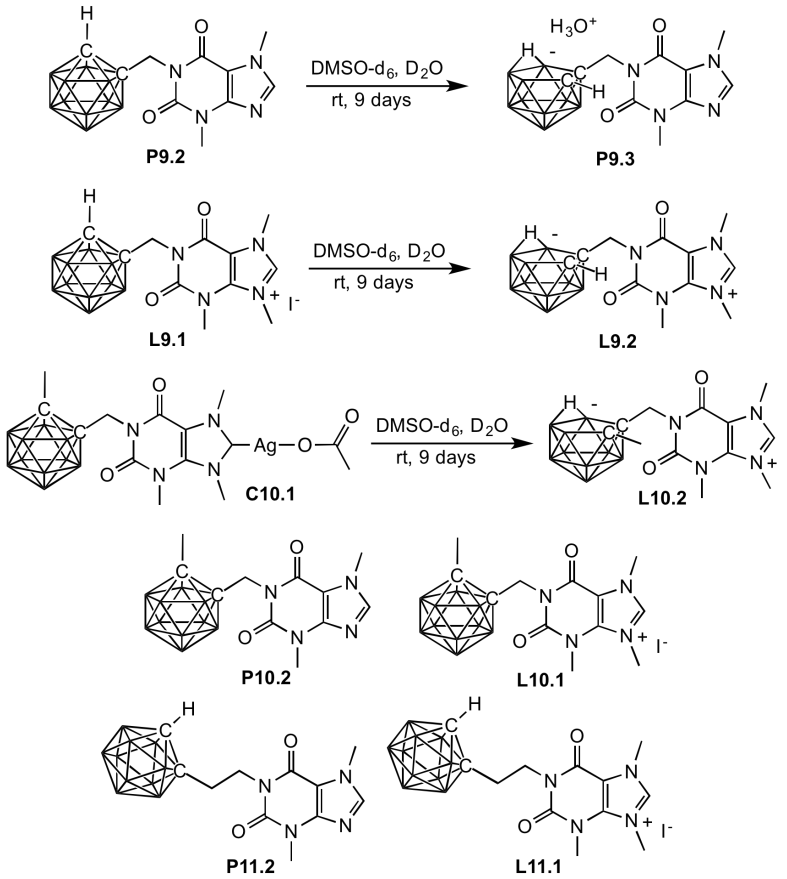

Compound	Deboronated product formed (% yield)*
P9.2	**P9.3** (5)
L9.1	**L9.2** (14)
P10.2	-
L10.1	-
C10.1	**L10.2** (100)
P11.2	-
L11.1	-

* refer to NMR spectra on the next page for an example of how % yield is measured.

To illustrate how the decomposition products are identified, the ^{1}H and $^{11}B\{^{1}H\}$ NMR spectra of **L9.1** dissolved in DMSO-d_6 (5 % D_2O) (**Figure 6.17**, **bottom**), and the ^{1}H and $^{11}B\{^{1}H\}$ NMR of the same sample recorded 9 days later (**Figure 6.17**, **top**) are provided. The decomposition product (**L9.2**) is indicated by the red dots. The appearance of an imidazolium peak further upfield at 9.21 ppm is likely due to the loss of hydrogen bonding interaction between the iodide counterion and the imidazolium proton, as **L9.2** is zwitterionic. The carboranyl proton, a broad singlet at 5.11 ppm for **L9.1**, becomes shielded with a shift to 2.15 ppm upon deboronation due to the increase in charge density of the cage upon loss of the B vertex. This is also the case for the methylene bridge protons, which appear further upfield at 4.31 ppm. The $^{11}B\{^{1}H\}$ NMR spectrum further clarifies this with the diagnostic resonances of a *nido*-cage at around −35 ppm.

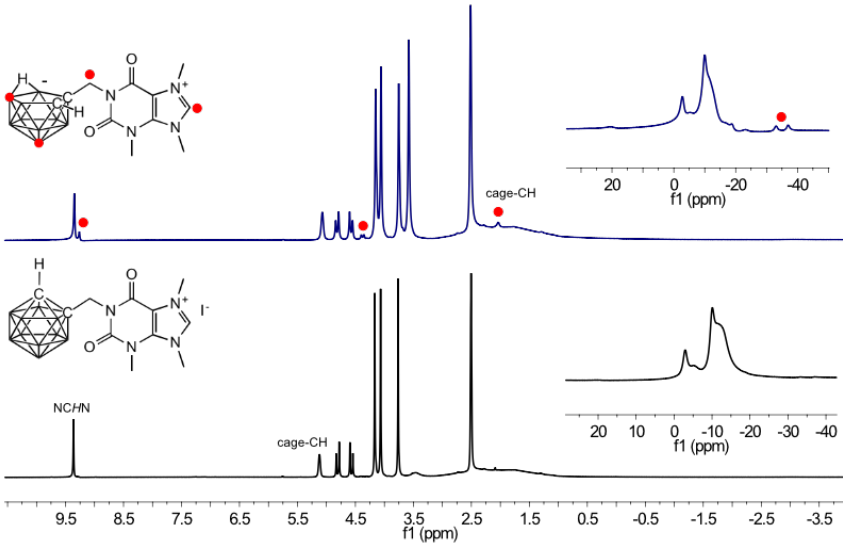

Figure 6.17 ^{1}H NMR spectrum (300 MHz, DMSO-d_6) (bottom) and $^{11}B\{^{1}H\}$ NMR (96 MHz, DMSO-d_6) spectrum (inset) for **L9.1** with 5 % D_2O, and ^{1}H NMR spectrum (300 MHz, DMSO-d_6) (top) and $^{11}B\{^{1}H\}$ NMR spectrum (96 MHz, DMSO-d_6) (inset) of the same sample recorded 9 days later (top).

The question that arises is why does **C10.1** fully deboronate to **L10.2**, when its precursors **P10.2** and **L10.1** are completely stable? It can be suggested that the silver withdraws electron density from the theobromine unit increasing the electrophilicity of the boron atoms, hence the susceptibility of the cage towards deboronation is increased. Alternatively, the weakly basic acetate unit may be involved in deboronation. It can be proposed from these observations that the stability of the Ag^{I}-OAc complexes (**C9.1-C11.1**) is not only linked to the susceptibility of the cage towards deboronation, but also whether the carboranyl unit possess an acidic CH proton. Future ligand design should look to further increase the stability of the cage whilst ensuring the cage CH proton is substituted if a more stable Ag^{I}-OAc complex is to be isolated. A route to a potentially more stable Ag^{I}-OAc carboranyl complex **C13.1** that could be looked at in the future is provided in Section 6.7.

6.6 Anticancer testing

Preliminary studies revealed that the $Ag(NHC)_2Br$ type complexes **C2.26** and **C8.1** (Section 6.3), and AgOAc xanthine-derived complexes **C10.1** and **C12.1** (Section 6.4.2) exhibit antiproliferative activity against the HCT116+/+ and HCT116−/− (colon) cancer cell lines (**Figure 6.18**).

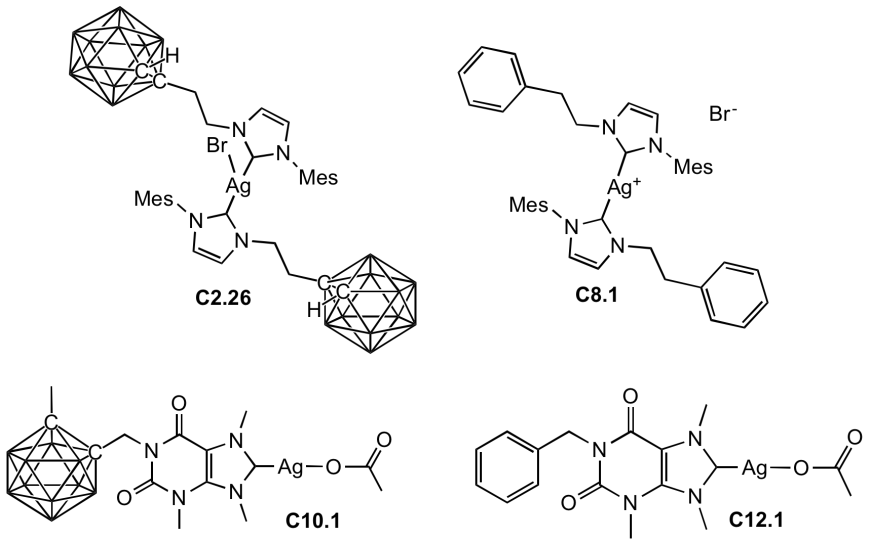

Figure 6.18 Ag-NHC complexes screened against the HCT116+/+ and HCT116−/− cancer cell lines.

The *in vitro* cytotoxicity of the complexes were determined using MTT-based assays involving a 96 hour complex-exposure period. The MTT based assay is a colorimetric assay for cellular growth and was the first homogeneous cell viability assay developed for a 96-well format that is highly effective for high-throughput screening.[32] Viable cells reduce MTT (yellow) to formazan (purple), which has an absorbance maximum near 570 nm (**Figure 6.19**). The quantity of formazan is measured by recording changes in absorbance in this region. Upon apoptosis (cell death), the ability to reduce MTT to formazan is lost, therefore colour is an effective marker to measure cytotoxicity (loss of viable cells) and is quantified as an IC_{50} value. IC_{50} is defined as the concentration of the complex required to achieve cell death in 50 % of the cells.

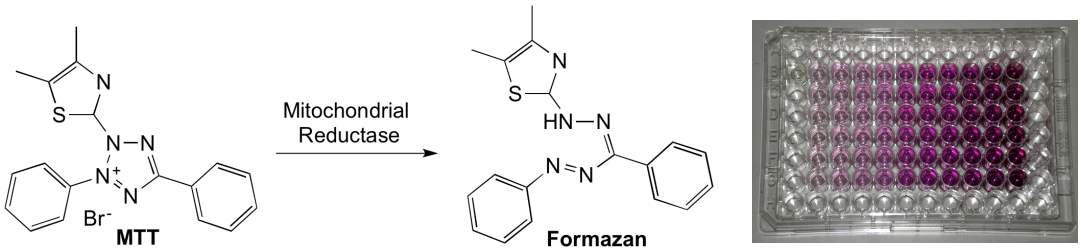

Figure 6.19 Reduction of MTT to formazan and representation of a 96-well MTT assay whereby increasing numbers of viable cells resulted in increased purple colouring.

Each of the complexes tested were screened a total of three times to give an average IC_{50} value, and in most cases results showed good reproducibility (**Table 6.5**). Interestingly **C2.26** was found to be most potent (entry 1), being more effective than the phenyl complex **C8.1** (entry 2). In comparison the xanthine-derived complexes are not as effective and a reverse of potency was observed with phenyl complex **C12.1** outperforming carboranyl derivative **C10.1** (entries 3 and 4). The greater antiproliferative activity of **C12.1** can be rationalised by its superior stability (Section 6.5.2), allowing for a slower release of Ag over the 96 hour period providing a superior cytotoxicity profile.

Another interesting observation is that the IC_{50} values for each complex are the same irrespective to the cell line they are screened against (HCT116+/+ or HCT116−/−). The difference between the two cell lines is that HCT116−/− does not possess the p53 gene, also known as the tumour suppressor protein, *i.e*. it prevents the formation of tumours. The p53 gene is the most commonly mutated gene in people who have cancer, hence, is involved in the complex mechanism leading to tumour formation.

By screening the complexes against the HCT116+/+ and HCT116−/− cell lines it could be determined whether cell apoptosis was dependant on the p53 gene. With the IC_{50} values unaffected across both cell lines it can be hypothesised that the Ag^{I} complexes induce apoptosis *via* an alternative mechanism independent of the p53 gene.

Table 6.5 IC_{50} (μM) for Ag-NHC complexes screened against the HCT116+/+ and HCT116−/− cell lines.

		HCT116+/+				**HCT116−/−**			
Entry	**Complex**	**Run 1**	**Run 2**	**Run 3**	**Average (SD)**	**Run 1**	**Run 2**	**Run 3**	**Average (SD)**
1	**C2.26**	1.5	1.0	1.3	1.3 ± 0.2	1.6	1.0	1.8	1.5 ± 0.4
2	**C8.1**	16.0	7.7	7.7	10.5 ± 4.8	14.0	7.6	7.7	9.8 ± 3.7
3	**C10.1**	17.7	15.4	19.7	17.6 ± 2.1	18.6	16.3	25.8	20.2 ± 5.0
4	**C12.1**	17.0	9.0	8.9	11.6 ± 4.6	16.7	8.5	8.7	11.3 ± 4.6

6.7 Conclusions and future work

A series of Ag^I NHC-carborane complexes have been prepared by reacting imidazolium salts in with Ag_2O (**Scheme 6.7**, **A**). It was found that when the α-substituent of the NHC was a sterically bulky ^{t}Bu group, an uncommon $Ag(NHC)_2Br_2$ type complex **C2.24** is formed which is unstable. A second complex (**C2.25**) was also present upon crystallisation of the product material, which is suspected to be a decomposition product of **C2.24**. Reducing the sterics of the NHC allowed a stable Ag^I-NHC carborane complex **C2.26** to be isolated (**Scheme 6.7**, **B**). A phenyl derivative **C8.1** was prepared by analogous procedure.

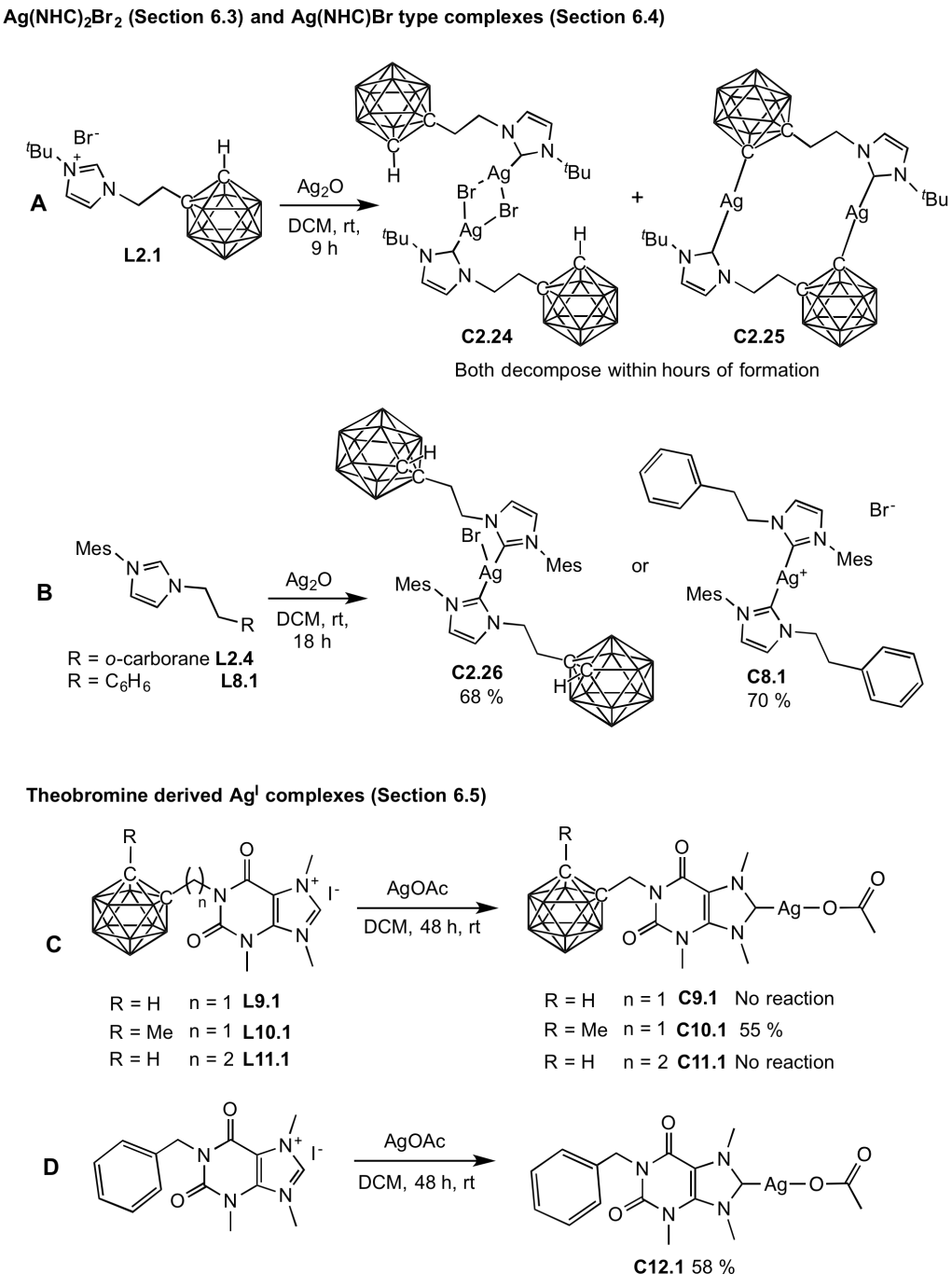

Scheme 6.7 Summary of ligands and complexes synthesised in this chapter.

In addition, a series of carboranyl xanthine derivatives **L9.1**-**L11.1** and a phenyl derivative **L12.1** were prepared (**Scheme 6.7**, **C** and **D**). When these ligand precursors were reacted with AgOAc it was determined that if the carborane possesses an acidic CH proton the complex was unstable and could not be isolated (**C9.1** and **C11.1**). Substituting this proton for a Me group (**L10.1**), or employing the phenyl ligand precursor **L12.1**, allowed the corresponding Ag^{I} complexes to be isolated in good yield (**Scheme 6.7 C** and **D**). Phenyl complexes **C8.1** and **C12.1** were prepared for useful comparison when evaluating the cytotoxic properties of the complexes against the HCT116 (colon) cancer cell line. **C2.24** was found to be the more potent than **C8.1**, with an IC_{50} value of 1.3 ± 0.2 (μM) compared to 10.5 ± 4.8 (μM) for **C8.1**. The xanthine-derived complexes showed a reverse of potency with the phenyl complex **C12.1** outperforming the carboranyl derivative **C10.1** (**Table 6.6**).

It is intriguing that **C2.24** outperforms **C8.1**. Why this is the case remains unclear and future efforts should look towards screening both complexes against other cancer cell lines, as research has shown Ag^{I}-NHC complexes can have selectivity towards specific cancers.[16] The complexes should also be screened against non cancerous cell lines to determine whether the complexes show selectivity for the cancer cells over healthy cells. With regards to **C10.1**, it is suspected that its relatively poor antiproliferative activity is a result of its poor stability. A more stable complex such as **C13.1** could be prepared by increasing the tether length between the electron withdrawing theobromine unit and the cage to reduce the susceptibility of the cage towards deboronation. A proposed synthesis is outlined in **Scheme 6.8**.

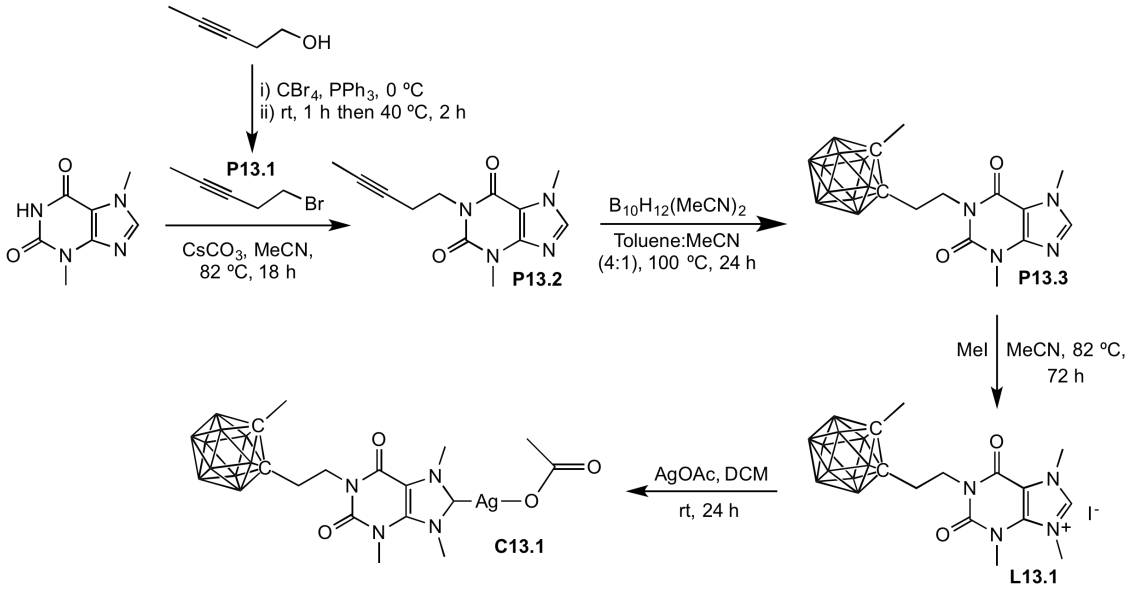

Scheme 6.8 Proposed synthesis of a potentially more stable xanthine derived Ag^{I}-OAc complex **C13.1**.

6.8 Experimental

All manipulations were carried out under an inert atmosphere by means of standard Schlenk line or glovebox techniques unless otherwise stated. Anhydrous solvents were prepared by passing over activated alumina to remove water, copper catalyst to remove oxygen and molecular sieves to remove any remaining water, *via* the Dow-Grubbs solvent system, and then freeze-pump-thaw degassed prior to use. All chemicals used in this work were bought from either Sigma Aldrich or Alfa and used without further purification. NMR spectra were recorded on a Bruker AV500, Bruker AV400 or a Bruker DPX300 spectrometer. ^{1}H NMR and ^{13}C{^{1}H} NMR chemical shifts were referenced against residual solvent peaks. Assignment of ^{1}H and ^{13}C{^{1}H} NMR spectra for all compounds was aided by the use of 2D ^{1}H^{1}H COSY, ^{1}H^{13}C HMQC, ^{1}H^{13}C HMBC and ^{13}C{^{1}H} DEPT 135 and DOSY experiments. Mass spectra were collected on a Bruker Daltonics (micro TOF) instrument operating in the electrospray mode. Elemental analyses were performed by Mr Stephen Boyer at London Metropolitan University. The preparation of NHC-carborane ligand precursors **L2.1** and **L2.4** can be found in Chapter 2.

6.8.1 Ligand Precursors

Preparation of **P9.1**.

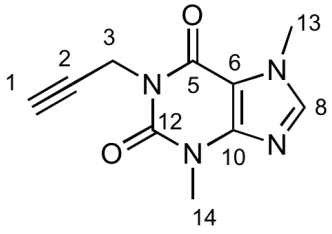

To an RBF was added MeCN (30 mL), theobromine (3.00 g, 16.70 mmol), $CsCO_3$ (10.80 g, 33.30 mmol) and propargyl bromide (2.27 mL, 25.00 mmol, 80 % wt toluene) and then heated at 80 °C for 18 hours. The reaction was then cooled to room temperature and the solvent removed *in vacuo*. DCM (50 mL) was added, filtered and H_2O (30 mL) added, and the organic phase was collected. This was further washed with H_2O (2 × 30 mL), dried over $MgSO_4$, filtered and the solvent removed *in vacuo*. The off white residue was recrystallised from DCM (20 mL) with pentane (50 mL) to give a white powder. Yield: 2.99 g, 13.70 mmol, (82 %). ^{1}H NMR (500 MHz, $CDCl_3$): δ (ppm) 7.52 (m, 1H, H^{8}), 4.79 (d, J = 2.5 Hz, 2H, H^{3}), 3.99 (m, 3H, H^{13}), 3.59 (s, 3H, H^{14}), 2.17 (t, J = 2.5 Hz, 1H, H^{1}). ^{13}C NMR (126 MHz, $CDCl_3$): δ (ppm) 154.5 (C^{5}), 151.0 (C^{12}), 149.3 (C^{10}), 141.9 (C^{8}), 107.7 (C^{6}), 78.8 (C^{2}), 70.6 (C^{1}), 33.8 (C^{13}), 30.6 (C^{3}), 29.9 (C^{14}). HRMS (ESI^{+}): *m/z* $[C_{10}H_{10}N_4O_2Na]^+$ 241.0700, calcd for $[M + Na]^+$ 241.0696.

Preparation of **P10.1**.

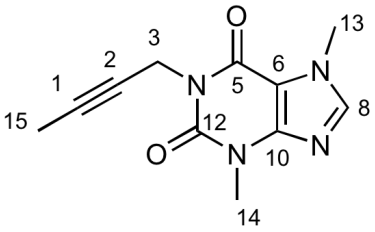

Prepared as described for **P9.1** from theobromine (3.00 g, 16.70 mmol), $CsCO_3$ (10.80 g, 33.30 mmol) and 1-bromo-2-butyne (1.60 mL, 18.40 mmol) in MeCN (30 mL). After work up the product was obtained as a white powder. Yield: 2.95 g, 12.70 mmol, 76 %. ^{1}H NMR (500 MHz, $CDCl_3$): δ (ppm) 7.50 (m, 1H, H^8), 4.72 (q, J = 2 Hz, 2.5 Hz, 2H, H^3), 3.98 (m, 3H, H^{13}), 3.58 (m, 3H, H^{14}), 1,76 (t, *J* = 2Hz, 3H, H^{15}). ^{13}C NMR (126 MHz, $CDCl_3$): δ (ppm) 154.7 (C^5), 151.1 (C^{12}), 149.1 (C^{10}), 141.7 (C^8), 107.7 (C^6), 78.3 (C^2), 73.9 (C^1), 33.7 (C^{13}), 31.1 (C^3), 29.9 (C^{14}), 3.8 (C^{15}). HRMS (ESI^+): *m/z* $[C_{11}H_{12}N_4O_2Na]^+$ 255.0857, calcd for $[M + Na]^+$ 255.0852.

Preparation of **P11.1**.

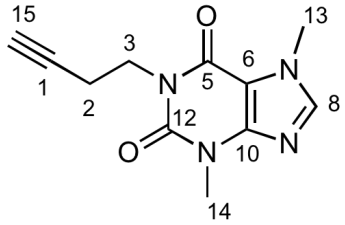

Prepared as described for **P9.1** from theobromine (3.00 g, 16.70 mmol), $CsCO_3$ (10.80 g, 33.30 mmol) and 4-bromo-1-butyne (1.88 mL, 20.00 mmol) in MeCN (30 mL). After work up the product was obtained as a white powder. Yield: 1.55 g, 6.68 mmol (40 %). ^{1}H NMR (300 MHz, $CDCl_3$): δ (ppm) 7.50 (s, 1H, H^8), 4.27–4.14 (m, 2H, H^2), 3.98 (s, 3H, H^{13}), 3.56 (s, 3H, H^{14}), 2.58 (td, *J* = 7.3, 2.7 Hz, 2H, H^3), 1.96 (t, *J* = 2.7 Hz, 1H, H^{15}). ^{13}C NMR (75 MHz, $CDCl_3$): δ (ppm) 155.1 (C^5), 151.4 (C^{12}), 149.0 (C^{10}), 141.7 (C^8), 107.7 (C^6), 81.0 (C^1), 69.9 (C^2), 39.7 (C^3), 33.7 (C^{13}), 29.8 (C^{14}), 17.8 (C^{15}). HRMS (ESI^+): *m/z* 255.0860 $[C_{11}H_{12}N_4O_2Na]^+$, calcd for $[M + Na]^+$ 255.0858.

Preparation of **P12.1**.

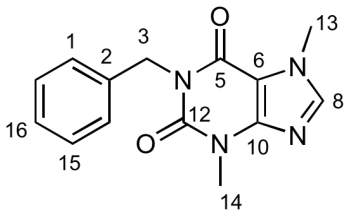

Prepared as described for **P9.1** from theobromine (3.00 g, 16.70 mmol), $CsCO_3$ (10.80 g, 33.30 mmol) and benzyl bromide (1.99 mL, 16.70 mmol) in MeCN (30 mL). After work up the product was obtained as a white powder. Yield: 3.62 g, 13.40 mmol (80 %). ^{1}H NMR (500 MHz, $CDCl_3$): δ (ppm) 7.49 (m, 3H, H^1, H^8), 7.30 (m, 2H, H^{15}), 7.24 (m, 1H, H^{16}), 5.19 (s, 2H, H^3), 3.98 (m, 3H, H^{13}), 3.57 (s, 3H, H^{14}). ^{13}C NMR (126 MHz, $CDCl_3$): δ (ppm) 155.4 (C^5), 151.8 C^{12}), 149.0 (C^{10}), 141.7 (C^8), 137.5 (C^2), 129.0 (C^1), 128.5 (C^{15}), 127.7 (C^{16}), 107.8 (C^6), 44.6 (C^3), 33.7 (C^{13}), 29.9 (C^{14}). HRMS (ESI^+): *m/z* $[C_{14}H_{14}N_4O_2Na]^+$ 293.1025, calcd for $[M + Na]^+$ 293.1009.

Preparation of **P9.2**.

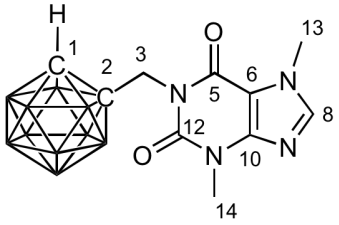

To a Schlenk flask was added **P9.1** (1.00 g, 4.58 mmol) and $B_{10}H_{12}(MeCN)_2$ (927 mg, 4.58 mmol) and degassed. Anhydrous toluene (10 mL) and anhydrous MeCN (3 mL) was added and slowly heated to 100 °C and kept at this temperature for 18 hours. The reaction was cooled to room temperature and the solvent was removed *in vacuo*. The product was extracted with Et_2O (2 × 15 mL) and filtered. This was washed with 1 M NaOH solution (2 × 10 mL) then H_2O (2 × 10 mL), dried over $MgSO_4$, filtered and solvent removed *in vacuo*. The residue was recrystallised from Et_2O (10 mL) with hexane (30 mL), filtered and solvent removed *in vacuo* to give a white powder. Yield: 807 mg, 2.40 mmol (52 %). ^{1}H NMR (500 MHz, $CDCl_3$): δ (ppm) 7.56 (s, 1H, H^8), 4.88 (d, J = 14.9 Hz, 1H, H^3), 4.60 (d, J = 14.9 Hz, 1H, H^3), 4.20 (br. s, 1H, H^1), 3.98 (s, 3H, H^{13}), 3.58 (s, 3H, H^{14}). ^{13}C NMR (126 MHz, $CDCl_3$): δ (ppm) 154.5 (C^5), 151.6 (C^{12}), 149.4 (C^{10}), 142.6 (C^8), 107.3 (C^6), 74.0 (C^2), 61.3 (C^1), 45.3 (C^3), 33.9 (C^{13}), 30.2 (C^{14}). ^{11}B{^{1}H} NMR (161 MHz, $CDCl_3$): δ (ppm) −1.4 (1B), −4.8 (1B), −10.0 (2B), −10.8 (2B), −12.9 (4B). HRMS (ESI^+): *m/z* $[C_{10}H_{21}B_{10}N_4O_2]^+$ 337.2670, calcd for $[M + H]^+$ 337.2667.

Preparation of **P10.2**.

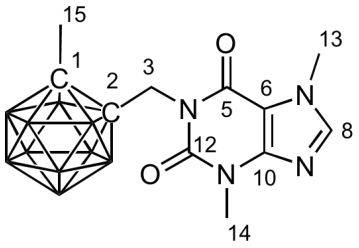

To a Schlenk flask was added **P10.1** (1.00 g, 4.31 mmol), $B_{10}H_{12}(MeCN)_2$ (871 mg, 4.31 mmol), anhydrous toluene (10 mL) and anhydrous MeCN (3 mL) and slowly heated to 100 °C and kept at this temperature for 18 hours. The reaction was cooled to room temperature and the solvent was removed *in vacuo*. The residue was dissolved in a minimum amount of DCM and purified by silica chromatography, which was eluted with ethyl acetate/hexane 1:2. The product fractions were combined and the solvent is removed *in vacuo*. The residue was dissolved in Et_2O (5 mL) and the product was precipitated as a white powder with hexane (30 mL), this was filtered and dried *in vacuo*. Yield: 573 mg, 1.63 mmol (38 %). ^{1}H NMR (500 MHz, $CDCl_3$): δ (ppm) 7.56 (d, J = 0.6 Hz, 1H, H^8), 4.86 (d, J = 14.8 Hz, 1H, H^3), 4.64 (d, J = 14.8 Hz, 1H, H^3), 3.99 (d, J = 0.6 Hz, 3H, H^{13}), 3.59 (s, 3H, H^{14}), 2.34 (s, 3H, H^{15}). ^{13}C NMR (126 MHz, $CDCl_3$): δ (ppm) 154.7 (C^5), 151.5 (C^{12}), 149.5 (C^{10}), 142.4 (C^8), 107.4 (C^6), 77.4 (C^2), 75.9 (C^1), 42.5 (C^3), 33.9 (C^{13}), 30.2 (C^{14}), 23.5 (C^{15}). ^{11}B{^{1}H} NMR (161 MHz, $CDCl_3$): δ (ppm) −3.2 (1B), −6.0 (1B), −9.9 (8B). HRMS (ESI^+): *m/z* $[C_{11}H_{23}B_{10}N_4O_2]^+$ 351.2824, calcd for $[M + H]^+$ 351.2824.

Preparation of **P11.2**.

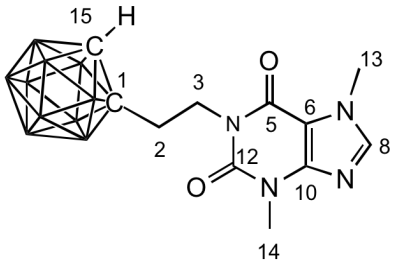

To a Schlenk flask was added **P11.1** (1.00 g, 4.31 mmol), $B_{10}H_{12}(MeCN)_2$ (871 mg, 4.31 mmol), anhydrous toluene (10 mL) and anhydrous MeCN (3 mL) and slowly heated to 100 °C and kept at this temperature for 18 hours. The reaction was cooled to room temperature and the solvent was removed *in vacuo*. The residue was dissolved in a minimum amount of DCM and purified by silica chromatography, which was eluted with ethyl acetate/hexane 1:2 and then the product is eluted with DCM/MeOH (10 %). The product fractions are combined and the solvent was removed *in vacuo*. The residue was dissolved in Et_2O (5 mL) and the product was precipitated as a white powder with hexane (30 mL), this as filtered and dried *in vacuo*. Yield: 680 mg, 1.93 mmol (45 %). ^{1}H NMR (300 MHz, $CDCl_3$): δ (ppm) 7.52 (s, 1H, H^8), 4.12 (m, 2H, H^2), 3.96 (s, 1H, H^{13}), 3.73 (br. s, 1H, H^{15}), 2.52 (s, 3H, H^{14}). ^{13}C NMR (75 MHz, $CDCl_3$): δ (ppm) 154.8 (C^5), 151.2 (C^{12}), 149.2 (C^{10}), 142.0 (C^8), 107.6 (C^6), 72.4 (C^{15}), 61.6 (C^1), 40.0 (C^3), 35.12 (C^2), 33.8 (C^{13}), 29.89 (C^{14}). ^{11}B{^{1}H} NMR (96 MHz, dmso-d_6): δ (ppm) −2.1 (1B), −5.3 (1B), −9.1 (2B), −11.6 (6B). HRMS (ESI^+): *m/z* $[C_{13}H_{23}B_{10}N_5O_2Na]^+$ 413.2600, calcd for $[M + MeCN + Na - H_2]^+$ 413.2716.

Preparation of **L9.1**.

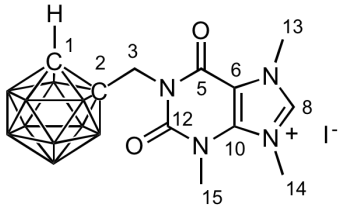

An ampoule was charged with MeCN (5 mL), **P9.2** (1.17 g, 3.48 mmol) and MeI (6.49 mL, 104.3 mmol) and heated at 80 °C for 7 days. The reaction was then cooled to room temperature and solvent removed *in vacuo*. To the residue was added Et_2O (30 mL) and then sonicated, filtered, washed with Et_2O (20 mL) and dried *in vacuo* to give a white powder. Yield: 631 mg, 1.46 mmol (42 %). ^{1}H NMR (500 MHz, DMSO-d_6): δ (ppm) 9.35 (s, 1H, H^8), 5.11 (br. s, 1H, H^1), 4.81 (d, J = 15.1 Hz, 1H, H^3), 4.58 (d, J = 15.1 Hz, 1H, H^3), 4.16 (s, 3H, H^{14}), 4.06 (s, 3H, H^{13}), 3.76 (s, 3H, H^{15}). ^{13}C NMR (126 MHz, DMSO-d_6): δ (ppm) 152.7 (C^5), 150.1 (C^{12}), 140.5 (C^8), 139.9 (C^{10}), 107.5 (C^6), 73.2 (C^2), 62.4 (C^1), 45.1 (C^3), 37.0 (C^{14}), 35.8 (C^{13}), 31.8 (C^{15}). ^{11}B{^{1}H} NMR (161 MHz, DMSO-d_6): δ (ppm) −2.9 (1B), −5.2 (1B), −10.0 (2B), −11.6 (3B), −12.9 (3B). HRMS (ESI^+): *m/z* $[C_{11}H_{23}B_{10}N_4O_2]^+$ 352.2800, calcd for $[M - I]^+$ 352.2800.

Preparation of **L10.1**.

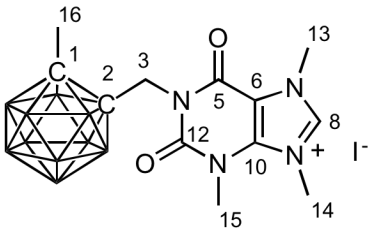

Prepared as described for **L9.1** from **P10.2** (500 mg, 1.43 mmol) and MeI (2.67 mL, 42.6 mmol) in MeCN (5 mL). After purification the product was obtained as a white powder. Yield: 287 mg, 0.64 mmol (45 %). ^{1}H NMR (500 MHz, DMSO-d_6): δ (ppm) 9.34 (s, 1H, H^{8}), 4.86 (d, J = 15.4 Hz, 1H, H^{3}), 4.64 (d, J = 15.4 Hz, 1H, H^{3}), 4.16 (s, 3H, H^{14}), 4.07 (s, 3H, H^{13}), 3.77 (s, 3H, H^{15}), 2.35 (s, 3H, H^{16}). ^{13}C NMR (126 MHz, DMSO-d_6): δ (ppm) 152.9 (C^{5}), 150.1 (C^{12}), 140.5 (C^{8}), 140.0 (C^{10}), 107.4 (C^{6}), 77.9 (C^{2}), 75.7 (C^{1}), 43.0 (C^{3}), 37.0 (C^{14}), 35.8 (C^{13}), 31.8 (C^{15}), 22.6 (C^{16}). ^{11}B{^{1}H} NMR (161 MHz, DMSO-d_6): δ (ppm) −2.9 (1B), −5.2 (1B), −10.0 (2B), −11.6 (3B), −12.9 (3B). HRMS (ESI^{+}): *m/z* $[C_{11}H_{23}B_{10}N_4O_2]^{+}$ 366.2963, calcd for $[M - I]^{+}$ 366.2944.

Preparation of **L11.1**.

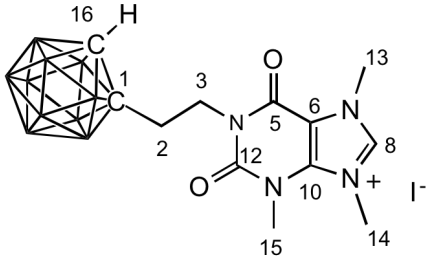

Prepared as described for **L9.1** from **P11.2** (450 mg, 1.28 mmol) and MeI (2.40 mL, 38.5 mmol) in MeCN (5 mL). After purification the product was obtained as a yellow powder. Yield: 189 mg, 0.86 mmol (67 %).^{1}H NMR (500 MHz, dmso-d_6): δ (ppm) 9.29 (s, 1H, H^{8}), 5.38 (br. s, 1H, H^{16}), 4.14 (s, 1H, H^{14}), 4.04 (s, 3H, H^{13}), 3.98 (m, 2H, H^{3}), 3.72 (s, 3H, H^{15}). ^{13}C NMR (75 MHz, dmso-d_6): δ (ppm) 152.8 (C^{5}), 149.7 (C^{12}), 139.1 (C^{8}), 139.5 (C^{10}), 107.8 (C^{6}), 73.0 (C^{1}), 63.6 (C^{16}), 36.9 (C^{14}), 35.6 (C^{13}), 33.0 (C^{3}), 31.4 (C^{15}). ^{11}B NMR (96 MHz, CD_3CN): δ (ppm) −2.83, −5.58, −9.47, −11.78, −12.93. HRMS (ESI^{+}): *m/z* $[C_{11}H_{23}B_{10}N_4O_2]^{+}$ 366.2960, calcd for $[M - I]^{+}$ 366.2944. (Note: only one of the CH_2 resonance is observed).

Preparation of **L12.1**.

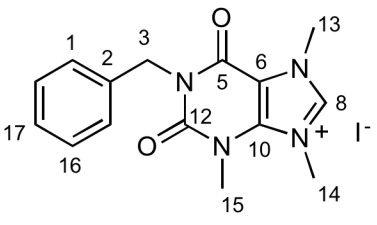

An ampoule was charged with MeCN (5 mL), **P12.1** (1.00 g, 3.70 mmol) and MeI (6.91 mL, 111 mmol) and heated at 80 °C for 100 hours. The reaction was then cooled to room temperature and solvent removed *in vacuo*. To the residue was added DCM (5 mL) and the product recrystallised with hexane (30 mL) this was then filtered yielding a sticky orange solid. This was dissolved in DCM (5 mL) and hexane (5 mL) is added, the solvent is removed *in vacuo* to give a fluffy golden solid, which is highly hygroscopic. Yield: 1.30 g, 3.15 mmol (85 %). ^{1}H NMR (500 MHz, DMSO-d_6): δ (ppm) 9.32 (s, 1H, H^{8}), 7.33 (m, 4H, $H^{1,16}$), 7.28 (m, 1H, H^{17}), 5.09 (s, 2H, H^{3}), 4.15 (s, 3H, H^{14}), 4.07 (s, 3H, H^{13}), 3.74 (s, 3H, H^{15}).

^{13}C NMR (126 MHz, DMSO-d_6): δ (ppm) 153.2 (C^5), 150.0 (C^{12}), 139.8 (C^8), 139.6 (C^{10}), 136.2 (C^2), 128.3 (C^1), 127.7 (C^{16}), 127.4 (C^{17}), 107.8 (C^6), 44.5 (C^3), 36.9 (C^{14}), 35.7 (C^{13}), 31.5 (C^{15}). HRMS (ESI$^+$): *m/z* $[C_{15}H_{17}N_4O_2]^+$ 285.1343, calcd for $[M - I]^+$ 285.1346.

Preparation of **L8.1**.

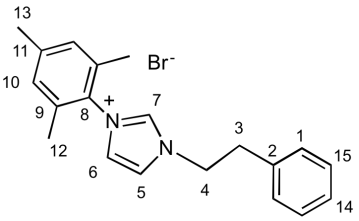

To an ampoule was added MeCN (2 mL), mesityl imidazole (576 mg, 3.09 mmol) and 2-bromoethyl-benzene (0.42 mL, 3.09 mmol) and heated at reflux for 18 hours. The reaction was cooled to room temperature and the product was precipitated with Et_2O (30 mL), filtered and dried *in vacuo* to give a white microcrystalline solid. Yield: 886 mg, 2.39 mmol (77 %). ^{1}H NMR (500 MHz, DMSO-d_6): δ (ppm) 9.35 (t, *J* = 1.5 Hz, 1H, H^7), 8.12 (t, *J* = 1.7 Hz, 1H, H^5), 7.87 (t, *J* = 1.8 Hz, 1H, H^6), 7.28 (m, 2H, H^{15}), 7.24 (s, 2H, H^1), 7.22 (m, 1H, H^{14}), 7.10 (s, 2H, H^{10}), 4.62 (t, *J* = 6.8 Hz, 2H, H^4), 3.26 (t, *J* = 6.8 Hz, 2H, H^3), 2.30 (s, 3H, H^{13}), 1.86 (s, 6H, H^{12}). ^{13}C NMR (126 MHz, DMSO-d_6): δ (ppm) 140.2 (C^{11}), 137.2 (C^7), 136.6 (C^2), 134.1 (C^9), 130.9 (C^8), 129.1 (C^{10}), 128.7 ($C^{1/15}$), 128.5 ($C^{1/15}$), 126.8 (C^{14}), 123.8 (C^6), 123.1 (C^5), 50.2 (C^4), 34.9 (C^3), 20.5 (C^{13}), 16.7 (C^{12}). HRMS (ESI$^+$): *m/z* $[C_{20}H_{23}N_2]^+$ 291.1870, calcd for $[M - Br]^+$ 291.1856.

6.8.2 Complexes

Preparation of **C2.26**.

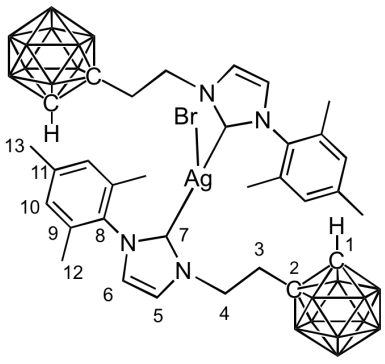

An ampoule was charged with **L8.1** (200 mg, 0.46 mmol) and Ag_2O (53 mg, 0.23 mmol) and degassed. Anhydrous DCM (5 mL) was added and the mixture is stirred at room temperature for 24 hours. The solution was filtered through Celite and the solvent was removed *in vacuo*. The residue was dissolved in Et_2O (5 mL) and the product was precipitated with hexane (15 mL), filtered and dried *in vacuo* to give a beige powder. Yield: 141 mg, 0.16 mmol (68 %). ^{1}H NMR (500 MHz, CD_2Cl_2): δ (ppm) 7.07 (d, *J* = 1.8 Hz, 1H, H^5), 6.97 (s, 2H, H^{10}), 6.87 (d, *J* = 1.8 Hz, 1H, H^6), 5.33 (br. s, 1H, H^1), 4.07 (m, 2H, H^4), 3.05 (m, 2H, H^3), 2.37 (s, 3H, H^{13}), 1.89 (s, 6H, H^{12}). ^{13}C NMR (126 MHz, DMSO-d_6): δ (ppm) 139.6 (C^{11}), 136.7 (C^8), 135.7 (C^9), 129.7 (C^{10}), 122.7 (C^6), 121.2 (C^5), 73.1 (C^2), 64.4 (C^1), 50.7 (C^4), 37.8 (C^3), 21.4 (C^{13}), 18.2 (C^{12}). ^{11}B{^{1}H} NMR (161 MHz, DMSO-d_6): δ (ppm) −3.2, −5.5, −10.0 (2B), −9.5, −13.0. HRMS (ESI$^+$): *m/z* $[C_{32}H_{56}B_{20}AgN_4]^+$ 819.5598, calcd for $[M - Br]^+$ 819.5562. Anal. Calcd for $C_{32}H_{56}B_{20}AgBrN_4$: C, 42.67; H, 6.27; N, 6.22. Found: C, 42.49; H6.16; N, 6.17.

Preparation of **C8.1**.

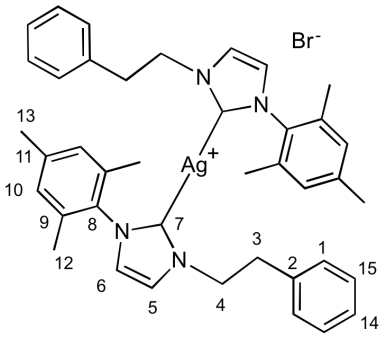

An ampoule was charged with **L8.1** (200 mg, 0.54 mmol) and Ag_2O (69 mg, 0.30 mmol) and degassed. Anhydrous DCM (5 mL) was added and the mixture is stirred at room temperature for 24 hours. The solution was filtered through Celite and the solvent removed *in vacuo* and methanol (5 mL) was added. The insoluble particulate was filtered and the product was precipitated with Et_2O (30 mL), filtered and dried *in vacuo* to give a white powder. Yield: 145 mg, 0.19 mmol (70 %). ^{1}H NMR (500 MHz, CD_2Cl_2): δ (ppm) 7.20 (s, 1H, H^5), 7.18 (m, 3H, $H^{14,15}$), 6.90 (m, 4H, $H^{1,10}$), 6.84 (s, 1H, H^6), 4.26 (t, J = 6.5 Hz, 2H, H^4), 3.00 (t, J = 6.5 Hz, 2H, H^3), 2.31 (s, 3H, H^{13}), 1.74 (s, 6H, H^{12}). ^{13}C NMR (126 MHz, DMSO-d_6): δ (ppm) 182.9 (C^7), 139.9 (C^{11}), 137.7 (C^2), 136.1 (C^8), 135.4 (C^9), 129.6 (C^{10}), 129.4 (C^1), 129.1 (C^{15}), 127.4 (C^{14}), 123.0 (C^6), 122.4 (C^5), 53.4 (C^4), 38.0 (C^3), 21.4 (C^{13}), 17.9 (C^{12}). HRMS (ESI^+): *m/z* $[C_{40}H_{44}AgN_4]^+$ 689.2621, calcd for $[M - Br]^+$ 689.2615. Anal. Calcd for C, 62.51; H, 5.77; N, 7.29. Found: C, 62.38; H, 5.89; N, 7.17.

Preparation of **C10.1**.

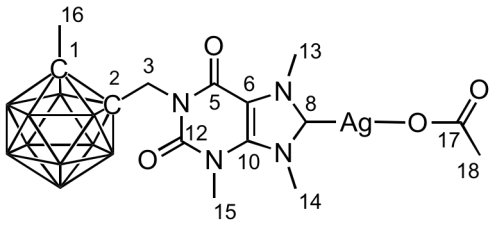

An ampoule was charged with **L10.1** (150 mg, 0.31 mmol), AgOAc (102 mg, 0.61 mmol) and anhydrous DCM (5 mL) and stirred at room temperature for 48 hours. The reaction mixture was filtered through Celite washed with DCM (5 mL) and the solvent volume reduced to 5 mL *in vacuo*. The product was precipitate with diethyl ether (30 mL), filtered and dried *in vacuo* to give a white powder. Yield: 90 mg, 0.17 mmol (55 %). ^{1}H NMR (500 MHz, CD_2Cl_2): δ (ppm) 4.88 (d, J = 14.9 Hz, 1H, H^3), 4.61 (d, J = 14.9 Hz, 1H, H^3), 4.21 (s, 3H, H^{14}), 4.11 (s, 3H, H^{13}), 3.81 (s, 3H, H^{15}), 2.32 (s, 3H, H^{16}), 1.95 (s, 3H, H^{18}). ^{13}C NMR (126 MHz, DMSO-d_6): δ (ppm) 188.4 (C^8), 178.8 (C^{17}), 153.3 (C^5), 151.2 (C^{12}), 141.2 (C^{10}), 110.1 (C^6), 78.2 (C^1), 75.8 (C^2), 43.6 (C^3), 40.5 (C^{14}), 39.2 (C^{13}), 32.9 (C^{15}), 23.7 (C^{16}), 22.9 (C^{18}). ^{11}B{^{1}H} NMR (161 MHz, CD_2Cl_2): δ (ppm) −3.3 (1B), −6.0 (1B), −9.9 (8B). Anal. Calcd for $C_{14}H_{27}AgB_{10}N_4O_4$: C, 31.65; H, 5.12; N, 10.54. Found: C, 31.58; H, 4.97; N, 10.37. Complex could not be characterised by HRMS due to scrambling.

Preparation of **C12.1**.

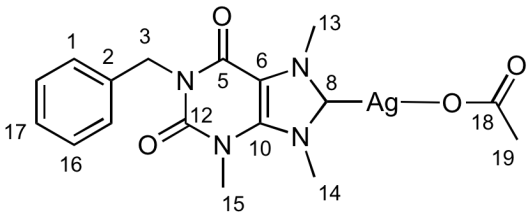

Prepared as described for **C10.1** from **L12.1** (300 mg, 0.73 mmol) and AgOAc (255 mg, 1.53 mmol) in anhydrous DCM (5 mL). and stirred at room temperature for 48 hours. After purification the product was obtained as a white powder. Yield: 191 mg, 0.42 mmol (58 %). ^{1}H NMR (500 MHz, CD_2Cl_2): δ (ppm) 7.42-7.39 (m, 2H, H^{1}), 7.33-7.24 (m, 3H, $H^{16/17}$), 5.15 (s, 2H, H^{3}), 4.16 (s, 3H, H^{14}), 4.11 (s, 3H, H^{13}), 3.76 (s, 3H, H^{15}), 1.94 (s, 3H, H^{19}). ^{13}C NMR (126 MHz, CD_2Cl_2): δ (ppm) 187.2 (C^{8}), 178.7 (C^{18}), 153.9 (C^{5}), 151.2 (C^{12}), 140.8 (C^{10}), 137.2 (C^{2}), 129.1 (C^{1}), 128.9 (C^{16}), 128.3 (C^{17}), 110.4 (C^{6}), 45.6 (C^{3}), 40.3 (C^{14}), 39.1 (C^{13}), 32.4 (C^{15}), 22.9 (C^{19}). Anal. Calcd for $C_{17}H_{20}AgN_4O_4$: C, 45.15; H, 4.46; N, 12.39. Found: C, 45.17; H, 34.10; N, 12.48. Complex could not be characterised by HRMS due to scrambling. The major peak molecular ion peak observed corresponded to *m/z* $[C_{30}H_{32}AgN_8O_4]^{+}$ 675.1602, calcd for $[Ag(NHC)_2]^{+}$ 675.1592.

Cytotoxicity Studies

In vitro cell tests were performed at the Cancer Pharmacology Institute at the University of Huddersfield by Mr. Suliman Atallah who works under the supervision of Prof. Roger Phillips. Cells were incubated in 96-well plates, at 2 × 103 cells per well in 200 µL of growth media (RPMI 1640 supplemented with 10 % foetal calf serum, sodium pyruvate (1 mM) and L-glutamine (2 mM)). Cells were incubated for 24 hours at 37 °C in an atmosphere of 5 % CO_2 prior to drug exposure. Silver compounds were dissolved in DMSO at a concentration of 25 mM and diluted with medium to obtain drug solutions ranging from 25 µM to 0.049 µM. The final DMSO concentration was 0.1 % (v/v) which is non-toxic to cells. Drug solutions were applied to cells and incubated for 96 hours at 37 °C in an atmosphere of 5 % CO_2. The solutions were removed from the wells and fresh medium added to each well along with 20 µL MTT (5 mg mL^{-1}), and incubated for 4 hours at 37 °C in an atmosphere of 5 % CO_2. The solutions were removed and DMSO (150 µL) was added to each well to dissolve the purple formazan crystals. A plate reader was used to measure the absorbance at 540 nm. Lanes containing medium only, and cells in medium only (no drug), were used as blanks for the spectrophotometer and 100 % cell survival respectively. Cell survival was determined as the true absorbance of treated cells divided by the true absorbance of controls and expressed as a percentage. The concentration required to kill 50 % of cells (IC_{50}) was determined from plots of % survival against drug concentration.

6.9 References

1 K. H. J., *Burns*, 2000, **26**, 117–130.

2 T. A. Bell, J. T. Grayston, M. A. Krohn and R. A. Kronmal, *Pediatrics*, 1993, **92**, 775–760.

3 C. L. Fox, *Arch. Surg.*, 1968, **96**, 184–188.

4 C. J. Fox and S. M. Modak, *Antimicrob Agents Chemother*, 1974, **5**, 582–588.

5 J. R. Morones-Ramirez, J. a Winkler, C. S. Spina and J. J. Collins, *Sci. Transl. Med.*, 2013, **5**, 1–11.

6 Y. Kim, H. S. Suh, H. J. Cha, S. H. Kim, K. S. Jeong and D. H. Kim, *Am. J. Ind. Med.*, 2009, **52**, 246–250.

7 A. Melaiye, R. S. Simons, A. Milsted, F. Pingitore, C. Wesdemiotis, C. A. Tessier and W. J. Youngs, *J. Med. Chem.*, 2004, **47**, 973–977.

8 A. Melaiye, Z. Sun, K. Hindi, A. Milsted, D. Ely, D. H. Reneker, C. A. Tessier and W. J. Youngs, *J. Am. Chem. Soc.,* 2005, **127**, 2285–2291.

9 A. K-Nebioglu, M. J. Panzner, J. C. Garrison, A. C. A. Tessier and W. J. Youngs, *Organometallics*, 2004, **23**.

10 A. K. Nebioglu, A. Melaiye, K. Hindi, S. Durmus, M. J. Panzner, L. A. Hogue, R. J. Mallett, C. E. Hovis, M. Coughenour, S. D. Crosby, A. Milsted, D. L. Ely, C. A. Tessier, C. L. Cannon and W. J. Youngs, *J. Med. Chem.*, 2006, **49**, 6811–6818.

11 A. S. Ahmad, N. Ormiston-Smith and P. D. Sasieni, *Br. J. Cancer*, 2015, **112**, 943–947.

12 A. Vessières, S. Top, W. Beck, E. Hillard and G. Jaouen, *Dalt. Trans.*, 2006, **47**, 529–541.

13 C. G. Hartinger, M. A. Jakupec, S. Zorbas-Seifried, M. Groessl, A. Egger, W. Berger, H. Zorbas, P. J. Dyson and B. K. Keppler, *Chem. Biodivers.*, 2008, **5**, 2140–2155.

14 J. M. Rademaker-Lakhai, D. van den D. P. Bongard, J. H. Beijnen and J. H. M. Schellens, *Clin. Cancer Res.*, 2004, **10**, 3717–3727.

15 H.-L. Zhu, X.-M. Zhang, X.-Y. Liu, X.-J. Wang, G.-F. Liu, A. Usman and H.-K. Fun, *Inorg. Chem. Commun.*, 2003, **6**, 1113–1116.

16 D. A. Medvetz, K. M. Hindi, M. J. Panzner, A. J. Ditto, Y. H. Yun, W. J. Youngs, D. A. Medvetz, K. M. Hindi, M. J. Panzner, A. J. Ditto, Y. H. Yun and W. J. Youngs, *Met. Based. Drugs*, 2008, **2008**, 384010.

17 M. Griffiths and H. Sundaram, in *Methods in Molecular Biology*, 2011, pp. 451–465.

18 H. A. Mohamed, B. R. M. Lake, T. Laing, R. M. Phillips and C. E. Willans, *Dalt. Trans.*, 2015, **44**, 7563–7569.

19 C. P. Newman, G. J. Clarkson and J. P. Rourke, *J. Organomet. Chem.*, 2007, **692**, 4962–4968.

20 C.-H. Cheng, D.-F. Chen, H.-B. Song and L.-F. Tang, *J. Organomet. Chem.*, 2013, **726**, 1–8.

21 C. Hemmert, A. Fabié, A. Fabre, F. Benoit-Vical and H. Gornitzka, *Eur. J. Med. Chem.*, 2013, **60**, 64–75.

22 H. A. M. A. Abdelgawad, *PhD Thesis, Unversity Leeds*, 2016.

23 J. C. Garrison and W. J. Youngs, *Chem. Rev.*, 2005, **105**, 3978–4008.

24 A. A. D. Tulloch, A. A. Danopoulos, S. Winston, S. Kleinhenz and G. Eastham, *J. Chem. Soc. Dalt. Trans.*, 2000, **36**, 4499–4506.

25 H. M. J. W. And and I. J. B. Lin, *Organometallics*, 1998, **17**, 972–975.

26 L. I. Zakharkin, V. A. Bratsev and A. Chapovskii Yu, *Zh. Obs. Khim*, 1965, **35**, 2160–2167.

27 A. A. Semioshkin, G. M. Ptashits, V. L. Ivanov, V. A. Artyomov, A. M. Shestopalov, V. I. Bregadze and V. P. Litvinov, *Tetrahedron*, 1997, **53**, 7911–7916.

28 M. J. Panzner, K. M. Hindi, B. D. Wright, J. B. Taylor, D. S. Han, W. J. Youngs and C. L. Cannon, *Dalt. Trans.* , 2009, 7308–13.

29 J. J. Schaeck and S. B. Kahl, *Inorg. Chem.*, 1998, **38**, 204–206.

30 L. O. Kononov, A. V. Orlova, A. I. Zinin, B. G. Kimel, I. B. Sivaev and V. I. Bregadze, *J. Organomet. Chem.*, 2005, **690**, 2769–2774.

31 C. L. Powell, M. Schulze, S. J. Black, A. S. Thompson and M. D. Threadgill, *Tetrahedron Lett.*, 2007, **48**, 1251–1254.

32 T. Mosmann, *J. Immunol. Methods*, 1983, **65**, 55–63.